944

# UNSTEADY FLOW IN COLLAPSIBLE TUBES

by

PAUL MORGAN

A thesis submitted to the University of London for the degree of Doctor of Philosophy in the Faculty of Engineering, 1985.

Physiological Flow Studies Unit
Imperial College
LONDON SW7 2AZ

## ABSTRACT

This work was motivated by the need to know more about the mechanisms of flow in biological vessels such as veins. Extensive experimental investigations into flow in thin-walled rubber tubes have provided some insight into the phenomena occurring in such biological vessels.

A mathematical model is developed to investigate, primarily, unsteady flow in a collapsible tube whose ends are tethered to rigid tubes and which is enclosed in a pressurised chamber. An incompressible fluid flows through the tube from an upstream reservoir and discharges at another reservoir downstream.

A one-dimensional distributed parameter model is used and the boundary conditions upstream and downstream are provided by lumped parameter models. An implicit differencing method is used for both the steady and unsteady flow equations. The method of specified time intervals is used to solve the system of hyperbolic equations of the unsteady model.

Steady flow results are presented and compared with results from a lumped parameter version of the model, and those of other authors' models and experiments. The importance of certain parameters is investigated.

Unsteady flow is investigated by starting from an equilibrium state obtained from the steady flow model and stepping on in time. An ad hoc method is used to predict the stability of the equilibrium state. This method is based on a linear stability analysis of both the model and

the boundary conditions, and the location of the operating point on the pressure-flow characteristic.

The effect of wave propagation on stability is investigated. Several types of instability, with features similar to those observed in experimental studies, are predicted. The importance of certain model parameters is emphasised.

CONTENTS


| | | | |
|---|---|---|---|
| ACKNOWLEDGEMENT | | | 9 |
| CHAPTER 1 | INTRODUCTION AND APPLICATIONS | | 10 |
| | 1.1 | Introduction | 10 |
| | 1.2 | Starling Resistor | 12 |
| | | 1.2.1 Flow Limitation | 13 |
| | | 1.2.2 Oscillations | 13 |
| | 1.3 | Physiological Applications | 14 |
| | | 1.3.1 Veins | 14 |
| | | 1.3.2 Arteries | 20 |
| | | 1.3.3 Autoregulation | 21 |
| | | 1.3.4 Pulmonary Circulation | 21 |
| | | 1.3.5 Pulmonary Airways | 22 |
| | | 1.3.6 Urethra | 23 |
| | | 1.3.7 Vocal Cords | 23 |
| | 1.4 | Medical Applications | 24 |
| | | 1.4.1 Korotkoff Sounds | 25 |
| | | 1.4.2 Intermittent External Pneumatic Compression | 26 |
| | | 1.4.3 Counterpulsation | 26 |
| | | 1.4.4 Artificial-Larynx | 28 |
| | 1.5 | Engineering Applications | 28 |
| | 1.6 | Conclusions | 29 |
| | Figs 1.2.1 - 1.2.5 | | 30 - 33 |
| | Figs 1.3.1 - 1.3.4 | | 33 - 35 |
| CHAPTER 2 | REVIEW OF PREVIOUS WORK | | 36 |
| | 2.1 | Introduction | 36 |
| | 2.2 | Experimental Background | 38 |

2.2.1 Effect of Varying Upstream Conditions 39

2.2.2 Effect of Varying Downstream Conditions 41

2.2.3 Effect of Varying External Pressure 41

2.3 Theoretical Background 41

2.3.1 Tube Law 46

2.4 Wave Propagation 52

2.5 Flow Limitation 56

2.6 Self-Excited Oscillations 63

2.7 Korotkoff Sounds 77

2.7.1 Dynamic Instability 77

2.7.2 Shock Wave 78

2.7.3 Self-Excited Oscillations 80

2.7.4 Turbulence 82

Figs 2.2.1 - 2.2.2 84 - 85

Table 2.3.1 86

Figs 2.3.1 - 2.3.3 87 - 88

Figs 2.5.1 - 2.5.4 88 - 90

Figs 2.6.1 - 2.6.2 91 - 92

Figs 2.7.1 - 2.7.2 92 - 93

CHAPTER 3 MATHEMATICAL MODEL 94

3.1 Introduction 94

3.2 Description of the Physical Model 95

3.3 Assumptions of the Theoretical Model 95

3.3.1 One-Dimensional Flow 95

3.3.2 The Tube Law 96

3.4 Formulation of the Theoretical Model 96

3.5 The Tube Model 99

3.5.1 Quasi-Static Tube Law 99

3.5.2 Limitations of the Tube Law 101

3.5.3 Wave Speed 103

3.6 The Flow Model 104

3.7 Boundary and Initial Conditions 106

3.7.1 Control-Volume Method 106

3.7.2 General Flow Equations 107

3.7.3 Upstream Boundary Condition 112

3.7.4 Downstream Boundary Condition 115

3.7.5 Initial Conditions 117

3.8 Non-Dimensional Variables 117

3.9 Non-Dimensional Equations 118

Fig 3.1.1 121

Fig 3.4.1 122

Figs 3.5.1 - 3.5.2 123 - 124

Figs 3.7.1 - 3.7.3 125 - 126

CHAPTER 4 STEADY FLOW 127

4.1 Introduction 127

4.2 Equations and Boundary Conditions 128

4.2.1 Boundary Conditions 128

4.3 Finite Difference Formulation 129

4.3.1 Solution Scheme 132

4.3.2 Boundary Conditions 133

4.4 Results 136

4.4.1 Non-Dimensional Variables 136

4.4.2 Parameter Values 137

4.4.3 Conrad's Experiment 140

| | | | |
|---|---|---|---|
| | 4.4.4 | Brower and Scholten's Experiment | 146 |
| | 4.4.5 | Parameter Variation | 148 |
| | Figs 4.4.1 - 4.4.24 | | 153 - 174 |
| CHAPTER 5 | UNSTEADY FLOW | | 175 |
| | 5.1 | Introduction | 175 |
| | 5.2 | Model Equations | 175 |
| | 5.3 | Method of Characteristics | 176 |
| | 5.3.1 | Integration of the Characteristic Equations | 178 |
| | 5.3.2 | Method of Specified Time Intervals | 181 |
| | 5.3.3 | Errors | 182 |
| | 5.4 | Boundary Conditions | 185 |
| | 5.4.1 | Upstream Boundary | 186 |
| | 5.4.2 | Downstream Boundary | 187 |
| | 5.5 | Initial Conditions | 188 |
| | 5.6 | Solution Scheme | 188 |
| | 5.7 | Test Cases | 192 |
| | 5.7.1 | LPM Equations | 192 |
| | 5.7.2 | The Complete Model | 193 |
| | Figs 5.3.1 - 5.3.5 | | 204 - 205 |
| | Figs 5.6.1 - 5.6.2 | | 206 |
| | Figs 5.7.1 - 5.7.22 | | 207 - 228 |
| CHAPTER 6 | INSTABILITIES | | 229 |
| | 6.1 | Introduction | 229 |
| | 6.2 | Types of Instability | 230 |
| | 6.2.1 | Milking Oscillations | 230 |
| | 6.2.2 | 'Stationary' Oscillations | 232 |
| | 6.2.3 | Exponential Instability | 233 |

6.3 Stability 233

6.3.1 Boundary Condition Instabilities 233

6.3.2 Collapsible Tube Instabilities 236

6.3.3 Combined Instabilities 237

6.4 Results 239

6.4.1 The Effect of Wave Propagation on Instabilities Associated with the Boundary Conditions 239

6.4.2 The Effect of Model Parameters on the Form of the Oscillations 249

6.4.3 Instabilities in Experimental Models (Starling Resistor) 253

Fig 6.2.1 263

Figs 6.4.1 - 6.4.37 264 - 300

CHAPTER 7 CONCLUSIONS AND FUTURE WORK 301

APPENDIX A ELLIPTIC TUBE RESISTIVITY 308

APPENDIX B METHOD OF CHARACTERISTICS 311

REFERENCES 314

ACKNOWLEDGEMENT

I would like to thank Dr Kim Parker for inspiration and guidance during the course of this research. Our numerous discussions were extremely valuable and contributed greatly to the advancement of this research. I would also like to thank Kim and Dr Bob Schroter for their advice and critical comments on drafts of this thesis.

I am also grateful to Drs Steve Maskell and Mike Patrick of the University of Exeter for their advice during the early stages of this research.

The research was completed while I was employed as a Research Assistant in the Department of Mechanical Engineering at University College, Cardiff, and I am grateful to Professor Eric Markland for his encouragement and understanding during this period.

I would like to thank my wife Paula for her support and encouragement throughout and also for typing the thesis.

Finally, I am grateful to the SRC for financial support during the first two years of this research.

# CHAPTER 1

# INTRODUCTION AND APPLICATIONS

## 1.1 INTRODUCTION

The study of physiological fluid flows is pursued by scientists from several different disciplines. The attraction of the subject arises from the abundance and diversity of the problems raised, which differ in many respects from those encountered in engineering fluid flows (Lighthill, 1972). Progress in this field has resulted from the close collaboration between specialists from physiology, engineering and the physical sciences.

Many physiological fluid flows, in higher life forms, occur in vessels which collapse during their normal function, for example, veins above the level of the heart. When collapse occurs the cross-section of such vessels becomes non-circular, and the relationship between the pressure gradient and the flow rate becomes very complicated. In these circumstances several interesting phenomena can occur.

The flow through these collapsible vessels can be investigated experimentally both in vivo and in vitro; a mathematical model incorporating all the physical properties would be forbiddingly complex. Alternatively, research into an artificial system, viz a collapsible rubber tube, which has been studied extensively in recent years, provides some insight into the phenomena occurring in physiological vessels; without the need for surgery. Also, a comprehensive mathematical model of such a tube,

although difficult to develop, is more tractable than a model of its physiological counterpart. This thesis is concerned with an investigation into phenomena which occur during flow through such collapsible tubes.

The majority of experiments on collapsible tubes have been conducted on the so-called Starling resistor. In the first section of this chapter this device is described together with some related experiments which exhibit phenomena similar to those occurring in physiological flows.

In the next section some areas of physiology to which research into flow in collapsible tubes can and has already been applied is indicated. This research has led to a greater understanding of some physiological phenomena.

Finally, biomedical applications of collapsible tubes, for example, in prosthetic devices, are considered, which have improved the quality of life of many people. Some engineering applications are also indicated.

This chapter serves mainly to introduce the areas to which the study of flow in collapsible tubes has relevance. Details of the phenomena observed in collapsible tube flow, the theories proposed to explain them and the application of these theories to naturally occurring flows (in physiology) is given in the next chapter.

## 1.2 STARLING RESISTOR

This is an experimental apparatus devised by Knowlton and Starling (1912). It was originally developed to simulate the resistance presented to an isolated mammalian heart (Fig 1.2.1) but has subsequently been used to simulate other physiological phenomena.

It consists of a thin-walled compliant tube (for example, colostomy tubing) which is attached at each end to a rigid tube and enclosed in a chamber at an adjustable external pressure, $p_e$. Numerous hydraulic tests have been carried out on this device (Holt, 1969; Conrad, 1969, among others) using an apparatus similar to that shown in Fig 1.2.2. The flow through the system can be changed by adjustment of the reservoir heights, the variable constrictions, or the external pressure. This versatility is useful in simulating physiological phenomena.

If the external pressure and downstream constriction (Fig 1.2.2) are held constant and flow varied by adjustment of the upstream reservoir or constriction, then a pressure drop versus flow rate or P-Q characteristic, similar to that shown in Fig 1.2.3, is obtained. An important property of this P-Q characteristic is the region of negative slope. In this region the Starling resistor exhibits a dynamic negative resistance and oscillations are often observed. A discussion of this phenomenon is given in section 2.7.3.

As an indication of the use of this device in simulating physiological phenomena, two experiments are now considered. In the first experiment flow limitation

occurs, which has been observed, for example, in forced expiration (Fry, 1958) and in the second, self-excited oscillations, which have been observed in veins under certain conditions (Brecher, 1952; Tsuji et al, 1978).

In the following discussion $P_1$ denotes the upstream pressure, $P_2$, the downstream pressure and $P_e$, the external pressure to the collapsible tube.

1.2.1 Flow Limitation

$P_1 - P_e$ = constant. If $P_2 - P_e$ is reduced, the flow rate, Q, increases as $P_1 - P_2$ increases provided that $P_2 - P_e$ is positive, ie the tube is inflated at the outlet. However, if $P_2 - P_e$ becomes negative, ie the tube is partially collapsed at the outlet, then Q is virtually independent of $P_1 - P_2$ (Fig 1.2.4). Flow limitation results because while a reduction in $P_2$ increases the driving pressure drop and hence the fluid velocity, the exit area is reduced due to collapse of the tube.

1.2.2 Oscillations

$P_2 - P_e < 0$. For a certain range of negative $P_2 - P_e$ the outlet area oscillates at a characteristic frequency. This range corresponds to a region of negative slope of the P-Q characteristic (Fig 1.2.3). This negative slope makes the system statically unstable. Dynamically, negative damping is present which means that the oscillation can grow. Eventually there is a build up of the oscillation to a limit cycle (Fig 1.2.5).

These are two examples of phenomena occurring in the Starling resistor which will be shown to have physiological implications. Physiological flows and the

many associated phenomena are now discussed for which experimental and theoretical research on collapsible tubes may provide some explanations.

A variety of physiological and medical applications of flow in collapsible tubes are cited in a paper by Shapiro (1977a).

## 1.3 PHYSIOLOGICAL APPLICATIONS

Since the studies of Hagen (1839) and Poiseuille (1840), the hydrodynamics of flow through rigid tubes has been widely developed. However, it is only relatively recently that detailed studies have been carried out concerning the flow through collapsible tubes, in regimes where collapse can occur, and these have been concentrated mainly on steady flow.

In considering the physiology of animals it is evident that the transport of fluids through the ureters, urethra, intestinal tract, blood vessels, etc involves flow through collapsible tubes. However, inspite of the abundance of such flows, it was not until the work of Holt (1941) that quantitative studies concerning flow through collapsible tubes were reported. This work examined the significance of the collapsibility of veins, a matter of great physiological interest.

In this section several examples of physiological flows in compliant vessels are given together with some of the phenomena which are observed in these vessels.

### 1.3.1 Veins

These are thin-walled, compliant vessels which

convey the blood to the heart. The systemic veins convey the deoxygenated blood from the periphery and the pulmonary veins convey oxygenated blood from the lungs (the corresponding arteries convey the blood to the periphery and lungs, repectively). Almost 80 per cent of the blood in the systemic vascular system is in the veins.

A typical ratio of wall thickness to diameter for these vessels would be in the range 0.01-0.02. The walls are non-homogeneous and their stress-strain relations are non-linear and time dependent (Attinger, 1969). The effective Young's modulus for circumferential stretch measured at the in vivo length and diameter for a large vein (inferior vena cava) is in the range $0.4\text{-}1.0 \times 10^5$ N $m^{-2}$.

The pressure in a vein is normally much lower than that in an artery at the same level and may be less than atmospheric. Taking the pressure at heart level as zero (relative to atmospheric) the pressure in a large vein at this level is about $0.7 \times 10^3$ N $m^{-2}$. Therefore the transmural pressure, $p_{tm}$ (pressure inside vessel - pressure outside vessel) is just positive. In veins significantly above heart level, for example, in a raised arm, $p_{tm}$ is normally sub-atmospheric and the veins collapse. In contrast, the transmural pressure in the foot is above $10^4$ N $m^{-2}$ due to the hydrostatic pressure.

The pressure external to veins can be increased by muscular action, thereby preventing too great a distension of veins well below the heart, but it cannot

be reduced to prevent collapse. This is not true for veins within the skull which is a constant volume chamber; a reduction in blood vessel volume generates a negative external pressure preventing further collapse.

When the transmural pressure is very low it has been observed that a reduction in the internal pressure at the downstream end has little or no effect on the flow rate, provided that it is less than the pressure outside the vessel. Since the systemic venous system extends from a region in which the external pressure is above atmospheric (abdomen) through to a region in which the pressure is normally sub-atmospheric (thorax), the veins will collapse on just entering the chest. Similar behaviour can also occur in the pulmonary venous system provided the intrathoracic pressure is sub-atmospheric. Holt (1941) proposed that this phenomenon is similar to that which occurs in a Starling resistor when $P_2 < P_e$ and the tube is partially collapsed (see section 1.2.1). He suggests that collapse of veins entering the chest may be a mechanism which ensures a normal flow of blood into the heart but prevents overfilling.

Brecher (1952) also investigated the effect of breathing on venous return. In an experiment on an open-chest dog, the effect of a negative intrathoracic pressure was substituted by suction at the peripheral end of the superior vena cava. When negative pressure was applied in this way two different stages were observed in the venous outflow, viz a depleting stage and a collapsed stage. The former was characterised by a continuous

reduction of the vein's filling state. The venous outflow increased with the pressure gradient while the resistance remained virtually constant. The collapsed stage occurred after the veins had partially emptied, the outflow remained constant and resistance increased with greater pressure gradients (Fig 1.3.1). Experiments with rubber tubes showed similar results (Fig 1.2.4). Brecher concluded that very deep inspiration can increase venous return initially but when veins collapse the flow rate is maintained virtually constant.

Vein collapse is also important in the auto-regulation of blood to various organs.

The collapse of veins resulting from, for example, raising an arm above heart level, does not necessarily alter the mean flow rate of blood through the cardio-vascular system. This is because the impedance of the system depends primarily on the viscoelastic properties of the arteries and the resistance of the microcirculation, venous calibre is relatively unimportant.

The distensibility, D, of a vessel may be defined as

$$D = \frac{1}{A}\frac{dA}{dp_{tm}} \quad , \qquad (1.3.1)$$

where A is the cross-sectional area and $p_{tm}$ is the transmural pressure. Veins are highly distensible over a certain range of transmural pressure. These vessels can therefore be sensitive to manoeuvres which change the transmural pressure, for example, respiration (see above).

The wave speed in veins is usually less than that in arteries provided $p_{tm}$ is less than about $3 \times 10^3$ N $m^{-2}$. The wave speed for the superior vena cava of a dog lies in the range 0.5-3 m $s^{-1}$.

An estimate of the wave speed in collapsible vessels can be obtained using the following formula

$$c^2 = (\rho D)^{-1}, \qquad (1.3.2)$$

where $\rho$ is the density of the fluid in the tube and D is the tube distensibility defined in (1.3.1). The predicted wave speed in the thoracic vena cava, determined from (1.3.2), varies from 5 m $s^{-1}$ or more at high transmural pressures, to a minimum of about 0.6 m $s^{-1}$ when the vein is collapsing, and increases again to about 3 m $s^{-1}$ when it is fully collapsed (Caro et al, 1978).

The collapsibility of veins makes the understanding of wave propagation in these vessels difficult. Wave reflections occur and the wave speed along a vessel can change significantly due to changes in distensibility. Thus waves may flatten or steepen; in the latter case an elastic jump may be formed (cf shock wave, hydraulic jump). Such phenomena have been proposed for the so-called venous pistol shot sounds which are associated with incompetence of the tricuspid valve (Anliker et al, 1971 - see Holenstein et al, 1984).

The study of flow in collapsible tubes can provide insight into venous flow and related phenomena. However, there are several important differences between the mechanical properties of a vein and a simple collapsible tube and these must be accounted for if a useful

simulation is to be made. Moreno et al (1970) performed some experiments on excised veins and collapsible latex tubes in which the vessels were distended from flattened to circular cross-sections. It was found that in this regime the perimeter of the collapsible latex tube remained constant, the cross-sectional area increasing exclusively by bending of the walls. Further increases in area were associated with circumferential stretching and a corresponding increase in the perimeter. This two regime behaviour did not occur in the experiment on a vein. A combination of bending and stretching was found to occur throughout the distension (Fig 1.3.2). The constancy of the perimeter of a collapsible tube at negative transmural pressure is one of the reasons why results obtained from model studies are only broadly indicative of the behaviour of this vessel.

The volume compliance of the latex tube is large when bending dominates and there is a sharp transition to a low compliance when circumferential tension dominates. The transition for the vein is smooth.

The distensibility of the vein was discussed earlier. From Fig 1.3.2 it appears that the maximum value of $dA/dp_{tm}$ occurs at a positive transmural pressure of about $0.5 \times 10^3$ N $m^{-2}$ whereas in the case of the collapsible rubber tube it occurs at a negative transmural pressure of about $-0.25 \times 10^3$ N $m^{-2}$. This difference is primarily due to the greater stiffness of the collapsible tube. Young's modulus for rubber has a value of about $2.1 \times 10^6$ N $m^{-2}$ whereas the corresponding

value for a vein, when circular, is $5 \times 10^4$ N $m^{-2}$. Thus a greater bending moment is required to cause bending of the walls of the collapsible tube from a circular cross-section. At high values of transmural pressure the area of the vein is much greater than that of the rubber tube due to the greater distensibility of the former.

The flow in systemic veins is further complicated by the presence of valves which break up the high hydrostatic fluid column, for example, in the leg, into small segments. This prevents overdistension of these vessels; the stress-strain characteristics also help to prevent overdistension. The presence of these valves will affect wave propagation in these vessels as will the non-homogeneity of the wall.

Another important difference between the two vessels is the presence of smooth muscle in the walls of veins, which is normally in a state of active tension (ie of tone). The tone can to some extent be simulated in the collapsible tube by imposing longitudinal tension.

### 1.3.2 Arteries

The majority of these vessels normally experience a positive transmural pressure and therefore do not collapse. However, during ventricular contraction the instigating muscular contraction of the heart muscle causes collapse of the coronary arteries (Rodbard, 1963).

Another case in which these vessels are collapsed is in the cuff measurement of blood pressure (see section 1.4.1).

### 1.3.3 Autoregulation

It has been observed that the flow of blood through the tissues of the brain, kidney, forearm, extremities, heart, liver and intestines remains essentially constant independent of the level of mean blood pressure. In an attempt to understand this phenomena Rodbard (1963) proposed the 'capilleron' model illustrated in Fig 1.3.3. The pressure in the chamber surrounding the collapsible tube is controlled largely by the pressure just upstream of the collapsible segment. An increase in upstream pressure tends to increase the flow through the tube, however, the chamber pressure is also increased further collapsing the tube and increasing the resistance to flow. By a suitable choice of inflow and outflow resistances to the surrounding chamber the system autoregulates.

Rodbard suggested that variations in the permeability of the capillary wall modifies the extravascular pressure (cf chamber pressure above), resulting in partial collapse of the capillary when this pressure exceeds the pressure in the-capillary.

### 1.3.4 Pulmonary Circulation

This is a low pressure, low resistance system which conveys the entire output of the right side of the heart to the lungs and returns it to the left side of the heart. Pulmonary capillaries located in the alveolae are essentially exposed to atmospheric pressure via the airways. These vessels may therefore collapse if the respiratory pressure is increased or the capillary

pressure decreased, by a small amount.

One of the factors affecting blood flow in the lung is the vertical elevation. Since there is a hydrostatic gradient of intravascular pressure down the lung and the alveolar pressure is roughly uniform and equal to atmospheric, the transmural pressure increases with decreasing height. This results in a greater blood flow in the lower part of the lung. In the upper part of the lung the hydrostatic level is low and the pulmonary veins appear collapsed due to alveolar pressure exceeding the pulmonary venous pressure.

1.3.5 Pulmonary Airways

These vessels convey air to and from the lungs and can be collapsed by a negative transmural pressure. An interesting phenomenon has been observed in these vessels, viz flow limitation. Experimental studies (Fry et al, 1954 – see Fry, 1958) have demonstrated a functional relationship between pressure exerted on the lung (pleural pressure) and the volume flow rate from the lung, measured at the mouth (Fig 1.3.4). It is apparent from these curves that for any given lung volume there is a maximum expiratory flow rate beyond which a subject cannot go regardless of effort.

Experimental and theoretical studies of flow in collapsible tubes have been undertaken to investigate the phenomenon of flow limitation. The possibility of the flow velocity equalling the wave speed at points along the airway, called choke points (which occur naturally) has been investigated by Dawson and Elliott (1977) and

Knudson and Schroter (1983).

1.3.6 Urethra

This vessel, which is approximately 5 cm in length in the female and 18-20 cm in the male, transports urine from the bladder to the exterior of the body. This process is called micturition.

The flow in this vessel has been investigated experimentally and theoretically in both the female (Griffiths, 1969a; 1969b) and the male (Griffiths, 1971a; 1971b). In the case of the female it was found that a critical elastic constriction (one in which the fluid velocity equals the speed of pressure waves at the constriction, while upstream and downstream it is less than the wave speed, ie subcritical) is present near the midpoint of the urethra, which controls the flow. Griffiths pointed out the importance of the flow velocity being comparable with the speed of pressure waves on the vessel. He paralleled his work on the male urethra with an experiment using a collapsible latex tube, which was supported on a rigid surface inclined at some angle to the vertical. The upstream end was attached to a rigid tube and two elastic constrictions were imposed on the collapsible tube. It appears that two similar critical constrictions occur naturally in the male urethra.

1.3.7 Vocal Cords

The vocal cords lie within the larynx and are thrown into vibration by air expelled from the lungs. The pitch is affected by the tension in the cords and their position which are controlled by small muscles.

The mechanism is similar to that of a Starling resistor in the negative resistance regime. In this analogy the external pressure acting on the collapsible tube is comparable to the active muscle tone of the vocal cords, tending to produce closure. Conrad (1980) has proposed a model of the vocal cords based on such an analogy (see also Conrad, 1983).

In section 1.4.4 a prosthetic vocal source is described which has been developed using a collapsible tube as a fluid mechanical oscillator.

It has been suggested that the study of flow in collapsible tubes may also possibly apply to flow in the eustachian tube and the drainage of aqueous humour from the eye. The eustachian tube is a small tube (3-5 cm in length) which extends from the middle ear to the back of the nose (nasopharynx). By means of this passage air can pass into or out of the middle ear. Shapiro (1977a) suggested that flow in this vessel may be similar to that of gas flow in a collapsible tube. The author knows of no research undertaken to investigate either of the above flows.

## 1.4 MEDICAL APPLICATIONS

Many people as a result of some disease or simply as an aid to recovery have benefited from the applications of research into flow in collapsible tubes. Several methods of diagnosis and numerous therapeutic devices have evolved and these have improved both the lifestyles and recovery periods of patients. Some of the main medical applications are now considered.

### 1.4.1 Korotkoff Sounds

Among the many diagnostic parameters used in clinical medicine is the arterial blood pressure. This is the lateral pressure exerted by the blood on the artery wall. The most common non-invasive method employed to determine the blood pressure is the auscultatory technique which was proposed by Korotkoff (1905). A cuff is inflated around a limb (usually the upper arm containing the brachial artery) until the pressure exceeds systolic arterial pressure and the artery is occluded. The cuff pressure is then gradually reduced while sounds are listened for through a stethescope placed above the artery downstream of the cuff. As cuff pressure falls below systolic arterial pressure short tapping sounds (Korotkoff sounds) can be heard in time with the heart beat. With further reduction in cuff pressure the tapping sounds change into murmurs, then into clear thud sounds and finally disappear altogether when the pressure is close to diastolic pressure. In this way both the approximate systolic and diastolic pressures can be determined.

It is still not fully understood what basic mechanism is responsible for producing these sounds. Some hypotheses proposed to explain them will be discussed in the next chapter. It is highly desirable to fully understand the mechanism involved, not only because of the reliance of clinical medicine on the auscultatory technique, but also (if the sounds are not dependent on measuring technique) from the point of view of developing

other non-invasive methods of determining blood pressure. The study of collapsible tubes in the partially occluded state may provide some insight into this phenomenon.

1.4.2 Intermittent External Pneumatic Compression

Thrombosis is prone to occur in the leg veins of persons who are confined to bed. In the recumbent position the blood remains static in the deep veins in the leg unless milked towards the heart by the action of the calf muscle pump or motion of the musculature of the thigh. As a result clotting may occur with its attendant risk of pulmonary embolism (Collins, 1976; Roberts and Cotton, 1975 - see Kamm and Shapiro, 1979).

Compression of the veins will result in flow towards the heart even if the valves are incompetent or absent altogether, since the capillary bed presents a very high resistance to flow in the opposite direction. A physical approach to prophylaxis against deep vein thrombosis is intermittent external pneumatic compression. This is accomplished with a boot or cuff on the leg which intermittently compresses the leg. The study of unsteady flow in collapsible tubes subjected to external pressure provides some insight into such a device (Kamm and Shapiro, 1979; Kamm, 1982; Olsen et al, 1982).

1.4.3 Counterpulsation

This is a temporary means of assisting a damaged heart. The objectives of the device are twofold;

(i) to take the work load off the heart,

(ii) to increase aortic pressure during diastole, resulting in effective perfusion of the coronary

arteries.

Basically counterpulsation requires low impedance during systole, thus reducing the work load of the heart, and during diastole high aortic pressure to perfuse the various organs.

One such method of accomplishing the counter-pulsation is the intra-aortic balloon pump (Laird et al, 1968; McMahon et al,1971). This requires implantation but involves very little surgery. A narrow balloon is inserted in the descending aorta through an incision in the femoral artery. During systole the balloon is deflated so that the cardiac volume enters the aorta without having to pressurise it. Then during diastole the balloon is inflated thus forcing the blood along the arteries away from the heart and perfusing the coronaries. The term counterpulsation results from the fact that the balloon is operated $180^{o}$ out of phase with the left ventricle.

Another means of assisting the diseased heart is by external counterpulsation. This involves a boot being applied to the leg which when pressurised displaces the blood volume in the arteries of the leg. This method has the advantage of being non-invasive. Another important difference between the balloon and the boot is that the latter not only squeezes the arteries, but also the veins, thus affecting the pressure in the inferior vena cava and hence the right atrium of the heart, which may alter cardiac stroke volume.

Investigations into the filling of partially collapsed compliant tubes (Jan et al, 1983) and external

pressurisation of collapsible tubes conveying a flow (Kamm and Shapiro, 1979) are examples of research with application to these devices.

### 1.4.4 Artificial Larynx

Every year many people lose the ability to speak as the result of a laryngectomy (removal of the larynx due to some pathological condition). A large number of these patients cannot master the esophogeal speech techniques and again others are disillusioned by the speech that is produced by them with the aid of an external mechanical vibrator. Schoendorfer and Shapiro (1977) have produced a prosthetic vocal source based on the use of a collapsible tube as a fluid mechanical oscillator; a system which they claim holds some promise for a more natural sounding speech. The mechanism arises from a distensible tube in the negative resistance regime, ie when the tube is operating in the oscillating mode. An attractive feature in such a device is the possibility of changing pitch (resulting in a more natural sound) by changing axial tension or external pressure of the tube.

Other areas of application of flow in collapsible tubes that have been proposed are: prosthetic heart devices, detection of stenoses using pressurised cuffs and flow limitation during withdrawal of blood from the body, as in the case of a kidney machine.

## 1.5 ENGINEERING APPLICATIONS

In the negative resistance region, collapsible tubes behave as oscillators and thus may have a potential as amplifiers, switches and logic devices (see Conrad,

1969).

When a collapsible tube is in the partially collapsed state it has potential as a flow controlling device (Rodbard, 1966). Such a device has been proposed by Vischer (1979) to keep reservoir discharges constant.

## 1.6 CONCLUSIONS

It has been shown in this chapter that the subject of flow in collapsible tubes has a wide application. In the next chapter a review of the literature involving theoretical and experimental studies of flow in collapsible tubes is presented. This will give some insight into the origin and mechanisms of the phenomena discussed in this chapter and indicates the current state of research in this field.

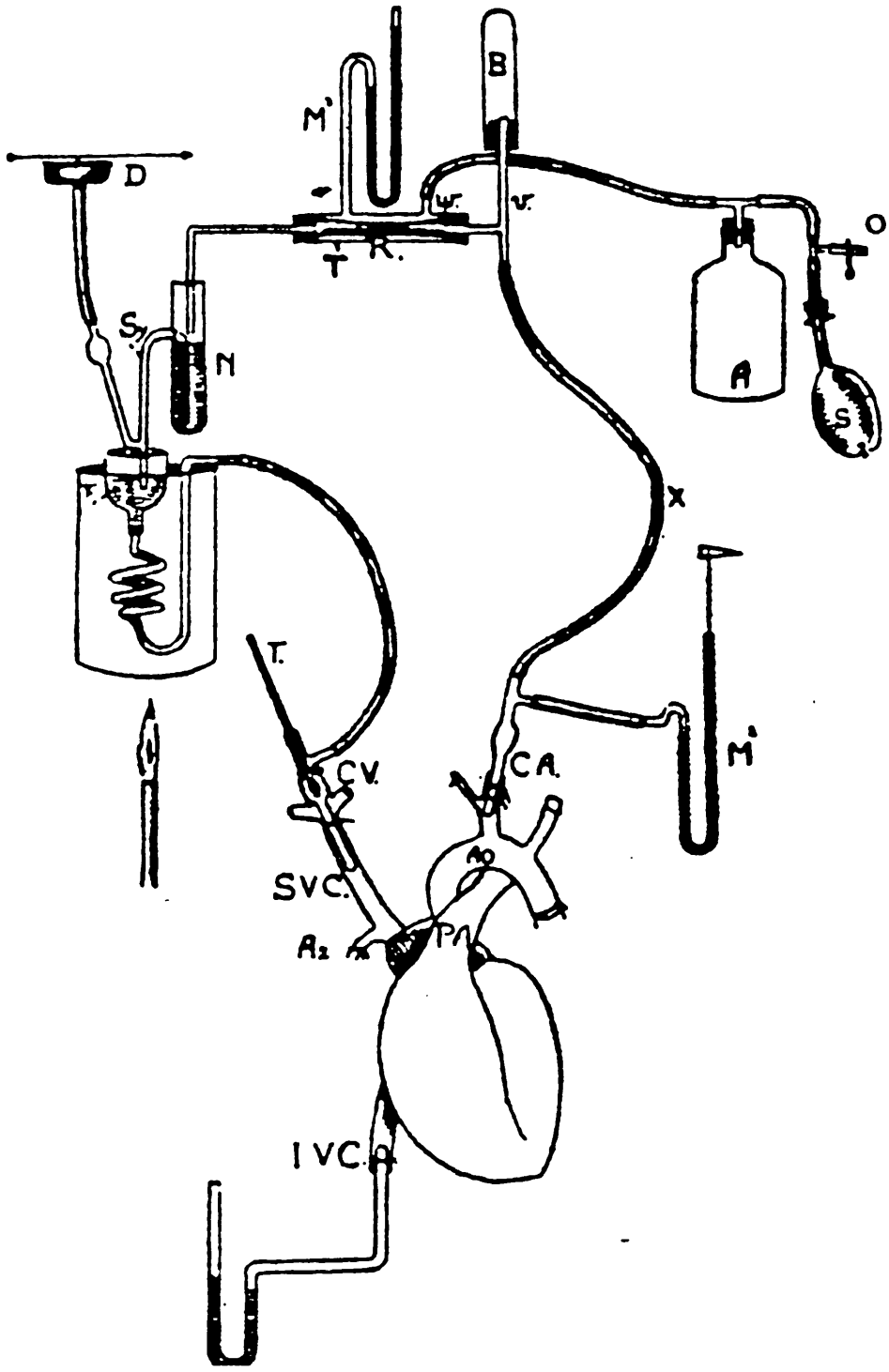



Fig 1.2.1 Apparatus used to investigate the influence of temperature and blood pressure variations on the performance of an isolated mammalian heart, showing the Starling resistor: R is the collapsible tube. (From Knowlton and Starling, 1912).

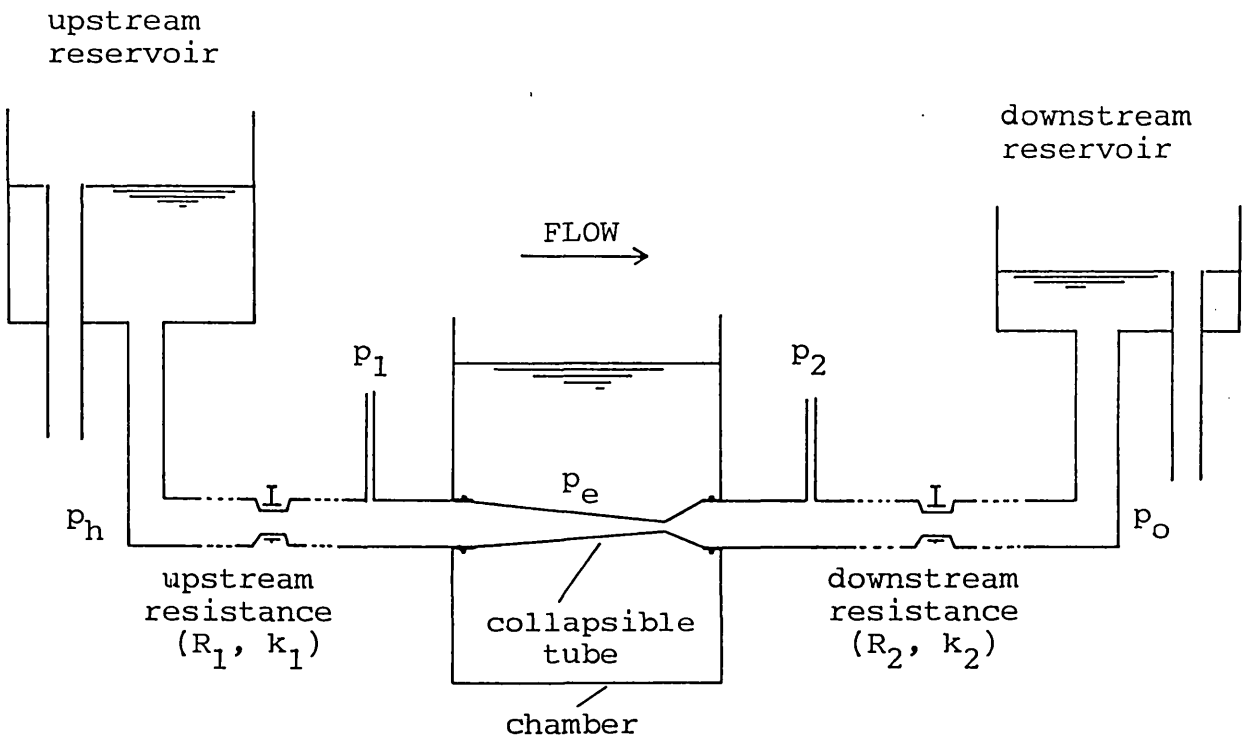



Fig 1.2.2 Typical experimental system used to investigate the flow through a collapsible tube.

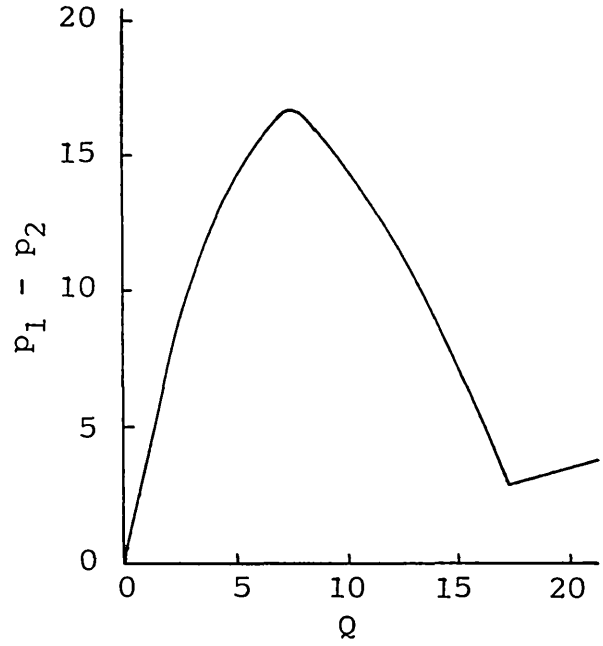



Fig 1.2.3 Typical P-Q characteristic obtained using an apparatus similar to that shown in Fig 1.2.2. The downstream resistance and the external pressure are held constant and the flow rate varied by adjustment of the upstream reservoir or constriction.

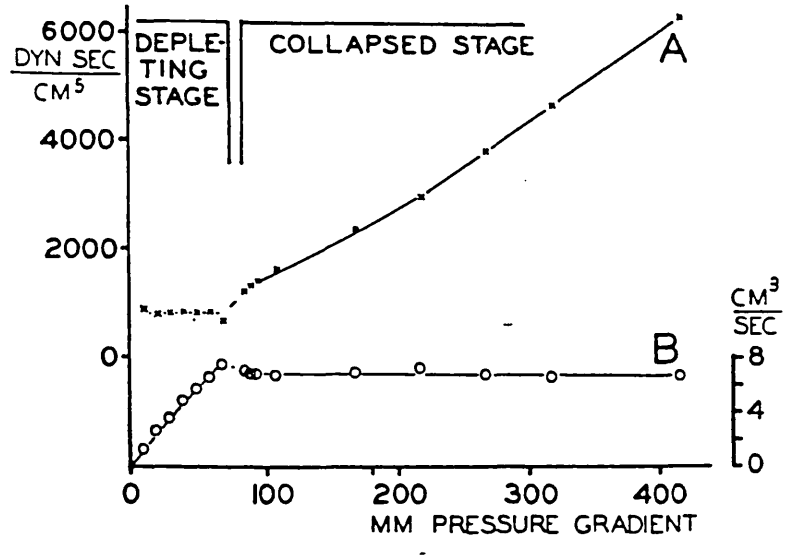



Fig 1.2.4 Experimental results from a physical model showing the relation of resistance (curve A) to flow rate (curve B) for a collapsible rubber tube, as the pressure downstream of the collapsible tube is reduced. Curve B shows the phenomenon of flow limitation. (From Brecher, 1952).

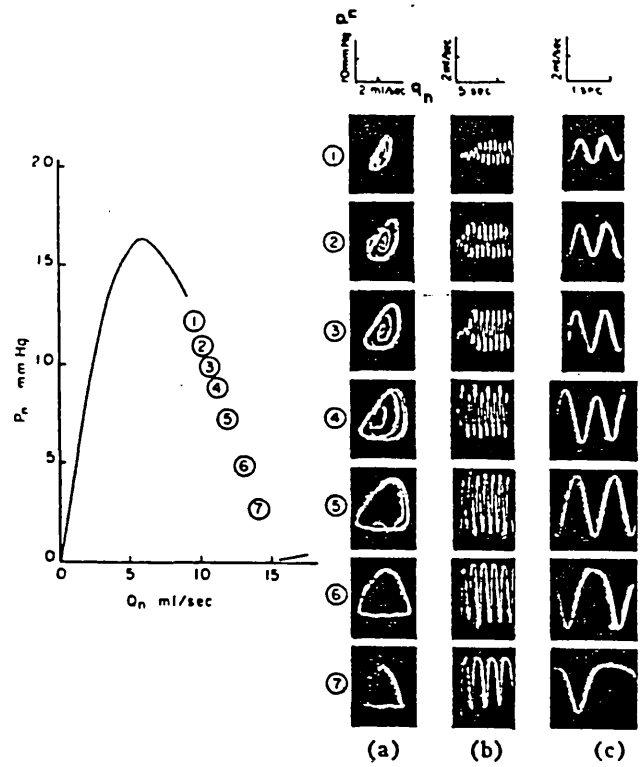



Fig 1.2.5 Relaxation oscillations in a collapsible tube as the static operating point moves through the region of negative slope. Note the build up of oscillation to a limit cycle. $p_n$ is the oscillatory pressure drop accross the tube and $q_n$ is the downstream oscillatory flow. $p_n$ and $q_n$ are perturbations about the static operating point ($P_n$, $Q_n$). (From Conrad, 1969).

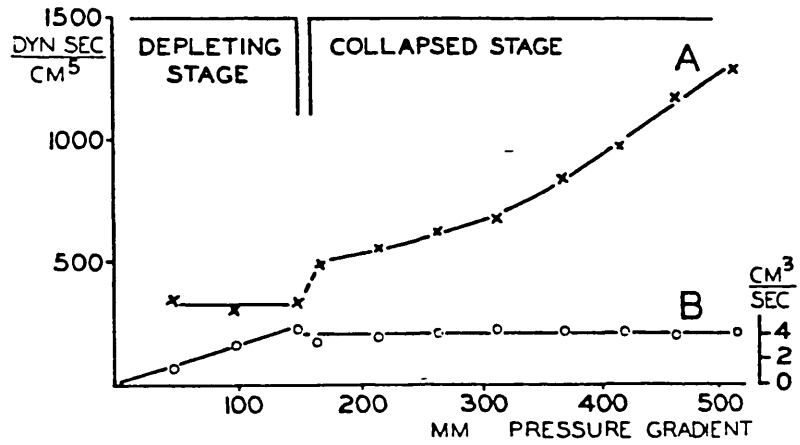



Fig 1.3.1 Experimental results from a dog showing the relation of resistance (curve A) to flow rate (curve B) for the superior vena cava, as the pressure downstream of this vessel is reduced. Curve B shows the phenomenon of flow limitation. (From Brecher, 1952).

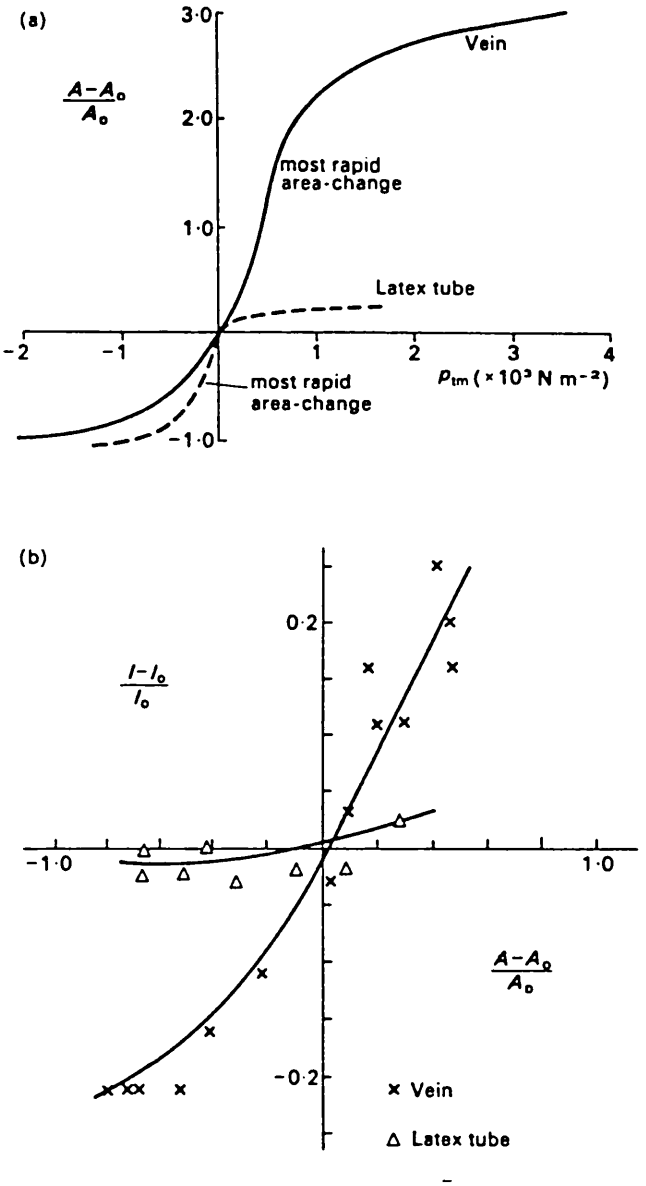



Fig 1.3.2 (a) Pressure-area relationships for a segment of vein and a thin-walled latex tube.
(b) Fractional change in perimeter plotted against fractional change in area for the vein and the latex tube.
$l_o$ and $A_o$ are the values of perimeter and area respectively at zero transmural pressure. (From Caro et al, 1978).

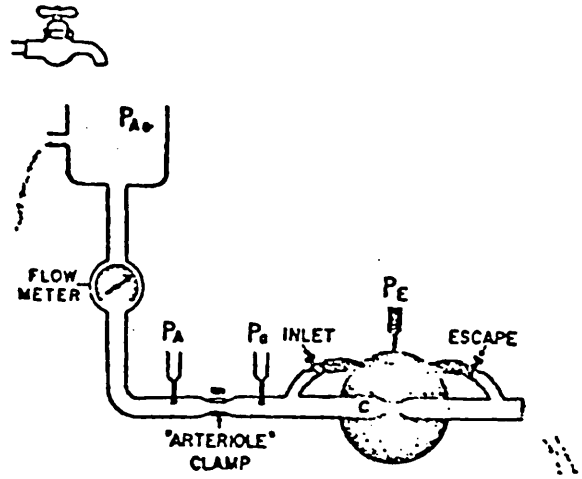



Fig 1.3.3 'Capilleron' model used for studying flow through a collapsible tube. C is the collapsible tube, $P_E$ is the chamber pressure and $P_a$ is the pressure upstream of the collapsible tube. (From Rodbard, 1963).

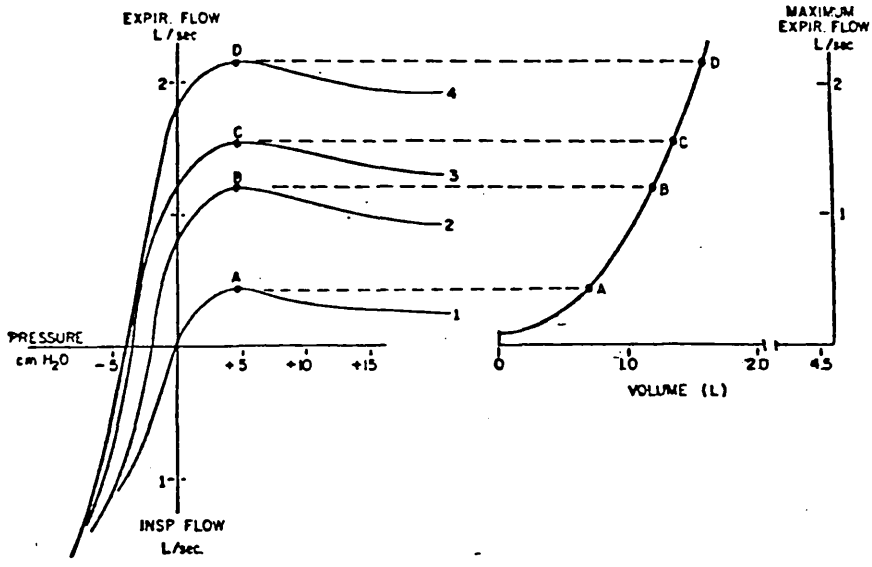



Fig 1.3.4 On the left is a family of isovolume pressure-flow curves obtained from a normal male subject. On the right is a plot of the flow and volume coordinates of the pressure flow curve maxima. (From Fry, 1958).

# CHAPTER 2

# REVIEW OF PREVIOUS WORK

## 2.1 INTRODUCTION

Investigations of flow in collapsible tubes fall into three main areas, viz:

(i) Experimental work: undertaken at the outset primarily by physiologists who wished to gain an understanding of certain phenomena occurring in blood vessels and airways. These experimental results have been obtained mainly from hydraulic tests on the Starling resistor (see section 1.2). A full understanding of this model is fundamental to its application in explaining physiological phenomena and also to its use in medicine, for example, artificial larynx (see section 1.4.4).

(ii) Fluid mechanical theories: proposed to explain several phenomena which have been observed both in vivo, for example, flow limitation, and in vitro, for example, self-excited oscillations. Such theories simplify the detailed structural mechanics of the tube itself and the equation of state is usually replaced by a relationship between the tube cross-sectional area and the transmural pressure; the so-called tube law (see section 2.3.1)

(iii) Solid mechanical theories: these concentrate on the detailed analysis of the mechanics of the

tube, normally at the expense of the fluid mechanics. The flow within the tube is usually assumed inviscid and treated by potential flow theory.

In this chapter the contributions made by each of these methods to a fuller understanding of the flow in collapsible tubes is examined. In the first section some simple experiments on the Starling resistor are considered.

The next section is devoted to a brief discussion of the theoretical background and introduces the tube law. This is followed by a section on wave propagation in elastic tubes which is fundamental to the understanding of the unsteady flow phenomena.

The next sections review the research undertaken to explain the phenomena of flow limitation and self-excited oscillations in connection with the Starling resistor. Experimental and theoretical studies not concerned with the Starling resistor but which aim to explain these phenomena in 'isolation' are also considered.

Finally, a brief review of a related fluid mechanics phenomenon which is sometimes observed in experiments on elastic tubes, viz the elastic jump, is made, together with a discussion of some experiments and theories that have been proposed to explain the phenomenon of Korotkoff sounds (see section 1.4.1).

## 2.2 EXPERIMENTAL BACKGROUND

The majority of the experimental results obtained to date are reports of hydraulic tests on the Starling resistor. Many of the results reported in the literature are difficult to interpret since the experimentalists treat the Starling resistor as a 'black box' with three controlling pressures rather than two controlling pressure differences. Brower and Noordergraaf (1973) clarified the situation and showed that for steady flow the collapsible tube can be characterised by the volume flow rate, Q and two of the three definable pressure differences $p_1 - p_2$, $p_e - p_2$ and $p_e - p_1$; where $p_1$, $p_2$ and $p_e$ are the upstream, downstream and external pressures respectively. They used the functional relationship $p_1 - p_2 = F(Q, p_e - p_2)$. A typical family of P-Q characteristics at constant $p_e - p_2$ is shown in Fig 2.2.1.

The importance of the external circuitry was not realised by most of the experimentalists until recently and as a result measurement of, for example, rigid tube length was not recorded. Such parameters are known to be important from results obtained using mathematical models of particular Starling resistor experiments (see, for example, Pedley, 1980). Thus quantitative agreement between mathematical model results and available experimental data is not really possible.

Attention is now focussed on a paper by Conrad (1969) which reports the most comprehensive (though still incomplete) set of data obtained from a model study. The only significant difference between the apparatus used by Conrad and that of other investigators is the

incorporation of micrometer controlled constrictions just upstream and downstream of the collapsible tube. The usual procedure in obtaining a set of results is to keep all the parameters, except one, constant.

2.2.1 Effect of Varying Upstream Conditions

In this case the downstream reservoir pressure, downstream resistance, and the external pressure, $p_o$, $R_2$ and $p_e$, respectively are held constant. The flow rate through the system is then varied by adjustment of the upstream pressure head, $p_h$ or the upstream resistance, $R_1$. The results of such an experiment are usually presented as a plot of pressure drop versus flow rate. A typical P-Q characteristic is shown in Fig 2.2.2 together with side views of the collapsible tube at different operating points on the curve. To obtain this 'N' type P-Q characteristic, $p_e$ and $R_2$ must be kept constant (Conrad et al, 1978). The P-Q characteristic can be divided into three distinct sections which reflect the flow regimes and state of collapse of the tube.

Region I

As Q is increased, the downstream pressure increases. The shape of the curve ($p_2$ versus Q) depends upon the choice of downstream resistance. For a constant resistance $p_2 = R_2Q$ (no constriction) the pressure increases linearly. However, in many of the experiments the downstream rigid tube contains a localised constriction; $p_2$ then increases monotonically with Q. For such a constriction $p_2$ exceeds $p_e$ for some Q and hence the pressure throughout the collapsible tube can

exceed the external pressure. The cross-section of the tube is then almost circular throughout and the tube stiffness very large. The pressure drop $P_1 - P_2$ is proportional to Q with an almost constant resistance (Fig 2.2.2).

Region II

Reduction of Q below a certain critical value results in a reduction of $P_2$ to a value close to or below $P_e$ at which the tube begins to collapse. Further reduction in Q results in a rapid reduction in cross-sectional area due to the high distensibility of the partially collapsed tube. The smaller area presents a greater resistance to the incoming flow for two reasons. Firstly, because the reduction in area results in a greater viscous resistance; secondly due to energy dissipation in the separated jet which forms (at least for values of the Reynolds number greater than 100) where the flexible segment widens from the constriction to its attachment to the rigid tube. Thus as the flow rate is decreased a greater pressure drop is required to overcome the increasing resistance. Self-excited oscillations are frequently observed in this region (see section 1.2.2).

Region III

When the whole segment is collapsed ( $P_1 < P_e$ ) the tube usually has a rather 'rigid' dumbbell shape which is maintained at lower flow rates; the tube cannot have zero cross-sectional area. The resistance to flow in this region is many times higher than before collapse.

2.2.2 Effect of Varying Downstream Conditions

The conditions downstream can be changed by an adjustment of $R_2$ or $P_o$. The effect of both of these parameters is to modify $P_2$ independently of $P_1$. When $P_2$ exceeds $P_e$ by a sufficient amount the flow rate is proportional to the pressure drop. However, when $P_2$ falls below $P_e$, collapse begins at the downstream end and is localised since $P_1$ remains high. Further reduction in $P_2$ has no effect on the flow rate - flow limitation (see section 1.2.1). In this mode the collapsible tube can be used as a constant flow device (Rodbard, 1966).

2.2.3 Effect of Varying External Pressure

If $P_e < P_2$ the tube is open along its entire length and the flow rate is nearly independent of $P_e$ (tube behaves as if it were nearly rigid). As $P_e$ is increased above $P_2$ the flow rate through the tube is governed by the pressure difference $P_1 - P_e$; ie the flow rate is virtually independent of the downstream pressure. Permutt and Riley (1963) postulated that this effect is like that of a waterfall, in which reductions of downstream water level below a certain critical level do not influence the flow. They coined the term 'vascular waterfall' to describe this phenomenon.

2.3 THEORETICAL BACKGROUND

This section is primarily concerned with the fluid mechanical theories. Rubinow and Keller (1972), Oates (1975a), Shapiro (1977b), Wild et al (1977), Kamm and Shapiro (1979) and Pedley (1980), among others, have all made theoretical advances in this field.

Griffiths (1969a, 1971a, 1971c) made a great contribution in this field by identifying the ratio u/c (= S, speed index) as a controlling parameter of one-dimensional steady flows. For S = 1 the flow is defined as critical and hence for S less or greater than unity the flow is sub or super-critical respectively.

Fluid dynamic theories of unsteady flow are few and the work of Kamm and Shapiro (1979) and Bertram and Pedley (1982) are probably the most informative. Earlier work by Olsen and Shapiro (1967) and Nicholson et al (1967) developed the criterion for non-linear steepening and flattening of waves based on the tube law. Much earlier Weber (1866) (see Shapiro, 1977a) derived the equation for the wave speed in area compliant vessels containing a liquid.

The usual theoretical approach is to assume one-dimensional flow. In this case the equations of continuity and momentum transport are fairly easily determined and then in order to close the problem an equation of state must be found. This of course should be a differential equation expressing the structural mechanics of the tube. However, such an equation is very complex and the usual approach is to introduce a relationship between the transmural pressure and the cross-sectional area, viz the tube law. Such a relationship has been used in the majority of theoretical models.

Griffiths (1969a) investigated the mechanics of micturition in females. Measurements of urethral pressure profiles in females (see section 1.3.6) had suggested that

there was an elastic constriction present near the mid-point of the urethra. A simplified model of urethral flow (inviscid flow in an elastic tube) with a constriction at the midpoint, was formulated. It was found that the flow from the bladder to the constriction was subcritical, while beyond the constriction the flow was either supercritical or free-flow (under zero pressure gradient), depending on the bladder pressure. This flow distribution results in an asymmetrical urethral profile about the constriction - funnelling down from the bladder to the constriction and thereafter remaining narrow. The pressure drop in the urethra takes place in a short section near the constriction. These results were in good agreement with a typical micturating cystogram (an x-ray film demonstrating the urinary bladder taken during the act of passing urine).

Griffiths (1971a) extended his earlier work on female micturition. In a simple experiment on an elastic tube with two elastic constrictions (imposed) he showed that if the flow was critical at the upstream constriction then an elastic jump (cf hydraulic jump in channel flow) is formed between the two constrictions. Making the downstream constriction more severe moves the jump upstream and ultimately it reaches the upstream constriction and disappears. A typical male micturating cystogram and urethral pressure profile suggests that two such critical constrictions are present in the male urethra.

In a later paper, Griffiths (1971c) suggested that an elastic constriction (transcritical) is present in the experiments of Conrad (1969) (this cannot be determined from Conrad's results). This constriction lies near the midpoint of the tube. The collapse of the tube downstream of the constriction suggests that the flow is supercritical. Then, since the flow in the rigid tubes is necessarily subcritical, an elastic jump is formed where the tube widens to attach to the downstream rigid tube. This elastic jump lies between an elastic constriction and the downstream rigid tube constriction (valve). Comparison with Griffiths (1971a) suggests that increasing the downstream resistance will move the elastic jump upstream until it ultimately disappears at the elastic constriction; the flow everywhere subcritical.

If the above theory could be applied to the Starling resistor then decreasing the downstream resistance would move the elastic jump downstream, making the area gradient more severe. With regard to oscillations it suggests that they may involve the interaction of the downstream rigid tube and the elastic jump. It has been observed by Rodbard and Saiki (1953) that part of the collapsible tube is carried into the downstream rigid tube during oscillations. It can only be conjectured that the increase in longitudinal tension and bending is somehow sufficient to force the tube open.

Brower and Noordergraaf (1978) proposed a quasi-three-dimensional model of a rectangular cross-section channel to analyse flow in a collapsible tube.

P-Q characteristics at constant values of $P_e - P_2$ were in qualitative agreement with experiments, ie concave to the flow axis (see Brower and Scholten, 1975). The longitudinal tube profiles (computed) show a constriction which moves downstream with increasing flow rate. They also showed that prestress significantly affects the pressure-flow relationship, tending to keep the vessel open. Viscosity was found to be important only at the lower flow rates.

Shapiro (1977b) demonstrated the analogy between the equations governing one-dimensional flow in a horizontal collapsible tube and those for corresponding flows in compressible gas dynamics and open channels with free surfaces (see Table 2.3.1). By virtue of these analogies he indicated the following characteristics of collapsible tube flows:

(i) wave propagation, as the prime mechanism of unsteady flow

(ii) a 'speed index', $S \equiv u/c$, whose central role is comparable in significance to that of the Mach number and the Froude number

(iii) in steady flow, opposite effects in subcritical ($S < 1$) and supercritical ($S > 1$) flows, for example friction causes a pressure drop in subcritical flow but a pressure rise in supercritical flow

(iv) choking and flow limitation when S reaches unity, as at the throat of a Laval nozzle or at the overflow of a dam

(v) the possibility of continuous transitions from subcritical to supercritical flow, as in a Laval nozzle;

(vi) rapid transitions from supercritical to subcritical flow (and vice versa?), as in gas dynamic shock waves and hydraulic jumps.

In a steady one-dimensional analysis for the case of negative transmural pressure, Shapiro made an extensive study of the effects of friction, gravity, S, etc on the flow and observed some of the features listed above.

The two main phenomena that will be discussed here are flow limitation and self-excited oscillations. However, before reviewing theories of these phenomena, it is necessary to define the tube law and an expression for the wave speed in collapsible tubes.

2.3.1 Tube Law

This is a functional relationship between the transmural pressure, $p_{tm}$ (pressure inside tube - pressure outside tube) and the cross-sectional area, $A$. This relationship couples the structural mechanics with the fluid mechanics and closes the equations in one-dimensional flow. Fig 2.3.1 shows the steady local tube law for a thin-walled latex tube. For $p_{tm} > 0$ the tube is inflated and the pressure load is supported by circumferential tension. For $p_{tm} < 0$ the tube is partially collapsed and the pressure load is supported by the bending stiffness of the tube wall. For $\alpha = \frac{A}{A_o} \leqslant \frac{1}{4}$ line contact occurs and the tube cross-section takes the form of two parallel conduits the shapes of which remain

self similar as $p_{tm}$ becomes increasingly negative. Flaherty et al (1972) have shown that in this regime

$$P = -\alpha^{3/2} , \qquad (2.3.1)$$

where $P \equiv (p - p_e)/K_p$ and $\alpha \equiv A/A_o$. Here $K_p$ is proportional to the bending stiffness of the tube wall. For a linear elastic material $K_p$ is proportional to the modulus of elasticity and to the cube of the thickness to radius ratio. $A_o$ is the area of the tube at $P = 0$. Equation (2.3.1) has been verified experimentally by Kamm and Shapiro (1979).

The form of the tube law usually used is

$$P = 1 - \alpha^{-3/2} , \quad \alpha < 1 , \qquad (2.3.2)$$

which approaches equation (2.3.1) as $\alpha \to 0$ and which produces the correct value $\alpha = 1$ when $P = 0$. This tube law only holds under certain conditions and some assumptions have to be made about both the tube and flow if it is to be incorporated in any theoretical model. This will be discussed in detail in the next chapter.

Kresch (1979) in a theoretical analysis demonstrated an abrupt change in the compliance $(dA/dp_{tm})$ of a flexible tube at point contact (Fig 2.3.2). The peak in compliance occurs when the transmural pressure is slightly negative. Conrad (1969) determined the compliance $(dV/dp_{tm})$ by graphically differentiating the pressure-volume characteristic which was determined experimentally (Fig 2.3.3).

It is difficult to measure the cross-section of a collapsible tube as many workers in this field have discovered. However, some recent work by

McClurken (1978) seems to have overcome this problem, at least in the steady case, by employing an electrical impedance technique, which is shape independent. Using this technique Shapiro (1977a) verified the similarity law of Flaherty et al (1972).

Cowley (1982) proposed that it may be better to determine the tube law directly for each experiment rather than to infer it from that for a uniformly pressurised tube, since the form of the tube law depends crucially on the tethering. For longitudinally tethered tubes he found that $P = P(A, \text{axial prestrain})$ while for untethered tubes $P = P(A, \text{time})$.

The form of the tube law may influence the phenomenon of elastic jumps. Such jumps are thought to provide an explanation of the so called 'pistol-shot' sounds heard in patients with incompetent heart valves (Anliker et al, 1971 - see Holenstein et al, 1984).

Oates (1975a) considered one-dimensional, viscous flow in soft-walled tubes. From the steady state equations for a horizontal tube with constant wall properties and reference area, he observed the following: in subcritical flow, the pressure forces are larger than the viscous forces and in the opposite direction. However, for supercritical flow the pressure and viscous forces combine to lead to possibly unstable deceleration. He proposes that the mechanical stability of the tube wall induced by supercritical flow is a greater contributing factor to the onset of an elastic jump than the rapid deceleration as argued by Griffiths (1971c).

The importance of the speed index with regard to mechanical stability and the formation of an elastic jump was emphasised. The analysis was quasi-steady and sidewall friction in the elastic jump was neglected.

In a later paper Oates (1982) incorporated Shapiro's tube law (see section 2.3.1) and obtained algebraic solutions supporting the analogy between a shock like transition in soft-walled tubes and shock waves in compressible flow. Calculations suggest that the effects of the magnitude of sidewall friction is important. Cowley did not take account of the viscous force on the wall in his analysis.

Kamm and Shapiro (1979) made an extensive study of unsteady flow in collapsible tubes subjected to body forces or external pressure. In the first section they considered small amplitude, linearised, inviscid flows. Using the method of characteristics they paralleled investigations in gas dynamics and considered wave propagation, super/subcritical flows, choking, etc. They then considered large amplitude motion with the associated strong non-linearities, and investigated the steepening of waves, development of shocks, flow limitation etc. They showed the importance of the tube law to these processes. Finally, experimental results were presented and compared with a one-dimensional mathematical model which was solved numerically. The experiment was similar to the usual hydraulic test on a Starling resistor, with one exception. The chamber enclosing the collapsible tube was constructed such that an external pressure was transmitted to the upstream half of the tube through a thin, highly

flexible compression sleeve, while the downstream part of the chamber was vented to the atmosphere. The inflow to the collapsible tube was constant in all their tests. They found that when the external pressure (upstream half) was increased the tube collapsed first at the downstream end of the pressurised region and the wave of collapse then propagated upstream. A flow limiting throat formed near the downstream end of the pressurised region where the flow velocity equalled the wave speed. Viscous effects became dominant as the length of the region of collapse increased. They considered the collapse process to consist of the following three phases,

(i) initial transient

(ii) quasi-steady emptying

(iii) viscous drainage.

The initial motivation for the above work was to improve upon the technique of external compression as prophylaxis against deep vein thrombosis (see section 1.4.2). The main aim of this method is to empty the veins in the leg as rapidly and a fully as possible. Their findings suggest that rapid compression rates are the most effective in achieving this.

Kamm (1982) and Olsen et al (1982) also presented numerical and experimental studies, respectively, of this technique of periodic external compression. Experiments were carried out on a simulated leg. This consisted of a thin-walled latex tube ('vein') surrounded by foam rubber ('tissue'). Three modes of compression were considered, viz uniform (cf Kamm and Shapiro, 1979), graded (decreasing from ankle to knee) and wavelike (from ankle to knee).

The conclusions of the numerical study were that wavelike compression appears to have some advantages over either of the other two modes. The greatest benefits occur when the pressure is applied rapidly, or in the case of a wavelike compression, the pressurisation wave moves most rapidly. The conclusions from the experimental results generally supported the theoretical findings.

Kececioglu et al (1981) investigated supercritical flow in a collapsible tube under negative transmural pressure, experimentally. Particular attention was payed to longitudinal tension effects. It was found that even a small amount of longitudinal tension or bending established standing waves ahead of a source of disturbance. Shock transitions were observed and values for the pressure recovery coefficient across the shock were measured. This pressure was found to lie between the loss-free pressure recovery and that given by the Borda-Carnot sudden expansion theory (Prandtl - Tietjens, 1934).
In an associated paper, McClurken et al (1981) present a theoretical analysis of the experimental observations in which the flow is assumed one-dimensional. The mechanics of the tube are represented by a modified tube law which includes the effects of longitudinal tension and bending. The experiments in part one confirm the one-dimensional theory for the mean gradients: in the absence of gravity, friction causes a pressure rise and a positive mean gradient of area; a downward slope can cancel gravity and lead asymptotically to a uniform state having zero gradients of pressure and area. An inviscid dispersion relation was developed which showed that the phase velocity

increases as the wavelength decreases. The group velocity therefore exceeds the phase velocity and consequently energy can propagate upstream and standing waves of area may appear.

The tube law plays a crucial role in the problem through its effect on the wave speed. The definition of wave speed is given in the next section.

## 2.4 WAVE PROPAGATION

The study of wave propagation in liquid filled elastic tubes has interested workers in fluid mechanics for over a century. Among some of the most well known contributers to the subject are Euler, Young and Love.

In connection with physiological flows much of the research was motivated by the problem of the propagation of the arterial pulse wave. The Moens-Korteweg expression for the wave speed, viz $c^2 = Eh/2r\rho$ , where $h$ = wall thickness; $E$ = Young's modulus; $r$ = tube radius; $\rho$ = fluid density, is based on a cylindrical thin-walled elastic tube whose compliance is the result of a uniform stress distribution everywhere in the tube wall. It does not allow for shape changes and is therefore only applicable to distended elastic tubes.

An equation for the wave speed which applies to both the inflated and partially collapsed elastic tube was obtained theoretically by Weber (1866) (see Shapiro, 1977a) and is given by the equation

$$c^2 = (\rho D)^{-1} = \frac{A}{\rho}\frac{dp}{dA} = \frac{A}{\rho}\frac{dp_{tm}}{dA} \quad , \qquad (2.4.1)$$

where $D$ is the distensibility of the tube.

This equation can be obtained from a simple linear theory in which viscous effects are neglected. The linearisation is based on considering the propagation along a single elastic tube with uniform undisturbed area and in which the wave amplitudes imposed are small enough for D to be taken as a constant and the convective acceleration to be neglected (for details see Lighthill, 1978). Equation (2.4.1) enables the calculation of the wave speed provided that the transmural pressure, $p_{tm}$, is known as a function of the cross-sectional area of the tube. This equation of state is usually the so-called tube law described earlier. It is evident that the wave speed depends directly on the form of the tube law used.

Some of the research on wave propagation in collapsible tubes which highlights the importance of the tube law is now examined.

Nicholson et al (1967) considered the behaviour of one-dimensional waves in liquid-filled elastic tubes. A theory was developed for inviscid flow which incorporated a tube law.

The non-linear equations were solved numerically using the method of characteristics. They showed how the form of the tube law affects the steepening tendencies of simple (non-reflecting) waves. In compressible gas dynamics simple compression waves will steepen and simple expansion waves will flatten provided that (Shapiro, 1954)

$$\frac{dv_w}{dp} = \frac{dv}{dp} + \frac{dc}{dp} > 0 \quad ,$$

where V and p are the fluid velocity and pressure, respectively and c the wave speed (which depends on the tube law in this analysis). A particular choice of tube law (that for a longitudinally constrained rubber tube with circular cross-section) resulted in non-distortion of large amplitude waves ( $dV_w/dp = 0$ ).

This had been demonstrated earlier by Olsen and Shapiro (1967) who concluded that 'every part of the wave moves with the same speed and that the wave neither steepens nor flattens. This extraordinary result depends on the particular pressure-area relationship for the tube'.

The same conclusions were reached by Beam (1968) who employed the Lagrangian form of the one-dimensional equations and obtained the solutions in closed-form.

Oates (1975b) obtained analytical solutions of the channel-flow equations. He investigated the interaction of two 'flat-topped' waves (effectively very long wavelength waves); one leftward running and one rightward running. Three different tube laws were used corresponding to soft rubber, elastically constrained and elastically unconstrained tubes. The first two of these laws, which are algebraically very different, surprisingly gave very similar results. The effects of changes in tube stiffness and cross-sectional area upon the transmitted and reflected waves were also examined. He found that for a soft rubber tube the wall stiffness had a pronounced effect on these waves. In the case of a stiff wall larger transmitted and reflected waves are produced from a given incident pressure pulse, while for

a softer walled tube a given compression pulse produces a reduced amplitude transmitted wave and the reflected wave changes sign.

Streeter et al (1963) investigated pulsatile flow in a distensible tube. The results agree favourably with experimental data obtained from the femoral artery. It was found that errors in the reverse flow results could be explained by investigation of the friction term. They assumed a laminar friction term based on Poiseuille flow which was found to be too small when compared with calculated flows, when flow reversal occurs. They put forward the hypothesis that the pressure gradient reverses during the cycle, thus effecting a separation of the boundary layer. This separation causes vortices at the wall, which spread through the flow giving rise to added energy losses. Flow in a converging tube tends to produce a thin boundary layer and smaller losses than for flow in a diverging tube (reverse flow in a converging tube). Thus losses are asymmetric - larger losses in reverse flow. Thus a different friction law is required when flow reverses.

Rodbard and Saiki (1953) also observed wave propagation in their experiments on a Starling resistor. They observed that during an oscillation a wave front was initiated when the tube opened at the downstream end. A wave propagated back and forth until the tube closed during the succeeding cycle and a new wave front was initiated.

Jan et al (1983) considered both experimentally and theoretically the equilibration process in a very long collapsible tube one end of which is partially collapsed

by means of an external pressure distribution. At time t = 0 the excess external pressure is released and the equilibration process begins. They investigated the effect of longitudinal tension, non-linearities and friction and showed that each affects the equilibration process. In this case wave propagation is essential for the equilibration process.

Bitbol et al (1982) employed a small segment of collapsible tube (mounted vertically, the upstream end attached to a rigid tube) in an experiment to model the closure of the mitral valve. Using a one-dimensional analysis it was found that the leading mechanism for the closure is the longitudinal flow deceleration. For large enough values of the Strouhal deceleration number‡, St, the closure process consists of an initial upstream collapse followed by a propagation of the collapse downstream. For small values of St the two phases merge into one with the tube closing uniformly.

## 2.5 FLOW LIMITATION

Under certain conditions in which the pressure surrounding an elastic tube (for example, in the tissue surrounding arteries, veins or the airways of the lung) is higher than the fluid pressure in the vessel, the flow is not increased by a decrease in the downstream pressure.

---

‡ The Strouhal number in this case is defined as $St = L/U_{max}\, T_D$, where L = length of collapsible segment; $U_{max}$ = maximum velocity of fluid through rigid tube; $T_D$ = time taken for fluid to decelerate from $U_{max}$ to zero.

This has also been observed in the Starling resistor experiments (see section 2.2.2) and a similar phenomenon occurs in a waterfall (see section 2.2.3). It is also analagous to 'choking' in gas dynamics.

Because of the analogy between the phenomenon observed in the Starling resistor and the physiological phenomenon, numerous authors have investigated flow limitation by a theoretical investigation of the Starling resistor.

The first mathematical approach to the phenomenon of flow limitation in expiratory flow was made by Fry (1958). A mathematical model of a simplified bronchial segment was proposed in which Poiseuille flow was assumed to hold and the radius of the vessel was represented as a function (independent of time) of the transmural stress. The model was further simplified by restricting the respiratory manoeuvre considered to the latter three-quarters of the total expiratory manoeuvre. It was proposed that the time derivatives of the stress acting on the inner wall and of the transmural stress would then be small except at the onset of-events. A pressure-flow equation was obtained and the resulting pressure-flow curves at constant volume exhibited a maximum flow rate (Fig 1.3.4).

A Starling resistor experiment was also undertaken using Penrose rubber tubing. The radius versus transmural stress relationship for the tube was determined experimentally. From the above pressure-flow equation an expression satisfying the maxima of the pressure-flow

curves ( $\partial Q/\partial p = 0$ ) was obtained. Simultaneous solution of this equation with the pressure-flow equation yielded an expression relating the maximum flow rate to the transmural stress and constants describing the physical properties of the segment. Qualitative agreement with the experimental results was obtained using this equation incorporating constants obtained from the radius versus stress curve.

Lambert and Wilson (1972) presented a mathematical model of the Starling resistor. The fluid mechanics was modelled by an inviscid flow and zero pressure recovery was assumed at the downstream end where the tube widened to attach to the rigid tube. The tube wall was treated as a thin beam. The model predicted that flow limitation should occur as the exit pressure is reduced.

Holt (1941) observed from experiments on dogs that the peripheral venous pressure remained constant when right atrium pressure was decreased greatly and that the veins collapsed. From experiments on the Starling resistor it was found that decreasing downstream pressure once the tube had begun to oscillate or collapse, either had no effect on the outflow or caused a slight decrease.

Rodbard(1955) tested, experimentally, the hypothesis that increasing the outlet resistance may paradoxically increase the flow. He found that when the tube was partially collapsed and oscillations (which he called flitter) were present, increasing the downstream resistance had either no effect on the flow or enhanced it.

In a theoretical analysis of pressure-flow relationships in arterioles Permutt and Riley (1963) used the pressure-flow relationship for a waterfall to characterise the flow between arterioles and capillaries in the presence of active tension. They coined the term vascular waterfall to describe the phenomenon which occurs in collapsible tubes in a region where $P_2 < P_e$ (see section 2.2.3). In this region reduction in $P_2$ has no effect on the flow rate. Under these conditions the flow rate depends upon $P_1 - P_e$ rather than $P_1 - P_2$ .

Dawson and Elliott (1977) presented a theoretical study of the mechanism which limits the expiratory flow. The flow was assumed quasi-steady and inviscid, and the local tube law used by Fry (1958), was incorporated. Assumptions regarding the tube law parameters were:

(i) the reference area decreases along the airway from a very large alveolar value to a minimum value‡ and then increases to the thoracic outlet

(ii) the elastic modulus is constant along the airway

(iii) the ratio of the maximum area to the reference area is constant along the airway corresponding to the value at the choke point.

They found that the shape of the maximum flow curves depends upon the tube law at the choke point. The magnitude of the critical flow rate depended upon the reference values of area and elastic modulus at the choke

---

‡ Several local minima of cross-sectional area occur naturally along the airways.

point, fluid density and the static recoil pressure. The critical rate of flow was found to be established when the fluid velocity reached the wave speed at the choke point. It was proposed that the effects of friction and longitudinal tension would be to decrease the critical flow rate.

In testing the critical flow condition for some experimental results the importance of evaluating the elastic modulus directly at this condition was emphasised. Evaluation of the elastic modulus without correction for longitudinal effects led to substantial discrepancies. They also proposed an explanation for negative effort dependence (reduction in forced expiratory flow rate with increasing effort) based on the effect of longitudinal tension on the distending pressure.

They proposed that the mechanism for maintaining the flow limitation is an elastic jump (see section 2.3.1) downstream of the choke point. Experiments to test the mechanism of flow limitation were made by the same authors (Elliott and Dawson, 1977). Dog tracheas and rubber membrane 'artificial tracheas' were used in a Starling resistor type apparatus; the 'tube' was mounted vertically and exposed to atmospheric pressure on the outside. The results supported the wave speed theory of flow limitation. Several observations and proposals by these authors are of interest. Firstly, the flow downstream of the choke point was found to become supercritical with reduction in downstream pressure, resulting in the narrowest area occurring downstream of the choke

point. When the dog tracheas were stretched axially, increasing longitudinal tension, their maximal flow rates were observed to increase. In this case when the downstream pressure was below that necessary to achieve flow limitation, the pressure just downstream affected the pressure at, and upstream of, the choke point (Fig 2.5.1). A similar effect of longitudinal tension, with regard to negative resistance, was observed and explained by Griffiths (1975a, 1975b, 1975c).

Negative effort dependence was not observed in the artificial tracheas (Fig 2.5.2). They proposed that this was due to a large lateral stretching of these tubes. The association of negative effort dependence with axial tension led them to the conclusion that the position of the in vivo choke point might influence this phenomenon. They proposed that if the choke point was in the trachea the situation would be similar to that of the excised dog trachea with reduction in flow after the peak. Whereas its occurrence intraparenchymally, where the parenchyma may give lateral support, would result in less negative effort dependence as in the artificial trachea.

Rubinow and Keller (1972) developed a theoretical model for steady, viscous flow in an elastic tube in which Poiseuille flow was assumed to hold locally and the tube radius determined as a function of the transmural pressure (cf tube law). The model results are in good agreement with steady flow results from experiments on rubber tubes, venous return and isolated cats' lungs. Flow limitation is evident in their results (Fig 2.5.3). The wave speed

did not appear in their analysis.

Wild et al (1977) extended the work of Rubinow and Keller (1972) in four ways:

(i) they considered tubes of elliptic cross-section

(ii) inertia effects were included

(iii) non-uniform external pressure

(iv) modelled a particular experiment with constant downstream resistance.

The analysis was based on lubrication theory and inertia was included as a perturbation to the basic lubrication theory solution. In applying this theory to collapsible tubes they incorporated a local tube law specified to fit an experimental curve corresponding to a vein. The external pressure distribution chosen was representative of a cuff inflated over part of the length of the segment. The results show a critical flow rate above which the area becomes very small just downstream of the peak external pressure and does not recover further downstream where the external pressure returns to zero. The results show sensitivity to inertia near the critical flow rate.

P-Q characteristics at different external pressures show the phenomenon of flow limitation. They also applied the model to the experiment of Conrad (1969) in which the downstream resistance is held fixed. The P-Q characteristics obtained show all the features of the experimental curves, for example, the flow rate is a multiple-valued function of the pressure drop (independent of inertia) (Fig 2.5.4).

Flow limitation in collapsible tubes subjected to body forces or external pressure was also investigated in section two of an extensive study of unsteady flow in collapsible tubes by Kamm and Shapiro (1979). Also, in an experiment on a Starling resistor they found that when the upstream half of the collapsible tube was subjected to a sudden increase in external pressure, a flow limiting throat formed near the downstream end of the pressurised region. Their results showed that the flow limiting throat has an important effect on the collapse process.

Grotberg and Davis (1980) considered incompressible, potential flow in a two-dimensional channel in which the walls have either a bending stiffness or are spring loaded. They identified a fluid speed (which they called the stasis velocity) above which all small amplitude fluid-elastic waves must travel downstream. This idea of flow limitation is similar to that of choking in gas dynamics.

## 2.6 SELF-EXCITED OSCILLATIONS

These oscillations are usually observed in experiments on the Starling resistor when the tube is in the partially collapsed regime (region II of Fig 2.2.2). They were first reported by Barry in 1824 (see Conrad, 1969). These oscillations in cross-sectional area and flow rate develop even when the upstream and downstream resistances and the external pressure are held fixed.

When $p_e$ and $R_2$ are held constant the well known 'N' type P-Q characteristic is produced with its region of negative slope. Conrad (1969) used the concept of negative resistance (see Mackay, 1958) in

an explanation of the oscillations in collapsible tubes. He proposed an electrical analog of his experiment on the Starling resistor in which the collapsible tube was represented by a flow controlled non-linear resistance. The equivalent circuit was described by van der Pol's equation. The analysis suggested that increasing the tube compliance should result in the oscillations being of relaxation type. Limit cycles obtained from Conrad's experimental results are shown in Fig 1.2.5. In approaching the valley of the P-Q characteristic the oscillations become more non-sinusoidal and the frequency and build up time decreases. Since the tube compliance is largest near the valley, this supports the above conclusion from Conrad's theory.

Conrad (1969) and Katz et al (1969) found that when the flow rate is varied by adjustment of upstream conditions (adjustment of $P_h$ or $R_1$), oscillations only occur for small values of the downstream resistance (Fig 2.6.1). It has also been shown (Katz et al, 1969) that when $R_2$ takes a value which does not result in oscillation an increase in $P_e$ and hence in collapse does not generate oscillations.

The frequency of the oscillations increases as the flow rate decreases, Fig 1.2.5. Conrad (1969) recorded frequencies in the range 0.6 to 1.7 Hz, while Ur and Gordon (1970) observed frequencies in the range 12 to 15 Hz. The latter authors also proposed self-excited oscillations as the mechanism for the generation of Korotkoff sounds (see section 2.7.3). Holt (1941) also

observed this well known phenomenon in experiments on the Starling resistor but he did not record the frequency of the oscillations.

Rodbard and Saiki (1953) observed oscillations in a collapsible tube which they called 'flitter'. The frequency was in the range 20 to 100 Hz. They recorded the sound produced during the oscillations on tape. The sound was heard as a constant low frequency note, however, when the playback speed was reduced to one-quarter of the original speed successive transient bursts could be heard. Vibration analysis revealed the sound to be composed of intermittent bursts of energy of the same frequency as the flitter. The frequency of the oscillations was found to increase with an increase in external pressure. This behaviour was also observed experimentally by Ohba et al (1984a) and is equivalent to Conrad's findings, viz that the frequency of the oscillations increases as the flow rate decreases. During the oscillations Rodbard et al also observed that part of the collapsible tube was carried into the rigid outlet tube.

Rodbard (1955) used a $3 \times 10^{-2}$ m length of relatively thick-walled latex tube of radius $3 \times 10^{-3}$ m in an experiment on a Starling resistor and observed oscillations of frequency 13 Hz. He also observed the paradox of a greater flow for a smaller pressure head. The effect of the downstream resistance on the oscillations was tested and it was found that increasing downstream resistance decreased the frequency of the oscillations or stopped them entirely. This is again equivalent to the

observations on the frequency of the oscillations made by Conrad, and Rodbard and Saiki.

Rodbard conducted numerous experiments in which several methods of varying the downstream resistance were used, for example, variable orifice, valve. At this time the Starling resistor was still considered to be a device with three controlling pressures rather than two controlling pressure differences (see section 2.2). In a later paper Rodbard (1966) devised a constant flow device which employed a collapsible tube in the negative resistance region. Relaxation oscillations were observed following changes in flow rate.

Some of the theoretical models proposed to simulate this phenomenon and its origin are now considered. Reyn (1974) presented a one-dimensional analysis for inviscid flow in an infinitely long tube and allowed for discontinuous solutions, viz an elastic jump. The hyperbolic equations were solved graphically using the method of characteristics. Starting from an unperturbed state, with the tube circular, a perturbation is applied and it is shown that the magnitude of the perturbation and whether collapse occurs, affects the resulting flow regime (sub/supercritical flow, elastic jump). Collapse of the tube tends to narrow the zone in which the perturbation has a significant effect on the wall deflection. In the first test the initial conditions were such that the velocity was given a linear perturbation over a finite distance; the flow was sub-critical and the cross-sectional area circular throughout.

The perturbation did not change the initial inflow and outflow. It was shown that an elastic jump could be formed by wave overtaking phenomena (see section 2.4).

He speculated that under the conditions of this test an oscillation would be described as consisting of waves bouncing up and down between the downstream end of the tube and an oscillating elastic jump.

In the second test the tube is again initially circular, however, the velocity perturbation takes place over a semi-infinite interval. The initial area is constant throughout and the flow subcritical. The perturbation gives an initial increase in the outflow. No elastic jump occurs in this case. The tube collapses near the middle of its length and the collapsed portion then moves downstream. This behaviour was in agreement with experiments undertaken in the laboratory at Delft (see Reyn, 1974) in which the outlet tube was short and of low resistance. In the experiments the tube reopened when the collapsed portion reached the downstream end of the tube. Reyn concluded that the frequency of these oscillations depends mainly on the travelling speed of the collapsed portion of the tube. Details of the solution procedure are given in Reyn (1975).

Holmberg and Wilson (1970) conducted an experiment in which an elastic tube extends from an orifice into a vessel where the pressure is higher than the external pressure. This is similar to the Starling resistor without the downstream rigid tube. The frequency of the oscillations was in the range 10 to 100 Hz for water and

approximately 2 kHz for air. A crude theoretical model (in which the oscillating part of the tube was represented by a block and spring) was proposed to simulate the phenomenon. Some qualitative agreement with the experiments was obtained but the model was not sophisticated enough to predict the frequency accurately.

In a series of papers Griffiths (1975a, 1975b, 1975c) investigated the mechanism for relaxation oscillations in an elastic tube resting on a solid surface which was inclined at some angle to the horizontal. The upstream end of the tube was attached to a rigid tube. Two elastic constrictions were imposed on the tube near the upstream and downstream ends. When both the constrictions were transcritical (ie the flow upstream of the constriction is subcritical and the flow downstream supercritical; the flow at the constriction critical) an elastic jump formed between the two constrictions. Strengthening the downstream constriction moved the elastic jump upstream, the pressure head remaining constant. When the upstream edge of the elastic jump reached the upstream constriction the pressure head fell suddenly before increasing again with further increase in pressure at the downstream constriction. The sudden fall in upstream pressure head is the result of the constriction becoming critical (flow upstream and downstream subcritical; flow critical at constriction). Griffiths (1975a) has shown experimentally that a critical constriction presents a lower resistance to flow than a transcritical one (according to a one-dimensional theory these resistances

should be identical). This difference in the resistance of the two constrictions results in a type of negative resistance in which $dp_1/dQ$ is negative ($p_1$ is the upstream pressure head). Relaxation oscillations were observed in the region of negative resistance which results from the interaction of the elastic jump and the upstream constriction. This negative resistance is different to that considered by Conrad (1969), viz negative value of $d(p_1-p_2)/dQ$ ; where $p_2$ is the downstream pressure. However, as pointed out by Griffiths, a very small negative resistance $dp_1/dQ$ is evident in Conrad's experiments (Fig 2.6.2).

In an attempt to explain the above experimental results a two-dimensional flow theory coupled with a one-dimensional elastic theory was used (Griffiths, 1975b). However, this analysis showed that the resistance of the critical configuration was greater in direct disagreement with the experimental results.

Finally (Griffiths, 1975c), a two-dimensional elastic theory was proposed coupled with the previous two-dimensional hydrodynamic theory. It was shown that if axial tension was included in the analysis or a careful treatment of the elastic behaviour of the material forming the constriction was made, then the theoretical results were in agreement with the experiments (Griffiths, 1975a). He explained that the deviation from the one-dimensional theory arose from non-local effects which are particularly important when the elastic properties vary rapidly along the tube, especially near an elastic

constriction. He proposes that the non-local deformations are associated with waves which travel much faster than pressure (Young) waves and so downstream conditions can have an effect on the elastic constriction even when the flow is supercritical.

Griffiths (1977) employed the theory developed in Griffiths (1971a, 1975a, 1975b, 1975c) to explain the oscillations observed in experiments similar to those conducted by Conrad (1969) and Holt (1969), ie experiments on the Starling resistor with either the tube horizontal or vertical; however no resistances were present in the semi-rigid inlet and outlet tubes. In the vertical configuration the instability takes the form of an oscillating elastic jump whose period depends upon the length of the outlet tube.

From the one-dimensional steady flow theory he concludes that oscillations occur when the mean fluid velocity is critical in the tube, the velocity downstream is necessarily subcritical (rigid tube) and the pressure at the constriction is greater than the downstream pressure. In this case he shows that a one-dimensional steady flow solution does not exist. The one-dimensional theory is sufficient to explain the motion of the elastic jump, apart from the rebound at the downstream end, which maintains the oscillations.

Brower and Scholten (1975) tested the hypothesis that oscillations in collapsible tubes are related to the fluid speed approaching the wave speed. Steady flow experiments suggested that there was a critical flow

characteristic only of the collapsible tube, which determines when oscillations are initiated. Experimental values of phase velocity and fluid velocity were plotted against transmural pressure. It was found that the fluid velocity could exceed the phase velocity for negative transmural pressures and flows greater than 10 ml $s^{-1}$. The theoretical expression for the wave speed, viz $c = [A \rho \, dA/dp]^{1/2}$ gave qualitatively the same behaviour as the experimentally determined wave speed.

Schoendorfer and Shapiro (1977) utilised the phenomena of self-excited oscillations as a basis for a prosthetic vocal source (see section 1.4.4). They developed a theoretical model of a Starling resistor type device to determine the conditions under which oscillations were produced and also to investigate the affect of several parameters on the frequency of the oscillations. Their stability condition showed that the smaller the frictional losses at the sudden expansion, the more likely the tube was to oscillate. This simple model contained several coefficients which were determined empirically. However, the sensitivity of the model to a change in a single coefficient (the others kept constant) was rather large.

Bonis and Ribreau (1977) investigated the phenomenon of self-excited oscillations empirically. Their apparatus was similar to the Starling resistor. The collapsible latex tube was supported along its length by a nylon thread and the connection between this tube and the chamber side walls was made through rubber

membranes; which they claim reduces end effects. This attachment obviously modifies the phenomenon of wave propagation in the tube and its associated stability. No oscillations were observed at subcritical flows. For supercritical flow they propose that small pressure fluctuations in the divergent (sudden expansion) part of the tube feed the unstable supercritical flow, which may lead to resonance. When the tube collapses the longitudinal tension at the constriction makes the tube stiffer and prevents further collapse. The wave speed increases due to the increased stiffness (calculated values are then not applicable) and it is not obvious whether the flow is supercritical after the instability has disappeared.

Conrad et al (1978) provide experimental evidence that conditions downstream of the elastic tube strongly influence the existence and frequency of the oscillations and as a result that a one-dimensional shock theory is inadequate to describe them. They also show that the oscillation condition given by Griffiths (1975a) is equivalent to that proposed by Conrad (1969) provided that the downstream resistance is linear. Ohba et al (1984a) have also emphasised the importance of the external circuitry in their experiments.

Further support for the influence of the downstream conditions was given in the mathematical model of Cancelli and Chiocchia (1979). Their model was similar to that of Katz et al (1969). However, in this lumped parameter model the cross-sectional area is a function

only of the time, while the pressure is a function of both time and the longitudinal coordinate. Griffiths (1977) had shown in his experiment that a critical constriction is fundamental to the origin of the oscillations. Cancelli et al modelled a Starling resistor (Holt, 1969) in which resistances were present upstream and downstream of the collapsible tube. They showed that for this type of experiment oscillations can occur when the flow is subcritical. They emphasised the importance of the external circuit (upstream and downstream rigid tubes) to the origin and frequency of the oscillations (Griffiths, 1977 did not incorporate rigid tube constrictions in his model). Two interesting points to note from this work are that pressure recovery was not included in the sudden expansion at the downstream end of the elastic tube and viscous dissipation in the elastic tube itself was not essential for oscillations to occur.

Bertram and Pedley (1982) proposed a lumped parameter model[I] of a Starling resistor experiment (Conrad, 1969) and examined the stability of the equilibrium states. The representation of the fluid mechanics in this model is an improvement on earlier models, for example, that of Katz et al (1969). Pressure recovery is included in the sudden expansion from the fixed (axial position) throat to the downstream rigid

---

I The derivation of the model is given in Pedley (1980).

tube. The resistances in the rigid tubes are linear. The tube mechanics is represented by a local tube law of the form described in section 2.3.1. Since this is a lumped parameter model wave propagation is not included.

Bertram and Pedley (1982) modelled two experimental situations;

(i) constant upstream pressure head

(ii) constant inflow.

From some general parameter variations they found that viscous dissipation in the collapsible tube was not as important as the inertia (cf Cancelli et al, 1979). The main conclusions of their paper were;

(i) that choking is not a prerequisite for self-excited oscillations in collapsible tubes - which agrees with the findings of Cancelli et al (1979) and

(ii) the most important fluid mechanical factors are pressure recovery at the throat and the properties of the external circuitry.

Cancelli et al (1979) could not test the importance of the pressure recovery since it was not included in their model, however, the importance of the external circuitry is well established.

At this stage it would be incorrect to conclude that pressure recovery is essential for oscillations since Cancelli et al (1979) produce oscillations in their model.

Bertram and Pedley (1982) represented the head loss in the diverging section of the tube by the quasi-steady Borda-Carnot expression. Because of the

importance of this head loss (as determined from the above theory) to the origin of the oscillations and the fact that the Strouhal number of the oscillations is somewhat greater than one (Bertram, 1982), they propose that some experimental work should be undertaken to determine the fully unsteady value. In a recent publication Bertram and Pedley (1983) have tried to gain some insight into this by experiments on a two-dimensional indented channel. (see also Stephanoff et al 1983).

Bertram (1982) observed two modes of oscillation in the Starling resistor. The first was a low frequency 'milking' oscillation in which local flattening occurred upstream which then moved downstream. The second was a local high frequency oscillation which occurred when the tube formed a neck at the downstream end. He called the latter a 'stationary' oscillation. It was found that these oscillations could occur simultaneously. The regions of instability were indicated on the steady P-Q characteristics where $p_e - p_2$ = constant.

A number of researchers have concentrated on the solid mechanics in attempting to explain the phenomenon of self-excited oscillations, which they refer to as 'flutter'. In this approach the fluid mechanics is modelled by a potential flow.

Paidoussis and Denise (1972) presented a theory based on Flügges equations for shell motion and a potential flow theory for the hydrodynamics. Their theoretical results gave qualitative agreement with their experiments on latex and silicone rubber tubes with regard

to oscillations. Oscillations are predicted for both cantilevered and clamp-clamped shells. No detailed information on the external circuitry was given. Of course their simplified flow theory may not benefit from such detail.

Weaver and Paidoussis (1977) presented two simple theories to determine the stability of thin-walled tubes conveying fluid. The tube is modelled as two parallel flattened plates. They show that two modes of flutter are possible; a flapping mode flutter arising from the divergence of the tube and shell mode flutter. They indicate that the flapping mode is the critical one for thin-walled tubes.

Matsuzaki and Fung (1977) obtained analytically an exact expression for the unsteady fluid pressure acting on the internal walls of simply-supported circular cylindrical tubes. From a linear stability analysis they produced a stability curve of flow rate versus length for a rubber tube conveying air. Their stability boundaries indicate that a shorter tube becomes unstable at lower flow rates than the longer tubes.

In a later paper Matsuzaki and Fung (1979) considered compressible, potential flow in a two-dimensional channel and concluded that a non-linear analysis of the fluid dynamics was necessary to understand the dynamic behaviour of the walls, for example, oscillations. They also suspected that unsteady flow separation would be important (cf Bertram and Pedley, 1982). They concluded from their theory that there are

no steady state oscillations if damping is present and no flutter is predicted at low Mach number.

## 2.7 KOROTKOFF SOUNDS

This phenomenon was described in section 1.4.1. Some of the hypotheses which have been proposed to explain the mechanism by which these sounds are generated are now examined.

In the last twenty years the four main hypotheses put forward to explain the Korotkoff sounds are: dynamic instability; shock wave; self-excited oscillations; excitation due to turbulent flow.

### 2.7.1 Dynamic Instability

Anliker and Raman (1966) proposed that the Korotkoff sounds at diastole (thud sounds) are due to a dynamic instability (oscillations with increasing amplitude) of the brachial artery, the instability being induced by the application of a pressure cuff. From direct visual observations and films of a translucent latex tube they drew the following conclusions:

(i) There is an established flow prior to the actual onset of the Korotkoff sounds, ie at cuff pressures slightly above systolic.

(ii) The simulated artery is not fully occluded during any phase of Korotkoff sound production.

(iii) At diastolic cuff pressures the simulated artery undergoes only small deformations and thus essentially retains its circular cylindrical shape during the entire cardiac cycle.

(iv) Flow visualisation with the aid of dye tracers

did not reveal any turbulent bursts or vortex shedding.

They presented a theoretical analysis of a fluid filled cylinder of infinite length which concentrated on the solid mechanics. The tube models proposed were a simple membrane and a shell, and the fluid mechanics was modelled as a potential flow. A linear stability analysis predicted stability of the brachial artery for cuff pressures less than 6 mm Hg ( 800 N $m^{-2}$) above diastolic. The frequencies and amplitudes of the sounds could not be determined from their analysis.

There does not appear to be any support for this hypothesis in the literature.

2.7.2 Shock Wave

Beam (1968) further developed his theory (see section 2.4) and derived the criteria for the transition of 'smooth' waves to sharp waves, which he called shock waves. He then used this analysis to support the hypothesis that the mechanism for Korotkoff sounds is the steepening of the pulse wave sufficiently to excite a response in the measuring system. The actual Korotkoff sounds being the response of the measuring system to this sharp wave. No oscillatory components of pressure were predicted from the analysis. Such oscillations, he proposes are characteristic of the measuring system used, for example, a stethescope.

In experiments on a rubber tube he found no turbulence when the sounds were heard, which agrees with the experimental findings of Anliker and Raman (1966). It was also found that sounds could be obtained when the

displacement of the tube contained no oscillatory components; supporting the hypothesis that the sounds are characteristic of the measuring system.

This shock wave hypothesis has been supported in a recent paper by Shimzu and Tanida (1983). They propose that the shock wave is the mechanism for generation of the thud sound when cuff pressure is in the vicinity of diastolic blood pressure. They conducted model experiments on a Starling resistor type device and also made a one-dimensional wave propagation analysis. From their experiments they concluded that '... the clear thud Korotkoff sound at diastole is generated by sudden expansion of a blood vessel due to the steep ascending limb of the transmission wave which is developed in the partially collapsed vessel segment under the cuff'.

Their theoretical analysis employed the method of characteristics in the solution of the equations. They showed that the steep ascending limb observed in the experiments is a wave front shock which builds up under the partially collapsed segment by an overtaking phenomenon (successive transmission waves travel at higher velocity and in overtaking, strengthen the shock), due to the non-linear tube law characteristics around zero transmural pressure. The first incident wave on reaching the collapsible tube produces a positive reflective wave and a positive transmission wave due to the sudden change in tube compliance. The cross-sectional area change in the transmission wave is relatively large and they call this a shock wave.

Subsequent transmission waves travel at higher velocity and so can overtake, strengthening the wave.

2.7.3 Self-Excited Oscillations

The third hypothesis is that Korotkoff sounds are generated by self-excited oscillations. These oscillations can be observed in certain experiments on the Starling resistor (see section 2.6). It was the similarity between the sounds produced by these oscillations and Korotkoff sounds which suggested to Ur and Gordon (1970) a common mechanism. Their model experiments on latex tubes and arteries produced similar results. Sound was observed when the transmural pressure was close to zero. Experiments on an isolated limb of a dog gave similar results. In both cases the frequency of the sound was 20 to 50 Hz. They also dismissed turbulence as the mechanism for Korotkoff sounds.

An earlier paper by Rodbard and Saiki (1953) also suggested that these oscillations (which they called flitter) were probably responsible for the generation of Korotkoff sounds. This evidence and that of Ur and Gordon, that relaxation oscillations are the mechanism for Korotkoff sound generation is primarily empirical.

Another approach, in support of the above hypothesis, has been made by Conrad et al (1980). It is known that relaxation oscillations are observed in experiments on the Starling resistor when the steady flow operating point is in the region of negative slope of the P-Q characteristic, ie when the dynamic resistance is negative. Conrad et al have shown that a compressed

artery under an occlusive blood pressure cuff also posesses a dynamic negative resistance P-Q characteristic. They then use this fact and the properties of systems with dynamic negative resistance to propose a description of Korotkoff sounds. They present a hypothetical brachial artery P-Q characteristic (Fig 2.7.1). P-Q characteristics corresponding to three differenct values of the cuff pressure are constructed (Fig 2.7.2). By drawing the load line (a plot of the equation of the external circuitry) corresponding to the systolic and diastolic driving pressures, they find the position of the static operating points corresponding to these pressures on the P-Q characteristic. These are the points at which the load lines cross the P-Q characteristics. They then establish the range of the excursion of the operating point on the P-Q characteristic between systolic and diastolic pressures for each P-Q characteristic (each corresponding to different values of cuff pressure). From this analysis and the results of previous authors, viz that the Korotkoff sound at diastole (thud sound) occurs when the cuff pressure is close to the proximal artery pressure, they propose that the operating point is somewhere on the positive slope of the P-Q characteristic between the systolic pressure and the diastolic pressure, and the artery opens briefly producing the sound.

Now when the cuff pressure is reduced the artery remains open for longer periods of the cardiac cycle. The operating point is then in the negative dynamic

resistance region and so transient flow perturbations will be amplified, giving rise to oscillations. From this analysis they conclude that the first Korotkoff sound or 'tap' is heard when the artery opens briefly, the operating point being near the peak of the P-Q characteristic. This could correspond to a shock wave.

The muffled sound, however, they show occurs when the operating point is in the region of negative dynamic resistance. In this region small disturbances can be amplified, giving rise to oscillations.

2.7.4 Turbulence

Gonzalez et al (1975) conducted an experimental and theoretical study to investigate the origin of Korotkoff sounds. The arterial sounds were recorded distal to a cuff with a microphone-amplifier set up containing various filters. The sounds were observed to have two components:

(i) a large amplitude, low frequency, thumping sound and

(ii) a much lower amplitude, high frequency murmur.

The first component was found to be related to the passing of the pulse wave under the cuff. The pressure wave steepens as it passes through the constricted artery resulting in a sudden expansion of the arterial walls downstream of the cuff. This is in agreement with the shock wave hypothesis. The second component, which was only heard immediately distal to the cuff, was found to result from turbulent jet formation. They showed that this murmur is dependent only on a critical jet velocity

which results from a Kelvin-Helmholtz instability. They conclude that this is why the first component can occur alone, while the second component is only found in connection with the first.

There seems to be strong evidence to support the hypothesis that the origin of the first Korotkoff sound (tap) involves the formation of a shock wave due to steepening of transmitted waves under the cuff. The origin of the second Korotkoff sound (thud), however, is far more difficult to assert. It may be due to a self-excited oscillation, as proposed by Conrad et al (1980), or may indeed result from turbulent jet formation (Gonzalez et al, 1975). The latter hypothesis seems very likely; however, turbulence has not been observed experimentally during simulated Korotkoff sounds (see for example section 2.7.1).

Further theoretical and experimental studies are needed in order to determine a fuller understanding of the mechanisms and origin of these sounds. It is hoped that investigation of unsteady flow in collapsible tubes will contribute to the discovery of their origin.

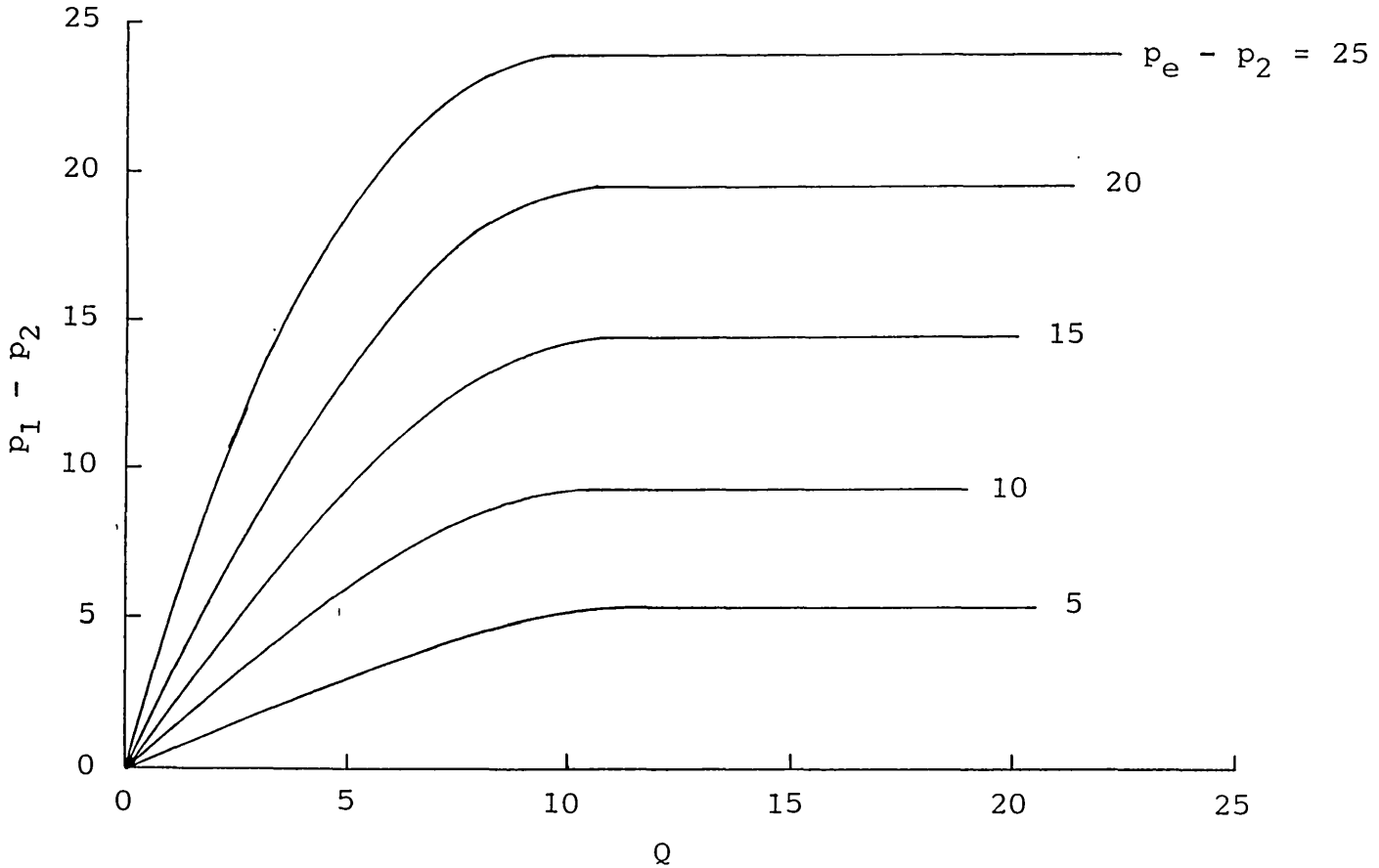



Fig 2.2.1 Typical family of P-Q characteristics. For each curve $p_e - p_2$ is a constant.

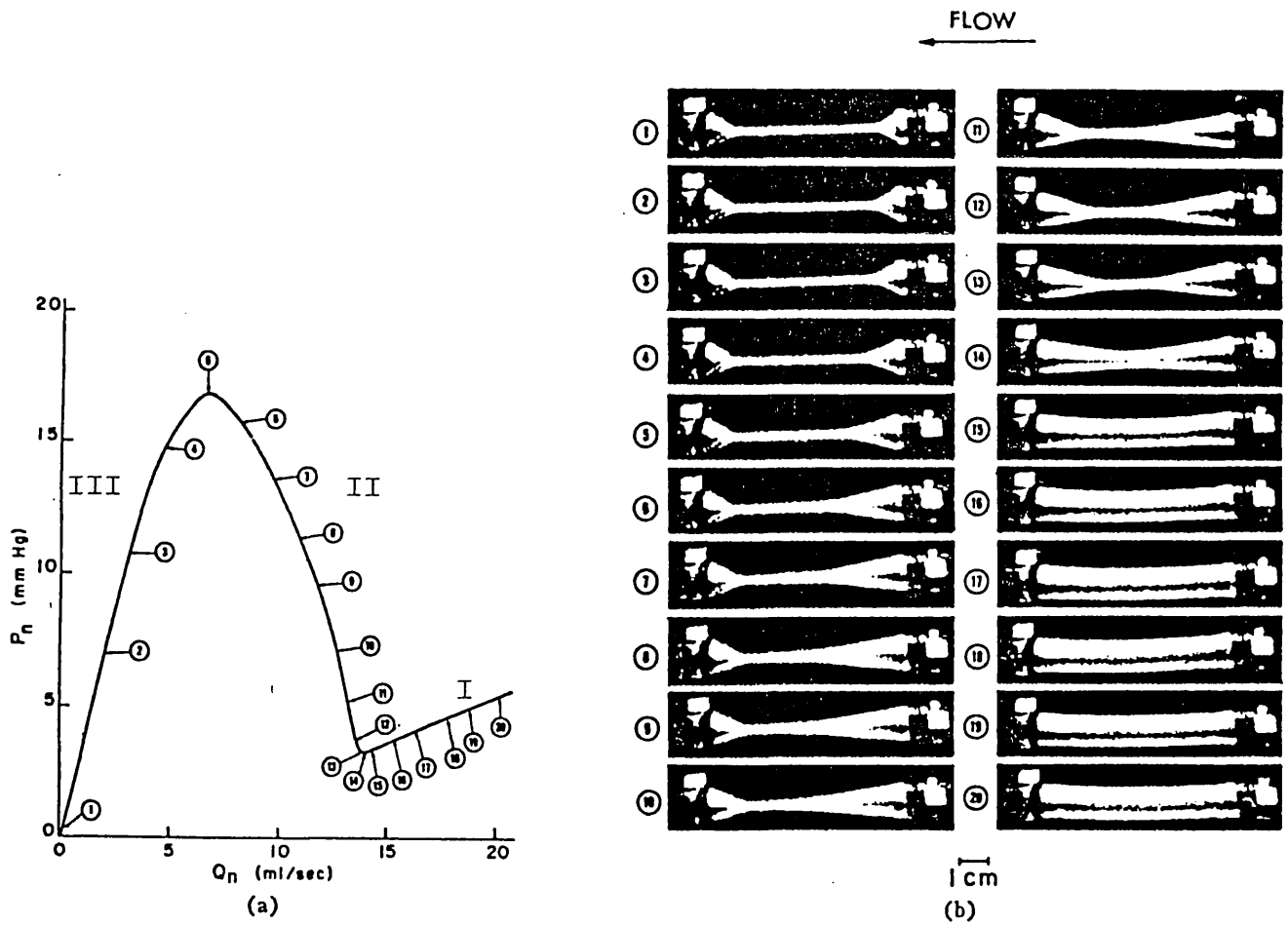



Fig 2.2.2 (a) Typical 'N' type P-Q characteristic for a collapsible tube at constant external pressure and downstream constriction.
(b) Side views of the collapsible tube at the indicated static operating points. (From Conrad, 1969).

Table 2.3.1 Analagous Physical Quantities

| | Flow in Collapsible Tube | Gas Dynamic Flow | Free-Surface Channel Flow |
|---|---|---|---|
| Speed | $u$ | $u$ | $u$ |
| Pressure | $p$ | $p$ | $p$ |
| Mass Storage Variable | $A$ | $\rho$ | $h$ |
| Eq'n. of State | $A = A(p-p_e)$ | $\rho = \rho(p)$ | $h = (p-p_{atm})/\rho g$ |
| Wave Speed | $c^2 = \frac{A}{\rho}\frac{dp}{dA} = \frac{A}{\rho}\frac{d(p-p_e)}{dA}$ | $c^2 = \frac{\rho}{\rho}\frac{dp}{d\rho} = \left(\frac{dp}{d\rho}\right)_{entropy}$ | $c^2 = \frac{h}{\rho}\frac{dp}{d\rho} = gh$ |
| Speed Index | $S \equiv u/c$ (Speed Index) | $M \equiv u/c$ (Mach No.) | $F \equiv u/c$ (Froude No.) |

(From Shapiro, 1977a).

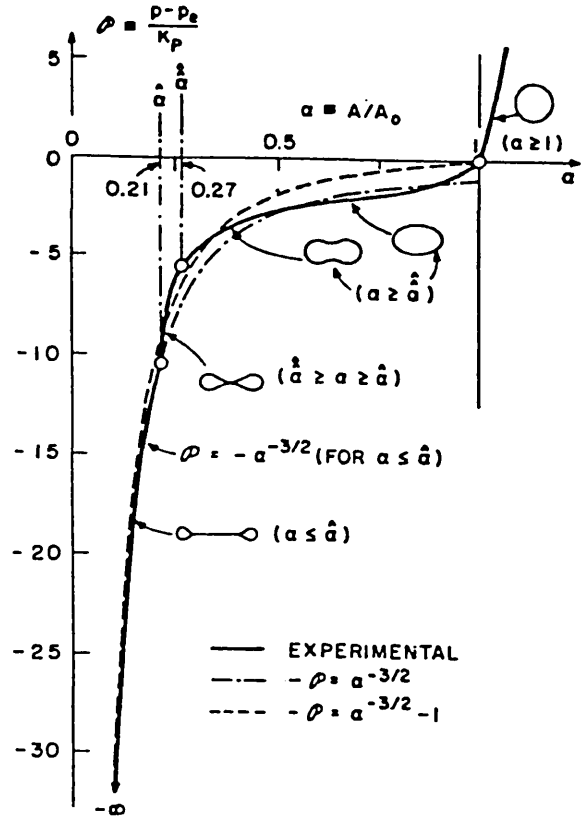



Fig 2.3.1 Steady local tube law for a thin-walled latex tube. (From Shapiro, 1977a).

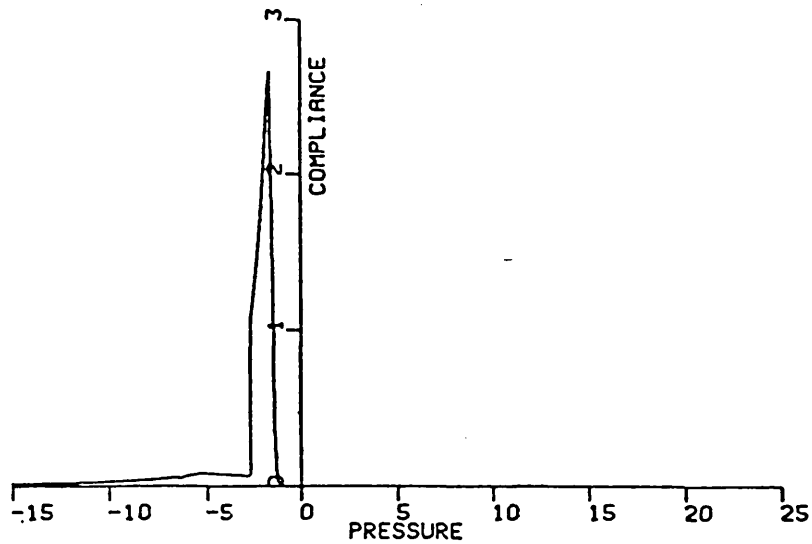



Fig 2.3.2 Theoretically determined change in compliance with transmural pressure for a flexible tube. (From Kresch, 1979).

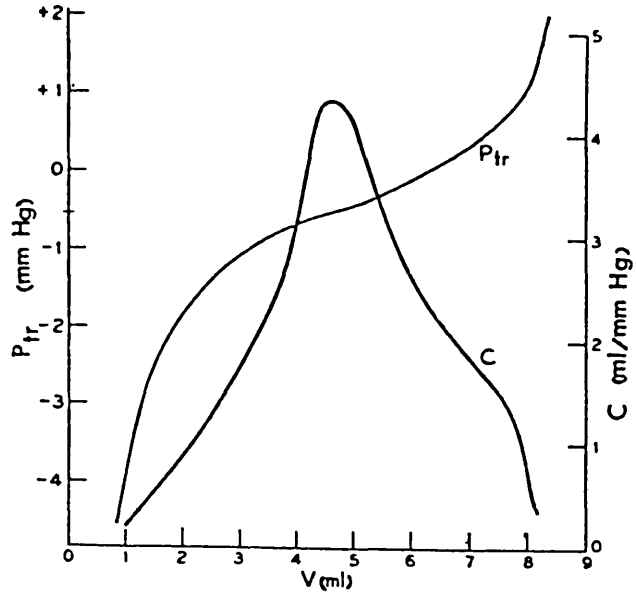



Fig 2.3.3 Experimentally determined compliance, C, of a thin-walled rubber tube. (From Conrad, 1969).

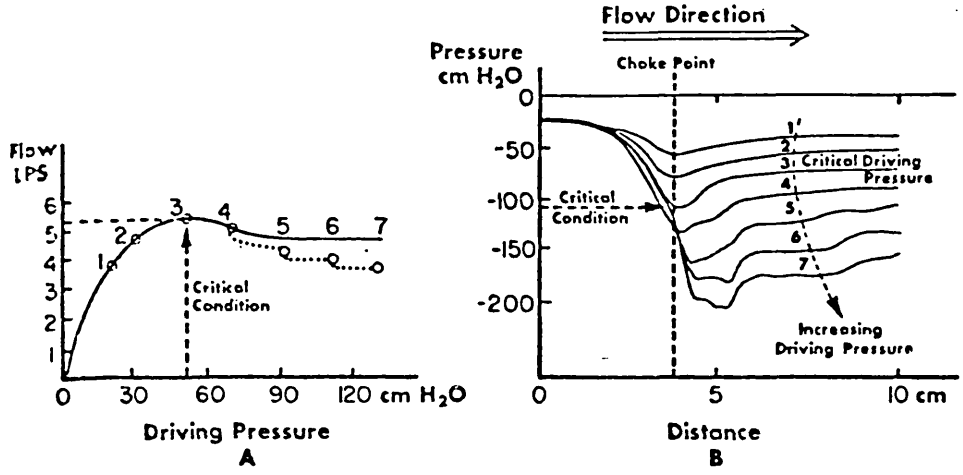



Fig 2.5.1 A:——, typical tracheal flow-driving pressure curve; ·····, same trachea with driving pressure held constant for brief intervals at indicated points.
B: corresponding pressure-distance curves at constant driving pressures. Choke point location is indicated.
(From Elliott and Dawson, 1977).

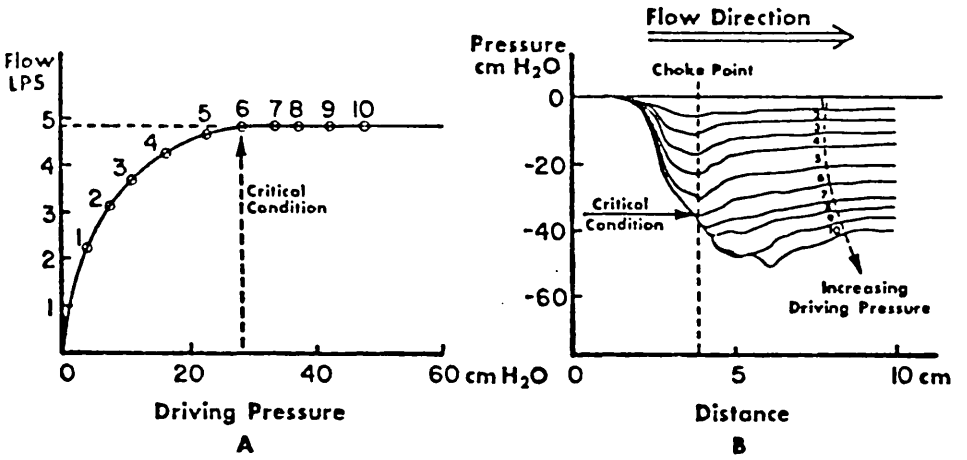



Fig 2.5.2 A: artificial trachea (rubber membrane) flow-driving pressure curve.
B: corresponding pressure-distance profile.
(From Elliott and Dawson, 1977).

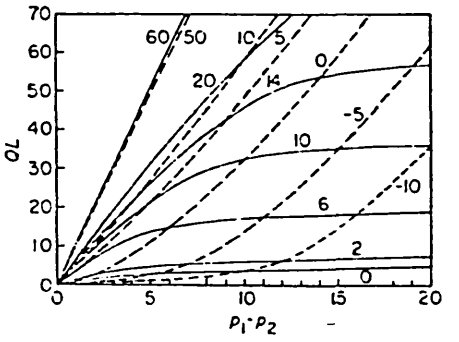



Fig 2.5.3 QL as a function of the difference between inlet pressure and outlet pressure, $p_1 - p_2$, for various values of $p_1 - p_e$ (solid lines) or $p_2 - p_e$ (dashed lines). (From Rubinow and Keller, 1972).

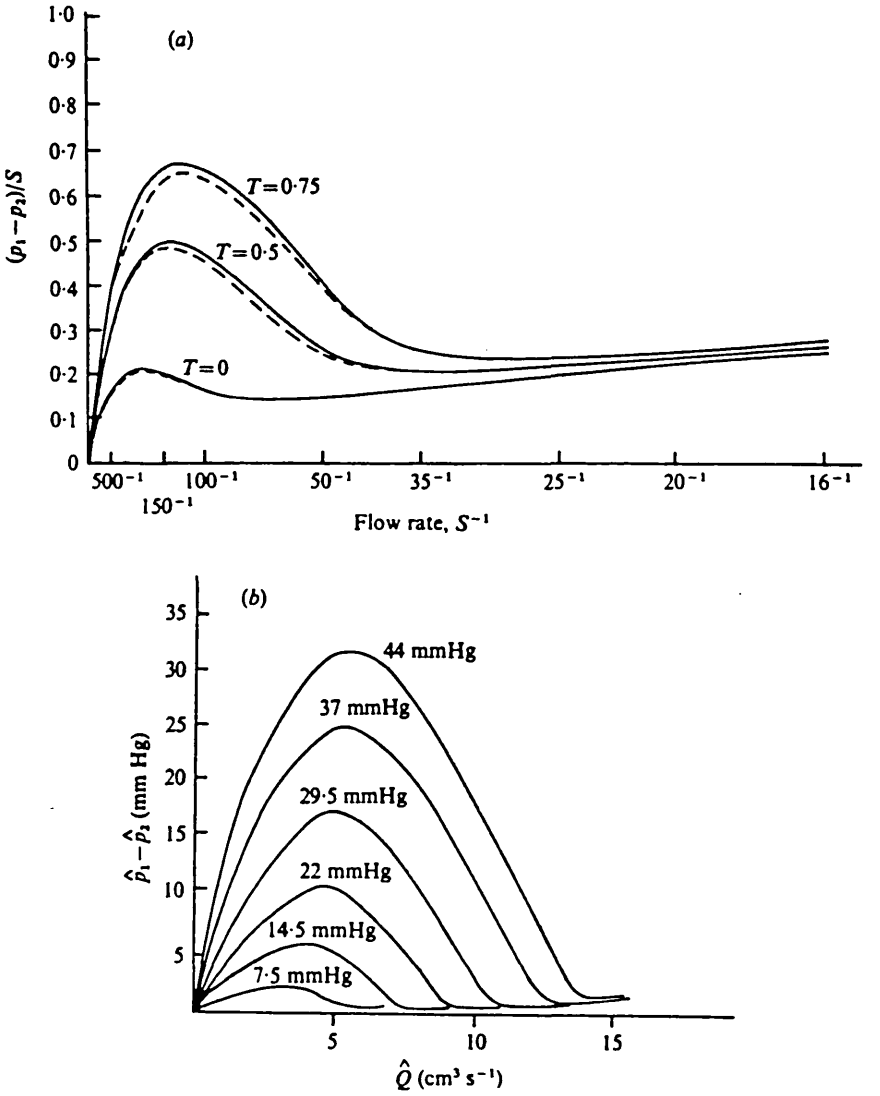
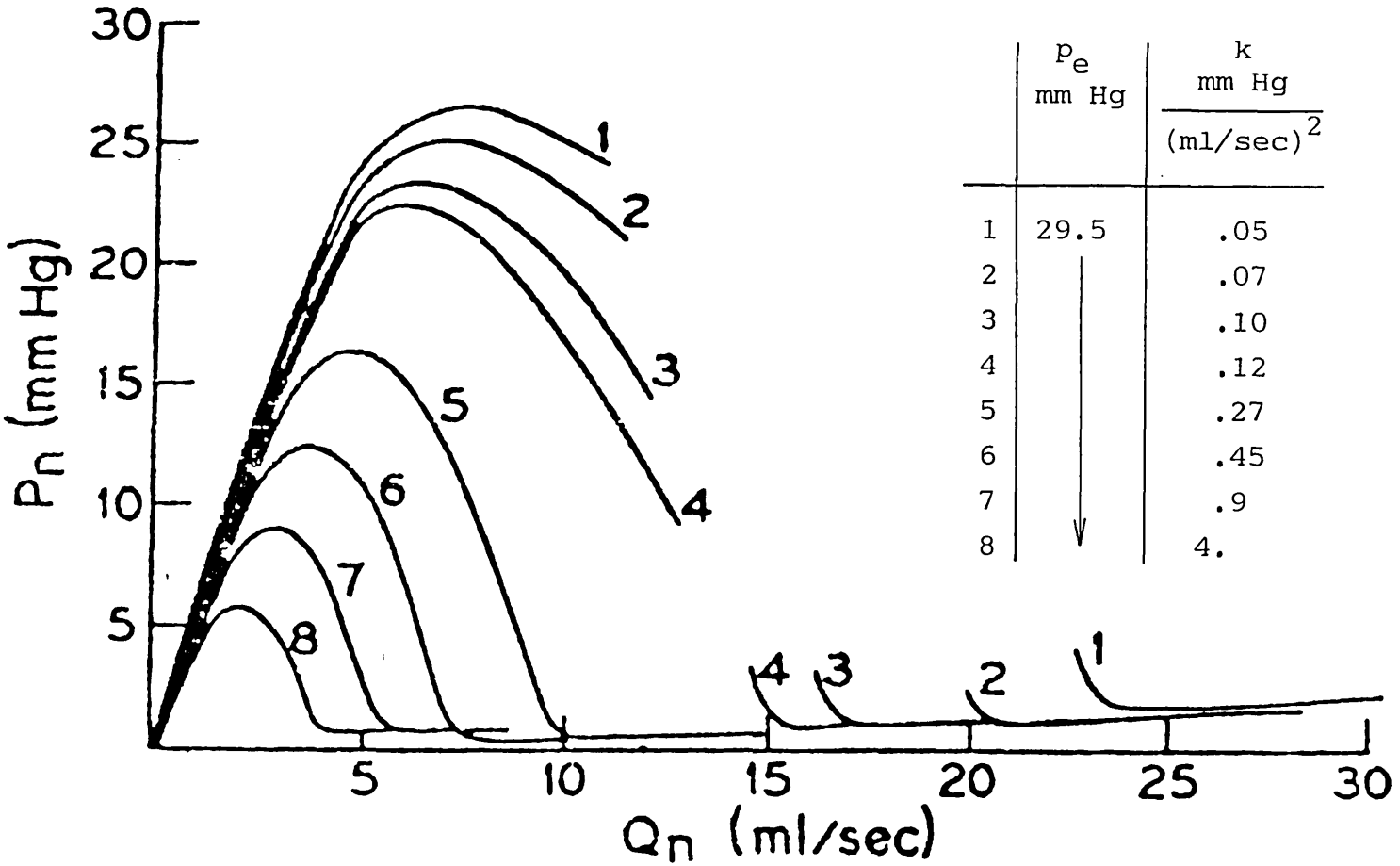



Fig 2.5.4 (a) Predicted P-Q characteristics for constant downstream resistance and various values of external pressure, T.

(b) Experimentally determined P-Q characteristics for constant downstream resistance and various values of external pressure. (Redrawn with curves smoothed from Conrad, 1969).
(From Wild et al, 1977).




| | $p_e$ mm Hg | k mm Hg / $(ml/sec)^2$ |
|---|---|---|
| 1 | 29.5 | .05 |
| 2 | | .07 |
| 3 | | .10 |
| 4 | | .12 |
| 5 | | .27 |
| 6 | | .45 |
| 7 | | .9 |
| 8 | | 4. |

Fig 2.6.1 P-Q characteristics for different settings of the downstream constriction. Breaks in curves represent regions of oscillations. Curve numbers refer to settings of downstream constriction, as indicated in the table. (From Conrad, 1969).

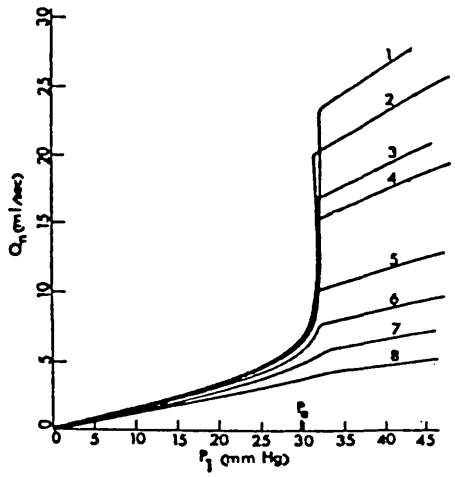



Fig 2.6.2 Upstream pressure as a function of flow rate for constant external pressure and different values of the downstream constriction. Curve numbers refer to settings of downstream constriction, as indicated in the table of Fig 2.6.1. (From Conrad, 1969).

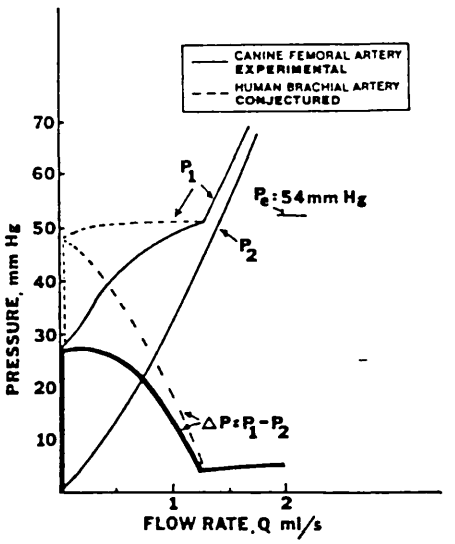



Fig 2.7.1 Typical P-Q characteristic and boundary pressures $P_1$ and $P_2$ for canine femoral artery with constant cuff pressure, $P_e$. Dotted lines represent a hypothetical human brachial artery characteristic and upstream boundary pressure. (From Conrad et al, 1980).

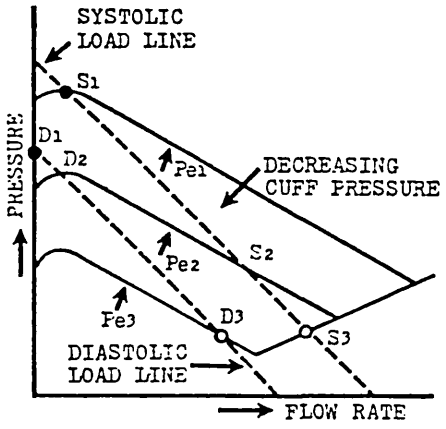



Fig 2.7.2 Hypothetical human brachial characteristics for three cuff pressures such that $P_{e1} > P_{e2} > P_{e3}$. The two dashed lines are steady flow or dc load lines which represent the system external to the compressed artery at the peak systolic and end-diastolic driving pressures. At the operating point $S_1$, the first Korotkoff sound or tap is heard, while at $D_3$, the sounds become muffled or cease. (From Conrad et al, 1980).

# CHAPTER 3

# MATHEMATICAL MODEL

## 3.1 INTRODUCTION

Until fairly recently the majority of theoretical studies of flow in highly compliant tubes were concentrated either on the solution of the steady flow problem or on that of unsteady flow at positive transmural pressure. The problem of unsteady flow in a collapsible tube, when the transmural pressure is negative, has received far less attention. Recent developments in this area have resulted from the work of Kamm and Shapiro (1979), Cancelli and Chiocchia (1979), Pedley (1980), Bertram and Pedley (1982), among others.

Flows of this type are very complex. The three-dimensional configuration of the tube, with its complicated variable cross-section, (see Fig 3.1.1) affects both the structural and fluid mechanics. Also, the mechanics of the flow and the structure are coupled and strong non-linearities are present. In an attempt to obtain some insight into this unsteady flow problem, a one-dimensional model is considered which includes many interesting phenomena, some of which correspond to those observed experimentally.

This chapter is totally devoted to the development of this model in which an incompressible, homogeneous, viscous fluid is flowing in a compliant, uniform, thin-walled tube whose ends are tethered to rigid tubes.

## 3.2 DESCRIPTION OF THE PHYSICAL MODEL

Numerous experiments have been undertaken on collapsible tubes both in the steady and unsteady flow regime (Conrad, 1969; Brower and Scholten, 1975; Kececioglu et al, 1981; Bertram, 1982, among others). The results of such experiments could be used to test a theoretical model. Therefore, a mathematical model is developed of what has now become a familiar experiment.

The majority of experimentalists have used an apparatus similar to that illustrated in Fig 1.2.2. It consists of a collapsible tube supported between two rigid tubes and enclosed in a pressurised chamber. The chamber contains air or water at an adjustable external pressure, $p_e$. The system is perfused with water from a constant head reservoir attached to the upstream rigid tube, and the downstream rigid tube is connected to a similar constant head device. Incorporated in the rigid tubes are variable constrictions. The flow through the collapsible tube can be modified by changing the height of the upstream or downstream reservoirs, by a change in the external pressure or by adjustment of one of the variable constrictions. Each of these changes can be made independently.

## 3.3 ASSUMPTIONS OF THE THEORETICAL MODEL

### 3.3.1 One-Dimensional Flow

It is assumed that the pressure, $p$, and velocity, $u$, can be represented by a mean pressure, $p(x,t)$ and a mean speed $u(x,t)$ at any cross-section of the tube; where $x$ is the longitudinal coordinate and $t$ the time.

It is shown later in this chapter that the problem

must be carefully formulated in order to employ a one-dimensional analysis. Further, the limitations of this derived model are discussed, for example it would not be valid for large amplitude local oscillations.

3.3.2 The Tube Law

It is assumed that all the properties of the tube can be represented by an unique relationship between the local transmural pressure and the local cross-sectional area: thus

$$P - P_e = P(A) \qquad (3.3.1)$$

The form of $P(A)$ used in the present model is derived from static experiments on thin-walled rubber tubes. In these experiments the elastic tube is attached at both ends to rigid tubes and has zero axial strain. The values of transmural pressure and cross-sectional area are determined simultaneously at a distance far from the points of attachment (Kececioglu et al, 1981). Thus this $P(A)$ is only valid in regions in which longitudinal tension and bending forces are negligible. This will be an important consideration in the formulation of the present model (see section 3.4).

With the above mentioned form of $P(A)$ the relation (3.3.1) is usually referred to as the 'local tube law'. The exact form of the function $P(A)$ and the assumptions involved in the application of the tube law to the present problem are discussed in detail in section 3.5.

3.4 FORMULATION OF THE THEORETICAL MODEL

In constructing the model it must be ensured that the one-dimensional flow approximation and the assumptions

under which the tube law can be employed, are not violated.

A distributed parameter model (DPM) is applied to the collapsible tube. This consists of the partial differential equations (of momentum and conservation of mass) governing one-dimensional flow in a collapsible tube, together with a constitutive relation for the tube wall, viz the local tube law. The region of application of this one-dimensional model is now examined.

Near the attachment points of the collapsible tube to the rigid end tubes, the area is constrained to adjust in a short distance to match the area of the rigid tube (Fig 2.2.2). In these regions longitudinal bending and tension are important and the employment of the local tube law could lead to significant error. Further, it is known from experiments that for much of the flow range, when the tube is 'collapsed', a throat forms near the downstream end of the collapsible tube. Immediately downstream of this point the fluid motion is essentially three-dimensional with turbulent mixing in the sudden expansion. In keeping with the one-dimensional approximation and the incorporation of a local tube law, lumped parameter models (LPM's) are used to provide the link between the DPM and the rigid tube LPM's. The proposed model, showing the transition zones, is depicted in Fig 3.4.1. Region 4 represents the DPM while regions 1, 3 and 5, $2^{\mp}$ are LPM's which provide the upstream and downstream boundary conditions respectively. By using

---

∓ The regions have been numbered so that the subscripts 1, 2, representing the upstream and downstream rigid tubes respectively, are consistent with those used by other authors (Conrad, 1969; Bertram and Pedley, 1982).

this formulation, in which the LPM's provide the boundary conditions, the model may be extended to other problems simply by modifying the boundary conditions. Further, with regard to the present problem, any new theories, eg on unsteady flow separation, can easily be incorporated as a change in a boundary condition.

The position of the DPM boundaries, are now chosen and are assumed to remain at a constant axial position. From Fig 2.2.2 it appears that for much of the flow range when the tube is 'collapsed', the narrowest point or constriction remains at an essentially constant axial position, near the downstream end of the tube. This position is chosen as the downstream boundary of the DPM and a LPM is employed to relate the behaviour at this station (subscript $c$) with that at the point in the downstream rigid tube where the flow is one-dimensional (subscript 2).

The position of the upstream boundary of the DPM is not so significant, with regard to the fluid mechanics, as that of the downstream boundary. At low flow rates (see Fig 2.2.2) the lengths of the sharply converging and diverging sections are approximately equal and the upstream boundary is chosen at the constant position (subscript $\beta$), which satisfies this condition. A LPM is again used to relate the values of the variables at this station to those at a point in the upstream rigid tube where the flow is fully developed (subscript 1). The actual length of the transition zone is determined from the longitudinal tube configuration at low flow rates, depicted in Fig 2.2.2.

The problem is then, in essence, to solve the DPM equations subject to boundary conditions provided by the LPM's. The equations of the DPM and the LPM's are derived in sections 3.5 - 3.7.

Pedley (1980) devised a LPM which exhibited some of the physical mechanisms present in flow through a collapsible tube. He examined the stability of the equilibrium states and by referring to a DPM indicated some mechanisms of instability, involving wave propagation, which can not be described by a LPM. It is expected that the combination of the DPM with the LPM boundary conditions will predict these mechanisms as a whole and so give more insight into the mechanisms responsible for instabilities occurring in experiments, than can be obtained from a purely LPM.

## 3.5 THE TUBE MODEL

### 3.5.1 Quasi-Static Tube Law

The local tube law represents the elastic properties of the tube wall. It relates the local transmural pressure to the local cross-sectional area and is usually expressed in the form (Shapiro, 1977a)

$$\frac{P - P_e}{K_p} = \mathcal{P}(\alpha) \quad , \qquad (3.5.1)$$

where $P_e$ is the external pressure; $P$ the internal fluid pressure; $K_p$ a parameter representing the circumferential bending or membrane stiffness and $\alpha = A/A_o$ : where $A_o$ is the value of $A$ at zero transmural pressure. The function $\mathcal{P}(\alpha)$ may be determined theoretically (Flaherty et al, 1972) or experimentally (for example, Kececioglu et al, 1981).

When the transmural pressure is such that the tube

is collapsed and opposite sides touch, a buckled state with n-fold symmetry ($n \geqslant 2$) is observed. Flaherty et al have shown that for transmural pressures equal to and below this buckling pressure the cross-sections of the lobes are self-similar. For the rubber tubes commonly used in Starling resistor type experiments n is typically 2. In this mode of collapse Flaherty et al have shown that for a perfectly symmetric tube the two cross-section are self-similar for $\alpha \leqslant 0.21$. Self-similarity arguments then show that

$$\mathcal{P}(\alpha) = -\alpha^{-3/2} \quad \text{‡} \quad . \tag{3.5.2}$$

Here, $K_p$ is the circumferential bending stiffness, which for a linear elastic material is given by

$$K_p = \frac{E(h/r_o)^3}{12(1-\sigma^2)} \tag{3.5.3}$$

where E is Young's modulus; $\sigma$ Poisson's ratio; h the wall thickness and $r_o$ the radius of a circle of area $A_o$. Pedley (1980), following Shapiro (1977a) (see Fig 2.3.1) used a function which is consistent with (3.5.2) at very small areas and which represents a change to circular cross-section at zero transmural pressure. This same form of relationship is employed in the present analysis, viz

$$P - P_e = P(A) \quad ,$$

where

$$\begin{aligned} P(A) &= c_1\left[1-(A_o/A)^{3/2}\right] \quad , \quad A < A_o \\ &= c_2\left[A/A_o - 1\right] \quad , \quad A \geqslant A_o \quad . \end{aligned} \tag{3.5.4}$$

Here, $c_1$ and $c_2$ are parameters representing the circum-

---

‡ This relationship has been confirmed by experiments carried out by Shapiro (1977a) and Kececioglu et al (1981).

ferential bending and membrane stiffnesses respectively and whose effect is tested in Chapters 4 and 6. It is assumed that the area at which the transition takes place is the area of the rigid tube‡. $P(A)$ is plotted in Fig 3.5.1, where $c_1$ is determined from (3.5.3) using values for $E$, $h$ and $r_o$ given by Conrad (1969) and $\sigma = 1/2$; $c_2$ is given the somewhat arbitrary value $100c_1$ to represent the greater stiffness of the circular cross-section.

3.5.2 Limitations of the Tube Law

The solid curve (see Fig 2.3.1) was obtained by Shapiro (1977a) from data determined with very long tubes under static conditions. The tubes used in model experiments can be relatively short in which case longitudinal tension and bending stiffness will become important. If the tube is under longitudinal tension $T$ and there is a local curvature $R^{-1}$ then this tension gives rise to a pressure difference roughly $TR^{-1}$ which will modify the relationship between cross-sectional area and transmural pressure. It is therefore assumed that $TR^{-1} \ll P_{tm}$. Longitudinal bending stiffness is also neglected; a tube law incorporating longitudinal bending stiffness and membrane stiffness due to longitudinal tension has been developed by McClurken et al (1981).

The attachment of the compliant tube to the rigid tubes, particularly in the vicinity of attachment, certainly affects the tube law. The law of course does not

---

‡ As pointed out by Pedley (1980) in reality this area may be slightly less than $A_o$ since some distension is required in attaching the collapsible tube to the rigid end tubes.

hold at the rigid tube itself and end effects, involving longitudinal tension and bending (see above), are important over some distance from the rigid tubes. This point was considered in section 3.4 when the boundaries of the DPM were chosen.

Incorporating a law based on experiments carried out under static conditions in an unsteady model is obviously a source of error. To account for unsteadiness in the tube law would require additional terms in $P(A)$ representing wall acceleration and viscoelasticity. Since very thin-walled tubes are being considered it is assumed that the inertia of the tube wall is negligible. It is further assumed that the tube exhibits no viscoelastic effects.

In the present model the effect of the fluid external to the tube is ignored. In most model experiments the tube is enclosed in a large chamber (many times greater than the volume of the tube) so that tube volume changes do not significantly affect the external pressure, $p_e$. During large amplitude local oscillations, however, the motion of the external fluid may modify the relationship between the transmural pressure and the cross-sectional area. However, as stated earlier, the model is not expected to be valid during such vigorous oscillations anyway. A difference in the densities of the two fluids gives rise to longitudinal tension in the tube wall[‡]. It is again assumed that this

---

‡ Conrad (1969) used water as the internal fluid and air as the external fluid in his experiment thus increasing the significance of longitudinal tension.

has a negligible effect on the relationship between cross-sectional area and transmural pressure.

With the above assumptions the tube law (3.5.4) is employed in the present model.

3.5.3 Wave Speed

The infinite wavelength phase velocity, c, for wave propagation in area compliant vessels containing an incompressible fluid (Weber, 1866; see Kececioglu et al, 1981) is

$$c = (\rho D)^{-1/2} , \tag{3.5.5}$$

where $\rho$ is the fluid density and D is the distensibility of the tube, viz

$$D = \frac{1}{A}\frac{dA}{dP_{tm}} , \tag{3.5.6}$$

the relative area increase per unit increase in excess pressure. Incorporating (3.5.4) in (3.5.6), yields

$$\begin{aligned} c &= \left[\frac{3}{2}\frac{c_1}{\rho}\left(\frac{A}{A_o}\right)^{-3/2}\right]^{1/2} , \quad A < A_o \\ &= \left[\frac{c_2}{\rho}\frac{A}{A_o}\right]^{1/2} , \quad A \geq A_o , \end{aligned} \tag{3.5.7}$$

which is discontinuous at $A = A_o$. c is plotted in Fig 3.5.2. For $A > A_o$ the distensibility is low and hence from (3.5.5) the wave speed is high. For very small areas, in which opposite sides of the tube are in point or partial line contact and smaller areas where the tube is in almost complete line contact, the distensibility is also small giving rise to a high wave speed. However, the range in between is one of high distensibility and hence low wave speed.

## 3.6 THE FLOW MODEL

There have only been a few investigations into unsteady flow in a collapsible tube subjected to negative transmural pressure, where a DPM has been used. Kamm and Shapiro (1979) solved the quasi- linear set of hyperbolic equations, resulting from the theory developed for flows generated by either externally applied pressures or by body forces. More recently Bitbol et al (1982) solved a similar set of equations in a collapsible tube model of the closure of the mitral valve. These are the only papers known to the author in which the one-dimensional partial differential equations governing unsteady, viscous flow in a collapsible tube have been solved.

The present DPM equations are similar to those used by the above authors. They are solved here in an attempt to investigate the instabilities which have been observed in model experiments on collapsible tubes. The main aim is to obtain some insight into the interesting phenomenon of self-excited oscillations.

The general equations of fluid motion are well documented and are simply stated here. These are the equations governing flow in region 4.

Continuity Equation

$$\frac{\partial A}{\partial t} + \frac{\partial (Au)}{\partial x} = 0 \ , \qquad (3.6.1)$$

where $\partial/\partial x$ and $\partial/\partial t$ denote differentiation with respect to axial distance and time respectively.

Momentum Equation

Here body forces have been neglected and wall

friction is taken into account by means of a resistance function R(A) (cf Pedley, 1980). The equation is

$$\frac{\partial u}{\partial t} + u\frac{\partial u}{\partial x} = -\frac{1}{\rho}\frac{\partial p}{\partial x} - \frac{R(A)Au}{\rho} , \qquad (3.6.2)$$

where R(A) is a resistance per unit length. For $A \geq A_o$ it is assumed that R(A) corresponds to the steady flow value for Poiseuille flow in a tube of circular cross-section:

$$R(A) = \frac{8\pi\mu}{A^2} , \qquad (3.6.3)$$

while for $A < A_o$ it is assumed it corresponds to that for an elliptic tube, which is approximated as:

$$R(A) = \frac{4\mu\pi}{A^2}\left[\frac{\pi^2 A_o}{4\mathcal{E}^2 A} + \frac{4\mathcal{E}^2 A}{\pi^2 A_o}\right] . \qquad (3.6.4)$$

where $\mathcal{E}$ is the elliptic integral of the second kind. For details see Appendix A. The influence of the parameter $\mathcal{E}$ is investigated in Chapter 4. For small values of A the assumption of an elliptic cross-section is obviously incorrect. The tube cross-section at point contact has n-fold symmetry, with the n=2 mode being the most commonly observed in Starling resistor type experiments (see section 3.5.1). For n=2 the tube cross-section at point contact resembles roughly two elliptic tubes and perhaps a better approximation for the resistance in this case would be 2R(A/2); where R(A) is given by (3.6.4). However, the fact that R(A) is based on the assumption of steady, laminar flow and (3.6.4) is not exact even for that special case, does not justify ellaboration and it is assumed that (3.6.4) holds for all $A < A_o$.

Tube Law

Closure of the equations in this region is accomplished by incorporating the tube law described in section 3.5.1 and which is restated here for completeness:

$$P - P_e = P(A) = c_1\left[1 - \left(\frac{A_o}{A}\right)^{3/2}\right], \quad A < A_o \qquad (3.6.5)$$

$$= c_2\left[\frac{A}{A_o} - 1\right], \quad A \geq A_o .$$

## 3.7 BOUNDARY AND INITIAL CONDITIONS

The choice of these conditions can greatly influence the type of solution permitted by a differential equation. The incorporation of pressure recovery in the downstream boundary condition (see region 5 analysis), for example, may be crucial in terms of whether oscillations can exist in the model (see Bertram and Pedley, 1982).

In this analysis each boundary condition takes the form of an algebraic equation. These equations (one upstream and one downstream) result from the LPM equations which after differencing in time, are reduced to a single algebraic equation in area and velocity. The details of the boundary condition formulation for the steady and unsteady flow cases will be given in Chapters 4 and 5 respectively.

### 3.7.1 Control-Volume Method

In the derivation of the fluid dynamic equations in regions 1, 2, 3 and 5 the familiar concept of a control volume is employed. For an incompressible fluid conservation of mass reduces to conservation of volume, viz

$$\int_{CS} (\underline{v}.\underline{n})\,dS + \frac{d}{dt}\int_{CV} dV = 0 \qquad (3.7.1)$$

and the linear momentum balance is

$$\sum \underset{\sim}{F} = \int_{CS} \rho \underset{\sim}{v}(\underset{\sim}{v}.\underset{\sim}{n})dS + \frac{d}{dt}\int_{CV} \rho \underset{\sim}{v}\, dV \quad , \tag{3.7.2}$$

where $\rho$ is the fluid density, $\underset{\sim}{v}$ is the velocity vector, $\underset{\sim}{n}$ is an outward pointing unit vector normal to the element of surface $dS$ and $\sum \underset{\sim}{F}$ is the sum of the external forces acting on the control volume. In the present one-dimensional analysis only the axial velocity component is relevant and so (3.7.1) and (3.7.2) become

$$\int_{CS} u\, dS + \frac{d}{dt}\int_{CV} dV = 0 \tag{3.7.3}$$

and

$$\sum F = \int_{CS} \rho u(\underset{\sim}{u}.d\underset{\sim}{S}) + \frac{d}{dt}\int_{CV} \rho u\, dV \quad , \tag{3.7.4}$$

where $u$ and $F$ are the axial components of velocity and external force respectively.

Before considering the boundary conditions in detail the types of flow which can be encountered in regions 3 and 5 are examined and it is shown that they can be represented by equations governing either attached or separated flow.

3.7.2 General Flow Equations

The equations governing the flow in regions 3 and 5 depend upon the degree of collapse or expansion of the tube at stations B and C respectively (see Fig 3.4.1) and also on the direction of the flow. The flow in these regions

may correspond to that in a tube which is

(i) gradually converging

(ii) sharply converging

(iii) gradually diverging

(iv) sharply diverging.

It is assumed that flow separation does not occur in the sharply converging section. Losses associated with such a separation are thought not to be critical in the present problem and are usually small compared with those for separated flow in a sharply diverging section. Cases (i) - (iii) above will then be governed by the same equations. Without loss of generality, flow in a gradually diverging section is considered as being representative of these three flows. Thus the flow in regions 3 and 5 is determined from

(a) the flow in a gradually diverging tube in which the flow does not separate or

(b) flow in a sharply diverging tube in which separation occurs.

For each of the above cases the continuity equation takes the same form and this equation is now derived.

Continuity Equation

Consider the deformable control volume depicted in Fig 3.7.1, in which the length, L, is fixed. The control surface consists of the tube walls and the upstream and downstream cross-sections at locations i and j respectively. The continuity balance is

$$\int_{A_j} u_j \, dA - \int_{A_i} u_i \, dA + \frac{d}{dt} \int_{V} dV = 0 \quad .$$

Hence,

$$u_j A_j - u_i A_i + \frac{dV}{dt} = 0 \quad , \tag{3.7.5}$$

where the expression for the volume, $V$, depends upon the geometry of the region. The geometry is actually very complex. The rigid tube end has a fixed circular cross-section while the other end can vary, for example, from a dumbbell shape, through an ellipse to a circular configuration (Fig 3.1.1). Thus it is very difficult to determine the volume of the collapsible tube exactly. An approximation to this volume is made by defining

$$V = (A_i + A_j)L/2 \quad , \tag{3.7.6}$$

where either $A_i$ or $A_j$ is equal to the constant rigid tube area $A_o$. This is a somewhat arbitrary choice but is preferred to other approximations, for example a cone, which make the subsequent analysis more involved and might well obscure the most important physical phenomena. Substituting for $V$ in (3.7.5) using (3.7.6), yields

$$u_j A_j - u_i A_i + \frac{L}{2}\frac{d}{dt}(A_i + A_j) = 0 \quad . \tag{3.7.7}$$

The momentum equation for attached flow is now derived.

Attached Flow

Momentum Equation

The external forces acting on the control volume are depicted in Fig 3.7.1. They include the pressure forces at stations $i$ and $j$ and forces due to the axial components of the normal pressure on the side wall and shear stress at the wall due to friction. The resultant

force is

$$\sum F = \int_{A_i} P_i \, dA - \int_{A_j} P_j \, dA - \int_{A_s} P_w \sin\theta \, dA_s - \int_{S} \tau_w \cos\theta \, dS ,$$

where $\theta$ is the angle the tube wall makes with the x-axis and $A_s$ is the side surface area of the control volume. Since $\sin\theta = dA/dA_s$ the third integral on the right hand side may be written in the form

$$\int_{A_j - A_i} P_w \, dA \quad .$$

If we now define the average wall pressure as

$$P_w = \beta (P_i + P_j) ,$$

where $\beta$ is a constant, then the axial component is

$$\beta (P_i + P_j)(A_j - A_i) .$$

The effect of the parameter $\beta$ is tested in Chapter 4. Thus the total force

$$\sum F = P_i A_i - P_j A_j + \beta (P_i + P_j)(A_j - A_i) - \tau_w \mathcal{P}_m L ,$$

where $L$ is the axial length of the control volume and $\mathcal{P}_m$ the mean perimeter. To be consistent with the equations in region 4 the resistance function $R(A)$ is incorporated and $\tau_w \mathcal{P}_m L$ is replaced by $R(A_m) L Q A_m$, where $A_m = (A_i + A_j)/2$ .

The momentum flux in the longitudinal direction is

$$\int \rho u (u \, d\underline{A}) = \rho u_j^2 A_j - \rho u_i^2 A_i .$$

The momentum increase in the control volume is

$$\frac{d}{dt} \int \rho u \, dV = \frac{d}{dt} \int_0^L \rho Q \, dx ,$$

where $Q = Au$ is the volume flow rate. Defining

$$\bar{Q} = \frac{1}{L} \int_0^L Q \, dx ,$$

then the momentum increase is given by

$$\rho L \frac{d\bar{Q}}{dt} \quad .$$

It is assumed, since there is no experimental data available, that

$$\bar{Q} = (1-\eta) Q_i + \eta Q_j \ ,$$

where $Q_i$ and $Q_j$ are the volume flow rates at stations $i$ and $j$ respectively and $\eta$ is a constant such that $0 \leq \eta \leq 1$ whose influence is tested in Chapter 6.

Equating the axial force to the sum of the momentum flux and momentum increase, yields

$$P_i A_i - P_j A_j + \beta (P_i + P_j)(A_j - A_i) - R(A_m) L Q A_m$$
$$= \rho u_j^2 A_j - \rho u_i^2 A_i + \rho L \left[(1-\eta)\frac{dQ_i}{dt} + \eta \frac{dQ_j}{dt}\right] \quad . \qquad (3.7.8)$$

Separated Flow

In this case the flow is similar to that encountered in a sudden expansion (Fig 3.7.2).

Momentum Equation

The external forces acting on the control volume are depicted in Fig 3.7.2. These include the pressure forces at stations $i$ and $j$ and the force due to shear stress exerted on the fluid by the tube walls. From experiments on sudden expansions it is found that the pressure on the downstream facing walls is approximately uniform and equal to the pressure, $P_i$ , at the expansion; otherwise a parallel jet would not be formed. Shear forces in the sudden expansion are difficult to evaluate. It can be argued that only stagnant fluid with very small velocity gradients is in contact with the wall and that

the shear forces are negligibly small compared with the pressure forces. The resultant force in the longitudinal direction is then

$$\begin{aligned}\Sigma F &= \int_{A_i} p_i \, dA - \int_{A_j} p_j \, dA + \int_{A_j - A_i} p_i \, dA \\ &= p_i A_i - p_j A_j + p_i (A_j - A_i) \\ &= (p_i - p_j) A_j \ .\end{aligned}$$

Now the momentum flux in the longitudinal direction is

$$\begin{aligned}\int_S \rho u (u_i \, \underset{\sim}{dA}) &= \int_{A_j} \rho u_j^2 \, dA - \int_{A_i} \rho u_i^2 \, dA \\ &= \rho A_j u_j^2 - \rho A_i u_i^2 \ .\end{aligned}$$

The rate of change of momentum within the control volume will be approximated as in the previous case, viz

$$\frac{d}{dt} \int \rho u \, dV = \rho L \frac{d\bar{Q}}{dt} \ ,$$

where it is assumed

$$\bar{Q} = (1 - \varepsilon) Q_i + \varepsilon Q_j \ .$$

Hence, the momentum balance for this control volume is

$$(p_i - p_j) A_j = \rho u_j^2 A_j - \rho u_i^2 A_i + \rho L \left[ (1-\varepsilon) \frac{dQ_j}{dt} + \varepsilon \frac{dQ_i}{dt} \right] \qquad (3.7.9)$$

Finally, two further assumptions are made concerning regions 3 and 5

(i) the areas $A_B$ and $A_C$ never increase far enough beyond $A_o$ for the flow to separate at the rigid tubes,

(ii) if $A_c < A_o$ and $u_2 > 0$ or $A_B < A_o$ and $u_B < 0$ it is assumed that the flow always separates.

3.7.3 Upstream Boundary Condition

This is obtained by combining the equations in

regions 1 and 3.

Region 1

This is the upstream rigid tube.

Continuity Equation

Since the tube walls are rigid (3.7.7) reduces to $u_1 = u_1(t)$ .

Momentum Equation

Consider the non-deformable control volume shown in Fig 3.7.3. The linear momentum balance is

$$\sum F = \int \rho u^2 \, dS + \int \rho \frac{du}{dt} \, dV \quad . \tag{3.7.10}$$

The external forces acting on the control volume are depicted in Fig 3.7.3. These forces include the pressure force at station 1 and that due to the pressure head, $p_h$ . There is also a force due to the shear stress at the tube, $\tau_w$ and a force expressing the losses at the variable constriction. It is assumed that this constriction gives rise to a pressure head loss $R u_1 + \rho k_1 u_1^2$ and thus a force $(R u_1 + \rho k_1 u_1^2) A_o$ . Thus the sum of the forces is

$$\sum F = \int p \, dS - \int \tau_w \, dS - R u_1 A_o - \rho k_1 u_1^2 A_o$$

$$= (p_h - p_1) A_o - \tau_w \mathbb{P} L_1 - R u_1 A_o - \rho k_1 u_1^2 A_o ,$$

where $\mathbb{P}$ is the perimeter of the tube; $L_1$ the tube length and $k_1$ is a constant which depends upon the degree of constriction. All pressures are relative to atmospheric.

The linear momentum in the control volume is

$$\int \rho \frac{du}{dt} \, dV = \rho \frac{du_1}{dt} \int dV = \rho A_o L_1 \frac{du_1}{dt} \quad .$$

Substituting the above expression for the momentum, into

(3.7.10) together with the expression for the force, yields

$$(p_h - p_1)A_o - \tau_w \mathcal{P} L_1 - R u_1 A_o - \rho A_o k_1 u_1^2 = \rho A_o L_1 \frac{du_1}{dt} .$$

It is now assumed that the average shear stress $\tau_w$ can be related to a skin friction coefficient $f$ in terms of the dynamic head to give $\tau_w = f\rho u_1^2/2$, where $f$ is the Fanning friction factor. For laminar flow $f = 16/Re = 16\mu/\rho d u_1$, where Re is the tube Reynolds number based on the diameter $d$. Substituting for $\tau_w$ in the momentum equation, yields

$$p_h - p_1 = \frac{8\mu \mathcal{P} L_1 u_1}{\rho A_o} + R u_1 A_o + \rho k_1 u_1^2 + \rho L_1 \frac{du_1}{dt} .$$

This equation can be written in the form

$$p_h - p_1 = R_1 A_o u_1 + \rho k_1 u_1^2 + A_o I_1 \frac{du_1}{dt} , \qquad (3.7.11)$$

where the effect of the linear part of the pressure loss at the constriction is lumped together with that of the shear stress (which will be very small in comparison). To investigate the case in which there is no constriction $k_1$ is set equal to zero and $R_1$ set equal to the resistance for Poiseuille flow in a circular tube (3.6.3).

By replacing $u_1^2$ by $u_1|u_1|$ equation (3.7.11) also holds if the flow reverses

$$p_h - p_1 = R_1 A_o u_1 + \rho k_1 u_1|u_1| + A_o I_1 \frac{du_1}{dt} . \qquad (3.7.12)$$

The inertance $I_1 = \rho L_1/A_o$, resistance $R_1$ and constriction factor $k_1$ are constants and are shown to be important parameters of the problem.

Region 3

This region provides the transition from the

upstream boundary of the DPM (subscript B) to the point in the upstream rigid tube where the flow is fully developed (subscript 1).

The governing equations are as follows:

Continuity Equation

Applying equation (3.7.7) to this region, yields

$$u_1 A_o - u_B A_B - \frac{L_3}{2}\frac{dA_B}{dt} = 0 \quad . \tag{3.7.13}$$

Momentum Equation

The form of the momentum equation depends upon the direction of flow and the value of $A_B$. For positive flow ($u_B > 0$) in a converging section ($A_o > A_B$) equation (3.7.8) is used. It is further assumed that $A_B$ does not increase far enough beyond the value of $A_o$ to result in flow separation at the rigid tube. Thus (3.7.8) also holds for $A_B \geq A_o$ with $u_B < 0$ or $u_B > 0$. Applying equation (3.7.8), yields

$$\begin{aligned} &P_1 A_o - P_B A_B + \beta(P_1 + P_B)(A_B - A_o) - R(A_m) L_3 Q A_m \\ &= \rho u_B^2 A_B - \rho u_1^2 A_o + \rho L_3 \left[(1-\eta)\frac{dQ_1}{dt} + \eta \frac{dQ_B}{dt}\right] \end{aligned} \tag{3.7.14}$$

$(A_B < 0,\ u_B > 0\ ;\ A_B \geq A_o,\ u_B < 0 \text{ or } u_B > 0)$.

For $u_B < 0$ and $A_B < A_o$ the flow may separate and in this case equation (3.7.9) is used, viz

$$(P_1 - P_B)A_o = \rho u_B^2 A_B - \rho u_1^2 A_o + \rho L_3 \left[(1-\varepsilon)\frac{dQ_1}{dt} + \varepsilon \frac{dQ_B}{dt}\right] \tag{3.7.15}$$

$(A_B < A_o,\ u_B < 0)$

3.7.4 Downstream Boundary Condition

This is obtained by combining the equations of motion in region 2 and 5.

Region 2

This is the downstream rigid tube. The equations are of exactly the same form as those in region 1:

Continuity Equation

$$u_2 = u_2(t) \quad .$$

Momentum Equation

$$p_2 - p_o = R_2 A_o u_2 + \rho k_2 u_2 |u_2| + A_o I_2 \frac{du_2}{dt} \quad , \qquad (3.7.16)$$

where subscripts h and 1 in (3.7.12) have been replaced by 2 and o respectively. The inertance $I_2 = \rho L_2 / A_o$, resistance $R_2$ and constriction factor $k_2$ are constants and are shown to be important parameters of the problem.

Region 5

This region provides the transition from the downstream boundary of the DPM (subscript c) to the point in the downstream rigid tube where the flow is fully developed (subscript 2).

The governing equations are as follows:

Continuity Equation

Applying equation (3.7.7) to this region, yields

$$u_c A_c - u_1 A_o - \frac{L_s}{2} \frac{dA_c}{dt} = 0 \quad . \qquad (3.7.17)$$

Momentum Equation

The form of the momentum equation depends upon the direction of flow and the value of $A_c$. For $u_2 > 0$ and $A_c < A_o$ it is assumed that the flow separates and the equation takes the form of (3.7.9), viz

$$(p_c - p_2) A_o = \rho A_o u_2^2 - \rho A_c u_c^2 + \rho L_s \left[\varepsilon \frac{dQ_2}{dt} + (1-\varepsilon)\frac{dQ_c}{dt}\right] \qquad (3.7.18)$$

$(A_c < A_o \, , \, u_2 > 0)$

For $u_2 < 0$ and $A_c < A_o$ the flow is converging and is governed by equation (3.7.8). As in region 3 it is assumed that $A_c$ does not increase far enough beyond $A_o$ to result in flow separation at the rigid tube. Thus equation (3.7.8) also holds for $A_c \geq A_o$ with $u_2 < 0$ or $u_2 > 0$. The form of the equation is

$$p_c A_c - p_2 A_o - \beta (p_c + p_2) \int_{A_c}^{A_o} - R(A_m) L_s Q A_m = \rho u_2^2 A_o - \rho u_c^2 A_c + \rho L_s \left[ \varepsilon \frac{dQ_2}{dt} + (1-\varepsilon) \frac{dQ_c}{dt} \right] \quad (3.7.19)$$

$(A_c \geq A_o, \; u_2 < 0 \text{ or } u_2 > 0)$.

3.7.5 Initial Conditions

Values of the dependent variables are required as the starting values ($t=0$) for the time dependent model. An equilibrium solution provides a convenient set of initial conditions and in the following chapter attention is concentrated on the somewhat simpler analysis of the steady flow equations.

3.8 NON-DIMENSIONAL VARIABLES

All of the equations required for the solution of this problem have now been derived. It is advantageous to write these equations in non-dimensional form. All the variables are non-dimensionalised with respect to the radius, $r_o$, of the rigid tubes and an arbitrary velocity $u_o$. Thus the normalising area is $\pi r_o^2$ $(= A_o)$ and the normalising pressure $\rho u_o^2$. Further, the normalising inertance is $\rho r_o / A_o$ and the normalising resistance $\rho u_o / A_o$; giving a normalising resistivity (resistance per unit length) $\rho u_o / r_o A_o$. The equations in non-dimensional form are given in the next section.

## 3.9 NON-DIMENSIONAL EQUATIONS

### Region 4

#### Continuity

$$\frac{\partial A}{\partial t} + \frac{\partial (Au)}{\partial x} = 0 .$$

#### Momentum

$$\frac{\partial u}{\partial t} + u\frac{\partial u}{\partial x} + \frac{c^2}{A}\frac{\partial A}{\partial x} + RAu = 0 .$$

#### Tube Law

$$p - p_e = P(A) ,$$

where

$$P(A) = \begin{cases} c_1(1 - A^{-3/2}) & , A < 1 \\ c_2(A - 1) & , A \geq 1 . \end{cases}$$

#### Wave Speed

$$c^2(A) = A\frac{dP(A)}{dA} = \begin{cases} \frac{3}{2} c_1 A^{-3/2} & , A < 1 \\ c_2 A & , A \geq 1 . \end{cases}$$

#### Resistivity

$$R(A) = \begin{cases} \frac{4\mu}{A}\left[\frac{1}{(2\xi A/\pi)^2} + \left(\frac{2\xi}{\pi}\right)^2\right] & , A < 1 \\ \frac{8\mu}{A^2} & , A \geq 1. \end{cases}$$

### Upstream Boundary (Regions 1 and 3)

#### Region 1

##### Momentum

$$p_h - p_1 = R_1 u_1 + k_1 u_1 |u_1| + I_1 \frac{du_1}{dt} .$$

Region 3

Continuity

$$A_B u_B - u_1 + \frac{L_3}{2}\frac{dA_B}{dt} = 0 \ .$$

Momentum

$(A_B < 1,\ u_B > 0\ ;\ A_B \geq 1,\ u_B < 0 \text{ or } u_B > 0)$:

$$p_1[1-\beta(1-A_B)] - p_B[A_B+\beta(1-A_B)] - R(A_m)QL_3A_m = u_B^2 A_B - u_1^2 + L_3\left[(1-\eta)\frac{du_1}{dt} + \eta\frac{d(A_B u_B)}{dt}\right] ,$$

where $A_m = \frac{1}{2}(1+A_B)$

$(A_B < 1,\ u_B < 0)$:

$$p_1 - p_B = u_B^2 A_B - u_1^2 + L_3\left[(1-\varepsilon)\frac{du_1}{dt} + \varepsilon\frac{d(A_B u_B)}{dt}\right]$$

Tube Law

$$p_B - p_e = P(A_B) \ .$$

Downstream Boundary (Regions 2 and 5)

Region 2

Momentum

$$p_2 - p_o = R_2 u_2 + k_2 u_2 |u_2| + I_2\frac{du_2}{dt} \ .$$

Region 5

Continuity

$$u_2 - A_c u_c + \frac{L_5}{2}\frac{dA_c}{dt} = 0 \ .$$

Momentum

$(A_c < 1,\ u_2 > 0)$:

$$p_c - p_2 = u_2^2 - A_c u_c^2 + L_5\left[(1-\varepsilon)\frac{d(A_c u_c)}{dt} + \varepsilon\frac{du_2}{dt}\right]$$

$(A_c < 1,\ u_2 < 0\ ;\ A_c \geq 1,\ u_2 < 0 \text{ or } u_2 > 0)$:

$$p_c[A_c - \beta(A_c - 1)] - p_2[1 + \beta(A_c - 1)] - R(A_m) Q L_3 A_m$$

$$= u_2^2 - A_c u_c^2 + L_5\left[(1-\eta)\frac{d(A_c u_c)}{dt} + \eta \frac{du_2}{dt}\right] ,$$

where

$$A_m = \frac{1}{2}(1 + A_c) .$$

Tube Law

$$p_c - p_e = P(A_c) .$$

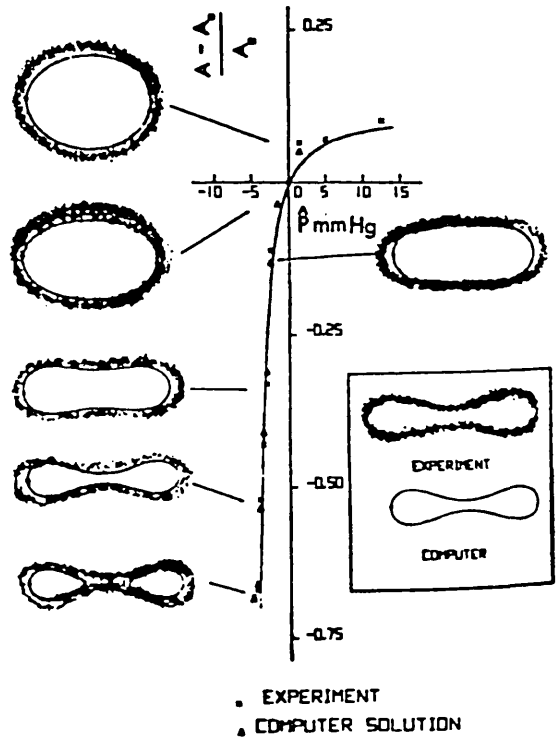



Fig 3.1.1 Comparison between changes in pressure-area relationships and configurations of cross-sectional areas obtained during distension of a thin-walled latex tube, and the corresponding computer solutions for the same values of the tube parameters. (From Moreno et al, 1970).

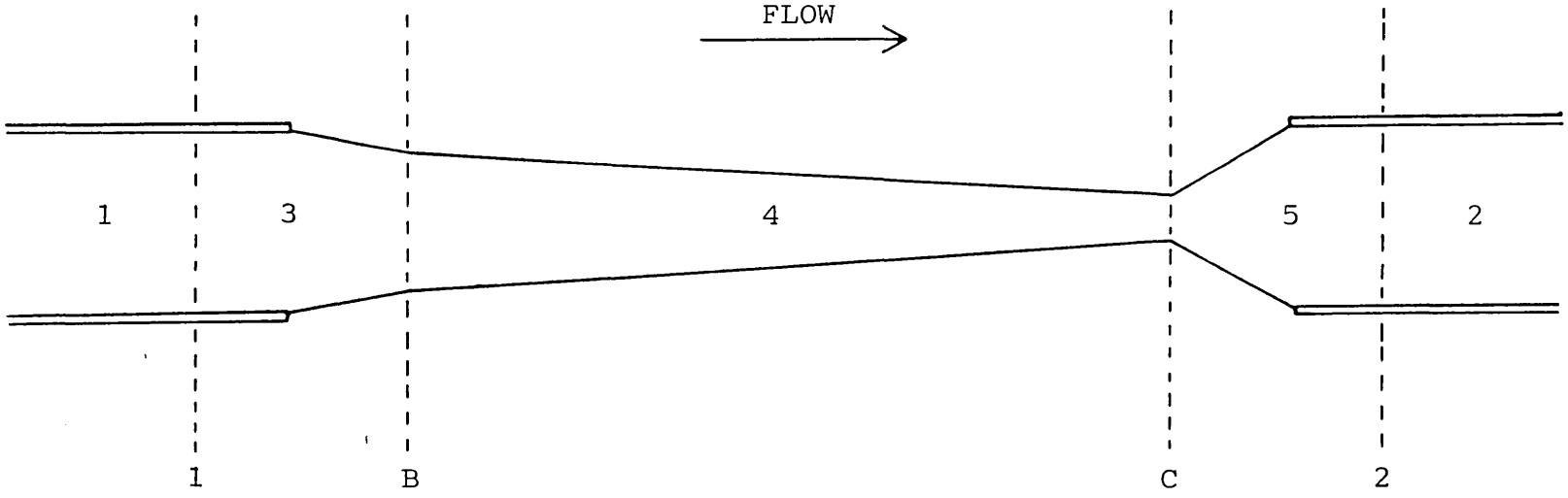



Fig 3.4.1 Sketch of the proposed model showing the different flow regions. The positions of the upstream and downstream boundaries of the distributed parameter model (region 4) are at the stations B and C, respectively. The transition regions 3 and 5 extend to positions 1 and 2 in the rigid tubes where the flow is assumed one-dimensional.

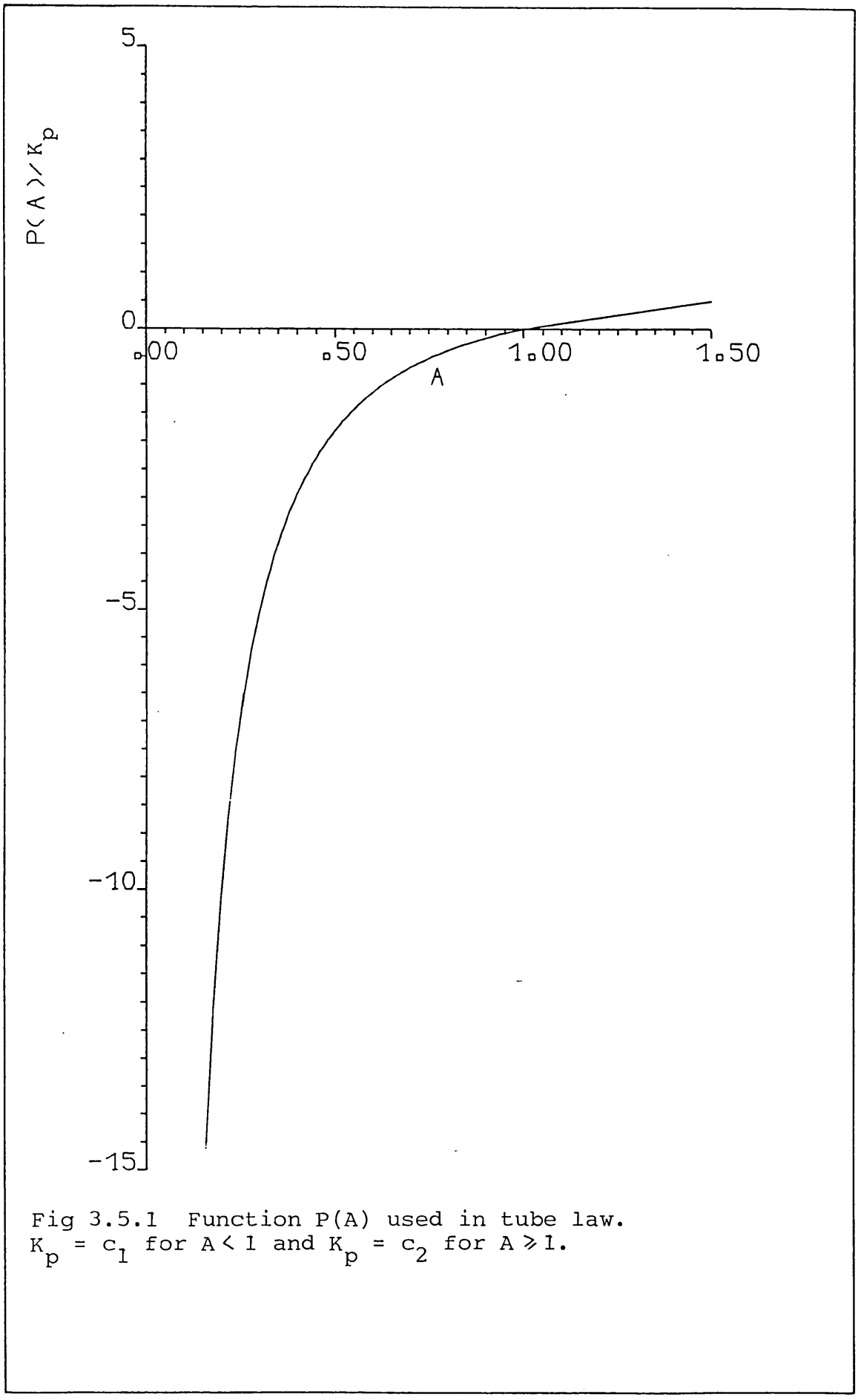



Fig 3.5.1 Function P(A) used in tube law.
$K_p = c_1$ for $A < 1$ and $K_p = c_2$ for $A \geq 1$.

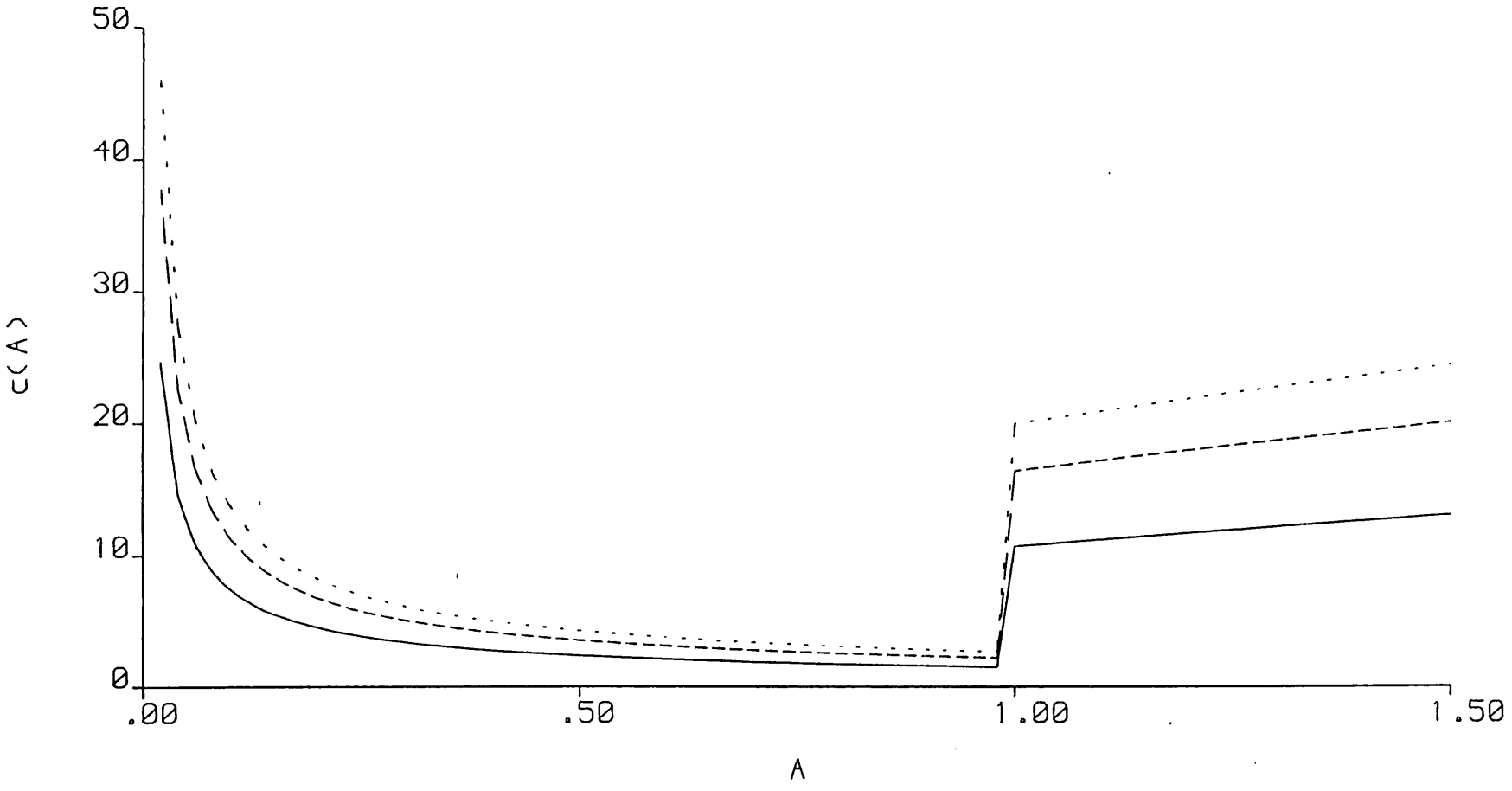



Fig 3.5.2 Wave speed c(A), for different values of $K_p$, based on tube law function P(A) plotted in Fig 3.5.1. $K_p = c_1$ for $A < 1$ and $K_p = c_2$ for $A \geqslant 1$. ———, $c_1 = 1.15$; - - - - -, $c_1 = 2.7$; · · · · ·, $c_1 = 4$.

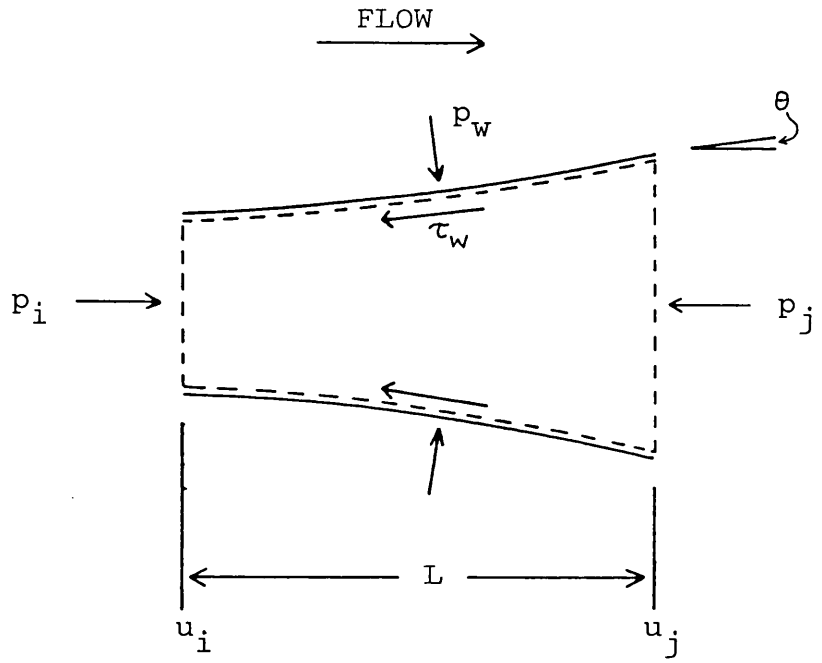



Fig 3.7.1 Control volume used in the analysis of the flow in a gradually diverging tube, in which the flow does not separate.

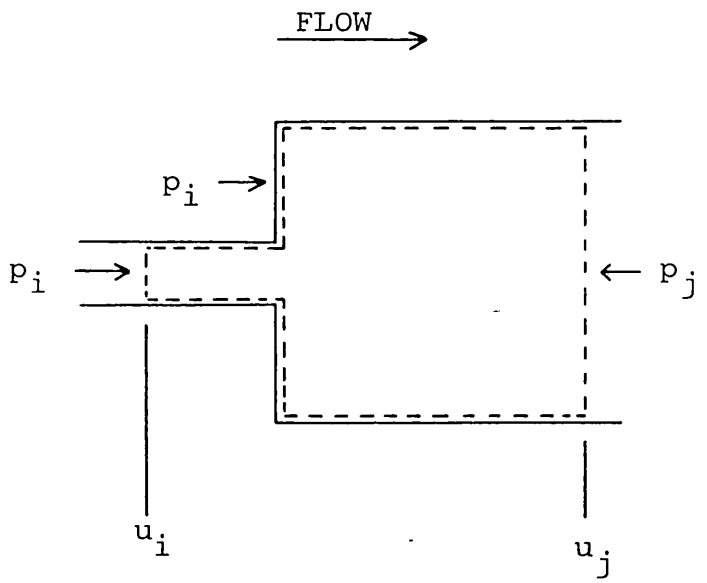



Fig 3.7.2 Control volume used in the analysis of the flow in a sharply diverging tube in which the flow separates.

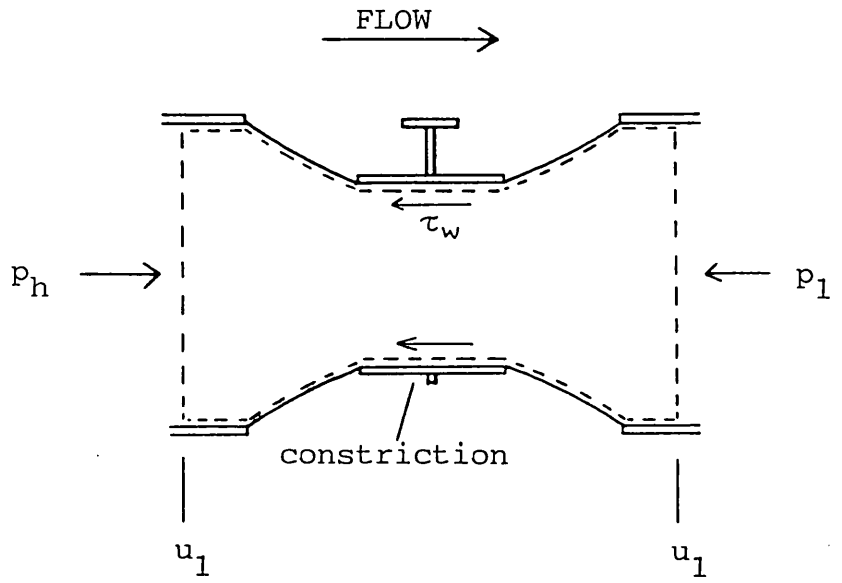



Fig 3.7.3 Control volume used in the analysis of the flow in region 1.

# CHAPTER 4

# STEADY FLOW

## 4.1 INTRODUCTION

Investigations into steady flow in compliant tubes have been extensive in recent years. The in vitro experimental studies have been concentrated mainly on the so-called Starling resistor (Conrad, 1969; Katz et al, 1969 among others). Theoretical models of this device have evolved (Katz et al, 1969; Pedley, 1980 among others) and also more general analyses of collapsible tube flow with the occurrence of elastic jumps, etc (Griffiths, 1971a; Oates, 1975a; Shapiro, 1977b among others).

Various methods have been used to solve the steady flow equations. Analytical methods applied to the linearised equations have provided insight into some of the possible flow regimes, choking, elastic jump, etc. Numerical methods on the other hand allow the full non-linear equations to be investigated and indeed supply the only means of solution for most of the real flow situations.

In this chapter the steady flow equations are solved using a numerical method based on the theory of finite differences. The solution is obtained at discrete points (grid points) along the collapsible tube. For a prescribed volume flow rate, $Q$, the steady flow equations constitute a 'marching' problem. The boundary condition is provided by the cross-sectional area which is obtained from the solution of the lumped parameter model (LPM)

algebraic equations at one of the boundaries. The LPM equations are chosen to correspond to particular experimental conditions. Conrad's experiment is used in the majority of cases since it gives the most complete record of the parameters of the problem and also because it has been compared most frequently with research undertaken by other workers. Thus results from the present problem can be compared with results obtained from models proposed by other authors.

The results obtained indicate the importance of certain parameters. The importance of the P-Q characteristic, with regard to the prediction of unstable regions of flow, is emphasised.

## 4.2 EQUATIONS AND BOUNDARY CONDITIONS

The equations for steady flow are obtained by setting the time derivative terms in the unsteady flow equations (see section 3.9) to zero: thus

$$\frac{d(Au)}{dx} = 0$$

$$u\frac{du}{dx} + \frac{c^2}{A}\frac{dA}{dx} + RAu = 0$$

$$p - p_e = P(A) \quad .$$

### 4.2.1 Boundary Conditions

Upstream Boundary

$$p_h - p_1 = R_1 u_1 + k_1 u_1 |u_1|$$

$$A_B u_B - u_1 = 0$$

$$p_B - p_e = P(A_B)$$

$(A_B < 1, u_B > 0;\ A_B \geq 1, u_B < 0 \text{ or } u_B > 0)$:

$$p_1[1-\beta(1-A_B)] - p_B[A_B+\beta(1-A_B)] - R(A_m)QL_3A_m = u_B^2A_B - u_1^2,$$

where $A_m = \frac{1}{2}(1+A_B)$.

$(A_B < 1, u_B < 0)$:

$$p_1 - p_B = u_B^2 A_B - u_1^2 .$$

Downstream Boundary

$$p_2 - p_o = R_2 u_2 + k_2 u_2 |u_2|$$

$$u_2 - A_c u_c = 0$$

$$p_c - p_e = P(A_c)$$

$(A_c < 1, u_2 > 0)$: $p_c - p_2 = u_2^2 - A_c u_c^2$

$(A_c < 1, u_2 < 0;\ A_c \geq 1, u_2 < 0 \text{ or } u_2 > 0)$:

$$p_c[A_c-\beta(A_c-1)] - p_2[1+\beta(A_c-1)] - R(A_m)QL_3A_m = u_2^2 - A_c u_c^2,$$

where $A_m = \frac{1}{2}(1+A_c)$.

## 4.3 FINITE-DIFFERENCE FORMULATION

Before discretizing the equations in region 4 it is convenient to introduce the volume flow rate, $Q (= Au)$. The equations then become:

$$\frac{dQ}{dx} = 0 , \qquad (4.3.1)$$

which when integrated, yields

$$Q = Au = \text{constant} . \qquad (4.3.2)$$

Incorporating (4.3.2) in the momentum equation, yields

$$\frac{dA}{dx} = \frac{RAQ}{(Q^2/A^2 - c^2)} , \qquad (4.3.3)$$

where $c = c(A)$ and $R = R(A)$ are known functions. The tube law now only serves to determine the pressure distribution from a given area distribution. Equation

(4.3.3) could be integrated analytically. This results in a transcendental equation, involving both the logarithmic and arctan functions, which could then be solved iteratively at each grid point. This approach is not used here but instead the integrations are performed numerically using the trapezoidal rule. There are three reasons for this, viz

(i) a change in the form of the resistance function $R(A)$ or the tube law $P(A)$ (with corresponding change in $c(A)$) would necessitate repeating the integration of (4.3.3) (analytical integration may not be possible) resulting in a new transcendental equation;

(ii) the steady flow solution should be a particular solution of the unsteady flow equations and since the trapezoidal rule is used to integrate the latter equations (see Chapter 5) it is advantageous to use the trapezoidal rule for the steady flow equations;

(iii) if $dR(A)/dx$ is large, a first order integration is too inaccurate to be of use (see Chapter 5).

Region 4 of the collapsible tube is divided into intervals of length $\Delta x = x_{i+1} - x_i$, where $x_{i+1}$ is downstream of $x_i$. The solution of equation (4.3.1) viz (4.3.2) is written in the form

$$Q = \text{constant} \; (= A_i u_i \; \forall \, i) \; . \qquad (4.3.4)$$

Integration of equation (4.3.3) using the trapezoidal

rule, yields

$$A_{i+1} - A_i = \frac{1}{2}\left\{\left(\frac{RAQ}{Q^2/A^2 - c^2}\right)_i + \left(\frac{RAQ}{Q^2/A^2 - c^2}\right)_{i+1}\right\}\Delta x, \quad (4.3.5)$$

where Q is a prescribed constant. Given the value of $A_{i+1}$, $u_{i+1}$ is determined from (4.3.4). In order to determine $A_i$, equation (4.3.5) is solved iteratively. The Newton Raphson method is used for this and the initial guess for $A_{i+1}$ is chosen as $A_i$. The converged solution of (4.3.5), $A_i$, is substituted in (4.3.4) to give $u_i$. Subsequent marching determines the values of $A_{i-1}$, $u_{i-1}$, etc. Here the solution procedure has been demonstrated for marching upstream, given the downstream boundary condition. Marching downstream is possible, and is probably the more obvious choice, however, it is not so convenient (see section 4.3.1).

There are several points to note regarding the solution scheme:

(i) For small A the resistance function, $R(A) \sim A^{-3}$, is very large. This makes a first order integration of the equations undesirable (Wylie and Streeter, 1978).

(ii) Another reason for choosing a second order integration is that the unsteady flow equations are solved in this way. This is necessary since the variation in the wave speed, $c(A)$, can be quite large increasing the curvature of the characteristics. Here, 'characteristic' refers

to a curve used in the solution procedure of the unsteady flow equations, viz the method of characteristics. Also, a first order integration of the unsteady flow equations would require a modification of the integration procedure for the positive slope characteristic (see Chapter 5).

(iii) The solution procedure ensures that conservation of mass is satisfied.

4.3.1 Solution Scheme

With the flow rate $Q$ prescribed, the ordinary differential equation (4.3.3) constitutes a 'marching' problem. The boundary condition is provided by specifying the area, $A$, at the upstream or downstream end.

In experiments on collapsible tubes the flow rate is usually modified by adjusting either the upstream pressure head, $p_h$, the upstream rigid tube constriction (RTC)[‡], $R_1$ and $K_1$, or the corresponding downstream quantities $p_o$ and $R_2$, $K_2$, respectively. Any one of these quantities could be used to adjust the flow rate in the present model. In choosing one of the RTC's it is more convenient (in some cases) to have only one variable, for example, to replace $R_1 u_1 + K_1 u_1 |u_1|$ by $R_1 u_1 (1 + k_1 |u_1|)$, where $k_1$ is the constant $K_1 / R_1$.

The direction of marching depends upon the boundary at which conditions on $A$ are specified, although

---

‡ Conrad (1969) found that adjusting the flow rate by changing the level of the upstream reservoir or by changing the upstream RTC, produced the same variations in pressure gradient across the tube.

it may not always be permissable to march upstream (see section 4.4.3). If the area is specified at the upstream boundary then marching downstream is performed. In this case either $k_2$ or $p_o$ would be determined, the other being fixed. Thus for a set of flow rates, a pressure drop versus flow rate characteristic could be determined in which the flow rate is modified by adjusting the downstream RTC or the height of the downstream reservoir. Similarly, knowing the area at the downstream boundary would mean marching upstream and determining $k_1$ or $p_h$ , the other remaining fixed. This would then give a pressure drop versus flow rate characteristic in which the flow rate is modified by adjusting the upstream RTC or the height of the upstream reservoir.

It has been decided to specify the boundary condition at the downstream end. There are two reasons for this:

(i) To determine the area at the downstream boundary involves the solution of a cubic equation, whereas at the upstream boundary a sixth order equation would have to be solved.

(ii) As stated earlier, Conrad's results were obtained by adjusting the upstream variable and one of the aims of this work is to simulate these results.

4.3.2 Boundary Conditions

Unlike the unsteady flow equations which constitute an initial boundary value problem, requiring boundary

conditions at both boundaries, the steady flow case can be reduced to a marching problem requiring a condition at only one boundary. Thus in this case one set of LPM equations (downstream) provides the boundary condition while the other set of LPM equations (upstream) have a free parameter ( $P_h$ or $k_1$ ), whose value is determined so that these LPM equations satisfy this boundary condition (upstream).

Downstream Boundary

The cubic equation obtained from combining the algebraic equations of the LPM is of the form

$$a_1 \mathcal{A}^3 + a_2 \mathcal{A}^2 + a_3 \mathcal{A} + a_4 = 0 \quad , \qquad (4.3.6)$$

where the form of the coefficients $a_1 \ldots\ldots a_4$ depend upon the magnitude of $A_c$. For $A_c < 1$ , $\mathcal{A} = A_c^{-1/2}$ and the coefficients are

$a_1 = c_1$

$a_2 = -Q^2$

$a_3 = 0$

$a_4 = P_2 + Q^2 - P_e - c_1$ ,

while for $A_c \geq 1$ , $\mathcal{A} = A_c$ and the coefficients are

$a_1 = c_2(1-\beta)$

$a_2 = P_e(1-\beta) + c_2(2\beta-1) - \beta P_2$

$a_3 = \beta(P_e - c_2) - P_2(1-\beta) - Q^2$

$a_4 = Q^2$ .

The solution of equation (4.3.6) is obtained using a subroutine from the NAG library, viz C02AEF. For $A_c < 1$ there is found to be only one positive real root. However, for $A_c \geq 1$ there can be three real roots. In trying to determine a pressure-flow characteristic it

is convenient to start at a low flow rate (with $A_c < 1$) and increase Q until A approaches unity. At this point small increments in Q are made until $A_c = 1$, at which point the root which gives an area $A_c > 1$ is chosen so as to remain on the same characteristic; subsequently the functions $R(A)$ and $P(A)$, together with the corresponding momentum equation, are chosen.

The values of $A_c$, $u_c$ and Q enable the values of $u_2$ and $p_2$ to be determined from the LPM equations.

Upstream Boundary

The final integration step in marching upstream determines the value of the area, $A_B$, and velocity, $u_B$. The LPM equations are then used to determine $u_1$, $p_1$ and finally the pressure head, $p_h$, which has provided the increase/decrease in flow rate.

As stated earlier, the pressure at each grid point in the collapsible segment is determined from the area distribution using the appropriate function $P(A)$ in the tube law.

Method of Solution

(i) Select Q, $p_o$ and the parameters $R_1$, $R_2$, $c_1$, etc.

(ii) Use LPM equations at the downstream boundary to determine $p_2$ and $u_2$ (= Q)

(iii) Solve the cubic equation (4.3.6) to determine $A_c$.

(iv) Substitute for $A_c$ in continuity equation (4.3.4) to obtain $u_c$.

(v) Move to the next grid point upstream and determine A using equation 4.3.5.

(vi) Apply equation (4.3.4) to determine u.

(vii) Repeat steps (v) and (vi) until the upstream boundary is reached.

(viii) Use LPM equations at upstream boundary to determine $u_1$ (= Q), $P_1$ and $P_h$.

(ix) Determine pressure distribution in the collapsible segment.

The above scheme is very flexible. The boundary conditions can be easily modified to include, for example, new information on flow separation. The computer program itself has been written in a modular form so that, for example, modification of an equation typically requires changing only a section (one or two lines) of a subroutine.

## 4.4 RESULTS

The main aim of this thesis is to investigate the unsteady flow phenomena which have been observed in experiments on the Starling resistor. However, this steady flow analysis is also useful in enabling identification of the regions of instability with regard to operating points on the pressure drop versus flow rate characteristic. It is felt that this is necessary in order to obtain the instabilities associated with a particular experiment, for example Conrad (1969).

### 4.4.1 Non-Dimensional Variables

The non-dimensionalising variables were chosen in Chapter 3. The actual values of these variables are chosen to correspond to the particular experiment that is simulated. For Conrad's experiment $\hat{r}_o$ = 6.35 mm, where the circumflex denotes a dimensional variable.

Following Bertram and Pedley (1982) the velocity scale $\hat{u}_o = 0.15\ ms^{-1}$ is chosen and so enables a direct comparison to be made with their results. The normalising time, flow rate and pressure are then 42.3 ms, 19.05 ml $s^{-1}$ and 22.5 N $m^{-2}$, respectively.

4.4.2 Parameter Values

These are chosen to correspond to the particular experiment under consideration. Again, since Conrad's experiment is the first and indeed the main experiment to be examined, the parameter values corresponding to his experiment are now discussed. It was suggested in Chapter 3 that $L_3 = L_5$. The value $L_3 = L_4/5$ appears to be a reasonable approximation (see Fig 2.2.2). The actual values given to these lengths are $L_4 = 10$ and $L_3 = L_5 = 2$. Thus $L_3 + L_4 + L_5 = 14$ corresponds to a dimensional length of 8.89 cm; Conrad's tube was about 8.9 cm in length. Fig 2.2.2 suggests that the length of collapsible tube quoted by Conrad included the parts of the tube supported by the rigid tubes. Thus $L_3 + L_4 + L_5$ may be slightly greater than the actual experimental value.

Conrad modified the flow through the system by adjusting either the upstream RTC or the upstream pressure head and observed that both methods of adjusting the flow produced the same variations in pressure gradient. For convenience, the upstream pressure head, $P_h$, is used in the present study. Since there is no means of determining the resistance of the upstream RTC and also since its role in steady flow is not crucial, the

values $R_1 = 0$ and $k_1 = 0$ are used.

At the downstream end of the tube the values of $R_2$ and $k_2$ are determined by a least squares fit of the $P_2$ versus $Q$ curves in Fig 4.4.1.

From the values of tube thickness, $h$, radius, $r_o$ and Young's modulus, $E$, quoted by Conrad, the value of

$$C_1 = \frac{E(h/r_o)^3}{12(1-\sigma^2)} = 2.7 \quad ,$$

where Poisson's ratio, $\sigma$, is given the value 0.5. There is some speculation as to the value of $h$ (= 0.093 cm) quoted by Conrad. Since the parameter $C_1 = f(h^3)$ is known to be significant (Pedley, 1980), it is essential that the correct value is used. Pedley (1980) states in a footnote that there was a misprint in Conrad's 1969 paper and that the actual thickness was much less than the value quoted. While the actual value of $h$ is not quoted, Pedley states that the value of $C_1$ based on the actual $h$ would be considerably smaller than unity: from experimental data given in the literature, Bertram and Pedley (1982) suggest that $0.4 < C_1 < 4$. It is interesting to note that Brower and Noordergraaf (1978) who also used Penrose tubing quoted the following values: $\hat{E} = 18 \times 10^6$ dynes cm$^{-2}$, $\hat{h} = 0.032$ cm. These values result in a value $C_1 \approx 1.14$.

The resistance function

$$R(A) = \frac{4\mu}{A}\left\{\frac{1}{(2\xi_e A/\pi)^2} + \left(\frac{2\xi_e}{\pi}\right)^2\right\} \quad , A < 1$$

$$= \frac{8\mu}{A} \quad , A \geq 1 \, .$$

was obtained in Chapter 3. The values of $\mu$ and $\mathcal{E}$ have to be specified. The fluid perfusing the tube in Conrad's experiment was water and hence $R_K = 4\mu = 0.00466$. From tables $1 \leq \mathcal{E} \leq 1.5678$. Thus for small A, $R|_{\mathcal{E}=1} \approx 2.5\ R|_{\mathcal{E}=1.5678}$. Following Pedley (1980) the value $(2\mathcal{E}/\pi)^2 = 1$ is used. This simplifies the form of the function, there being no rational reason to choose a different value of $\mathcal{E}$.

Hence,

$$R(A) = \frac{R_K}{A}(1 + A^{-2}) \qquad , A < 1$$

$$= 2\frac{R_K}{A} \qquad , A \geq 1 ,$$

where $R_K = 4\mu$. It was indicated in Chapter 3 that the resistance function could be modified when point contact occurred, for example

$$R(A) = \frac{R_f R_K}{R_A A}\left[1 + (R_A A)^{-2}\right] , \qquad (4.4.1)$$

where $R_f$ corresponds to the number of lobes, $n$, and $AR_A = A/n$, the area of each lobe. As an example, consider this function R(A) when A = 0.21. For $R_A = R_f = 1$, $R(A) \approx 0.5$ whereas for $R_A = \frac{1}{2}$, $R_f = 2$ (corresponding to 2 lobes, dumbbell configuration, see Fig 4.4.2), $R(A) \approx 8.1$. The difference between the values of these two forms of R(A) is even more pronounced for smaller A. $R_A$ and $R_f$ can have a much more significant effect than the elliptic integral, $\mathcal{E}$. In some of the calculations in this chapter (steady flows) the expression for R(A) given in (4.4.1) is

used. In subsequent chapters (unsteady flows) the values $R_A = R_f = 1$ are used; there being no justification to modify R(A) in this way for an unsteady, possibly turbulent flow.

The downstream pressure head takes the value $p_o = 0$. Finally, the value $\beta = 0.58$ is chosen. This is a somewhat arbitrary choice, however, no information is available on the force exerted by the sidewalls in such a complicated geometry. The value $\beta = 0.5$ would of course correspond to a linear pressure gradient in the region.

4.4.3 Conrad's Experiment

Fig 4.4.1 shows the change in $p_2$ with flow rate for different values of the downstream resistance ($p_e = 29.5$mm Hg). From a least squares fit of these curves, using the momentum equation

$$p_2 = R_2 Q + k_2 Q^2,$$

the following values of $R_2$ and $k_2$ are determined:

| Curve no | $R_2$ | $k_2$ |
|---|---|---|
| 1 | 18 | 99 |
| 2 | 28 | 129 |
| 3 | 52 | 175 |
| 4 | 66 | 204 |
| 5 | 113 | 466 |

These parameter values are now used in modelling some of the steady flow experiments carried out by Conrad. The results from the mathematical model are presented in the form of pressure versus flow rate curves; the P-Q characteristic being the most familiar of these. The

region of each P-Q characteristic for which $A > 1$ is not shown since the pressure drop is usually extremely small. Further, the main objective of the current research is to investigate flow in the collapsed regime ($A < 1$) and so this region ($A > 1$) is not of interest.

(i) With $R_A = 0.7$, $R_f = 3$ the P-Q characteristics shown in Fig 4.4.3 are obtained. Each of these characteristics (and subsequent ones in this chapter) is obtained by making positive increments in the flow rate and then determining the increase in $p_h$ which produces this increase in flow. At a certain flow rate (marked with an 'x') on several of the characteristics, a further increment in flow rate, Q, (no matter how small) results in a decrease in $p_h$. While this is still an acceptable steady flow solution it does not correspond to an operating point on the same characteristic as the previous flow rates. In some cases this point corresponds to $S \approx 1$, ie the flow is almost choked, while in others S is as small as $\frac{1}{3}$. It is interesting to note that these points occur on the negative slope of the characteristic, in the region where instabilities have been observed. Indeed, as mentioned above, in some cases $S \approx 1$, which suggests that a further increase in $p_h$ would perhaps result in an instability involving choking. This possibility is explored in Chapter 6.

Returning to Fig 4.4.3 it is seen that these results are in good agreement with the results of Conrad (1969) (cf Fig 2.6.1), with regard to the magnitudes of $(\Delta p)_{max}$ for each curve. The positive slopes are steeper than those in the experimental curves and the position of each $(\Delta p)_{max}$ occurs at a slightly lower flow rate. This is primarily due to the large value of R(A). Of course reducing R(A) by choosing $R_f = R_A = 1$ would decrease the values of $(\Delta p)_{max}$ and would not improve the agreement with experimental results.

Figs 4.4.4 and 4.4.5 show the variations in $p_2$ and $p_1$, respectively with change in flow rate, Q. The $p_2$ curves are of course the same as the experimental curves since a curve fit of the experimental data is used. The $p_1$ curve gives very good agreement with the experimental results up to the transition (at A = 1) to the equations valid for $A \geq 1$. As stated earlier the transition to a different P(A) relationship at A = 1 is fairly reasonable, however, the change in the flow regime in region 5 from a sudden expansion (with the flow separated) to that in which the flow is attached, does not in reality take place at A = 1. Thus this change over in the momentum equations is one possible explanation of the $p_1$ behaviour near A = 1. However, the results are qualitatively in agreement with Conrad's

experimental results.

(ii) $c_1 = 1.15$; $R_A = R_f = 1$. This value of $c_1$ corresponds to the Penrose tube used by Brower and Noordergraaf (1978). Since Conrad also used Penrose tubing and there was a misprint in his paper (see section 4.4.2), then this value may be a more appropriate choice. The results obtained using this value of $c_1$ are illustrated in Figs 4.4.6-4.4.8. The agreement with Conrad's curves is even better than before. Both the magnitude of $(\Delta p)_{max}$ and its postion, for each curve, is in very good agreement with Conrad's results. The positive slope has been decreased by the smaller value of R(A).

It is interesting to see that in curves 1, 2 and 3 no steady state solution exists beyond a certain flow rate. The flow chokes at this point on the curves. In order to remain on this characteristic the flow has to go supercritical and in this case the simple steady flow solution scheme breaks down. This is because when $S > 1$ at some point, events downstream of that point cannot influence those upstream, and hence it is incorrect to march upstream. However, the steady flow solution (if one exists) can be obtained by using the unsteady flow program. Starting from a steady state with $S < 1$, $p_h$ could be incremented and a new steady

state obtained; or the flow may become unstable (see Chapter 6). The unsteady flow solution scheme can be used to determine the steady flow characteristics by incrementing/decrementing $p_h$, $p_o$, $R_1$, $R_2$, etc. Indeed, this is exactly how a P-Q characteristic is obtained experimentally. However, this is more tedious than marching, and far more expensive, and the steady flow solution scheme is used for subcritical flows. Since no information regarding the lengths of Conrad's rigid tubes is available, it is impossible to determine his steady states using the unsteady flow model.

An investigation of these regions of the characteristics (on the negative slope) is made in Chapter 6. The breaks in the curves of Fig 4.4.6 are in a similar position to those observed in Conrad's results (see Fig 2.6.1). Comparison of Figs 4.4.3 and 4.4.6 suggest that there are instabilities associated with choking in the latter, while in the former, if instabilities do exist, they are probably associated with some other phenomenon. This possibility is examined in Chapter 6.

(iii) This is similar to case (ii). However, $L_4 = 0$, $L_3 = 12$ and the lumped parameter model of Bertram and Pedley (1982) is used. In addition $k_2$ is included so that the model benefits from

the fitted $p_2$ curves ($k_1$ and $k_2$ did not appear in Bertram and Pedley's model). The results are shown in Figs 4.4.9 - 4.4.11. The agreement with Conrad's results is not as good as that obtained using the present distributed parameter model (cf Figs 4.4.6-4.4.8). The position of $(\Delta p)_{max}$ occurs at a greater flow in each curve and its magnitude extends from being much too low for curve 5, to being much too high for curve 1. The $p_1$ versus Q curve (Fig 4.4.11) bears little resemblance to the experimental curve.

These results suggest that a distributed parameter model is superior to a lumped parameter model in simulating the experiment. The author's lumped parameter model is equally ineffective in simulating such flows; in fact it is probably worse. The reason for this is that the momentum equation has been used which involves 'shape' and Bertram and Pedley used the Bernoulli equation which does not. To clarify this, consider the two flow regimes illustrated in Fig 4.4.12. At medium/high flow rates both lumped parameter models would give reasonable results. However, at low flow rates the longitudinal configuration is such that the force exerted by the wall is very much over estimated in the author's lumped parameter model since the equations include the term $(p_1 + p_c)(1 - A_c)$ instead of

$(p_1 + p_B)(1 - A_c)$ (note that the wall force could be neglected by setting $\beta = 0$).

The equations in region 3 were derived on the basis that $L_3$ would be very short and simply provide a transition zone from the distributed parameter model to the rigid tube. For this purpose the author believes it is superior to the Bernoulli equation.

4.4.4 Brower and Scholten's Experiment

Brower and Noordergraaf (1973) pointed out that all results on the Starling resistor could be collapsed onto a single family of curves in which $p_1 - p_2$ is plotted against Q with $p_e - p_2$ kept constant. The subsequent results in this chapter are presented in this way.

(i) In this case results of the present model are compared with those obtained experimentally by Brower and Scholten (1975). In their experiments there were no rigid tube constrictions and so $R_1 = R_2 = k_1 = k_2 = 0$. Of course by choosing $R_1 = R_2 = 0$ the viscous losses in the rigid tubes are neglected. These losses are very small and are not thought to be significant in this problem; the main aim is to compare the shapes of the P-Q characteristics at constant $p_e - p_2$. Brower and Noordergraaf (1978) state that the length of the collapsible tube was 7 cm, but again it appears (as in Conrad, 1969) that they have included the

length supported by the rigid tubes in this figure. Using the lengths estimated from their figure, $L_4$ is given the value 6.3 and $L_3 = L_5 = 1.7$. The value of $c_1 = 1.15$. The experimental curves are illustrated in Fig 4.4.13 and the results obtained using the distributed parameter model are illustrated in Fig 4.4.14. The theoretical curves, like the experimental ones, are convex to the flow axis ($p_1 - p_2 = 0$). The maximum Q in each curve of Fig 4.4.14 corresponds to the flow rate at which choking occurs. This is not in exact agreement with the onset of oscillations illustrated in Fig 4.4.13 but it is very close. Further, in their experiments Brower and Scholten have proposed that oscillations result from the fluid velocity approaching the phase velocity. The present results suggest that this is possible and this is investigated in Chapter 6.

Although in modelling Brower and Scholten's experiment a similar apparatus to Conrad's is being used, the qualitative agreement with the experimental results of the former is something which previous workers have failed to achieve. This is illustrated in the following case.

(ii) Here, some dimensionless results obtained using $L_3 = L_5 = 2$, $L_4 = 10$ and several different values of $p_e - p_2$ (all other parameters as in (i)) are compared with those obtained using

the lumped parameter model of Bertram and Pedley (1982). In the case of the lumped parameter model the value of $L_3 = 12$ (= $L_3 + L_4$ in the distributed parameter model). The results of the distributed parameter model and lumped parameter model are illustrated in Figs 4.4.15 and 4.4.16, respectively. The lumped parameter model fails to simulate not only the shape of the characteristic (concave to the flow axis instead of convex), but also the magnitude of the pressure drop; being about twice as big as that predicted by the distributed parameter model (which has already been shown to be in good agreement with Brower and Scholten's experimental results).

It is therefore concluded that the present distributed parameter model is very effective in simulating steady flow behaviour in Starling resistor type experiments. A brief discussion is now made of the effects of several parameters on the pressure flow characteristic using this model.

4.4.5 Parameter Variation

All of the results presented in this section are concerned with the effects of parameter changes on the standard case (curve $p_e - p_2 = 100$) shown in Fig 4.4.15. This curve is plotted separately, on a different scale, in Fig 4.4.17.

(i) Length of region 3. Fig 4.4.18 shows the effect of doubling $L_3$ (= 4). This has no observable effect. Doubling $L_3$ effectively doubles the resistance

to flow in this region. It appears that the resistance is not significant in this case.

(ii) Length of region 4. The result of halving $L_4$ (= 5) is shown in Fig 4.4.19. In this case the resistance to flow is smaller and increases linearly with Q. Fig 4.4.20 shows the effect of doubling the length $L_4$ (= 20). It appears that the resistance has increased, as would be expected, and the shape of the curve is more convex to the axis Q = 0. As stated earlier, experimental results exhibit this convex behaviour, while the lumped parameter model of Bertram and Pedley does not. This suggests, at first sight, that resistance is an important quantity in these experiments and a lumped parameter model cannot effectively model this quantity (see (i)).

Another important property of the resistance, which cannot be examined using a lumped parameter model, is its effect on the longitudinal area gradient. This may have some influence on whether or not choking occurs (choking cannot be investigated in a lumped parameter model).

(iii) The flexural rigidity of the tube, $c_1$, is known to have an important effect on the stability of the flow (Bertram and Pedley, 1982). Its effect on the steady flow results is equally important. The two extremes of the range of $c_1$ proposed by Bertram and Pedley, viz $c_1$ = 0.4 and 4, are now

considered.

$c_1$ = 0.4: These results are presented in Fig 4.4.21. In this case the throat area is much smaller than in the standard case ($c_1$ = 1.15) and consequently the resistance is much larger, giving rise to the steep positive slope. The region near Q = 0, over which the resistance is linear, is the same as in the standard case. The flow breaks down with $S \approx 1$ at a flow rate approximately half of that found in the standard case. Thus, since $c_1$ can influence the choking phenomena, which has been proposed to explain oscillations in collapsible tubes (Brower and Scholten, 1975), it will be interesting to test the effect of this parameter in the unsteady flow case. While other workers in this field have briefly tested the effect of $c_1$ on the stability (for example, Bertram and Pedley, 1982), their use of a lumped parameter model prevented any check on whether choking was influenced by $c_1$ and perhaps, in part, responsible for some of the instabilities.

$c_1$ = 4: In this case the curve is concave to the axis Q = 0 (Fig 4.4.22) and choking is postponed, occurring at a much higher flow rate. The resistance to flow is reduced since the larger value of $c_1$ gives rise to a larger area at the

same flow rate. Thus the resistance (see (ii)) and $c_1$ significantly affect the flow through the system. Bertram and Pedley (1982) chose $c_1 = 4$ (in part to try and avoid the choking phenomena) and obtained curves similar to Fig 4.4.22. However, it should be added here that this is not the prime reason for the disagreement with the experimental results in their case. It has already been shown that with a smaller value of $c_1$ (see Fig 4.4.16) their lumped parameter model could not produce curves convex to the axis $Q = 0$ (cf Fig 4.4.15). This suggests the importance of the resistance itself, and not just the effect on the resistance of $c_1$ which must be modelled accurately.

(iv) Another means of changing the resistance is by varying the viscosity. This is equivalent to choosing a new $R_k$. The value $R_k = 0.0466$, a tenfold increase, produces the curve shown in Fig 4.4.23. The resistance at low flow rates is very high (cf Fig 4.4.21, virtually an identical slope). Further increase in Q has little or no effect on the pressure drop, ie up to as far as $Q \approx 0.6$, at which point there is a sudden steep increase in pressure drop before the flow chokes. In the region $0.025 \lesssim Q \lesssim 0.04$ the pressure drop is constant.

A tenfold reduction in $R_k$ (= 0.000466) produces

a curve which is concave to the axis Q = 0 (Fig 4.4.24). This is similar to the curves produced using a lumped parameter model. Again this emphasises that the lumping of the resistance is a major source of error in modelling steady flow experiments.

The present distributed parameter model and its associated lumped parameter model boundary conditions, give results which agree qualitatively with those obtained from experiments on the Starling resistor (Conrad, 1969; Brower and Scholten, 1975). Regions on the negative slopes of some of the P-Q characteristics (Fig 4.4.6) cannot be determined since $S \approx 1$. On other characteristics there are regions which correspond to a decrease in $p_h$ for an increase in Q and therefore do not belong to that characteristic (although they are acceptable steady states). It is likely that these regions correspond to those on the experimentally determined characteristics, Fig 2.6.1, which are regions of unstable flow. This can be tested by determining a steady state solution corresponding to an operating point on the characteristic and using this solution as the initial conditions for the unsteady flow equations. Then by increasing/decreasing $p_h$, a point corresponding to the break in the curve is approached. In this way an unstable region corresponding to a particular characteristic is determined.

Thus this steady flow analysis provides a useful starting point for the investigation of unstable flows which are examined in Chapter 6.

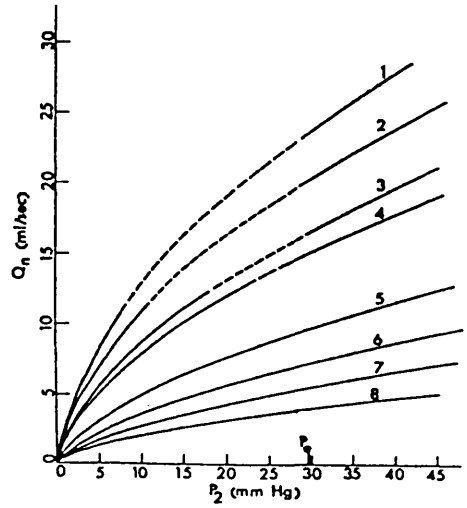



Fig 4.4.1 Downstream pressure as a function of flow rate for constant external pressure and different values of the downstream constriction. Curve numbers refer to settings of downstream constriction, as indicated in the table of Fig 2.6.1. (From Conrad, 1969).

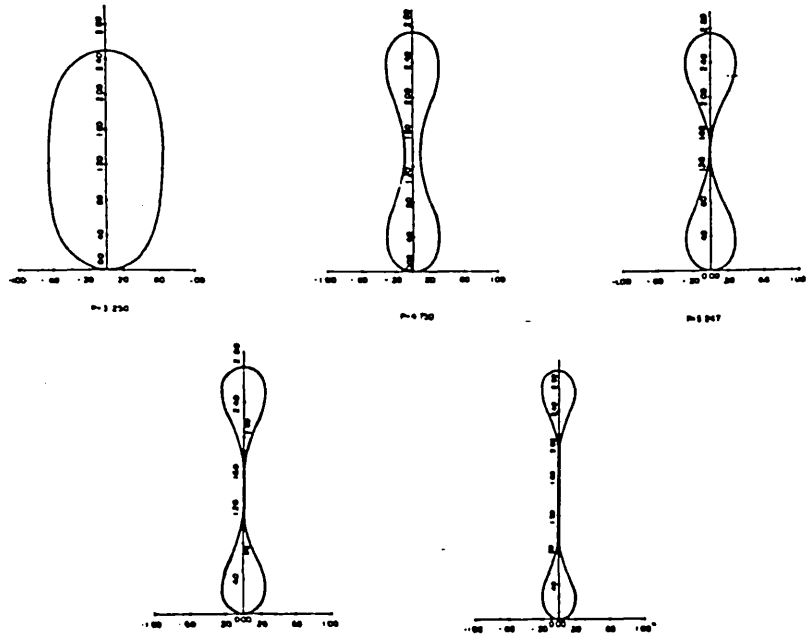


Fig 4.4.2 Possible configurations of the cross-section of a collapsible tube at negative values of transmural pressure. (From Flaherty et al, 1972).

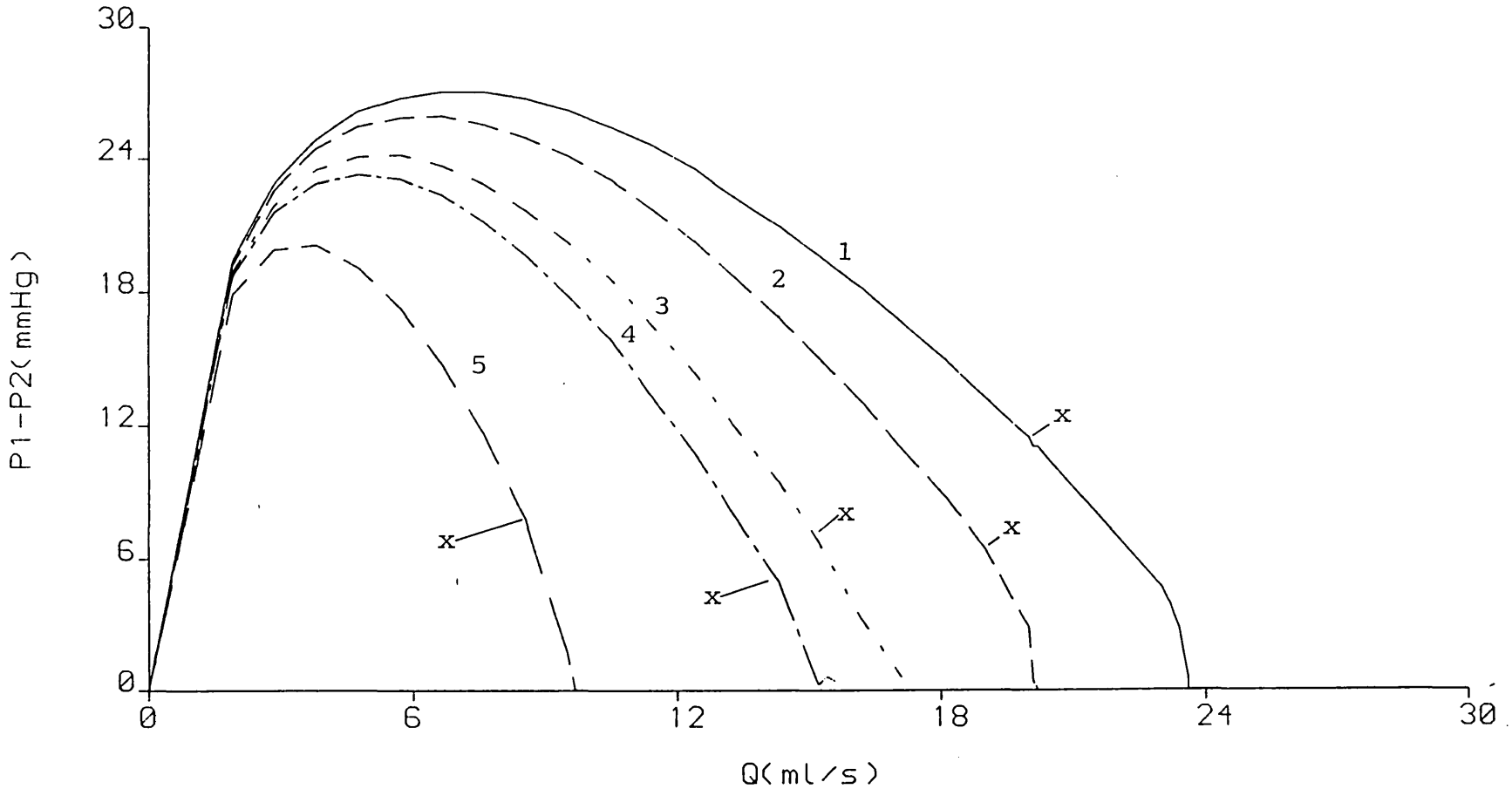



Fig 4.4.3 P-Q characteristics for different values of the downstream resistance ($R_2$, $k_2$), using the distributed parameter model, and data from Conrad (1969). The curve number corresponds to the downstream resistance given in the text and a 'x' indicates the point on the curve beyond which an increase in Q results in a decrease in $p_h$. $R_A$ = 0.7, $R_f$ = 3, $c_1$ = 2.7.

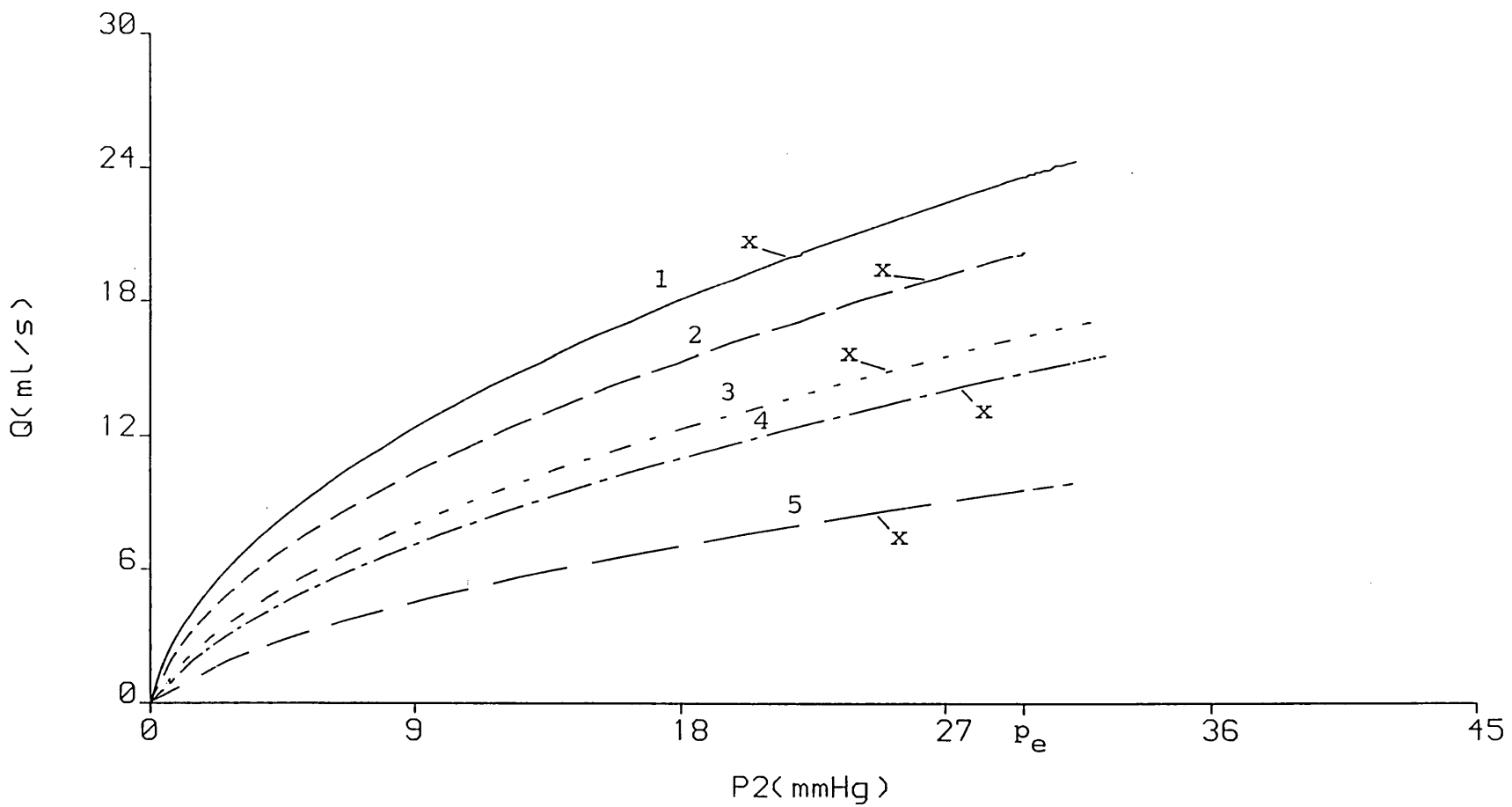



Fig 4.4.4 Downstream pressure as a function of flow rate for different values of the downstream resistance ($R_2$, $k_2$), using the distributed parameter model, and data from Conrad (1969). $R_A$ = 0.7, $R_f$ = 3, $c_1$ = 2.7. (Curve symbols are defined in Fig 4.4.3).

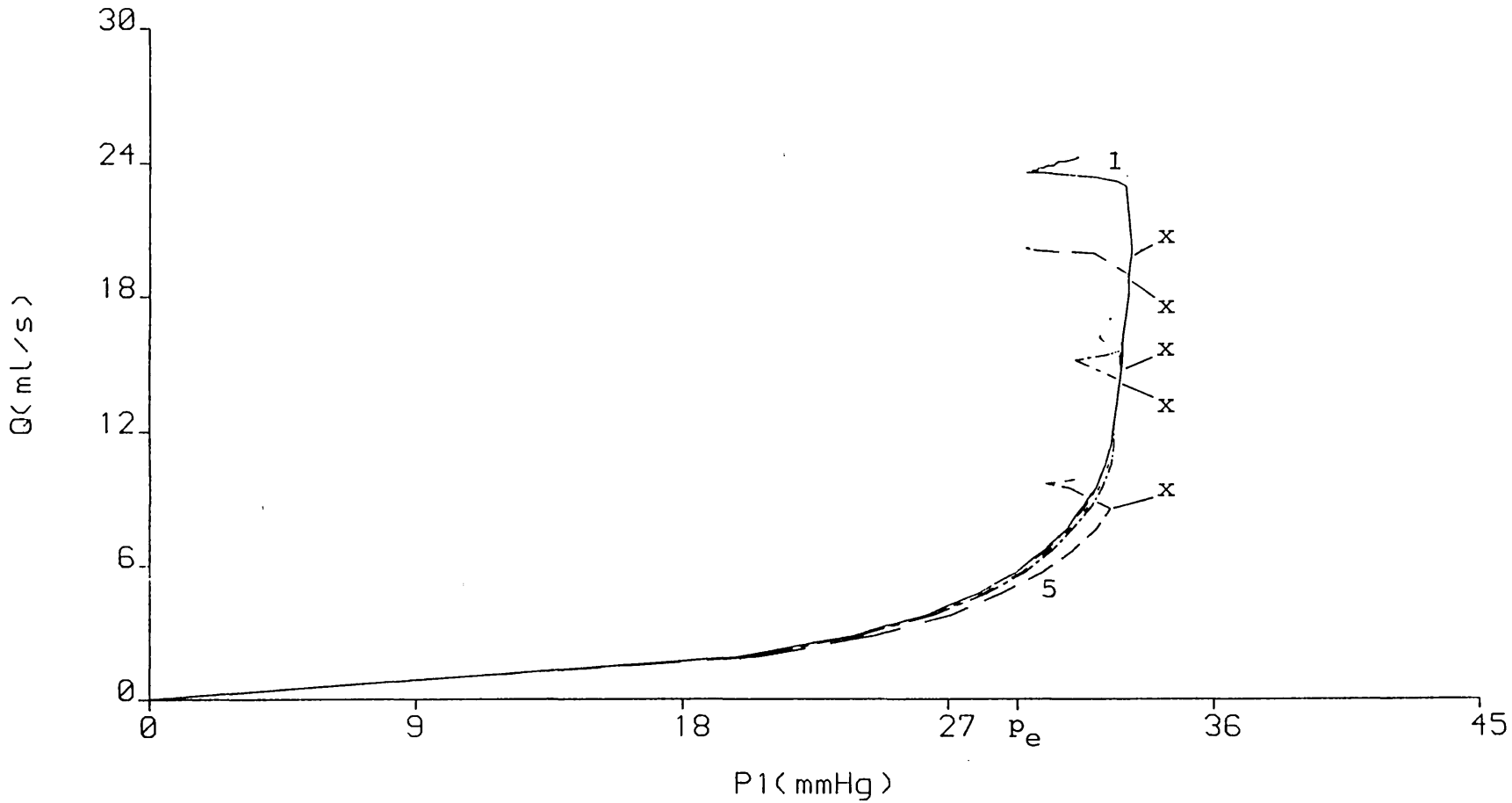



Fig 4.4.5 Upstream pressure as a function of flow rate for different values of the downstream resistance ($R_2$, $k_2$), using the distributed parameter model, and data from Conrad (1969). $R_A$ = 0.7, $R_f$ = 3, $c_1$ = 2.7. (Curve symbols are defined in Fig 4.4.3).

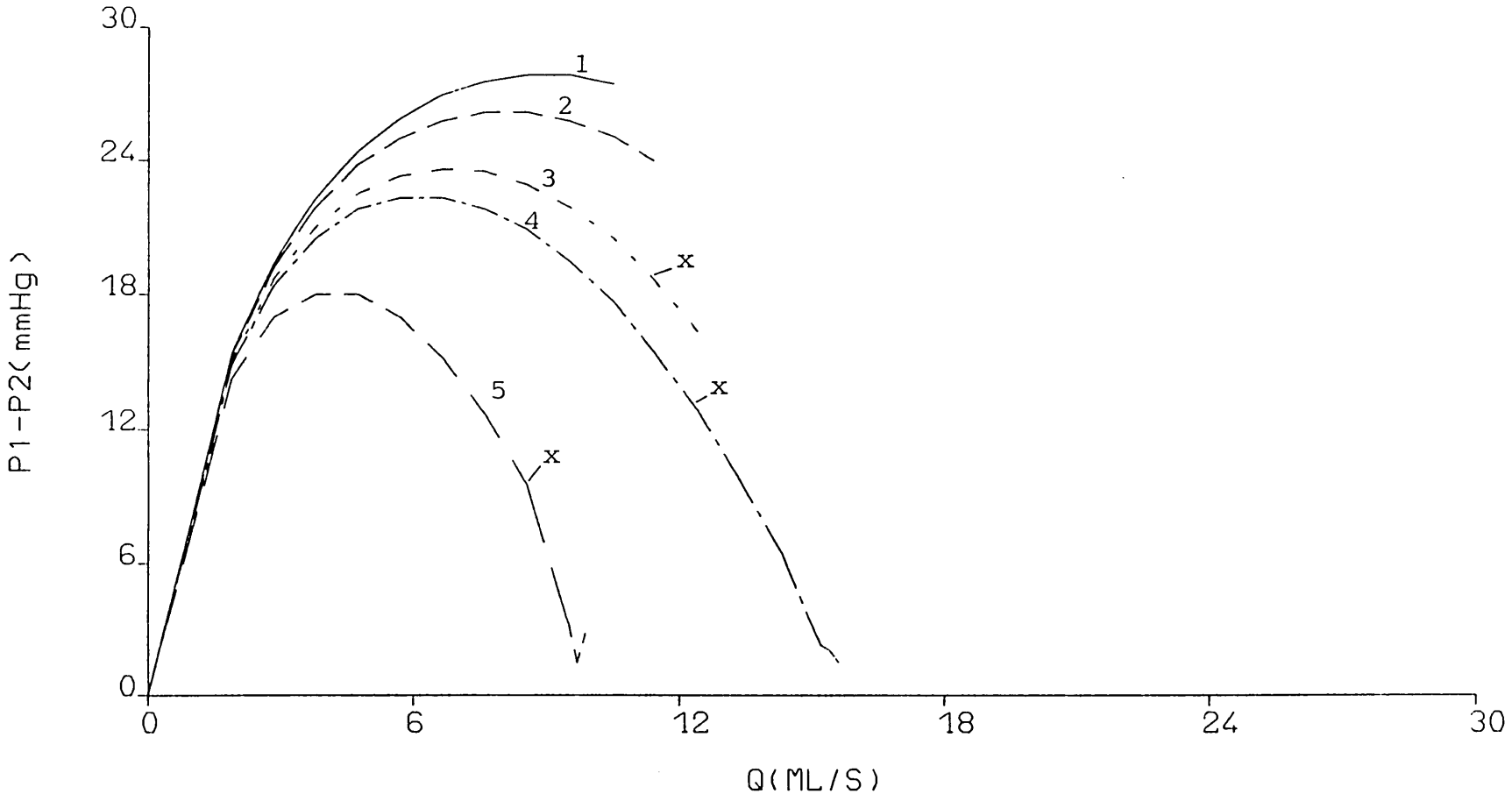



Fig 4.4.6 P-Q characteristics for different values of the downstream resistance ($R_2$, $k_2$), using the distributed parameter model, and data from Conrad (1969); except for the parameter h (tube wall thickness). $R_A = R_f = 1$, $c_1 = 1.15$. (Curve symbols are defined in Fig 4.4.3).

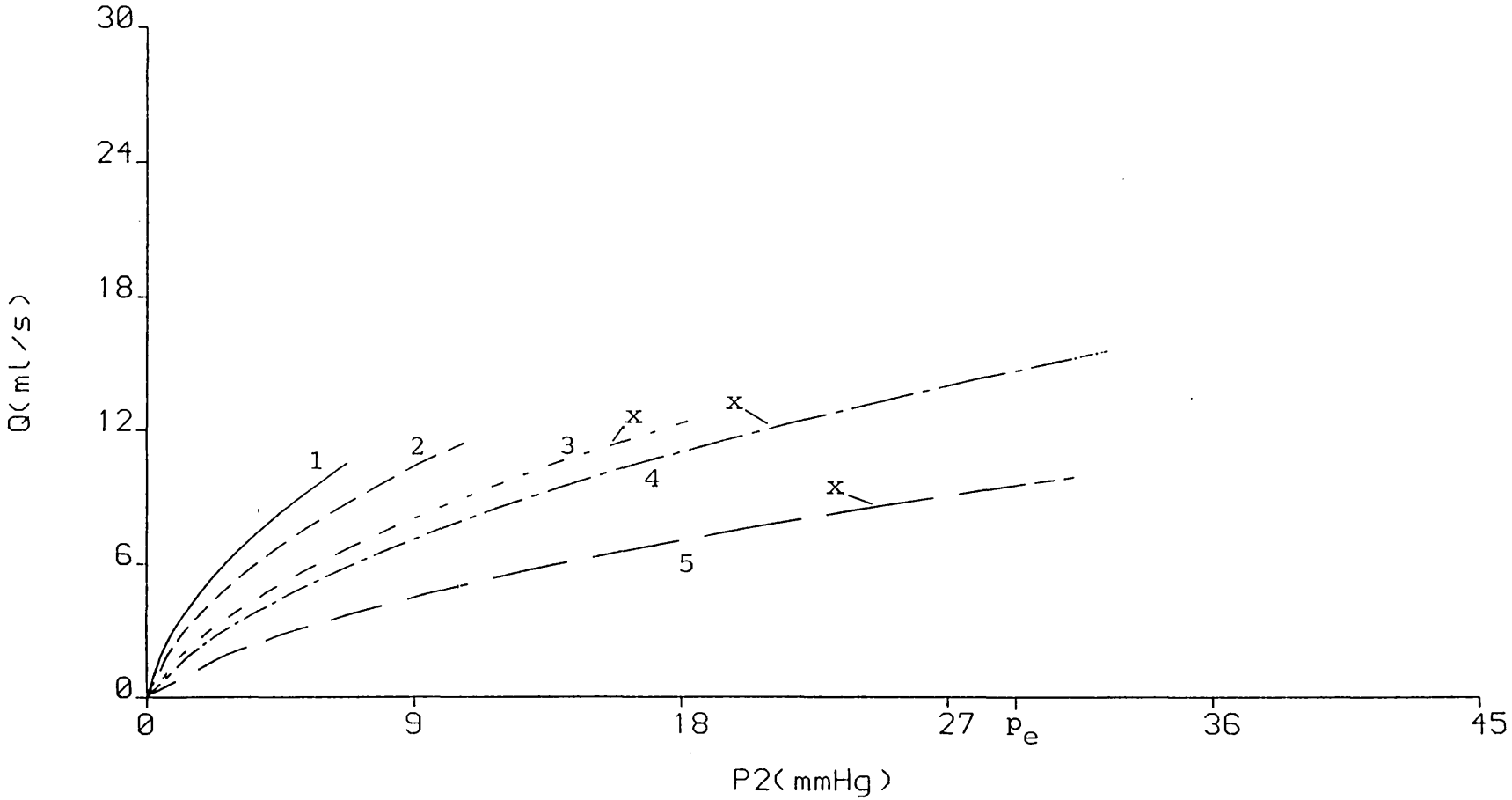



Fig 4.4.7 Downstream pressure as a function of flow rate for different values of the downstream resistance ($R_2$, $k_2$), using the distributed parameter model, and data from Conrad (1969); except for the parameter h (tube wall thickness). $R_A = R_f = 1$, $c_1 = 1.15$. (Curve symbols are defined in Fig 4.4.3).

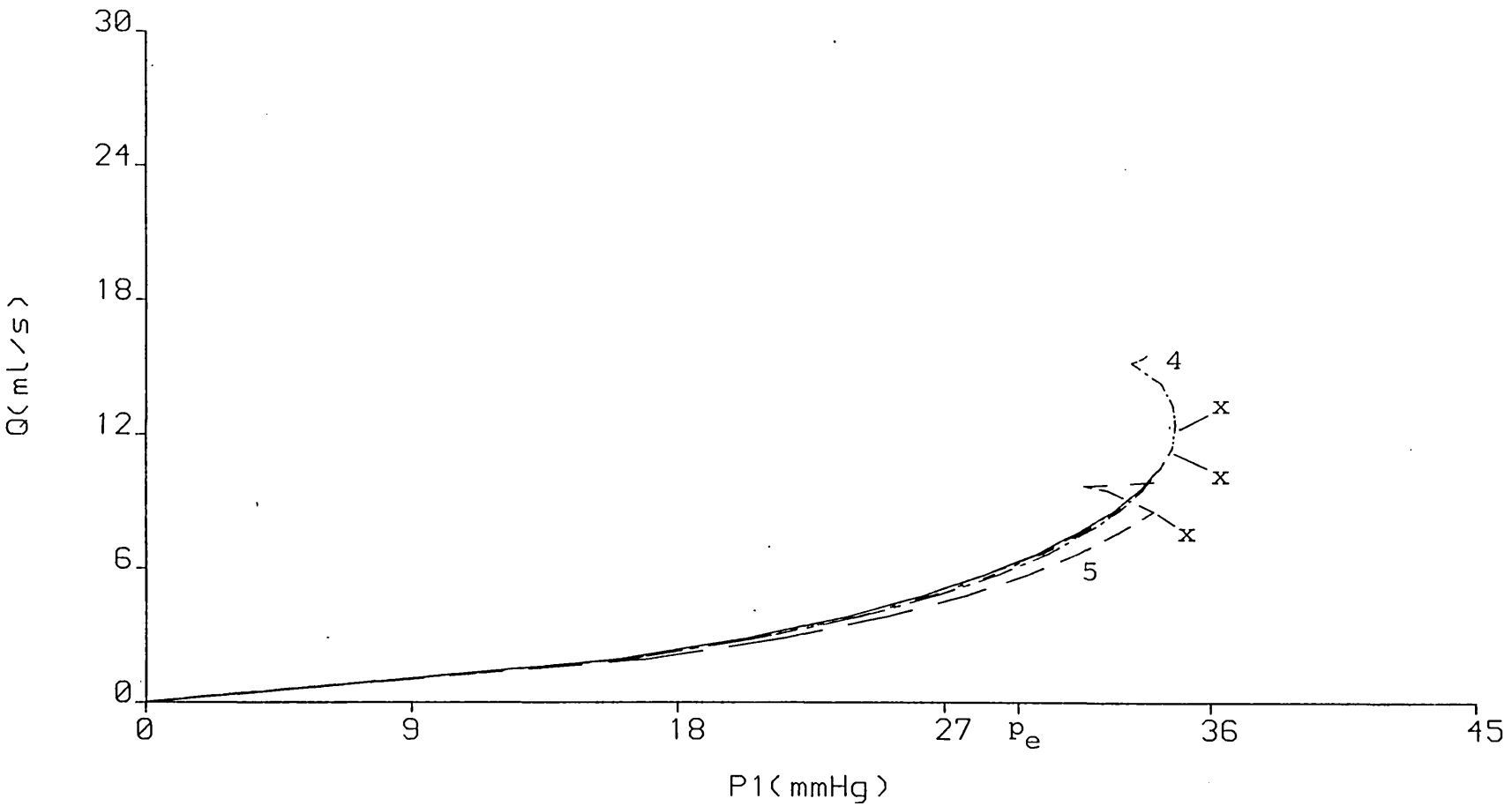



Fig 4.4.8 Upstream pressure as a function of flow rate for different values of the downstream resistance ($R_2$, $k_2$), using the distributed parameter model, and data from Conrad (1969); except for the parameter h (tube wall thickness). $R_A = R_f = 1$, $c_1 = 1.15$. (Curve symbols are defined in Fig 4.4.3).

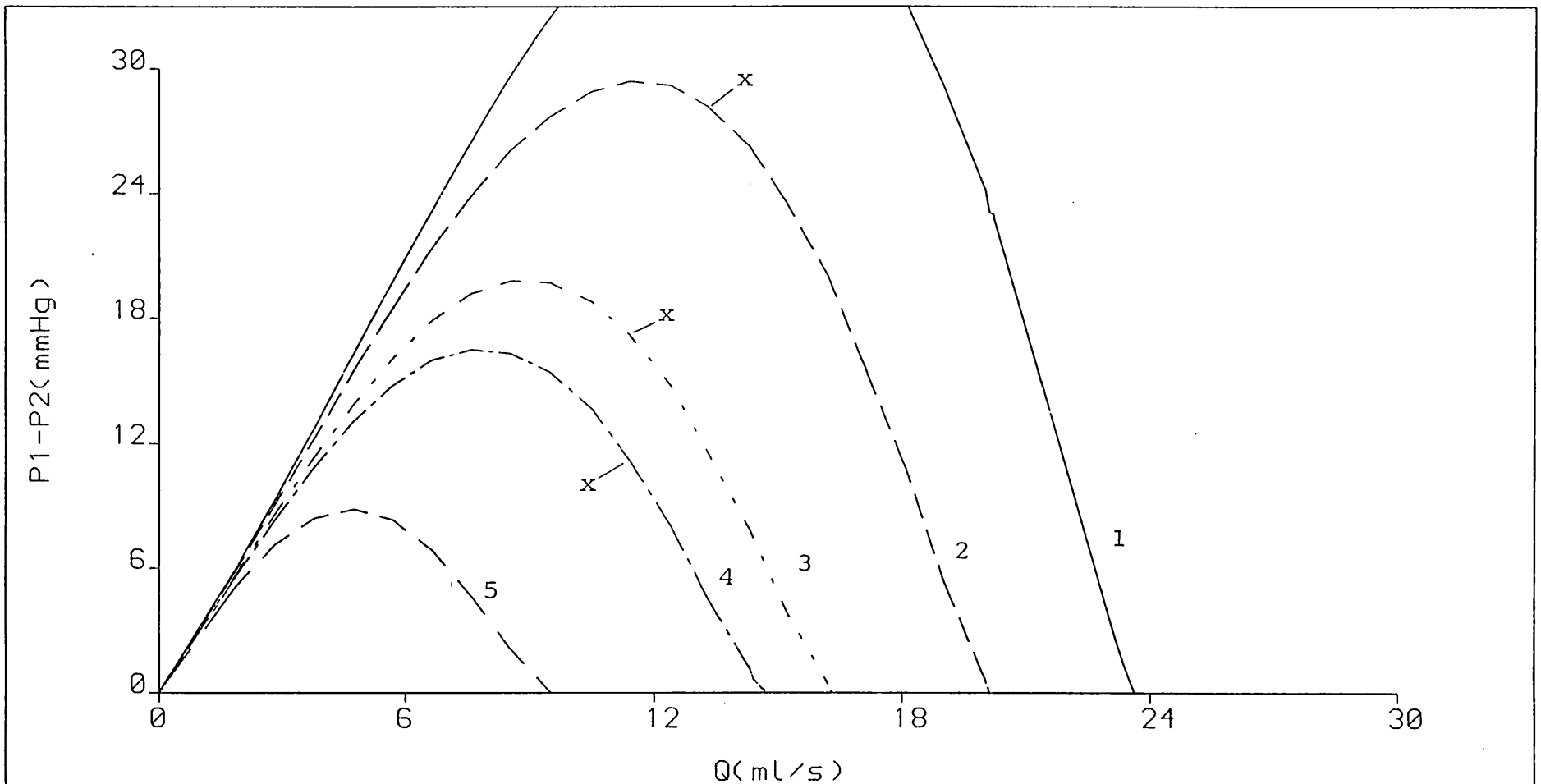



Fig 4.4.9 P-Q characteristics for different values of the downstream resistance ($R_2$, $k_2$), using the lumped parameter model of Bertram and Pedley (1982), and data from Conrad (1969); except for the parameter h (tube wall thickness). $R_A = R_f = 1$, $c_1 = 1.15$. (Curve symbols are defined in Fig 4.4.3).

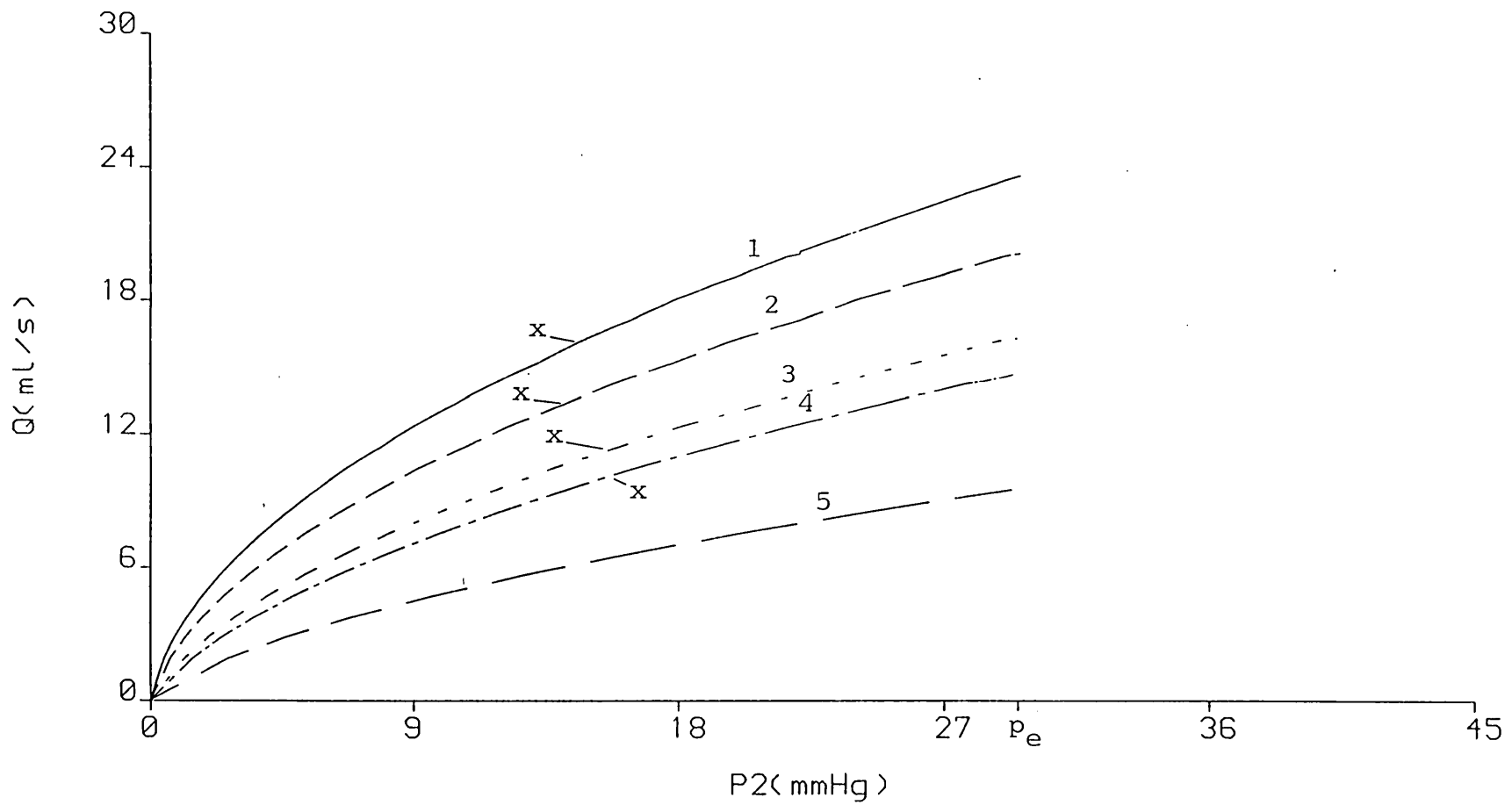



Fig 4.4.10 Downstream pressure as a function of flow rate for different values of the downstream resistance ($R_2$, $k_2$), using the lumped parameter model of Bertram and Pedley (1982), and data from Conrad (1969); except for the parameter h (tube wall thickness). $R_A = R_f = 1$, $c_1 = 1.15$. (Curve symbols are defined in Fig 4.4.3).

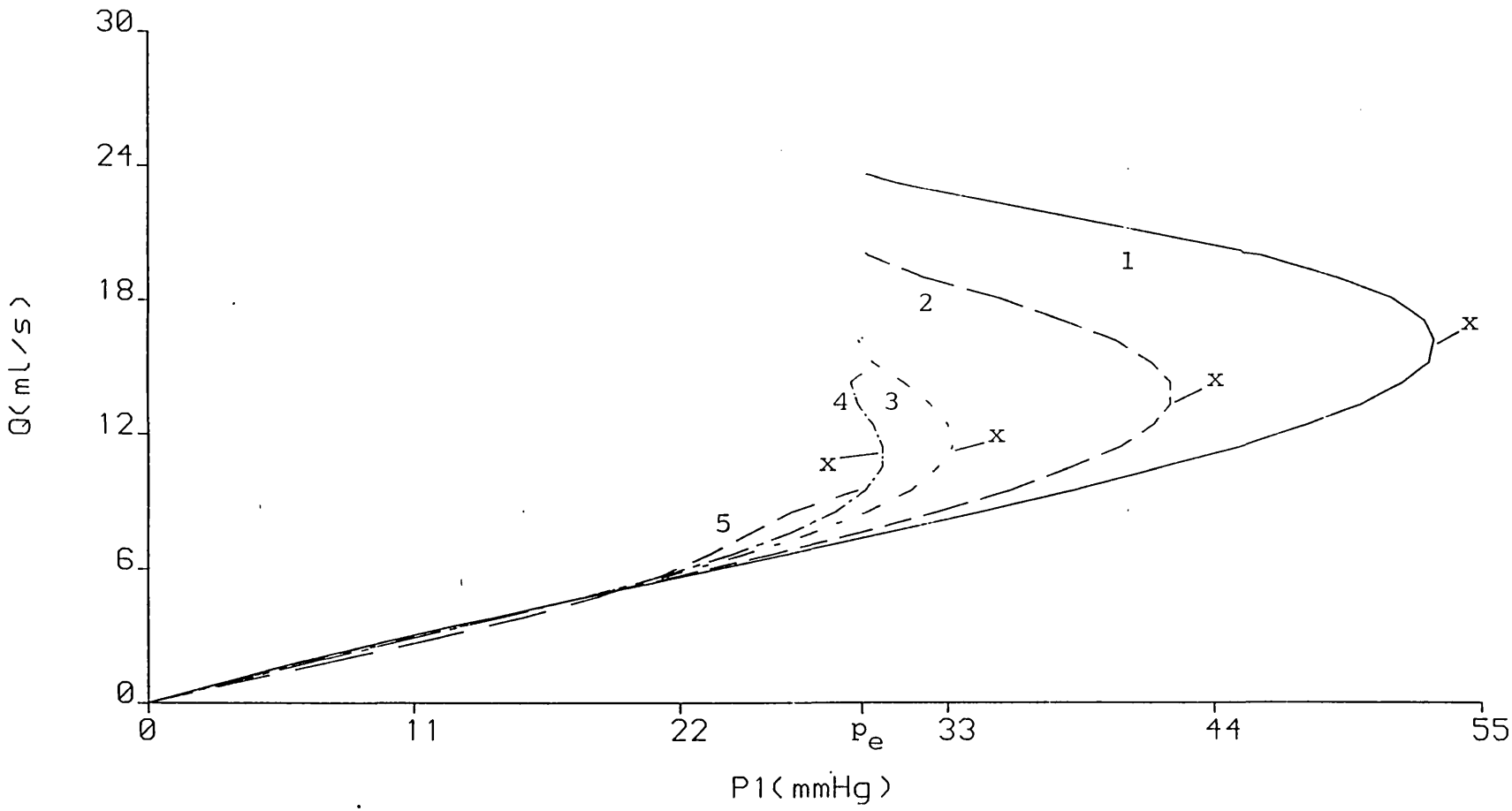



Fig 4.4.11 Upstream pressure as a function of flow rate for different values of the downstream resistance ($R_2$, $k_2$), using the lumped parameter model of Bertram and Pedley (1982), and data from Conrad (1969); except for the parameter h (tube wall thickness). $R_A = R_f = 1$, $c_1 = 1.15$. (Curve symbols are defined in Fig 4.4.3).

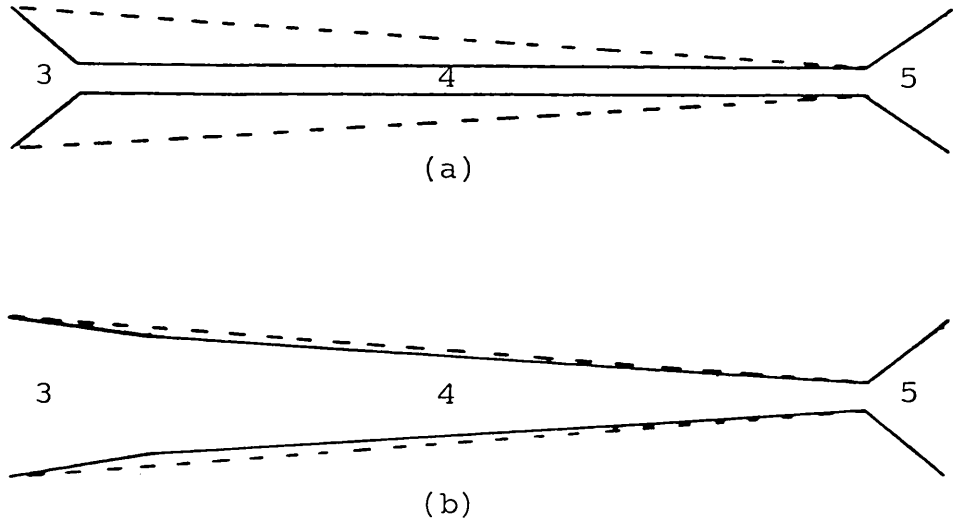



Fig 4.4.12 Typical side views of collapsible tube at (a) low flow rate and (b) medium/high flow rate; ---- corresponds to lumped parameter model approximation.

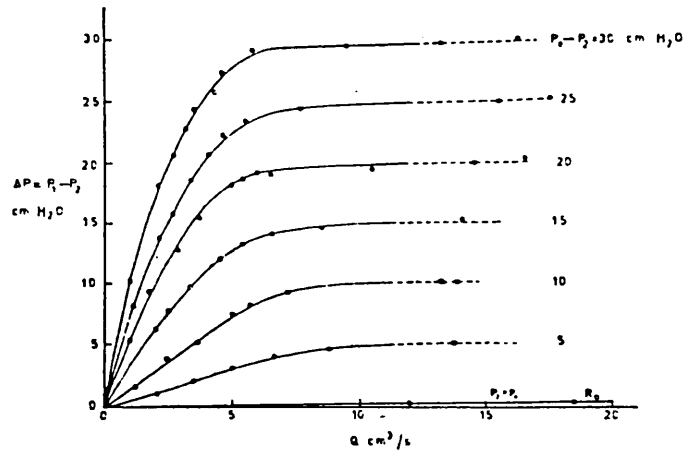



Fig 4.4.13 Experimentally determined P-Q characteristics at different values of $p_e - p_2$ = constant. (From Brower and Noordergraaf, 1978).

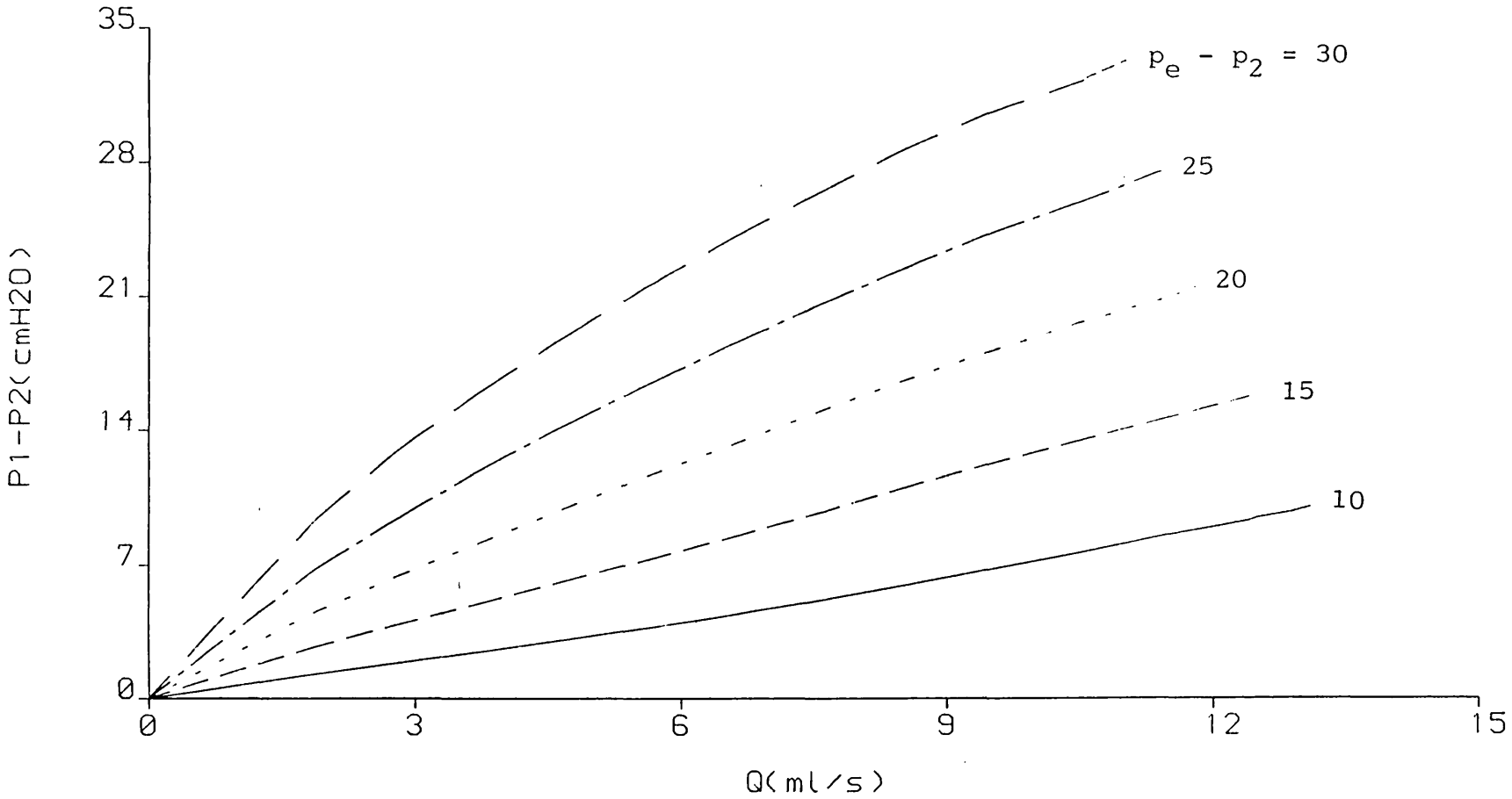



Fig 4.4.14 P-Q characteristics for different values of $p_e - p_2$ = constant, using the distributed parameter model, and data from Brower and Scholten (1975). The maximum Q in each curve corresponds to the flow rate at which choking occurs (cf Fig 4.4.13).

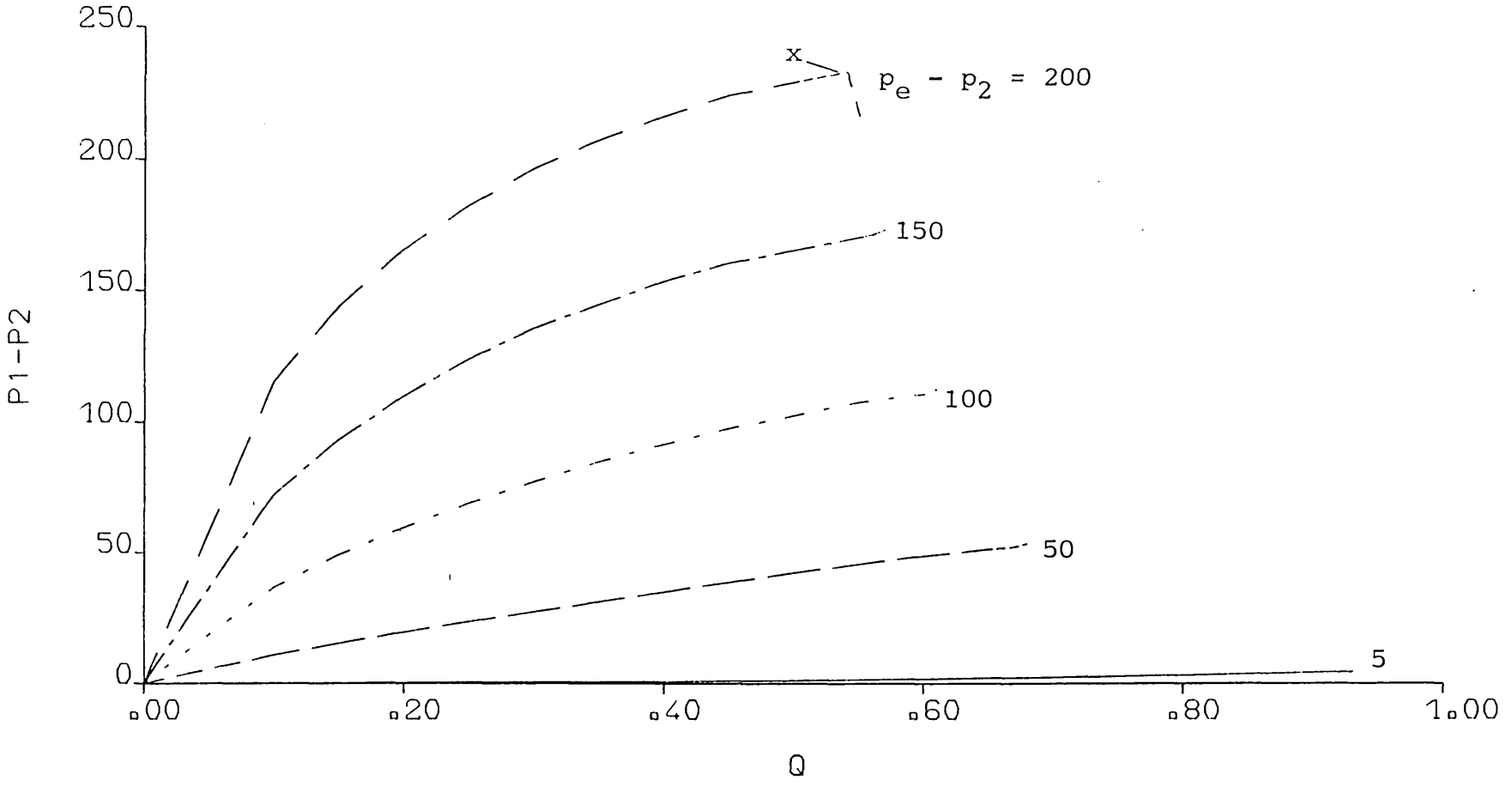



Fig 4.4.15 P-Q characteristics for different values of $p_e - p_2$ = constant, using the distributed parameter model. $L_3 = 2$, $L_4 = 10$, $c_1 = 1.15$. ('x' is defined in Fig 4.4.3).

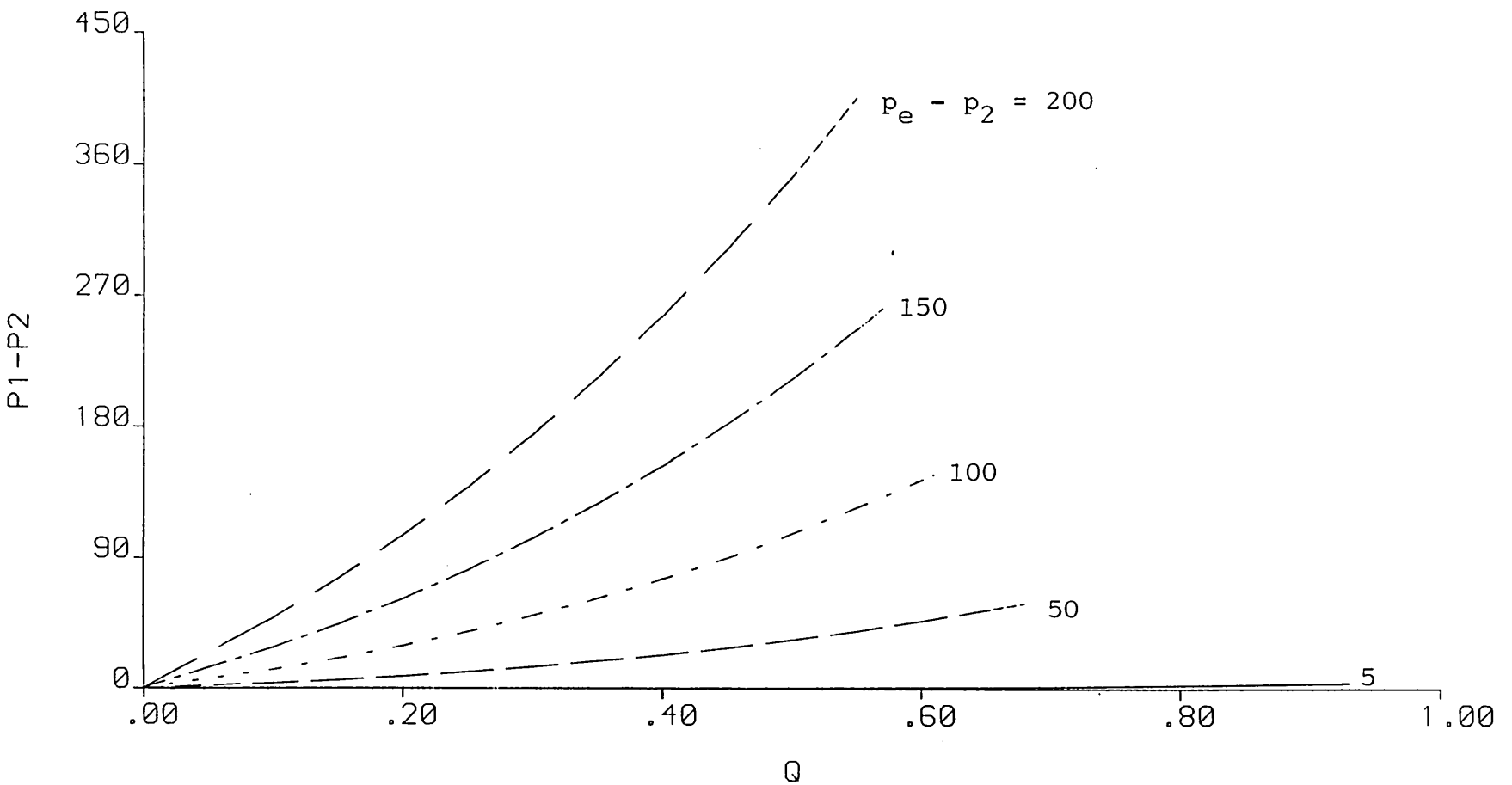



Fig 4.4.16 P-Q characteristics for different values of $p_e - p_2$ = constant, using the lumped parameter model of Bertram and Pedley (1982). $L_3 = 12$, $c_1 = 1.15$. Characteristics concave to Q = 0 axis (cf Fig 4.4.15).

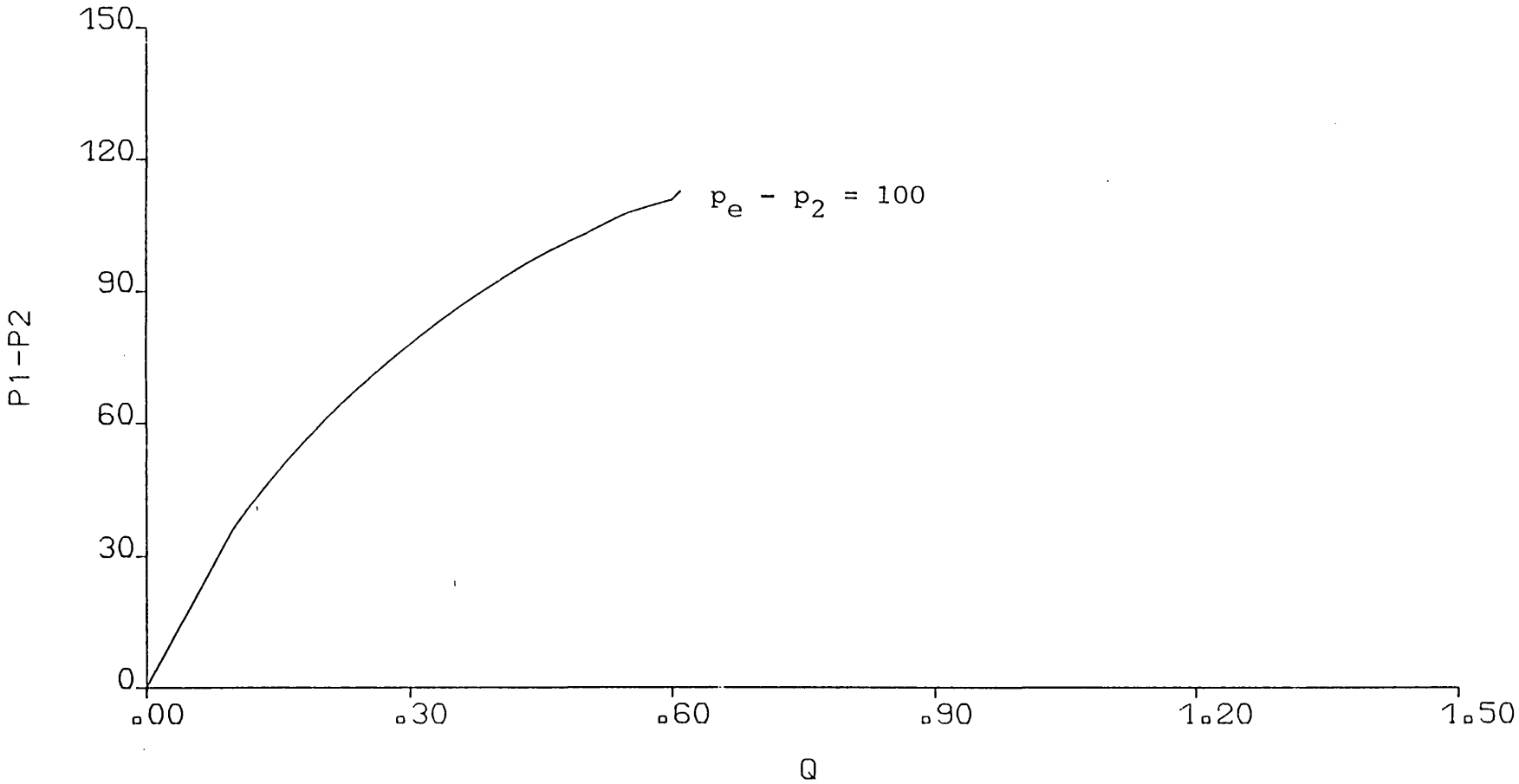



Fig 4.4.17 P-Q characteristic for $p_e - p_2 = 100$, taken from Fig 4.4.15.
Standard case: $L_3 = 2$, $L_4 = 10$, $c_1 = 1.15$, $R_k = 0.00466$.

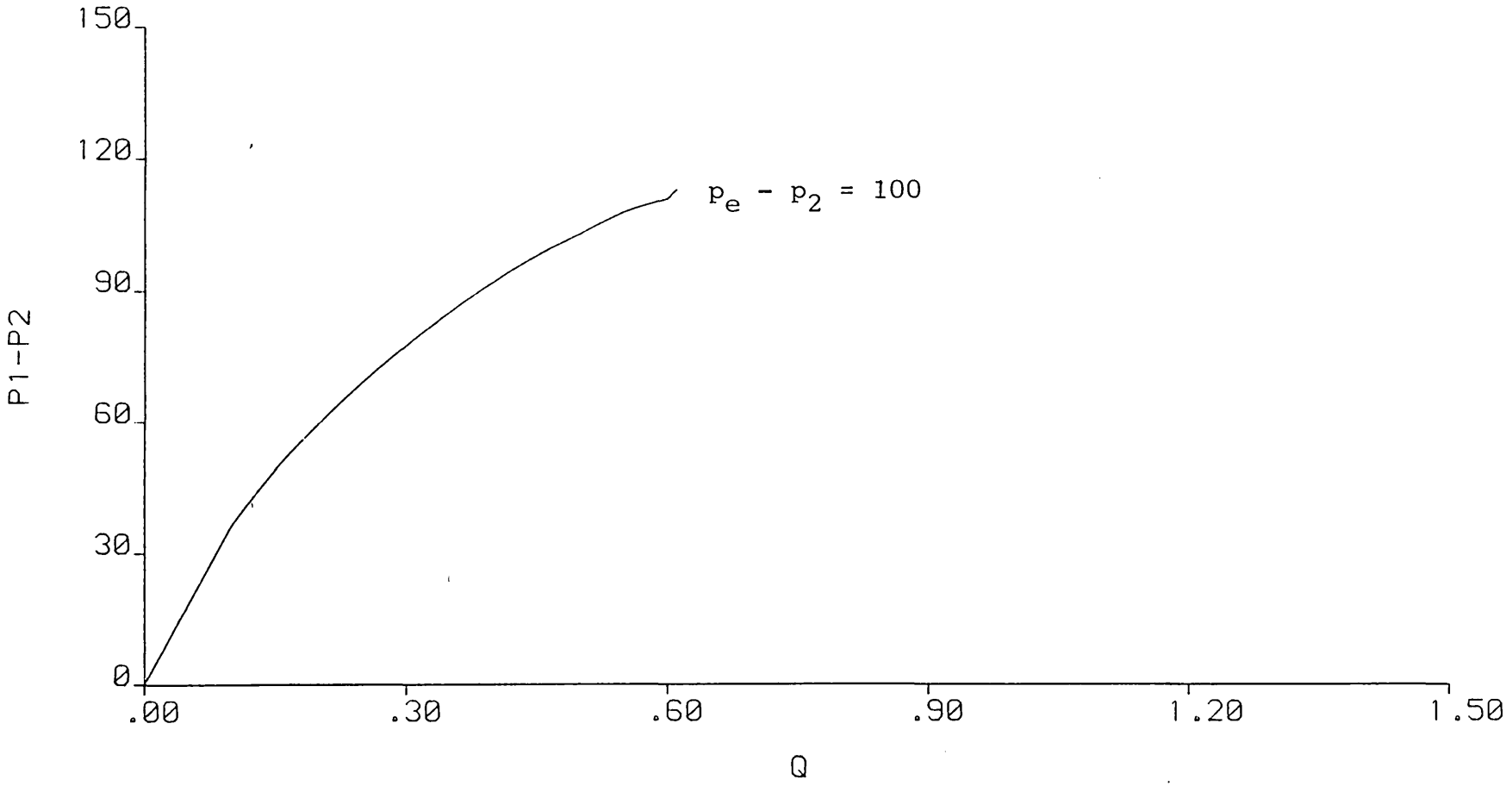



Fig 4.4.18 Effect on standard case of doubling $L_3$ (= 4) (cf Fig 4.4.17).

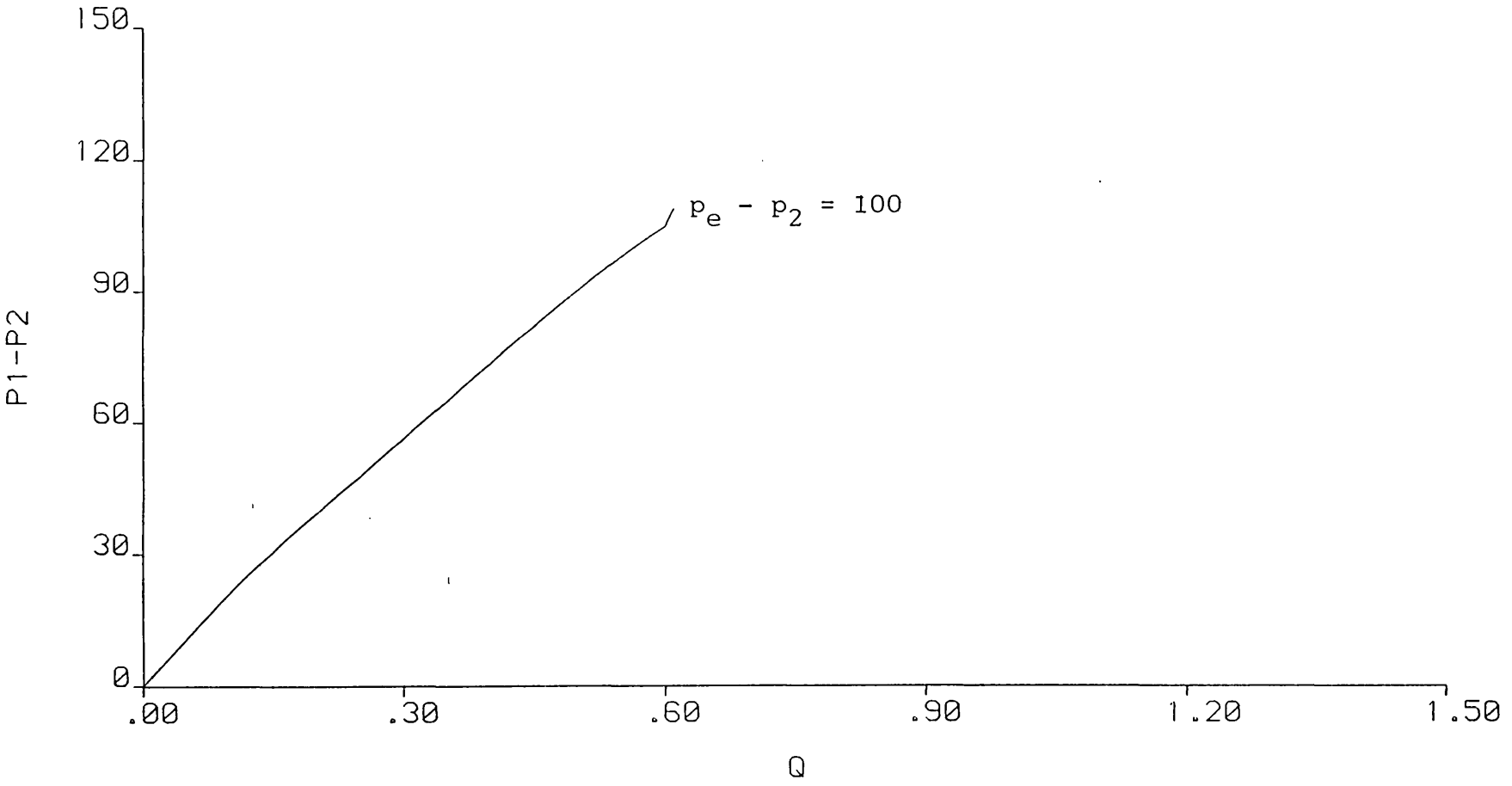



Fig 4.4.19 Effect on standard case of halving $L_4$ (= 5) (cf Figs 4.4.17 and 4.4.20).

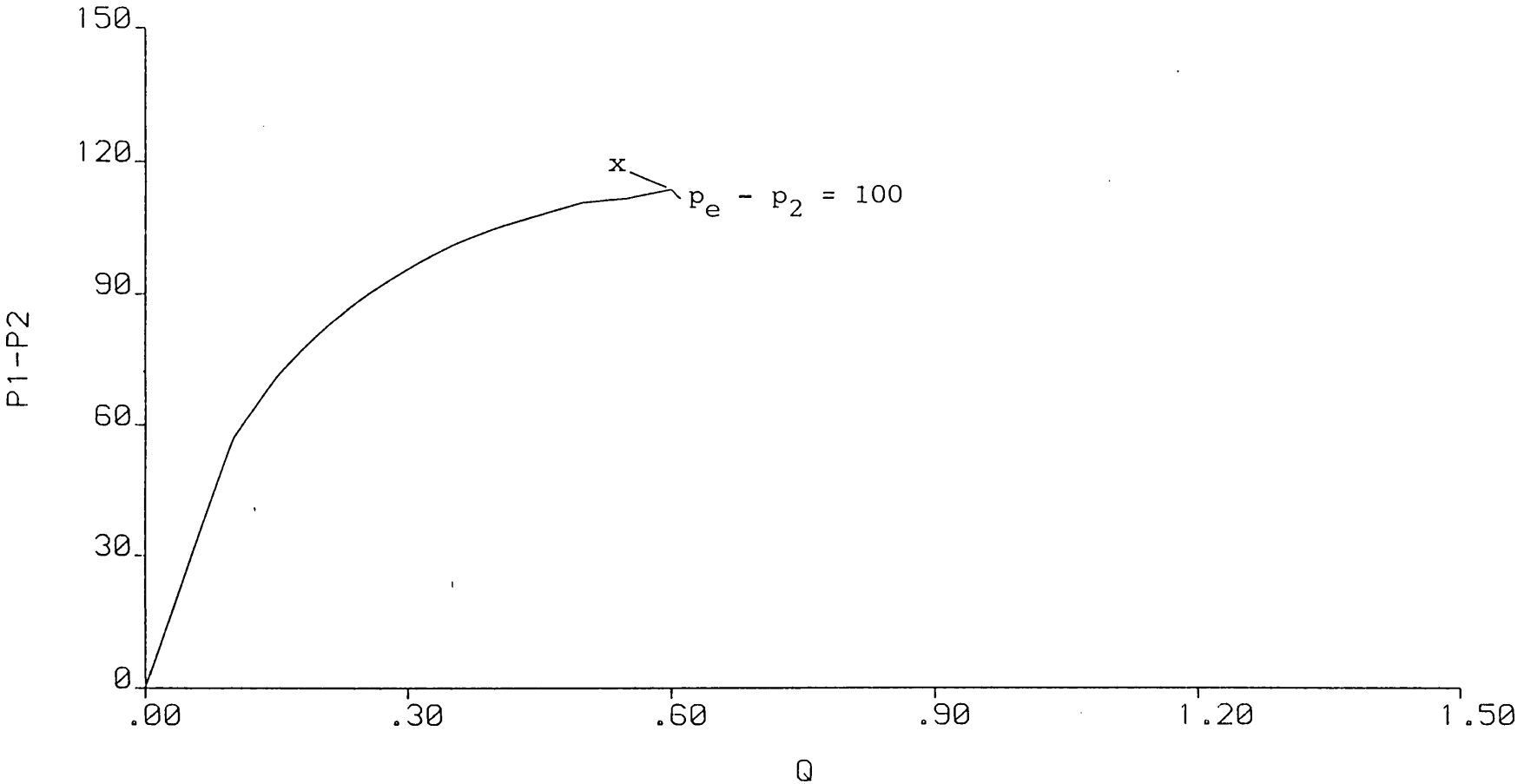



Fig 4.4.20 Effect on standard case of doubling $L_4$ (= 20) (cf Figs 4.4.17 and 4.4.19).

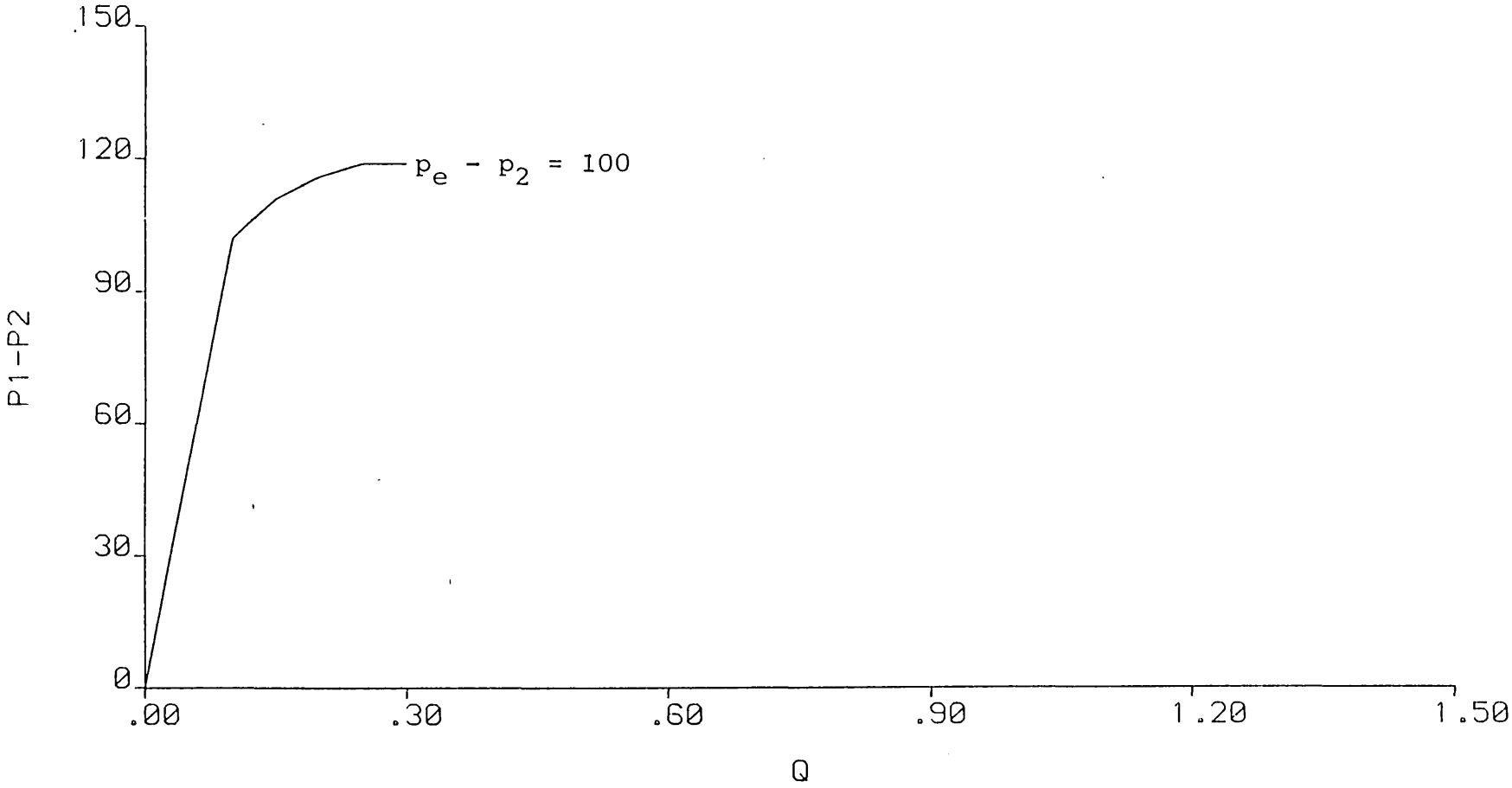



Fig 4.4.21 Effect on standard case of reducing $c_1$ (= 0.4) (cf Figs 4.4.17 and 4.4.22).

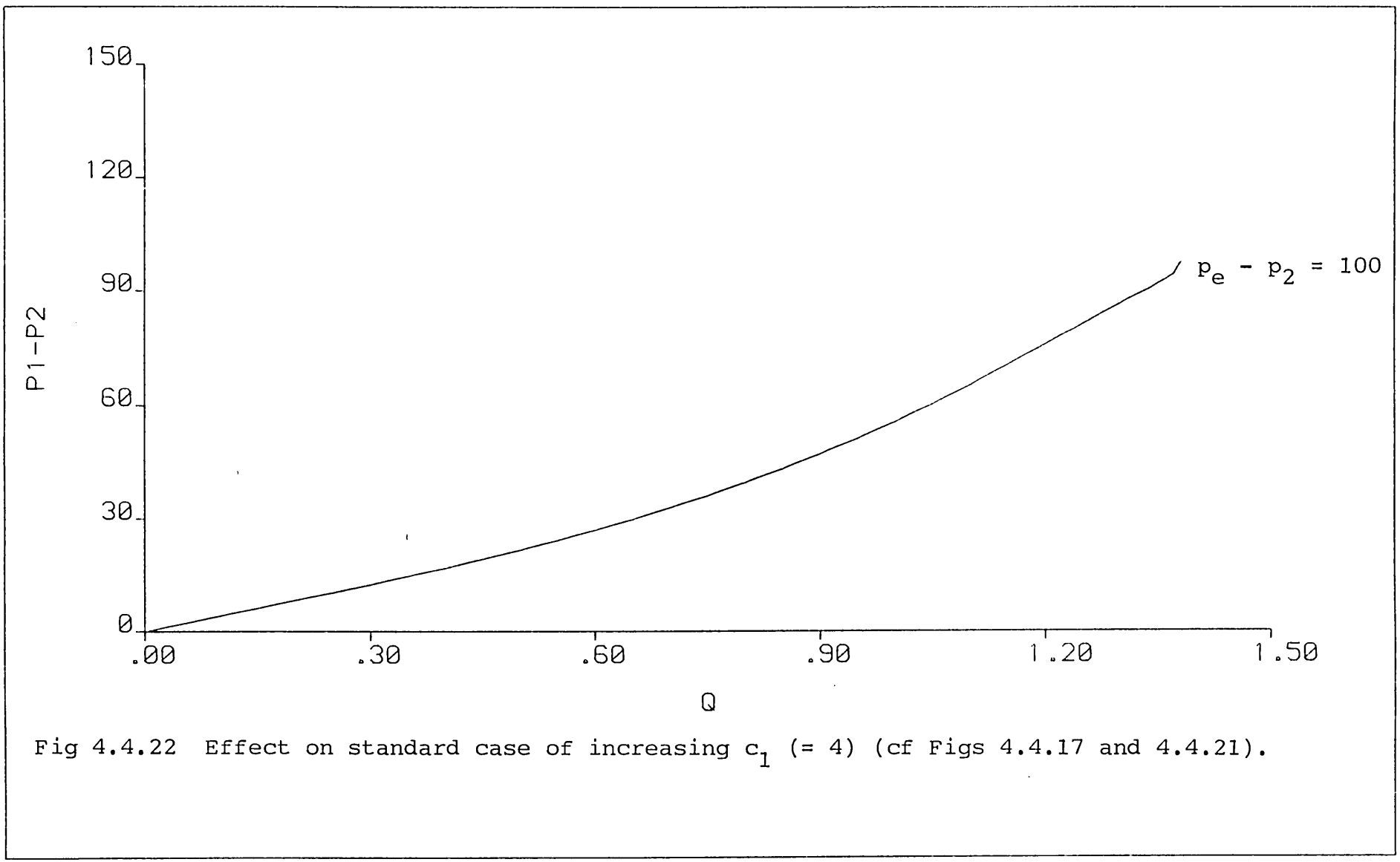



Fig 4.4.22 Effect on standard case of increasing $c_1$ (= 4) (cf Figs 4.4.17 and 4.4.21).

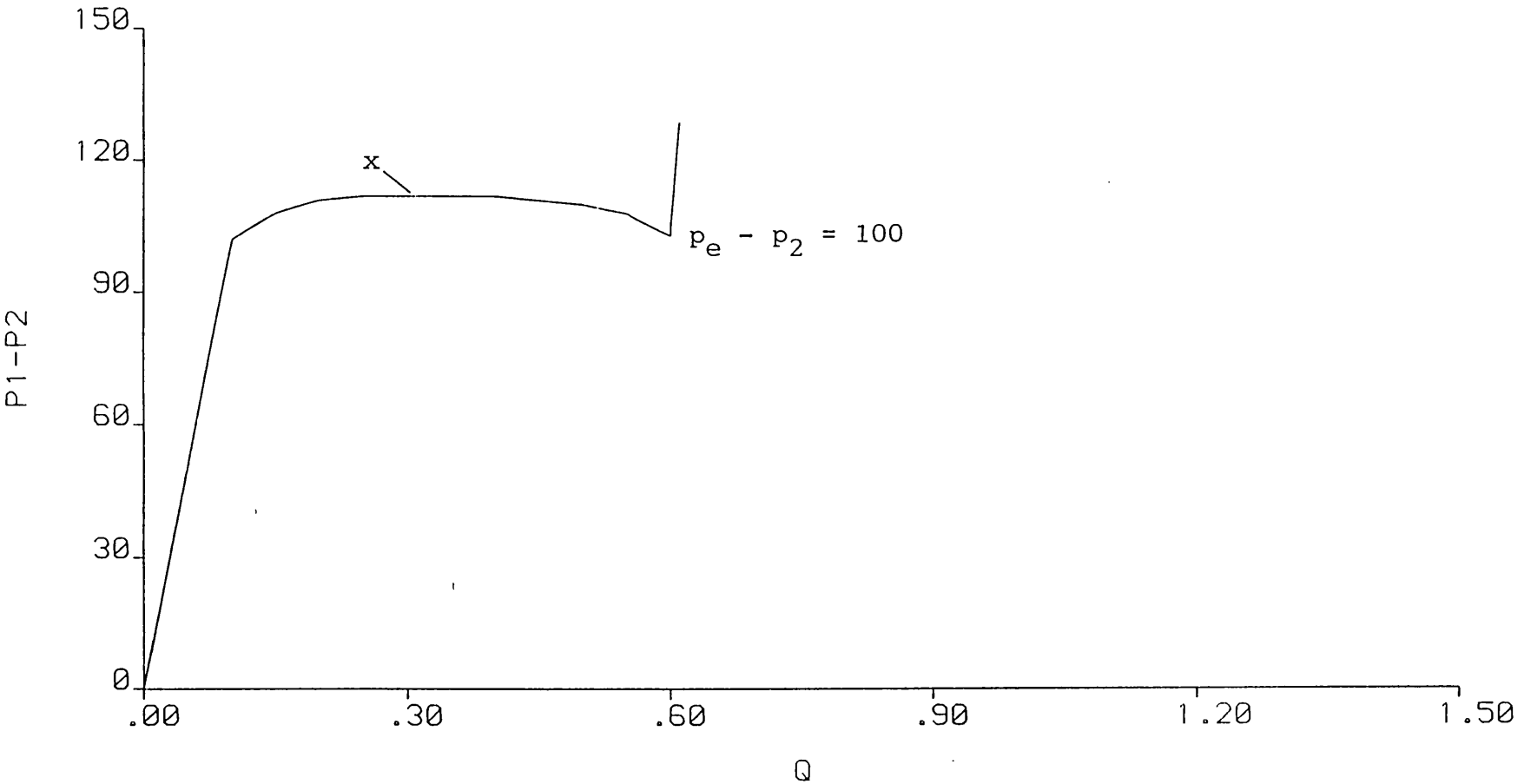



Fig 4.4.23 Effect on standard case of a tenfold increase in $R_k$ (= 0.0466) (cf Figs 4.4.17 and 4.4.24).

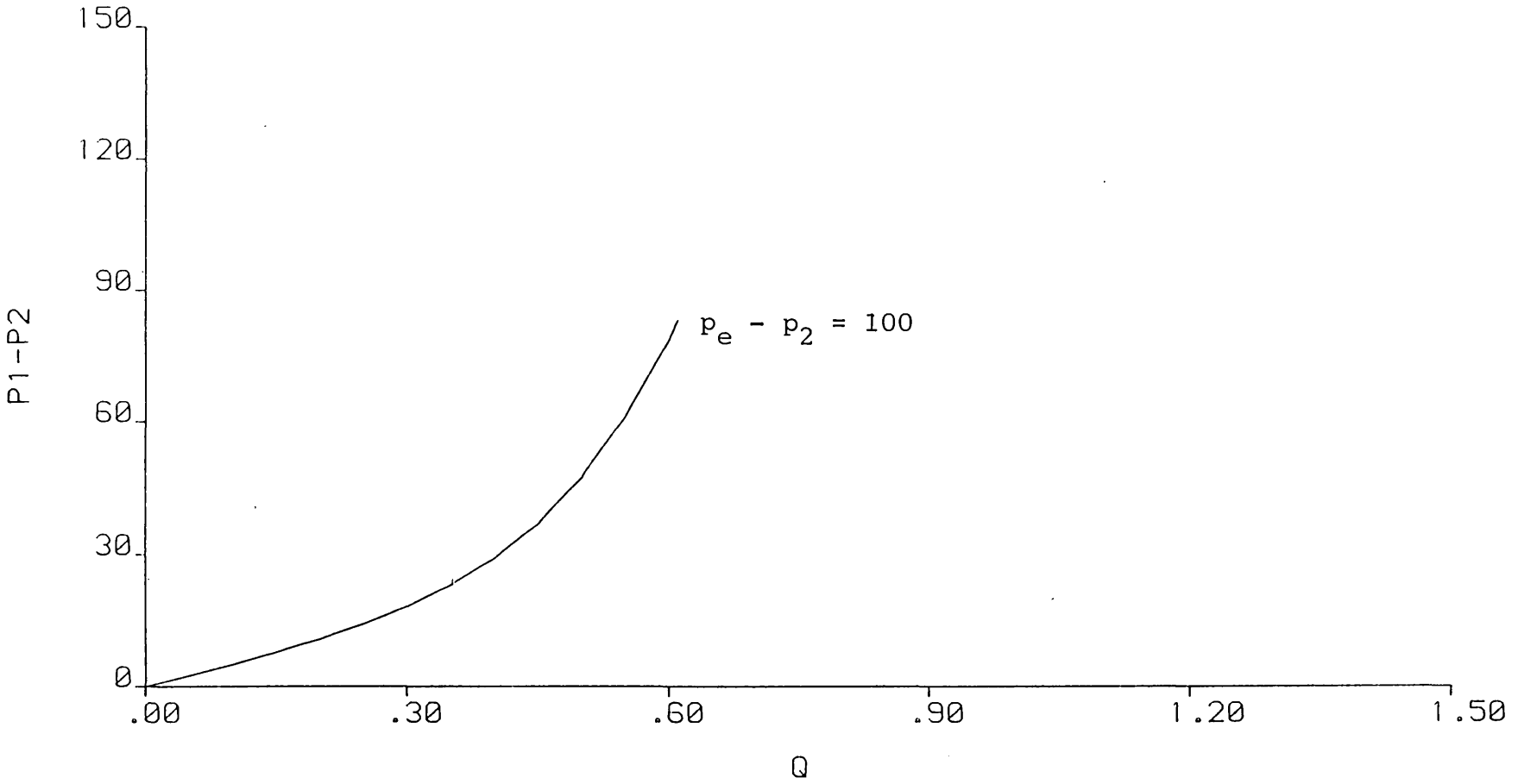



Fig 4.4.24 Effect on standard case of a tenfold decrease in $R_k$ (= 0.000466) (cf Figs 4.4.17 and 4.4.23).

# CHAPTER 5

# UNSTEADY FLOW

## 5.1 INTRODUCTION

Theoretical studies of unsteady flow in compliant vessels are fairly recent and have been primarily concerned with the tube in the distended regime (Streeter et al, 1963; Nicholson et al, 1967, among others). Some progress in understanding the 'collapsed' regime has been made through investigations by Kamm and Shapiro (1979), Bertram and Pedley (1982), among others.

In this chapter the equations governing unsteady flow in a collapsible tube are set out in a form which can be readily solved on a digital computer. The solution method used is based on the method of characteristics. This method is preferred to the finite difference methods which were tried at the early stages of this research. Some general test cases are examined to verify the applicability of the solution scheme to the present problem.

The main aim of this chapter is to develop an accurate, stable solution scheme which will be used in the next chapter to investigate the phenomenon of self-excited oscillations.

## 5.2 MODEL EQUATIONS

The dimensionless equations governing unsteady flow in region 4 are stated in Chapter 3 (see section 3.9):

$$\frac{\partial A}{\partial t} + A\frac{\partial u}{\partial x} + u\frac{\partial A}{\partial x} = 0 \qquad (5.2.1)$$

$$\frac{\partial u}{\partial t} + u\frac{\partial u}{\partial x} + \frac{c^2(A)}{A}\frac{\partial A}{\partial x} + R(A)Au = 0 \qquad (5.2.2)$$

$$p - p_e = P(A), \qquad (5.2.3)$$

where the choice of the functions $R(A)$ and $P(A)$ (and hence $c(A)$) depends upon the area of the cross-section of the tube and are defined as follows:

$(A < 1)$

$$R(A) = \frac{R_K}{A}(1 + A^{-2}) \qquad (5.2.4)$$

$$P(A) = c_1(1 - A^{-3/2}) \qquad (5.2.5)$$

$$c(A) = \left(A\frac{dP}{dA}\right)^{1/2} = \left(\frac{3}{2}c_1 A^{-3/2}\right)^{1/2} \qquad (5.2.6)$$

$(A \geq 1)$

$$R(A) = 2R_K A^{-2} \qquad (5.2.7)$$

$$P(A) = c_2(A - 1) \qquad (5.2.8)$$

$$c(A) = (c_2 A)^{1/2}. \qquad (5.2.9)$$

The tube law has already been used to eliminate the pressure from the momentum equation and now serves only to provide the pressure distribution from the calculated area distribution.

Equations (5.2.1) and (5.2.2) are a hyperbolic pair of quasi-linear, partial differential equations in the two dependent variables A and u and independent variables x and t. A solution scheme for these equations is now developed which is based on the method of characteristics.

## 5.3 METHOD OF CHARACTERISTICS

Numerous methods are availabe for the numerical solution of hyperbolic equations (see, for example Smith, 1978). Each of the methods has its merits, however, the

method of characteristics provides a greater physical understanding of the problem and in many cases is found to be the most accurate method (Evangelisti, 1969; Yevjevich et al, 1970; Fox, 1977). The method of characteristics, in essence, transforms the partial differential equations into particular total differential equations. These latter equations are then integrated to yield finite difference equations which are solved numerically.

Equations (5.2.1) and (5.2.2) are transformed into four ordinary differential equations by the method of characteristics (Appendix B),

$C_+$

$$\frac{dA}{dt} + \frac{A}{c}\frac{du}{dt} + \frac{RA^2u}{c} = 0 \qquad (5.3.1)$$

$$\frac{dx}{dt} = u + c \qquad (5.3.2)$$

$C_-$

$$\frac{dA}{dt} - \frac{A}{c}\frac{du}{dt} - \frac{RA^2u}{c} = 0 \qquad (5.3.3)$$

$$\frac{dx}{dt} = u - c . \qquad (5.3.4)$$

Equation (5.3.1) is the condition which must be satisfied along the $C_+$ characteristic (Fig 5.3.1) whose direction is given by equation (5.3.2). Similarly, equation (5.3.3) holds in the direction given by equation (5.3.4). No mathematical approximations have been made in this transformation of the original partial differential equations. Thus every solution of this set of equations is a solution of the original equations (5.2.1) and (5.2.2).

5.3.1 Integration of the Characteristic Equations

Since R(A) and c(A) (and hence the slope of the characteristics) can vary substantially along the tube, a second order approximation is used to integrate equations (5.3.1) - (5.3.4). The result of using a first order approximation for high friction flow can in extreme cases lead to instability in the solution (Wylie and Streeter, 1978). Equations (5.3.1) and (5.3.3) can be put in a variety of forms before integration. In fact to determine the 'correct' form the steady flow equations must also be considered; since the steady flow solution should be a special case of these unsteady equations. Introducing the volume flow rate Q,

where $$Q = Au$$

then $$dQ = A\,du + u\,dA \,. \qquad (5.3.5)$$

Combining equations (5.3.1) and (5.3.5) results in the equation

$$dA - \frac{dQ}{u-c} - \frac{RA^2u}{(u^2-c^2)}\,dx = 0 \,, \qquad (5.3.6)$$

and combining equations (5.3.3) and (5.3.5),yields

$$dA - \frac{dQ}{u+c} - \frac{RA^2u}{(u^2-c^2)}\,dx = 0 \,. \qquad (5.3.7)$$

If dQ = 0 then both equations (5.3.6) and (5.3.7) agree with the steady flow equation in the differential form (equation (4.3.3)). Integration of equations (5.3.6) and (5.3.7) using the trapezoidal rule, yields

$$(A_P - A_R) - \frac{1}{2}\left[\frac{1}{(u-c)_P} + \frac{1}{(u-c)_R}\right](Q_P - Q_R)$$

$$- \frac{1}{2}\left[\left(\frac{RA^2u}{u^2-c^2}\right)_P + \left(\frac{RA^2u}{u^2-c^2}\right)_R\right](x_P - x_R) = 0 \qquad (5.3.8)$$

and

$$(A_P - A_S) - \frac{1}{2}\left[\frac{1}{(u+c)_P} + \frac{1}{(u+c)_S}\right](Q_P - Q_S)$$

$$\frac{1}{2}\left[\left(\frac{RA^2u}{u^2-c^2}\right)_P + \left(\frac{RA^2u}{u^2-c^2}\right)_S\right](x_P - x_S) = 0. \qquad (5.3.9)$$

It is assumed that $x_R$, $u_R$, $A_R$ and the corresponding values at the point s are known (Fig 5.3.2). For steady flow the subscript $P$ can be replaced by the subscript $C$ and $Q_C = Q_S = Q_R$. Equations (5.3.8) and (5.3.9) then agree with the steady flow equation applied to the points $R$, $C$ and $S$. Integration of equations (5.3.2) and (5.3.4), yields

$$t_P - t_R = \frac{1}{2}\left[\left(\frac{1}{u+c}\right)_P + \left(\frac{1}{u+c}\right)_R\right](x_P - x_R) \qquad (5.3.10)$$

and

$$t_P - t_S = \frac{1}{2}\left[\left(\frac{1}{u-c}\right)_P + \left(\frac{1}{u-c}\right)_S\right](x_P - x_S), \qquad (5.3.11)$$

respectively where it is assumed that $t_R$ and $t_S$ are known. Equations (5.3.8) - (5.3.11) are written in the form

$$(A_P - A_R) - \frac{1}{2}\left[(\zeta_-)_P + (\zeta_-)_R\right](Q_P - Q_R) \qquad (5.3.12)$$

$$- \frac{1}{2}\left[F_P + F_R\right](x_P - x_R) = 0$$

$$t_P - t_R = \frac{1}{2}\left[(\zeta_+)_P + (\zeta_+)_R\right](x_P - x_R) \qquad (5.3.13)$$

$$(A_P - A_S) - \tfrac{1}{2}[(\zeta_+)_P + (\zeta_+)_S](Q_P - Q_S) - \tfrac{1}{2}[F_P + F_S](x_P - x_S) = 0 \qquad (5.3.14)$$

$$t_P - t_S = \tfrac{1}{2}[(\zeta_-)_P + (\zeta_-)_S](x_P - x_S) \quad , \qquad (5.3.15)$$

where $F = RA^2u\zeta_+\zeta_-$ and $\zeta_+ = \frac{1}{u+c}$ , $\zeta_- = \frac{1}{u-c}$ .

The above equations involve the four unknowns $A_P$, $u_P$, $x_P$ and $t_P$. There are two possible approaches to the numerical solution (see for example Wylie and Streeter, 1978): (i) the grid of characteristics, (ii) the method of specified time intervals. The latter method uses a rectangular grid and $x_P$ and $t_P$ are assigned definite values throughout the computation. It is then very easy to introduce boundary conditions at predefined times. Further, since the values of the variables at predefined positions in space and time are usually required, this method is very desirable. One penalty to pay for using this method, however, is that interpolation is required to determine the values at R and S (see Fig 5.3.2), which decreases the computational accuracy‡.

The characteristics grid (Fig 5.3.3) avoids the possibility of the interpolation error by using a direct solution of (5.3.12) - (5.3.15). The grid is not imposed on the characteristics as in (ii) but develops naturally as the characteristic curves intersect. It is apparent

---

‡ These interpolations also produce a slight incompatability with initial conditions obtained from the steady flow equations. This is usually very small.

that there is no control over the position of the points of intersection in the x-t plane and indeed an interpolation is required to obtain values at a prescribed position.

The method of specified time intervals (STI) is employed in the present problem because it gives the information required at the points in the x-t plane specified by the user. Interest here is not in the detail of an event, for example, the development of an elastic jump (a problem for which the pure method of characteristics is ideally suited), but rather the overall behaviour of the collapsible tube when such a phenomenon occurs.

5.3.2 Method of Specified Time Intervals

The solution of the steady flow equations provides the initial conditions (at $t=0$) for the unsteady flow equations. The values of A and u are therefore known at discrete points (grid points) on the line $t=0$ in the x-t plane (Fig 5.3.2). To obtain the values of A and u at a typical point P (at $t=\Delta t$) the values of these variables at the points R and S are required. A first order interpolation is used, viz

$$u_R = u_C\left[1-(\zeta_+)_P^{-1}\theta\right] + u_A\,\theta(\zeta_+)_P^{-1} \qquad (5.3.16)$$

$$A_R = A_C\left[1-(\zeta_+)_P^{-1}\theta\right] + A_A\,\theta(\zeta_+)_P^{-1} \qquad (5.3.17)$$

$$u_S = u_C\left[1+(\zeta_-)_P^{-1}\theta\right] - u_B\,\theta(\zeta_-)_P^{-1} \qquad (5.3.18)$$

$$A_S = A_C\left[1+(\zeta_-)_P^{-1}\theta\right] - A_B\,\theta(\zeta_-)_P^{-1}\ , \qquad (5.3.19)$$

where $\theta = \Delta t/\Delta x$. There is no difficulty in using a higher order interpolation in the current scheme, however,

it proves to be inconvenient in the scheme presented later in this chapter.

With the interpolation formulae given above, the values of the variables at the points R and S depend upon those at A and C, and C and B, respectively.

5.3.3 Errors

All differencing schemes are subject to numerical errors. Some of the important errors which arise in the present scheme are now indicated together with the steps taken to minimise them.

Interpolation

The STI method has the advantage of enabling a common time increment to be applied to each point of the tube (cf characteristics grid). The major disadvantage is that interpolations are necessary which introduce an artificial (numerical) damping into the solution. As an example consider inviscid flow in a tube (Fig 5.3.4). A sharp transient at B should be felt at the other end of the tube at point D. However, if two grid lengths are used and there is a 50 per cent interpolation ( $\theta\zeta_-^{-1} = 0.5$ ) then 50 per cent of the change is transferred to point S and therefore is transferred to point U at time $\Delta t$. Furthermore 50 per cent of this change is transferred to point W and therefore to point Y. Thus 25 per cent of the original disturbance arrives at the other end of the tube ahead of time and is reflected back to the source in advance of the physical wave, thereby dampening the transient.

These errors can be reduced by increasing the

number of grid points. If $\Delta x$ were halved in the above example then the disturbance reaches the other end of the pipe at the same time as before, however, its magnitude is reduced by a factor of 4. The disadvantage of increasing the number of grid points is that the computer time required is increased due to both the extra grid point calculations and the increased number of time steps.

Another means of reducing these errors is to make the interpolation smaller (ie $\theta\zeta^{-1}$ close to unity). This may require the characteristic curves to cross more than a single reach (Fig 5.3.5). The values of the variables at $R$ and $S$ are then determined by interpolation in the interval $\Delta x$ in which they lie. This requires only a slightly more sophisticated computer program. It is more difficult to incorporate a higher order interpolation formula in such a scheme, however, as shown by Vardy (1976) a linear interpolation is quite adequate.

High Friction and Attenuation

If the energy losses due to viscous effects are quite large then a first order approximation may be inadequate. This would occur when the tube is 'collapsed' and therefore a second order integration is used (see earlier section).

Characteristic Curvature

Over most of the length of the tube, $(u-c)$ remains virtually constant (except near a throat), whereas $(u+c)$ can change by quite a large amount. Therefore it is important to use a sufficiently fine grid in order to minimise the curvature of the characteristics. Further,

to improve convergence, iteration on the slope of the characteristic is used; in the case of the $C_+$ characteristic, this involves the slope at both R and at P. Using this method convergence is usually achieved in about 4 iterations.

The above errors are characteristic of this solution scheme. An error which is common to any calculation procedure which uses a computer is now considered.

Rounding

These errors result from the inability of a computer to reckon with more than a limited number of significant figures. In the solution of the present problem all calculations are performed in double precision which means that each variable is represented by sixteen digits. Thus these errors are relatively small.

Some compromise always has to be made between accuracy and computing time. The number of grid points required to give acceptable accuracy in the present problem depends upon, for example, the curvature of the characteristics. Some test cases are discussed in order to determine the optimum procedure which achieves both speed and accuracy in the computing.

In conclusion the main advantages of the STI method are:

(i) The variables are determined at positions in space and time prescribed by the user.

(ii) Boundary conditions are easily programmed.

(iii) It is the most accurate of any of the finite difference methods for the solution of hyperbolic

equations (Evangelisti, 1969; Yevjevich and Barnes, 1970).

(iv) Since a steady state must satisfy the unsteady equations, an error in programming shows up as an immediate departure from the steady state[I].

5.4 BOUNDARY CONDITIONS

At the boundaries of the distributed parameter model (DPM) only one of the characteristics is available[II]. At the upstream boundary it is the $C_-$ characteristic and at the downstream boundary the $C_+$ characteristic. Each of the compatability equations involves the unknown variables $u_p$ and $A_p$. These equations are solved simultaneously with the corresponding boundary condition, each of which takes the form of a non-linear equation in $u_p$ and $A_p$.

The reduction of the lumped parameter model (LPM) equations at the upstream and downstream boundaries to a single non-linear equation in the boundary values $A_p$ and $u_p$ is now examined. For the sake of brevity (this reduction takes several pages of algebra) only the main details of the procedure are outlined.

---

I As stated earlier the interpolations introduce a very small incompatability and should not be confused with a program error.

II This is true for subcritical flow. However, for supercritical flow at the downstream boundary two characteristics are available, while for supercritical flow at the upstream boundary no characteristics are available.

5.4.1 Upstream Boundary

The LPM equations are:

$$A_B u_B - u_1 + \frac{L_3}{2}\frac{dA_B}{dt} = 0 \tag{5.4.1}$$

$$P_h - P_1 = R_1 u_1 + k_1 u_1 |u_1| + I_1 \frac{du_1}{dt} \tag{5.4.2}$$

$$P_B - P_e = P(A_B) \tag{5.4.3}$$

$(A_B < 1, u_B > 0 \; ; \; A_B \geq 1, u_B < 0 \text{ or } u_B > 0)$:

$$P_1[1-\beta(1-A_B)] - P_B[A_B + \beta(1-A_B)] - R(A_B) Q L_3 A_B = u_B^2 A_B - u_1^2 + L_3\left[(1-\eta)\frac{du_1}{dt} + \eta \frac{d(A_B u_B)}{dt}\right] \tag{5.4.4}$$

$(A_B < 1, u_B < 0)$:

$$P_1 - P_B = u_B^2 A_B - u_1^2 + L_3\left[(1-\varepsilon)\frac{du_1}{dt} + \varepsilon \frac{d(A_B u_B)}{dt}\right] .$$

These equations are differenced using an implicit formulation. Such a scheme is unconditionally stable. Equation (5.4.1) for example, when differenced, yields

$$\frac{(A_B u_B)^{j+1} + (A_B u_B)^j}{2} - \frac{(u_1^{j+1} + u_1^j)}{2} + \frac{L_3}{2}(A_B^{j+1} - A_B^j) = 0 ,$$

where the superscripts denote the time step. In general differencing of equations (5.4.1) - (5.4.4) results in a set of equations of the form

$$g_1(A_B^{j+1}, u_B^{j+1}, u_1^{j+1}, f_1) = 0$$

$$g_2(P_1^{j+1}, A_B^{j+1}, P_B^{j+1}, u_B^{j+1}, u_1^{j+1}, f_2) = 0$$

$$g_3(P_B^{j+1}, A_B^{j+1}, f_3) = 0$$

$$g_4(P_h^{j+1}, P_1^{j+1}, u_1^{j+1}, f_4) = 0 \quad ,$$

where $f_1 - f_4$ are known functions of variables evaluated at time step $j$ . The pressure head, $p_h^{j+1}$ , is specified for all time. It may be prescribed to vary in some way, for example, providing a forced oscillation, or it could be set equal to $p_h^j$ , implying a constant pressure head ( $dp_h/dt = 0$ ). Thus equations (5.4.1) - (5.4.4) are four equations in the five unknowns, viz $A_B^{j+1}$ , $u_B^{j+1}$ , $p_B^{j+1}$ , $u_1^{j+1}$ and $p_1^{j+1}$ . These are reduced to a single equation in the two unknowns $u_B^{j+1}$ and $A_B^{j+1}$ :

$$g_s(A_B^{j+1}, u_B^{j+1}, f_s) = 0 \quad , \qquad (5.4.5)$$

where $f_s$ is a known function of the variables at time $j$ . Equation (5.4.5) is solved simultaneously with equations (5.3.14) - (5.3.15). These equations are non-linear and therefore require an iterative method of solution.

When $A_B^{j+1}$ and $u_B^{j+1}$ are calculated they are substituted in the relevant LPM equations to determine $u_1^{j+1}$ , $p_1^{j+1}$ and $p_B^{j+1}$ . Details of this procedure are given in section 5.6.

5.4.2 Downstream Boundary

A similar procedure is undertaken at this boundary. The LPM equations reduce to a single equation of the form:

$$h_s(A_C^{j+1}, u_C^{j+1}, m_s) = 0 \quad , \qquad (5.4.6)$$

where $m_s$ is a known function of the variables at time $j$ . This equation is solved simultaneously with the equations of the $C_+$ characteristic, viz, equations (5.3.12) - (5.3.13). The calculated values of $A_C^{j+1}$ and $u_C^{j+1}$ are then used to determine $u_2^{j+1}$ , $p_2^{j+1}$ and $p_C^{j+1}$ .

In principle all the equations and boundary

conditions are now defined and it only remains to specify the initial conditions.

## 5.5 INITIAL CONDITIONS

Before stepping forward in time the initial ($t = 0$) values of all the variables must be specified. These initial conditions are at the disposal of the program user and can correspond to countless different flow situations, including physically unrealisable states. In the majority of cases an equilibrium solution obtained from the steady flow equations (see Chapter 4) is used. A steady state solution is a special case of the unsteady flow equations and so provides a check of the STI scheme. The equilibrium state may be stable or unstable. For a stable equilibrium the equations should hold the initial state indefinitely whereas for an unstable equilibrium the equations initially predict the starting conditions but subsequently a departure from this state occurs (see section 5.7).

Although much of the present solution scheme follows the STI method some important differences are employed which decrease computing costs without decreasing the accuracy of the solution. Indeed, improved accuracy is almost always achieved.

## 5.6 SOLUTION SCHEME

The STI method used by the majority of authors is based on the characteristics lying within one reach ($\Delta x$) of the grid point considered (Fig 5.3.2). The reason for this is not made clear in the literature. When using a finite difference approach to the problem

the CFL (Courant, Friedrichs and Lewy, 1928 - see Courant et al, 1952) condition has to be satisfied. This states that 'the domain of dependence of the difference equations must be at least as big as the domain of dependence of the differential equations'. Consider the following example. Assume that a first order hyperbolic equation has been approximated by a difference equation of the form

$$u_i^{j+1} = au_{i-1}^j + bu_i^j + cu_{i+1}^j \quad .$$

Then $u_p$ (Fig 5.6.1) depends on the values at the grid points A, B and C. Therefore the domain of dependence of the point P is the 'triangle' PAC. Thus according to the difference equations the only values at the $j^{th}$ level that can affect the values of the variables at P must lie within AC. Now suppose that the characteristic curve through P of the differential equations meets the $j^{th}$ time level at D. This obviously violates the CFL condition. Events at P, according to these difference equations, depend on events in the triangle PAC. Thus D has to lie within AC.

Now consider the STI method in which the values at P depend on those at R and S. The only reason to restrict, for example, point R to the interval AB (Fig 5.3.2) is that the interpolation formulae are defined on that interval. In the author's view this restriction has nothing at all to do with the CFL condition as stated in some previous studies (for example, Lister, 1960). The CFL condition applies only to a finite difference scheme in which the domain of dependence of a given point (according to the difference equations) is fixed.

Integration along a characteristic proceeds from some point at time t to another point at time $t + \Delta t$. In the case of the $C_+$ characteristic, for example, integration proceeds from the point R to the point P (Fig 5.3.2). Provided the values of the variables at the point R can be determined then the problem can be solved. Since R can lie in an interval other than AC a more sophisticated method is required to determine the interval in which R lies. It is important to realise that the restriction on $\Delta t$ imposed by the CFL condition applies to a basic finite difference scheme (with a fixed domain of dependence) but not to a characteristics scheme.

Another way of looking at this is to consider a characteristics grid in which it is well established that the CFL condition is not required. Then to superimpose on this a regular grid. Indeed to obtain information about the variables at prescribed locations in space and time, a rectangular grid is often superimposed on a characteristics grid and interpolation from the characteristics grid to the rectangular grid is used. This is the reverse procedure of the proposed scheme.

Of all the literature consulted in connection with this problem only Vardy (1976) has used such a scheme. Furthermore, by allowing the characteristics to cross more than one reach ($\Delta x$) the interpolation errors are reduced, and of course $\Delta t$ can take larger values, hence reducing computer time.

Another modification to the STI method which is

used here is iteration on the slope ($\zeta$) of the characteristic‡. The method is as follows:
(without loss of generality the $C_+$ characteristic is considered)

(i) For the first time step assume the slope at P is equal to the slope at C (subsequently assume slope at P is $\frac{1}{2}[(\zeta_+)_P + (\zeta_+)_R]$).

(ii) Find $x_R$ (position at which characteristic crosses the $j^{th}$ time level)

(iii) Interpolate to find $u_R$ and $A_R$. If during the computation at time level $j+1$ a characteristic crosses a boundary (Fig 5.6.2) then interpolation takes place at the boundary between time levels $j$ and $j+1$.

(iv) Determine slope at R, $\zeta_R = 1/(u_R + c_R)$.

(v) Solve compatability equations and determine $u_P$ and $A_P$.

(vi) Determine new slope at P.

(vii) Determine new guess at slope as

$$\frac{1}{2}[(\zeta_+)_P^{new} + (\zeta_+)_R^{new}].$$

(viii) If the difference between the above new slope and the old slope is less that some parameter $\epsilon$ then convergence; proceed to the next grid point.

(ix) If the slope has not converged return to (i) and

---

‡ This was suggested to the author by Dr Bernardo de Bernardinis and has proved very effective in achieving convergence.

assume the slope at $P$ is the calculated new slope (vii).

Step (vii) could have used $(\zeta_+)_P^{new}$ as the guess at the new slope. However, such a method is not so effective when the characteristics are curved.

## 5.7 TEST CASES

The effect of $\Delta t$, $\Delta x$, etc on the solution of some typical flow states is now examined. Since no analytical solution is available to verify the results the program has to be run over and over again using progressively smaller values of $\Delta x$ and $\Delta t$. When two successive values of $\Delta x$ are found to give acceptably similar answers the larger value is used. This is of course based on the principle that the truncation error tends to zero as $\Delta x, \Delta t \to 0$ and hence the difference equation tends to the differential equation.

### 5.7.1 LPM Equations

The boundary conditions are a set of equations and the solution method for these equations can be tested by choosing a LPM version of the program in which region 4 is omitted. The upstream boundary equation in the variables $A$ and $u$ is solved simultaneously with the corresponding downstream equation.

The LPM equations are chosen to correspond to those used by Bertram and Pedley (1982). This enables a comparison to be made between the results obtained using the present solution procedure (which is derived so as to link with region 4 when considering the DPM) and those obtained using a standard library routine; as used by

Bertram and Pedley. The program is started from a set of initial conditions corresponding to a subcritical, unstable equilibrium state with Q = 1 and the following parameter values:

$R_2 = 75$ $R_1 = 37.5$

$I_2 = 25$ $I_1 = 12.5$

$p_e = 200$

$L_3 = 10$ $L_5 = 0$

$P_K = 4$

$R_K = 0.00466$

$p_h = 172.985$

Starting from the equilibrium state, obtained from the steady flow program, no change in the initial conditions is observed. However, when the value $p_h = 173$ (value used by Bertram and Pedley) is imposed at t = 0 a limit cycle is established, Figs 5.7.1 - 5.7.2. The amplitude and frequency are in excellent agreement with the results of Bertram and Pedley. The value of $\Delta t$ used here is 0.02. Halving the value of $\Delta t$ produces the same results. Thus $\Delta t = 0.02$ is sufficiently small to produce acceptable results in this case. Of course the value of $\Delta t$ appropriate to a particular problem has to be determined in the same way. A smaller value of $\Delta t$ would be required for a higher frequency oscillation.

5.7.2 The Complete Model

The solution procedure for the partial differential equations could be tested in isolation, however, since the solution of the problems of interest here requires the solution of both the DPM and LPM equations, the complete

solution scheme is tested. The validity of the solution scheme for the LPM equations in isolation has already been tested (see above).

The difference equations now involve $\Delta x$ as well as $\Delta t$. Thus values are required for both of these independent variables. Nearly all of the authors who use the STI method satisfy the CFL condition which was stated earlier. This imposes a restriction on $\Delta t$ for a given $\Delta x$ (or vice versa) in that the following condition must be satisfied:

$$\Delta x \geq (|u|+c)_{max} \Delta t \quad . \qquad (5.7.1)$$

As stated in section 5.6, it is not thought that (5.7.1) need be satisfied when using the current scheme and indeed some penalties are payed for satisfying this condition. In order to emphasise this, some tests in which the CFL condition is satisfied are now considered. For these tests the value $(|u|+c)_{max} \Delta t/\Delta x = 1$ is chosen. In the first five tests the values of $L_3$, $L_4$ and $L_5$ are 2, 10 and 2, respectively.

(i) Steep ramp: here the upstream pressure head, $\rho_h$, is increased by 10% with $d\rho_h/dt = 75$. In this case $\rho_h$ reaches its maximum value before the wave reaches the downstream end. The results for $\Delta x = 0.5$ (21 grid points) are shown in Fig 5.7.3. The three curves correspond to the upstream (grid point 1), midstream (grid point 11) and downstream (grid point 21) locations. The final values of Q at each point differs by a small amount, cf the upstream and downstream values.

It is known that method of characteristics schemes are non-conservative, however, the error in this case is mainly the result of too large a value of $\Delta x$ and the consequent interpolation errors. Fig 5.7.4 shows the effect of halving $\Delta x$ (= 0.25; 41 grid points). This is one way of reducing the interpolation errors (see section 5.3.3) but is very costly if the CFL condition is satisfied; indeed it increases the computer time 4-fold‡. A more desirable method of reducing the interpolation errors is considered later.

(ii) Gentle ramp: $d\rho_h / dt$ =7.5. In this case $\rho_h$ reaches its maximum value after the wave reaches the downstream end. This is a more severe test on the scheme than the steep ramp due to wave reflections. The results for $\Delta x$ = 0.5 are shown in Fig 5.7.5 and those for $\Delta x$ = 0.25 in Fig 5.7.6. Halving the value of $\Delta x$ has reduced the error but it is not as small as in the case of the steep ramp, Fig 5.7.4.

---

‡ Suppose the value $\Delta t_1 = \frac{\Delta x_1}{(|u|+c)_{max}}$ is chosen. If the space step is halved then $\Delta t_2 = \frac{\Delta x_2}{(|u|+c)_{max}} = \frac{\frac{1}{2}\Delta x_1}{(|u|+c)_{max}}$ $= \frac{1}{2}\Delta t_1$. Also, since there are twice as many points, each time level calculation takes twice as long.

(iii) Single sinusoidal variation in $\rho_h$ : this is of the form $\rho_h = \rho_h(0)[1 + b \sin\omega t]$ where b is 5%, $0 \leq t \leq 2\pi$, giving an amplitude of 10% p to p (peak to peak). $\omega = 2\pi f$ is the angular frequency. Fig 5.7.7 shows the results for $f = 5$ with $\Delta x = 0.5$ and Fig 5.7.8 shows the effect of halving $\Delta x$. Figs 5.7.9 - 5.7.10 show corresponding results for $f = 0.5$.

All of the previous results have satisfied the CFL condition (5.7.1). Some values of $\Delta t$ are now chosen which violate this condition thus allowing the characteristics to extend further than one reach ($\Delta x$). In the first test the conditions are those imposed in (iii) with $f = 0.5$ and $\Delta x = 0.5$. The results for the conditions

$$(|u| + c)_{max} \frac{\Delta t}{\Delta x} = 2, 4,$$

are shown in Figs 5.7.11 and 5.7.12, respectively. The result of doubling $\Delta t$ (Fig 5.7.11) is to produce virtually the same results as in Fig 5.7.10. However, in this case only 225 time steps are required whereas for the results shown in Fig 5.7.10, 900 time steps are required. Further, only 21 grid points are used in this case compared with 41 for Fig 5.7.10. The computer time is thus reduced by up to a factor of 8[I]. The results of

---

I Of course by allowing the characteristics to extend over more than one reach their curvature is increased and hence a greater number of iterations on the slope is probably required, thus reducing this figure slightly.

doubling $\Delta t$ again (Fig 5.7.12) are not quite as good but are still acceptable and of course the decrease in computer time over the standard case (Fig 5.7.10) could be as much as 16 times.

These increases in the magnitude of $\Delta t$ produce benefits in terms of reduction in computer time and often an increase in accuracy. However, the values of $\Delta t$ are chosen somewhat arbitrarily and are 'fixed' in the sense that for each time step

$$(|u| + c)_{max} \frac{\Delta t}{\Delta x} = \text{constant.} \qquad (5.7.2)$$

The constant value chosen may not result in an optimum value for $\Delta t$ for every time increment or even one of them.

The above tests do not really show the full potential of allowing the characteristics to cross more than one reach in terms of reducing interpolation errors. Also, further reduction in the number of grid points is possible with this method, thus decreasing computer time. This very important point is considered in a later section where an attempt to optimise this method so as to reduce both computer time and interpolation errors is explored.

(iv) In the solution of the equations, two parameters are involved, viz $\epsilon$ the maximum allowable relative change in characteristic slope and $\tau$ the maximum allowable relative change in successive calculated values of area and velocity at each grid point. Thus the following conditions must be satisfied at each grid point before convergence

is accepted

$$\left| \frac{\zeta^{new} - \zeta^{old}}{\zeta^{new}} \right| < \epsilon$$

and

$$\left| \frac{\phi^{new} - \phi^{old}}{\phi^{new}} \right| < \tau \quad ,$$

where $\zeta$ denotes the slope of the positive or negative characteristic and $\phi$ denotes the cross-sectional area or velocity. In the previous tests the values chosen were $\epsilon = \tau = 10^{-3}$. Fig 5.7.13 shows the results for $\epsilon = \tau = 10^{-5}$ (cf Fig 5.7.9). It appears that $\epsilon = \tau = 10^{-3}$ is sufficient to ensure an acceptably accurate solution.

The following tests were used by Yevjevich and Barnes (1970) to determine the accuracy of the STI scheme for the solution of the equations of one-dimensional, unsteady free-surface flow.

(v) Starting from the equilibrium state used in the previous tests and with $\Delta x = 0.5$ the program was run for 450 time steps. The maximum local error in flow rate was at grid point one and its magnitude was less than 1%. In fact this maximum was achieved within a small number of time steps and is due to the adjustment from the steady flow program, which does not use the same solution scheme. Once this value is reached, no further change takes place. This shows that the

scheme can hold a steady state solution.

In the second test the area at the 'midpoint' of the tube is increased by 10% at $t = 0$. This settles down within 450 time steps to the solution obtained in the previous test.

In another test a 10% increase in area at all of the grid points is imposed at $t = 0$. This again settles down to the same solution within 450 time steps.

Finally, the values $\epsilon = \tau = 10^{-5}$ are chosen with no perturbation applied. This produces the same results as the first of these tests which used $\epsilon = \tau = 10^{-3}$.

Optimised Scheme to Determine $\Delta t$

Consider the characteristics depicted in Fig 5.7.14. This is typical of the distribution in the partially collapsed tube when the CFL condition is satisfied. Of course in some flow regimes, for example, when a wave is propagating, the distribution is somewhat different, however, in general there is a region of low wavespeed and a region of high wavespeed. In order to safisfy the CFL condition viz $(|u| + c)_{max} \Delta t/\Delta x \leq 1$, large interpolations are required at the upstream end: these are undesirable since they give rise to numerical damping. Indeed it is shown later in this chapter that large interpolations can suppress the growth of an instability, which is very undesirable in the present study.

It has already been shown that decreasing the value of $\Delta x$ reduces the error at the expense of a considerable increase in computer time. Higher order interpolations could be used and these generally produce improved results for smooth transients. However, for the step function, such an interpolation can introduce extraneous fluctuations (Wylie and Streeter, 1978).

Vardy (1976) is the only paper known to the author in which the CFL condition has been violated. In this paper a spatially varying grid was also used positioning extra points where detailed information was required. Such a grid is not easily accommodated in the present problem since the region requiring detailed calculation is not fixed. The effect of allowing the characteristics to cross more than one reach is illustrated in Fig 5.3.5. It is seen that the interpolations are greatly reduced in the low wavespeed region. Vardy's results show this method to be very advantageous for high Mach number flows and its use in the present model has proved very successful.

The choice of the constant in (5.7.2) is now discussed. The value

$$(|u|+c)_{max}\,\Delta t/\Delta x = n\,(\text{constant}),$$

where $n > 1$ may be advantageous for the initial time step, however, at some later time this value may be inappropriate. The tube, for example, may collapse further, modifying the gradient in the wavespeed along the tube; a different value for $n$ may then be appropriate. Thus it is useful to have a scheme in which $n$ is not

fixed but depends in some way on the slopes of the characteristics. Such a scheme is now devised. Firstly, the maximum value of $|u| + c$ along the tube is determined. Then the minimum value of $||u| - c|$ along the tube is found. $n$ is defined as

$$n = \text{int}\left[\frac{(|u| + c)_{max}}{||u| - c|_{min}}\right] .$$

The function $\text{int}(z)$ returns the integer part of $z$ nearest to zero. For example, if $z = 2.41$, then $n = 2$. This means that the positive characteristic with minimum slope crosses two reaches (no interpolation) and the other characteristics have their interpolation reduced.

Of course there is a limit to the number of reaches crossed, above which accuracy is reduced. This is due, for example, to the curvature of the characteristics over $n$ reaches. A more sophisticated optimisation procedure based on the curvature of the characteristics could be devised but is not attempted here. Instead a limit on the value of $n$ is determined empirically.

Some results using the optimised method are now discussed.

Consider the unstable equilibrium state shown in Fig 5.7.1. The frequency of the limit cycle $\approx .86$. Fig 5.7.15 shows the result of imposing a forced oscillation in $\rho_h$ at this frequency and of amplitude 1% of $\rho_h$ p to p. The oscillation grows much faster than in Fig 5.7.1, however, the same limit cycle is established (a slight low frequency modulation is present).

The DPM is now introduced by choosing $L_4 = 1$

with $\Delta x = 0.1$ (11 grid points). An oscillation develops which increases in amplitude with the minimum value of $A \rightarrow 0$ (Figs 5.7.16 - 5.7.17). Ultimately the model breaks down, predicting a negative area. As stated in Chapter 3, the model is not expected to work during such large amplitude oscillations.

It is interesting to see that the maximum area fluctuation occurs at the downstream boundary and the maximum flow rate fluctuation at the upstream boundary. The area curves are plotted on a different scale in Fig 5.7.18 for the time interval $0 \leq t \leq 5$ . Fig 5.7.18 provides a useful comparison with subsequent tests.

The effect of halving $\Delta x$ is shown in Fig 5.7.19. The oscillation appears and $A \rightarrow 0$ earlier than in the previous case.

Halving $\Delta x$ (= 0.025; 41 grid points) again, results in an even earlier onset of instability and eventual breakdown with $A \rightarrow 0$ (Fig 5.7.20).

Further reduction in the size of $\Delta x$ (= 0.0125; 81 grid points) makes little difference (Fig 5.7.21). The onset of the oscillation and the breakdown occur at approximately the same time. The amplitude is slightly larger in this case and the shape of the waveform more asymmetric. These results suggest that $\Delta x = 1/40$ gives acceptabe accuracy in the present problem if the CFL condition is satisfied. The cost of computing this problem with $\Delta x = 1/40$ is up to 16 times more expensive than using $\Delta x = 1/10$. However, the latter value of $\Delta x$ is too large to give the required accuracy when the CFL

condition is satisfied.

Condider the effect of using the new scheme with $\Delta x = 1/10$. For the same equilibrium state this results in an initial value of $n = 6$. The results are shown in Fig 5.7.22. There is very good agreement with Fig 5.7.21 (81 grid points) both with regard to the shape, amplitude and onset of the oscillation. In both cases $A \rightarrow 0$ at approximately the same time, however, in Fig 5.7.21 the area recovers from a value very close to zero and the oscillation continues for one more cycle. The cruder grid is probably responsible for the discrepancy in the position of the breakdown point, however, the position of this point is not crucial in the present problem. As stated earlier, interest here is in the origin of the instability not in the detail of the resulting oscillations.

Consider the difference in the number of spatial grid points and time steps required in each case:

Fig 5.7.21 81 grid points 7000 time steps

Fig 5.7.22 11 grid points 124 time steps.

It is evident that the saving in computer time by using the new method is enormous.

This exhaustive testing of a solution scheme is essential in a numerical model, especially one which is to be used to predict stability (numerical instabilities arising, for example, from violating conservation of mass can drive oscillations). The results of the above tests give confidence in using the present scheme to investigate instabilities which occur in unsteady flow in collapsible tubes. This is the subject of the next chapter.

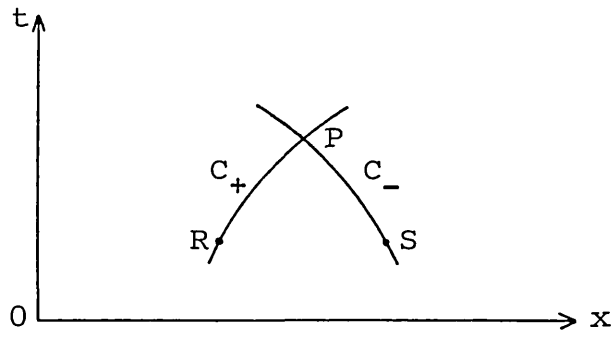



Fig 5.3.1 Typical pair of characteristics.

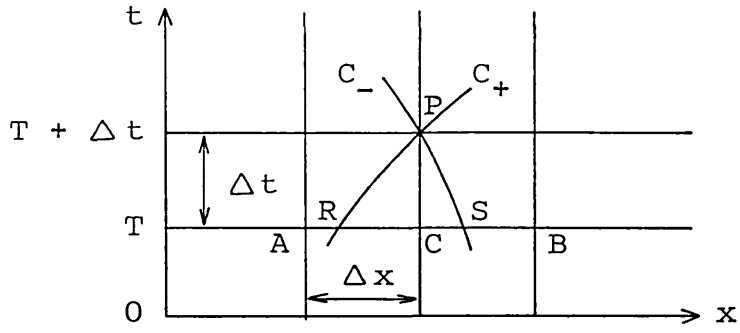



Fig 5.3.2 Typical pair of characteristics intersecting a fixed rectangular grid at the points $x_P$, $x_R$ and $x_S$. Variables are defined at intersection of grid lines (grid points) only. Values of the variables at R and S are determined by interpolating in the intervals AC and CB, respectively.

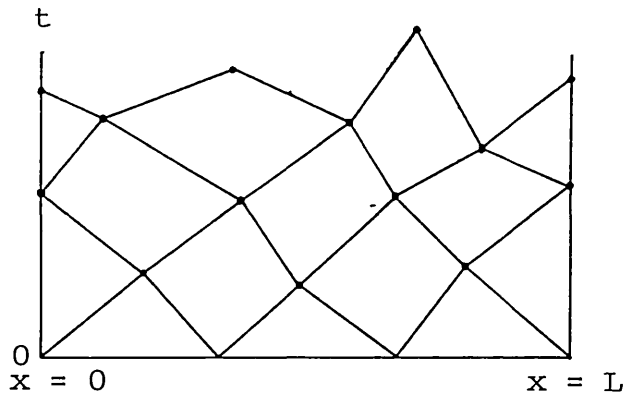



Fig 5.3.3 Characteristics grid.

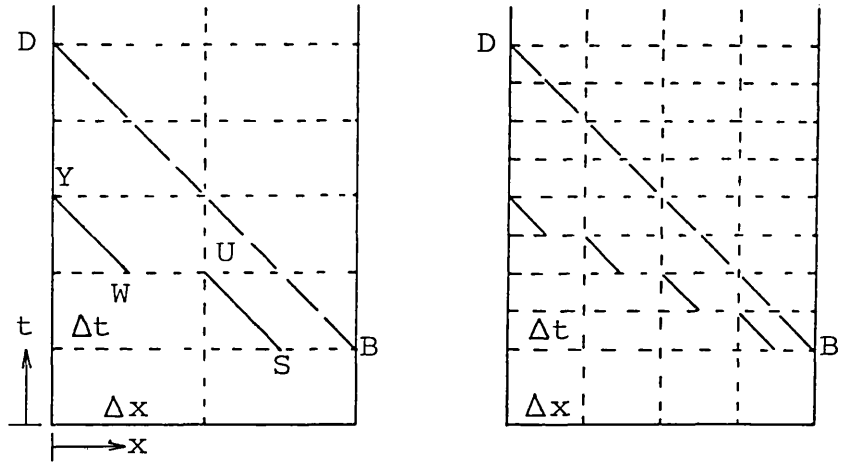



Fig 5.3.4 Propagation of a sharp transient through inviscid flow in a tube. Transient at B should be felt at the other end of the tube at point D. Interpolations produce a damping effect. This damping can be reduced by increasing the number of grid points (see text for explanation of the above x-t diagrams).

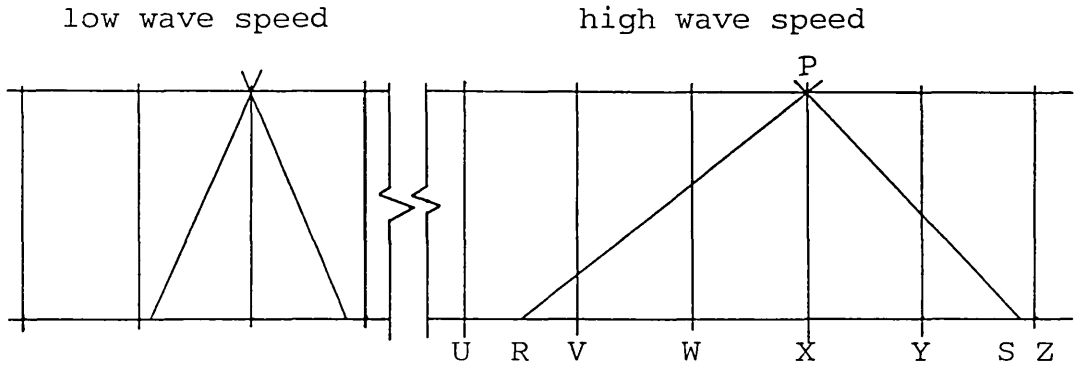



Fig 5.3.5 The interpolation in the low wave speed region is reduced by allowing the characteristics in the high wave speed region to cross more than a single reach. The values at the points R and S are found by interpolation in the intervals UV and YZ, respectively.

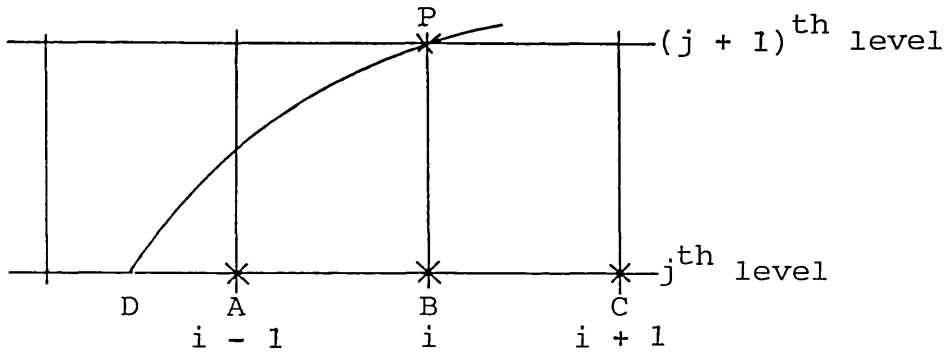



Fig 5.6.1 The point D must lie in the interval AC if a finite difference scheme is used which has a fixed domain of dependence for each point, for example, the domain of dependence of the point P according to such a difference scheme is the 'triangle' PAC.

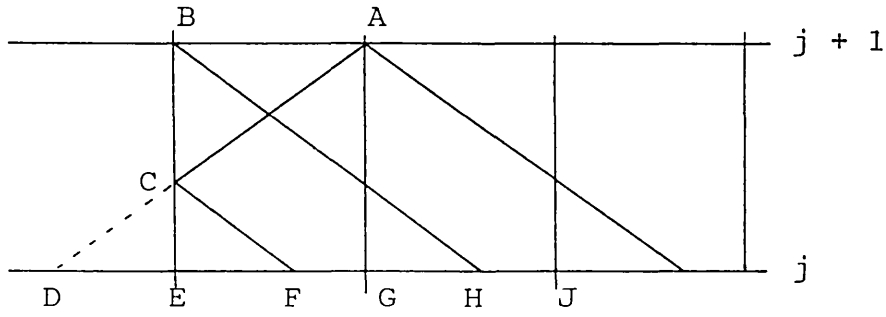



Fig 5.6.2 Values at the point C (boundary) are found by interpolation in the interval EB.

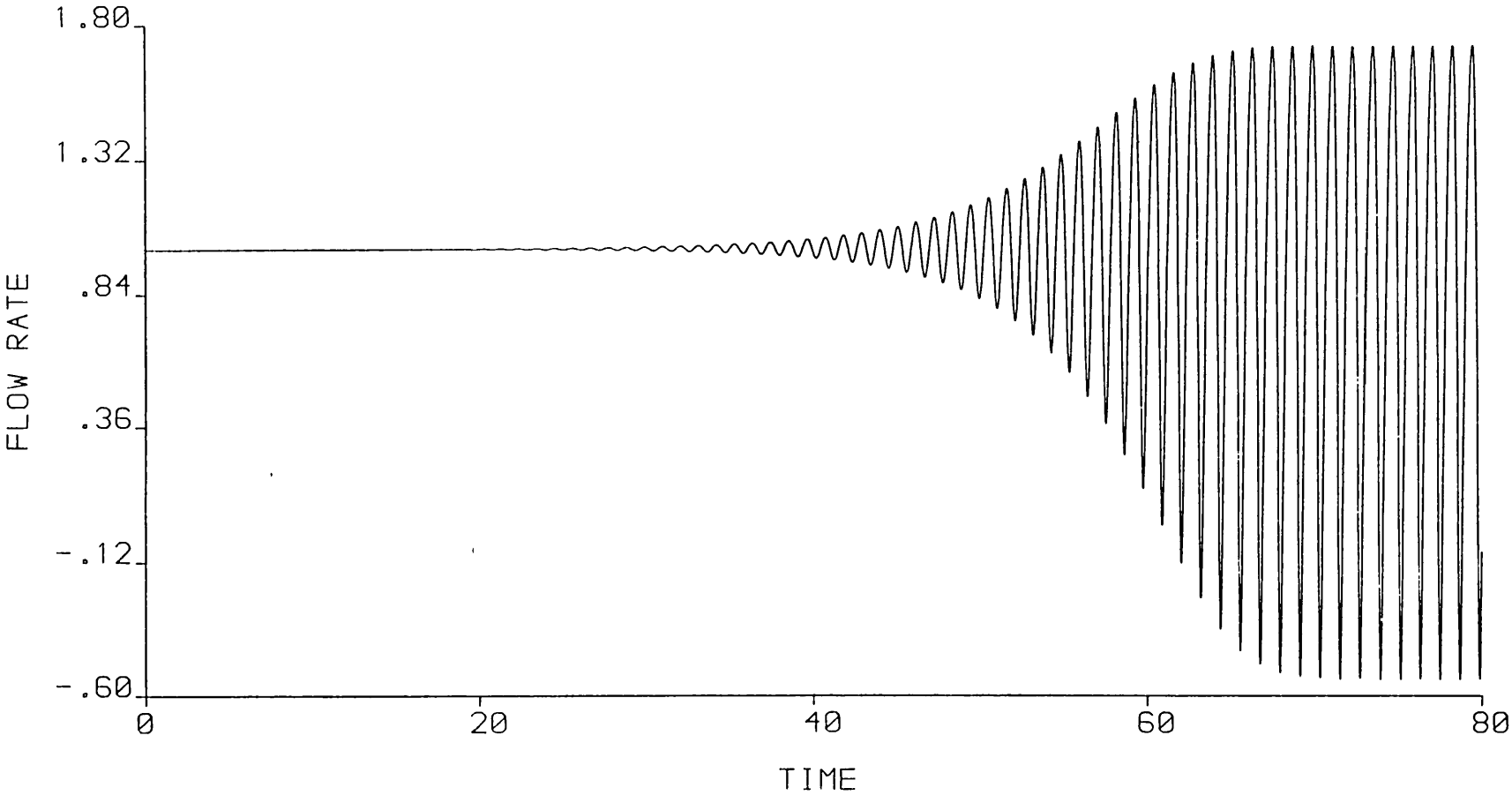



Fig 5.7.1 Limit cycle obtained using the lumped parameter model of Bertram and Pedley (1982) and the present solution scheme. $\Delta t = 0.02$.

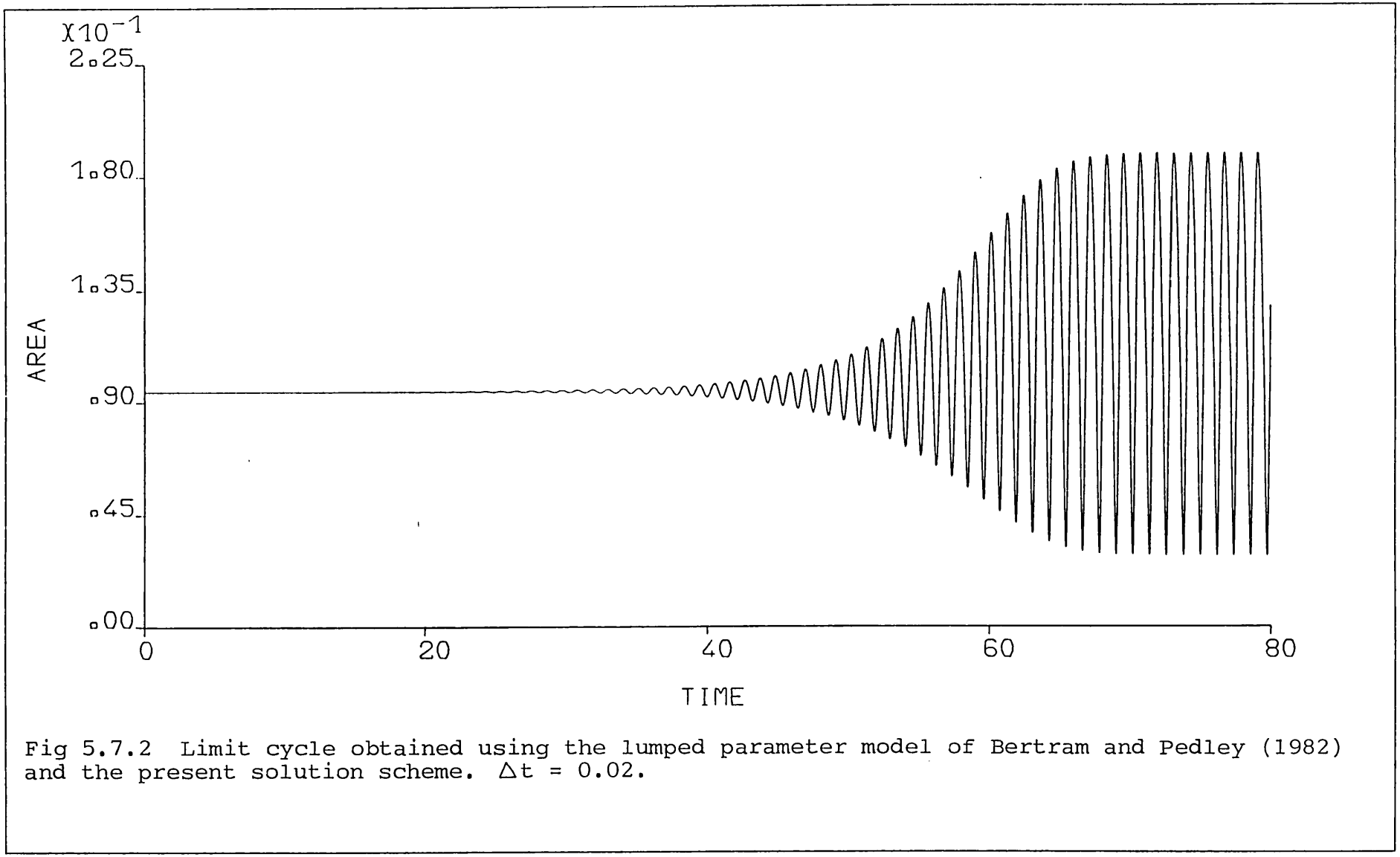



Fig 5.7.2 Limit cycle obtained using the lumped parameter model of Bertram and Pedley (1982) and the present solution scheme. $\Delta t = 0.02$.

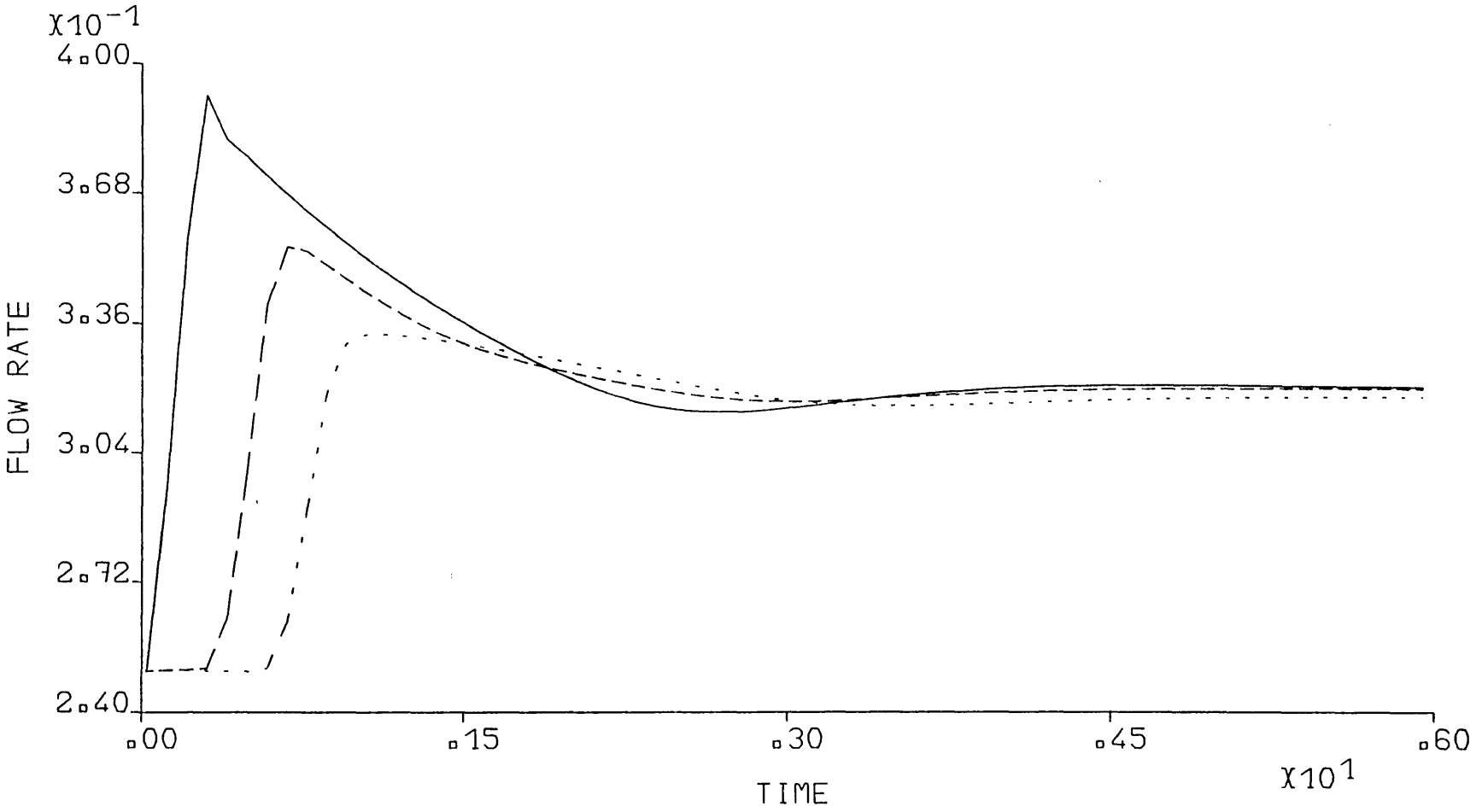



Fig 5.7.3 Steep ramp: the upstream pressure head $p_h$ is increased by 10% with $dp_h/dt = 75$. $p_h$ reaches its maximum value before the wave reaches the downstream end. In this and subsequent plots in this chapter (unless stated otherwise) the following notation is used: —— upstream boundary;- - - - midstream;- - - - - -downstream boundary. $\Delta x = 0.5$. Every 4th time step is plotted.

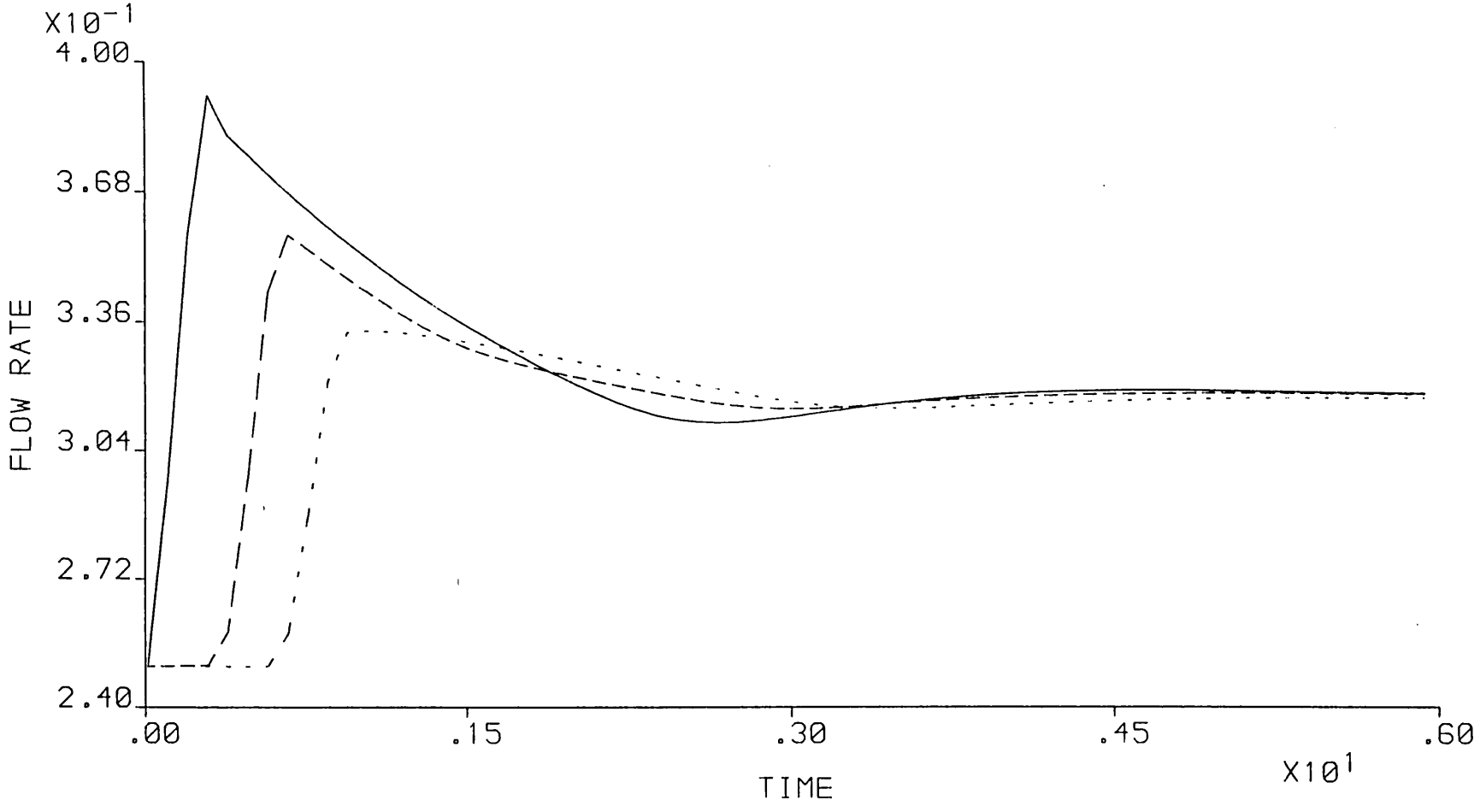



Fig 5.7.4 Effect of halving $\Delta x$ for the case of the steep ramp (cf Fig 5.7.3). $\Delta x = 0.25$. Every 8th time step is plotted.

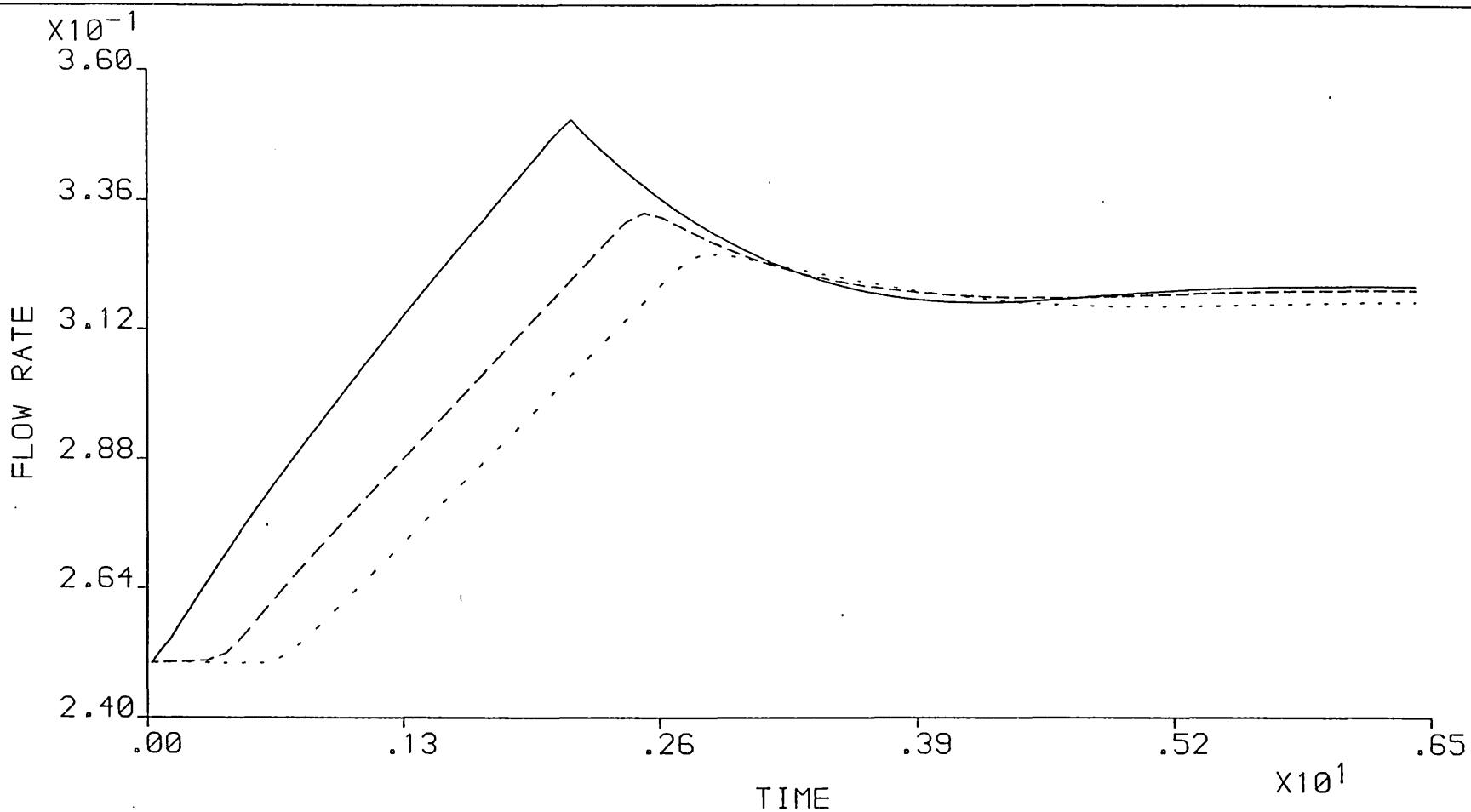



Fig 5.7.5 Gentle ramp: the upstream pressure head $p_h$ is increased by 10% with $dp_h/dt = 7.5$. The wave reaches the downstream end before $p_h$ reaches its maximum value. $\Delta x = 0.5$. Every 4th time step is plotted.

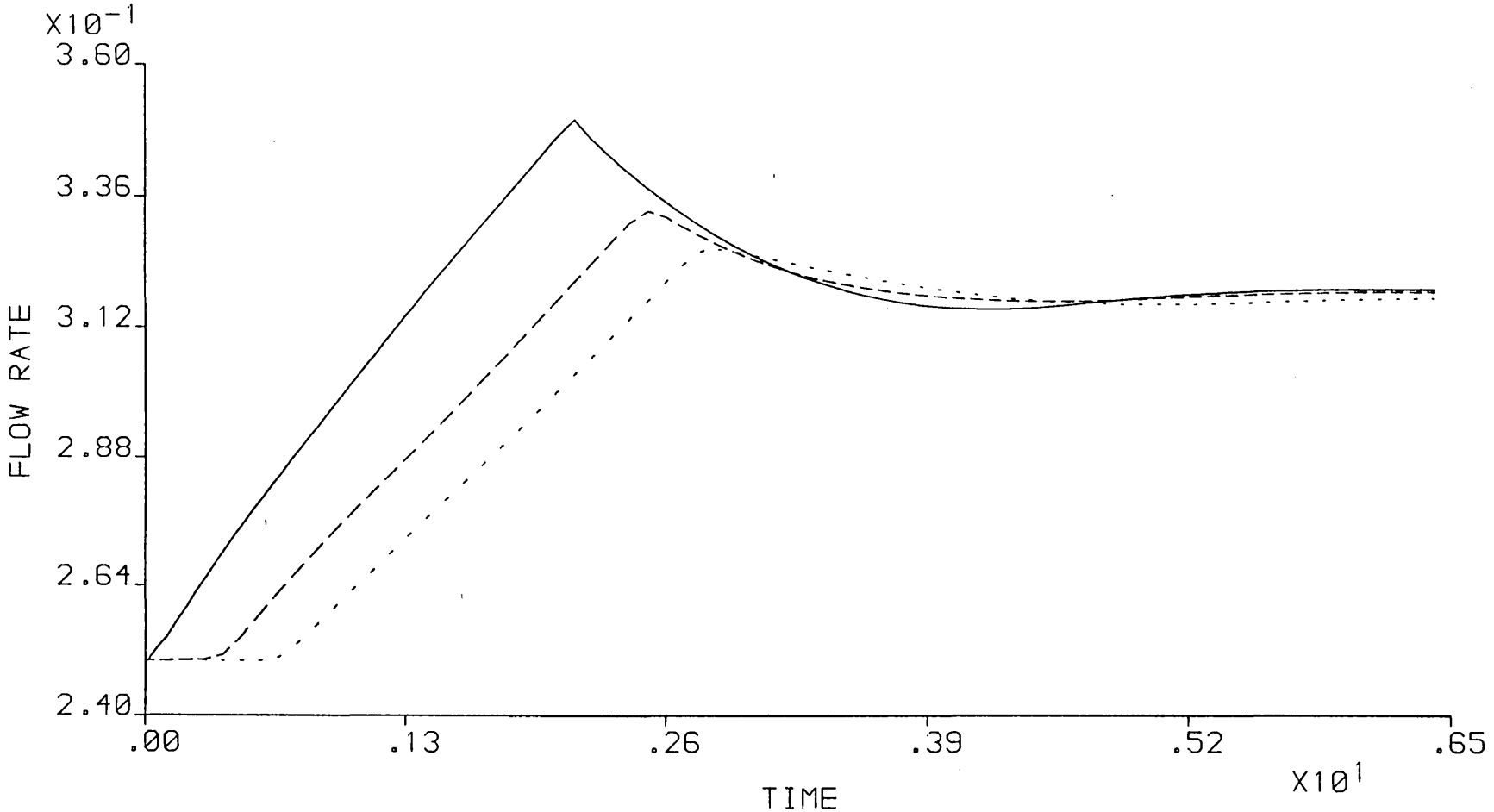



Fig 5.7.6 Effect of halving $\Delta x$ for the case of the gentle ramp (cf Fig 5.7.5). $\Delta x = 0.25$. Every 8th time step is plotted.

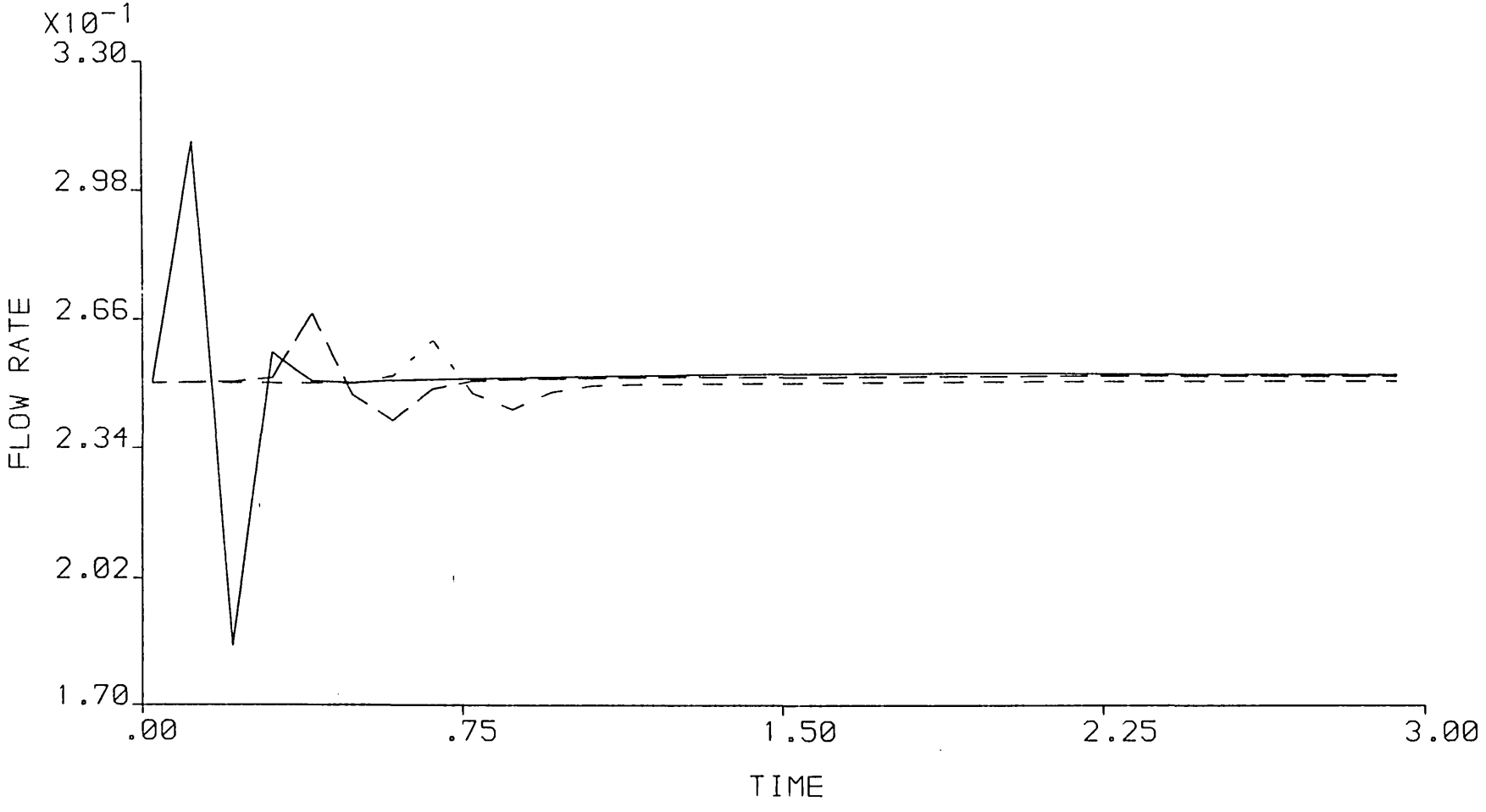



Fig 5.7.7 Single sinusoidal variation in $p_h$ of the form $p_h = p_h(0)(1 + b\sin 2\pi ft)$, where b = 5%, f = 5. $\Delta x = 0.5$. Every 4th time step is plotted.

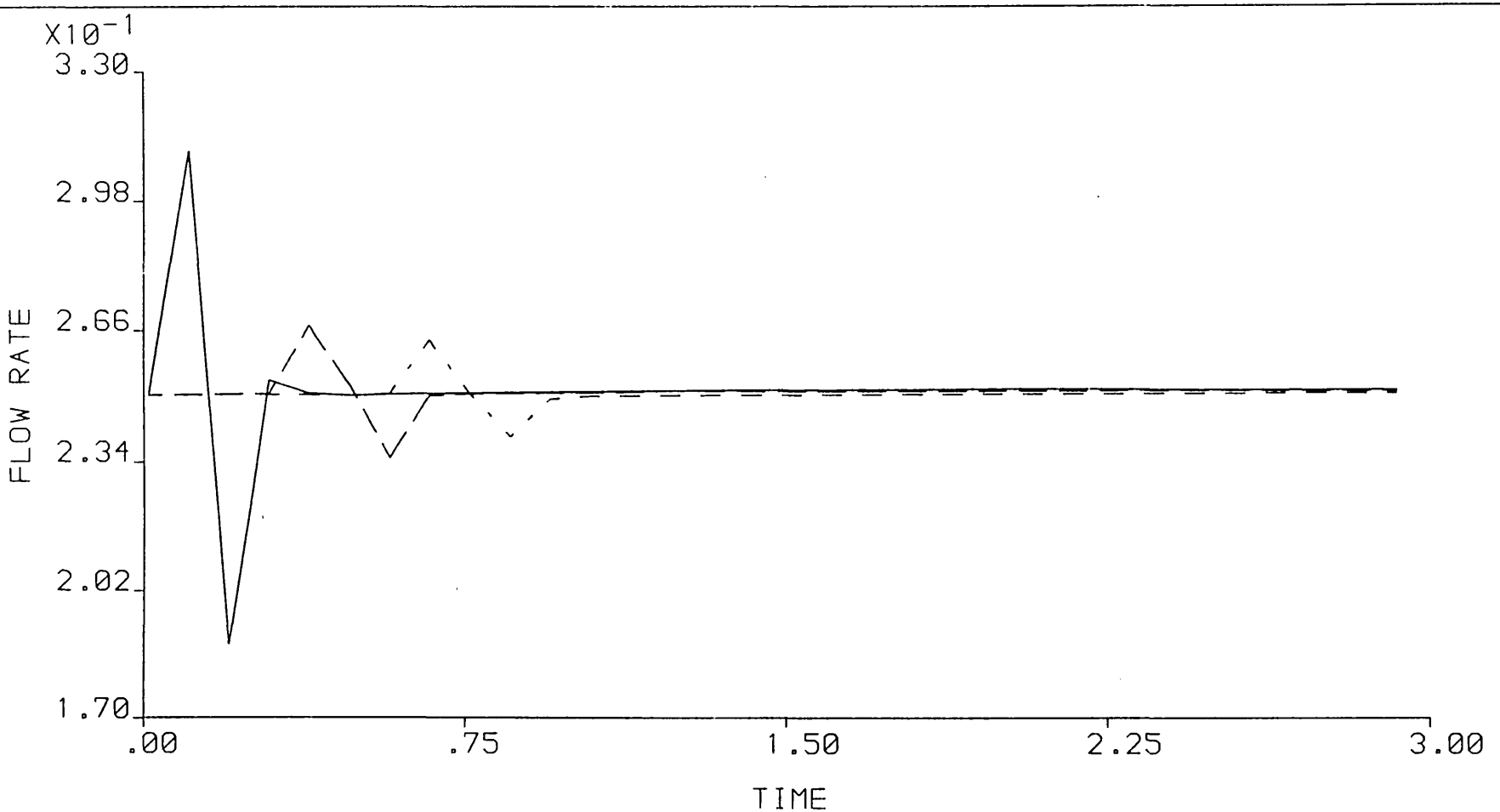



Fig 5.7.8 Effect of halving $\Delta x$ for the case of the single sinusoidal variation in $p_h$ (cf Fig 5.7.7). $\Delta x = 0.25$. Every 8th time step is plotted.

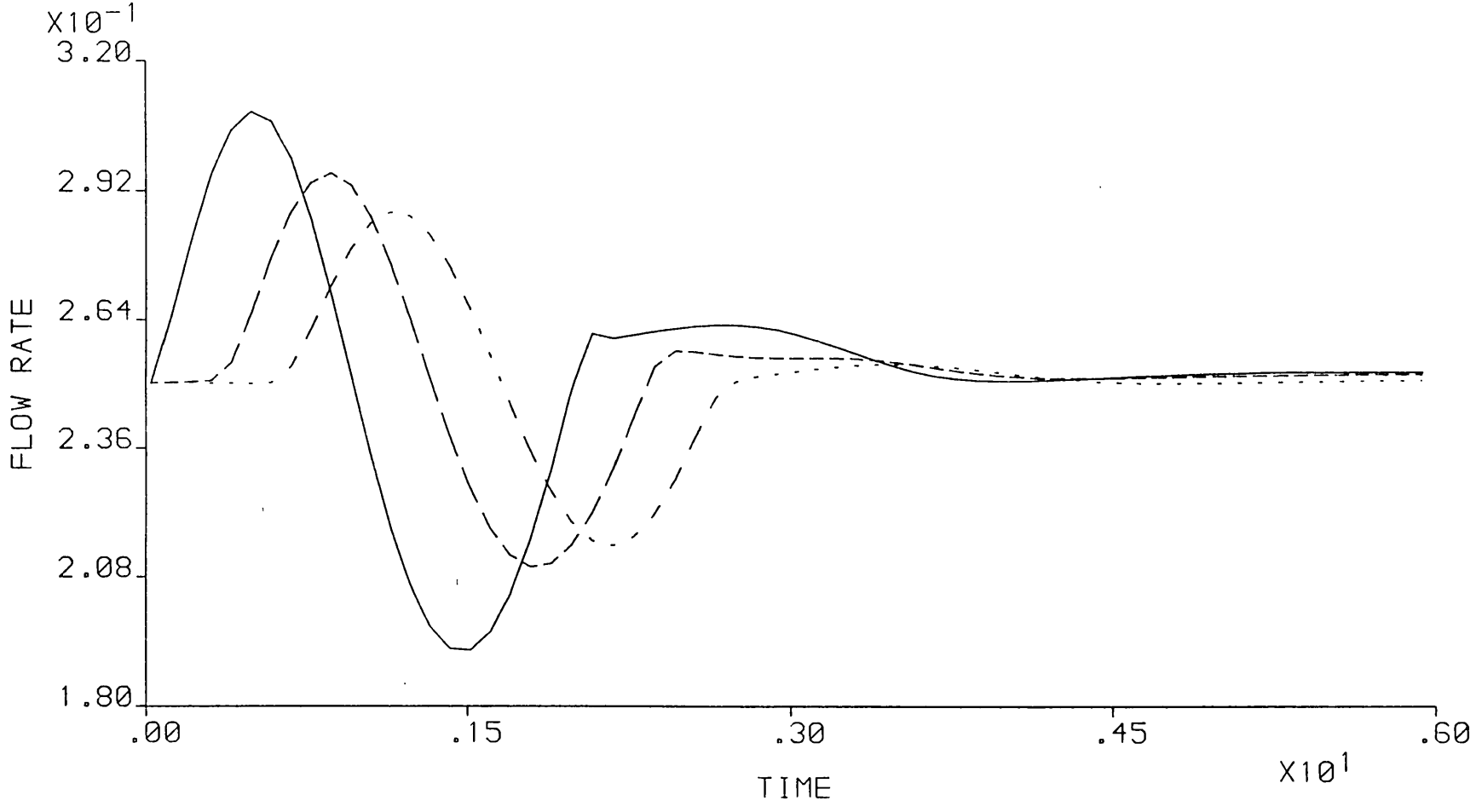



Fig 5.7.9 Single sinusoidal variation of $p_h$ of the form $p_h = p_h(0)(1 + b\sin 2\pi ft)$, where b = 5%, f = 0.5. $\Delta x = 0.5$. Every 4th time step is plotted.

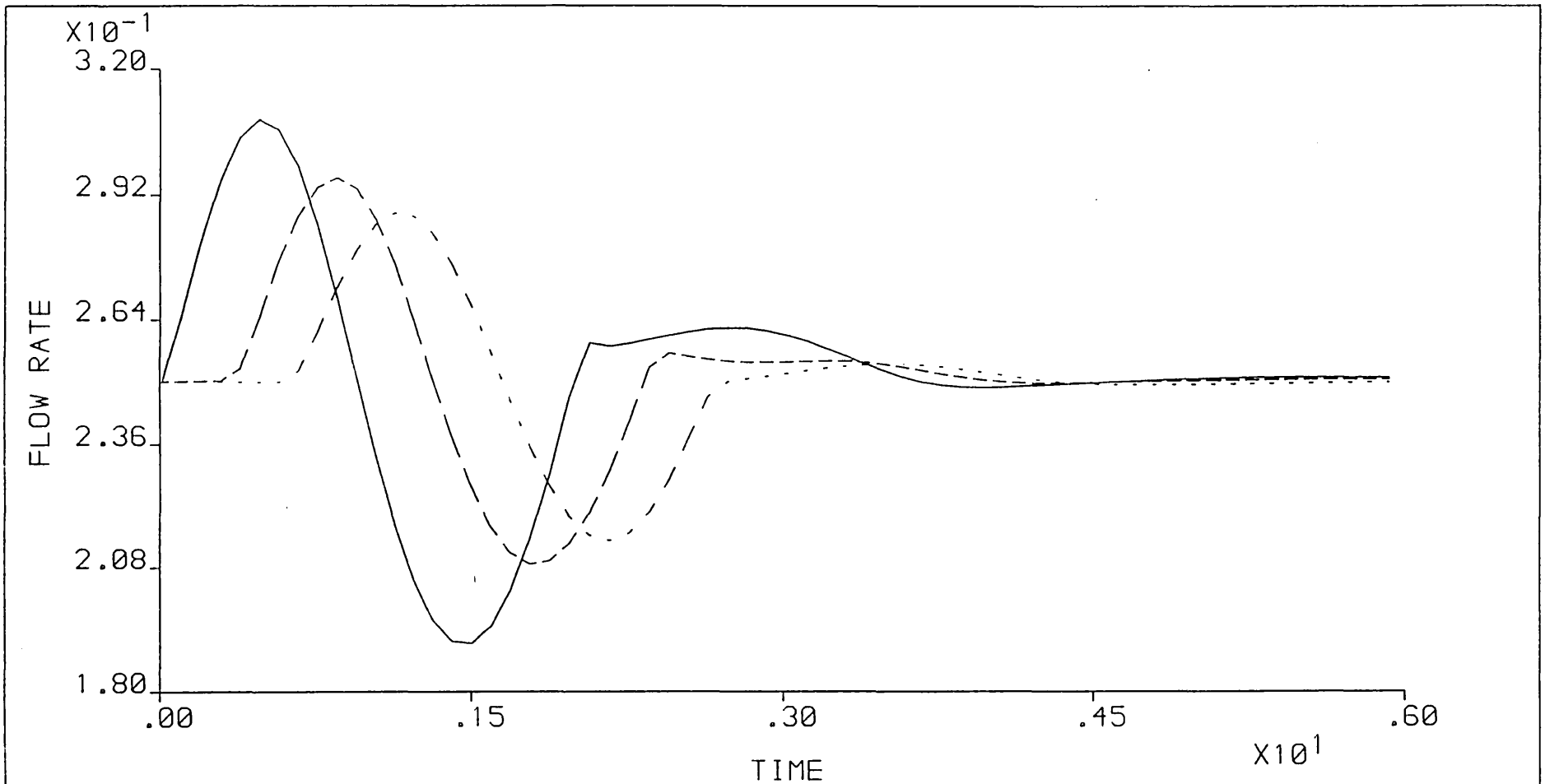



Fig 5.7.10 Effect of halving $\Delta x$ for the case of a single sinusoidal variation in $p_h$ (cf Fig 5.7.9). $\Delta x = 0.25$. Every 8th time step is plotted.

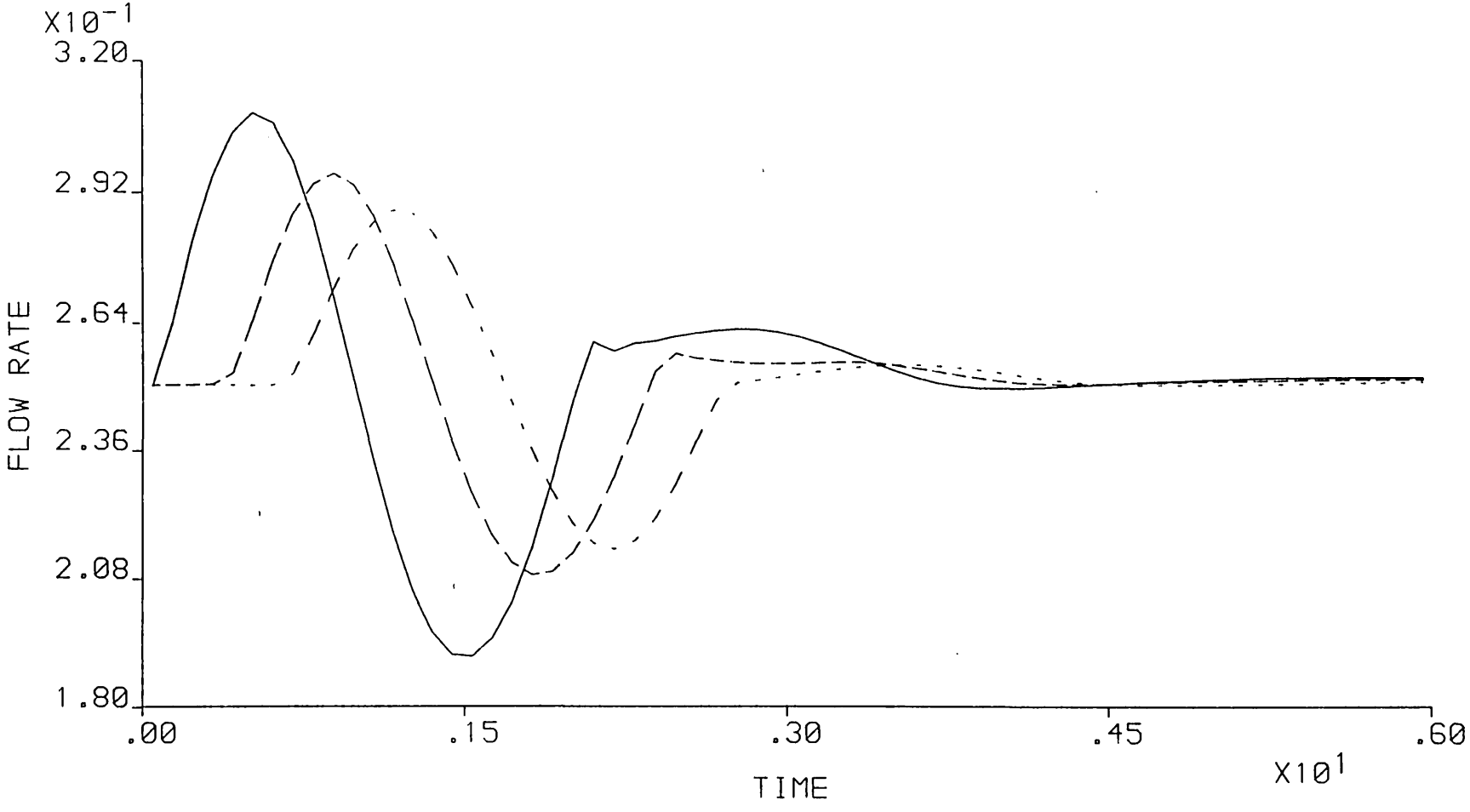



Fig 5.7.11 Effect of allowing the positive characteristic with the gentlest slope to extend over two reaches ($2\Delta x$) for the case of the single sinusoidal variation in $p_h$ (cf Fig 5.7.10).

$\Delta x = 0.25$. Every 2nd time step is plotted.

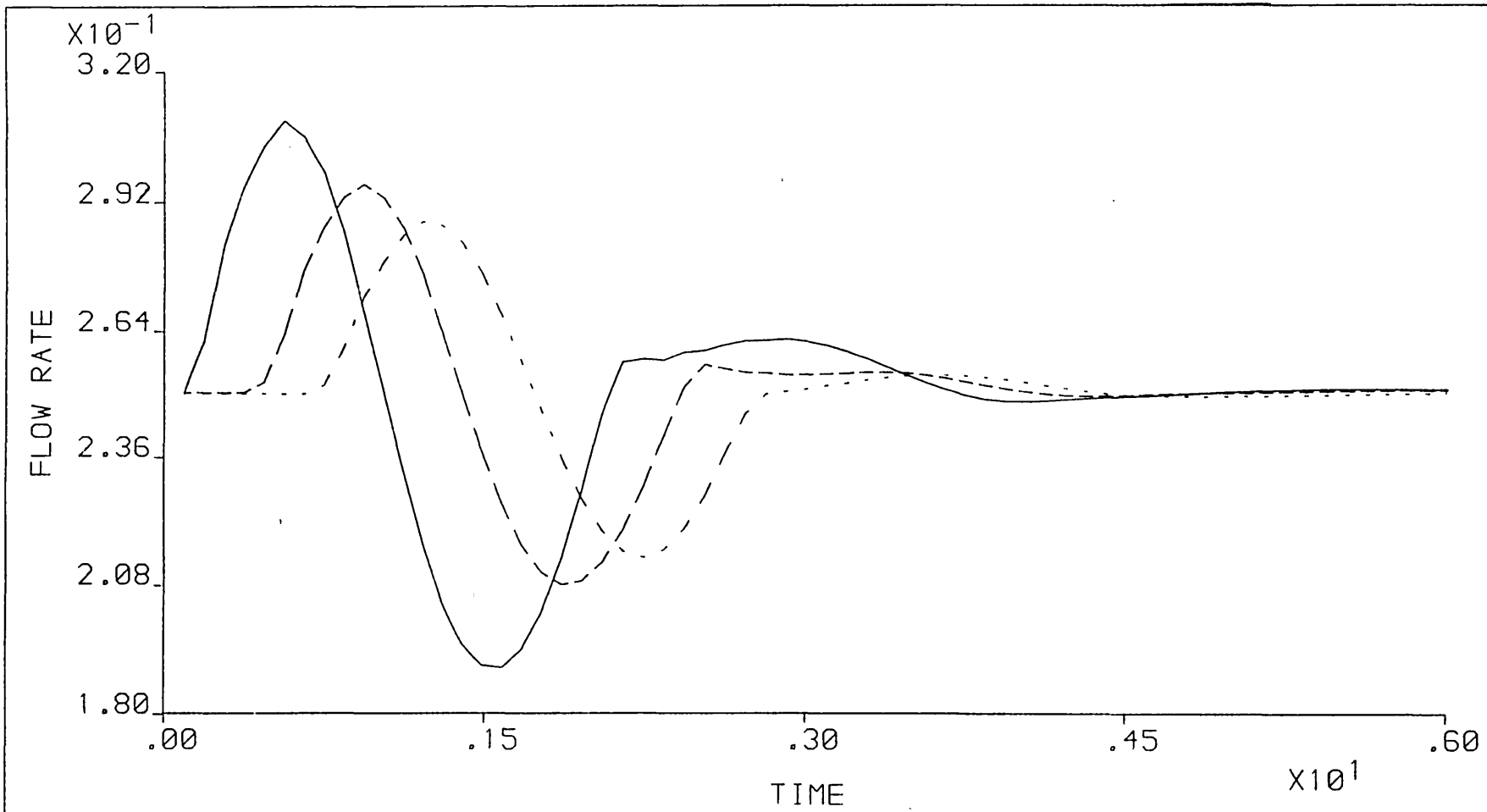



Fig 5.7.12 Effect of allowing the positive characteristic with the gentlest slope to extend over 4 reaches ($4\Delta x$) for the case of the single sinusoidal variation in $p_h$ (cf Fig 5.7.10).

Every time step is plotted.

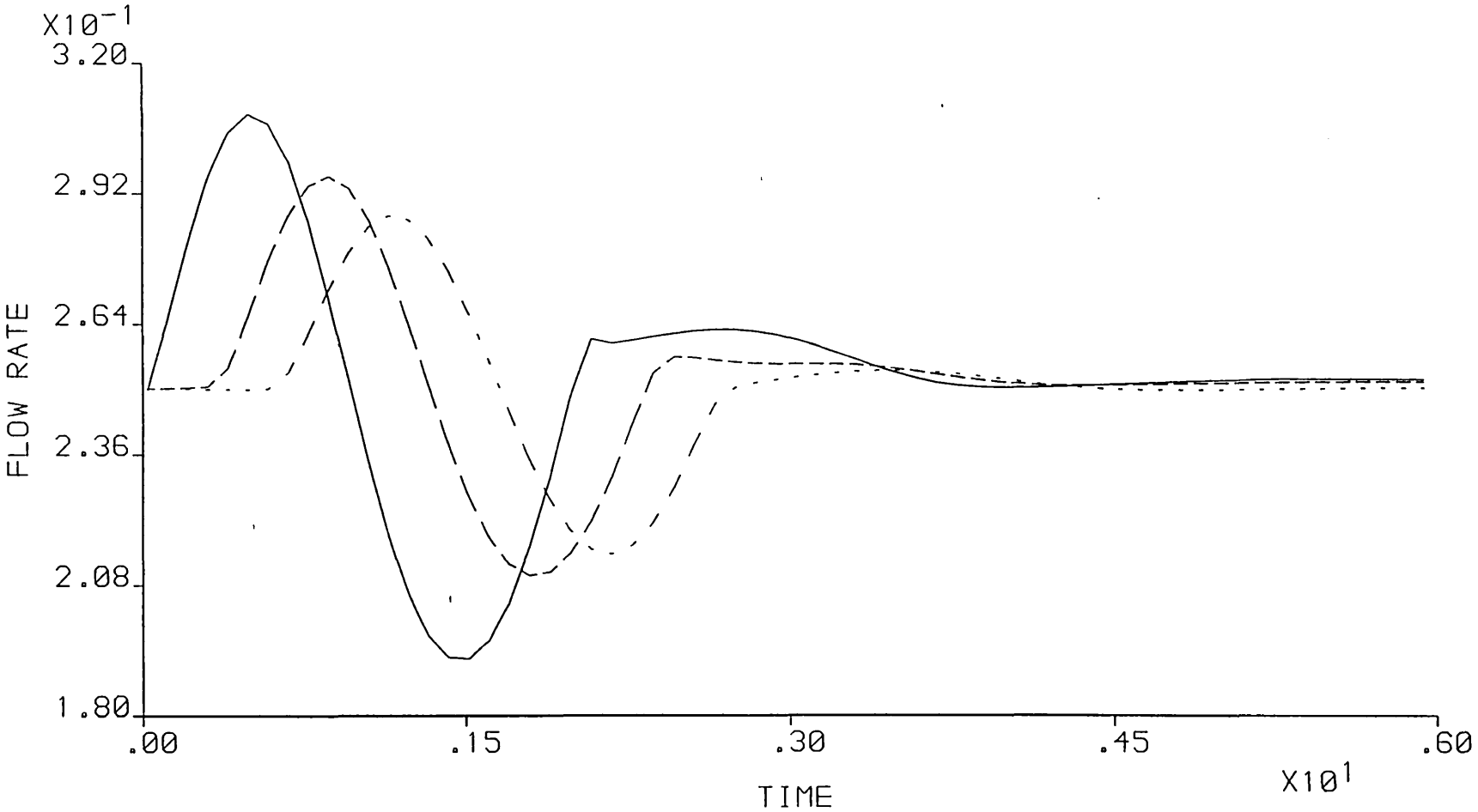



Fig 5.7.13 Effect of using a smaller value for each convergence parameter, viz $\epsilon = \tau = 10^{-5}$ (cf Fig 5.7.9 which uses $\epsilon = \tau = 10^{-3}$). $\Delta x = 0.5$. Every 4th time step is plotted.

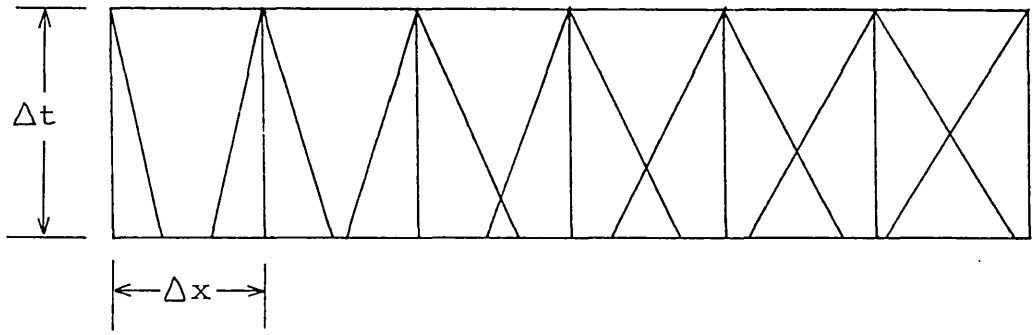



Fig 5.7.14 The grid ratio, $\Delta t/\Delta x$, is much too small in the low wave speed region (LHS) in order that it may satisfy the CFL condition in the high wave speed region (RHS).

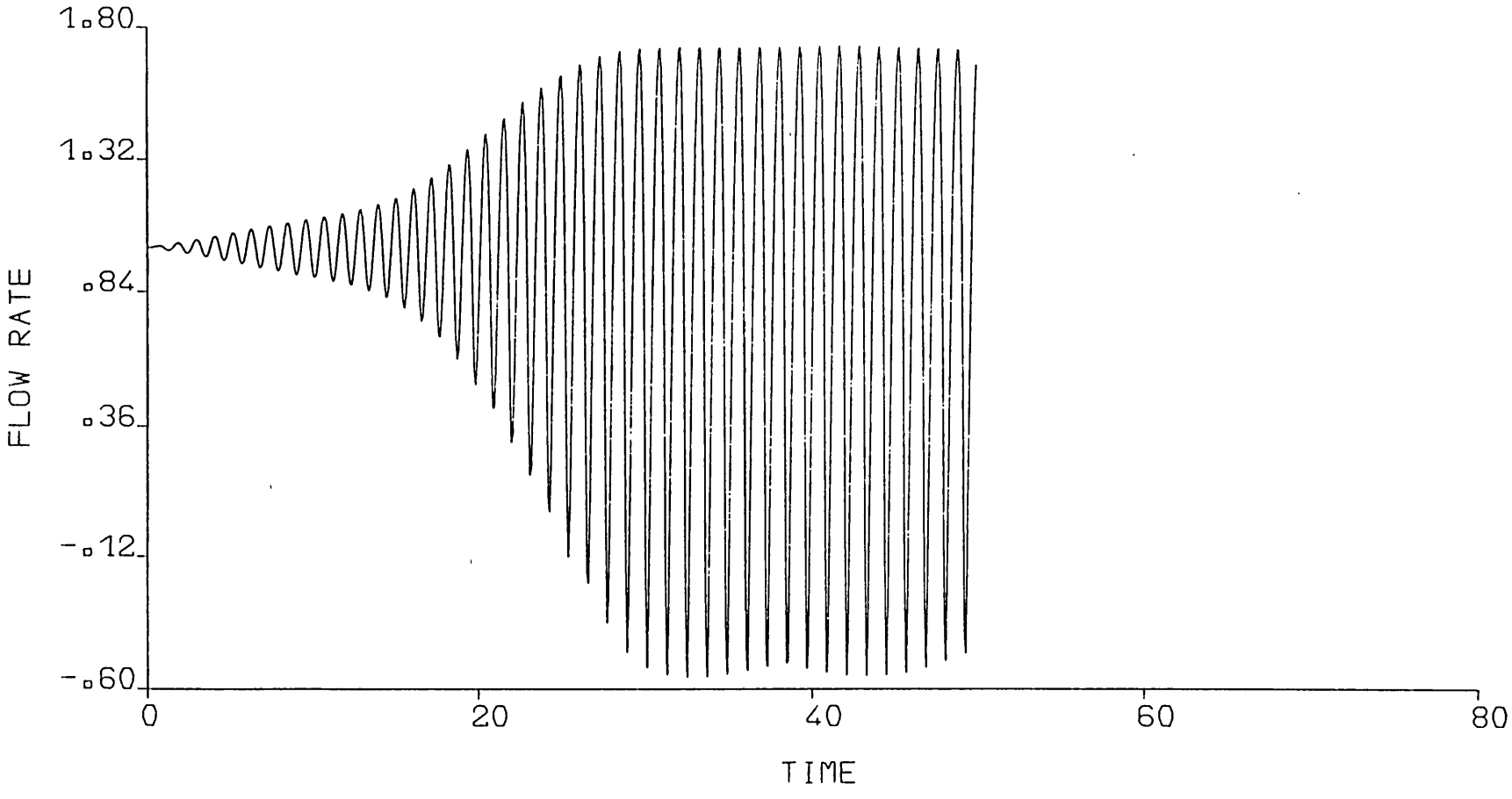



Fig 5.7.15 Effect of imposing a perturbation in $p_h$ on the unstable equilibrium state used in Fig 5.7.1. The frequency of the perturbation is 0.86 (frequency of the limit cycle in Fig 5.7.1) and the amplitude 1% of $p_h$ peak to peak. $\Delta t = 0.02$.

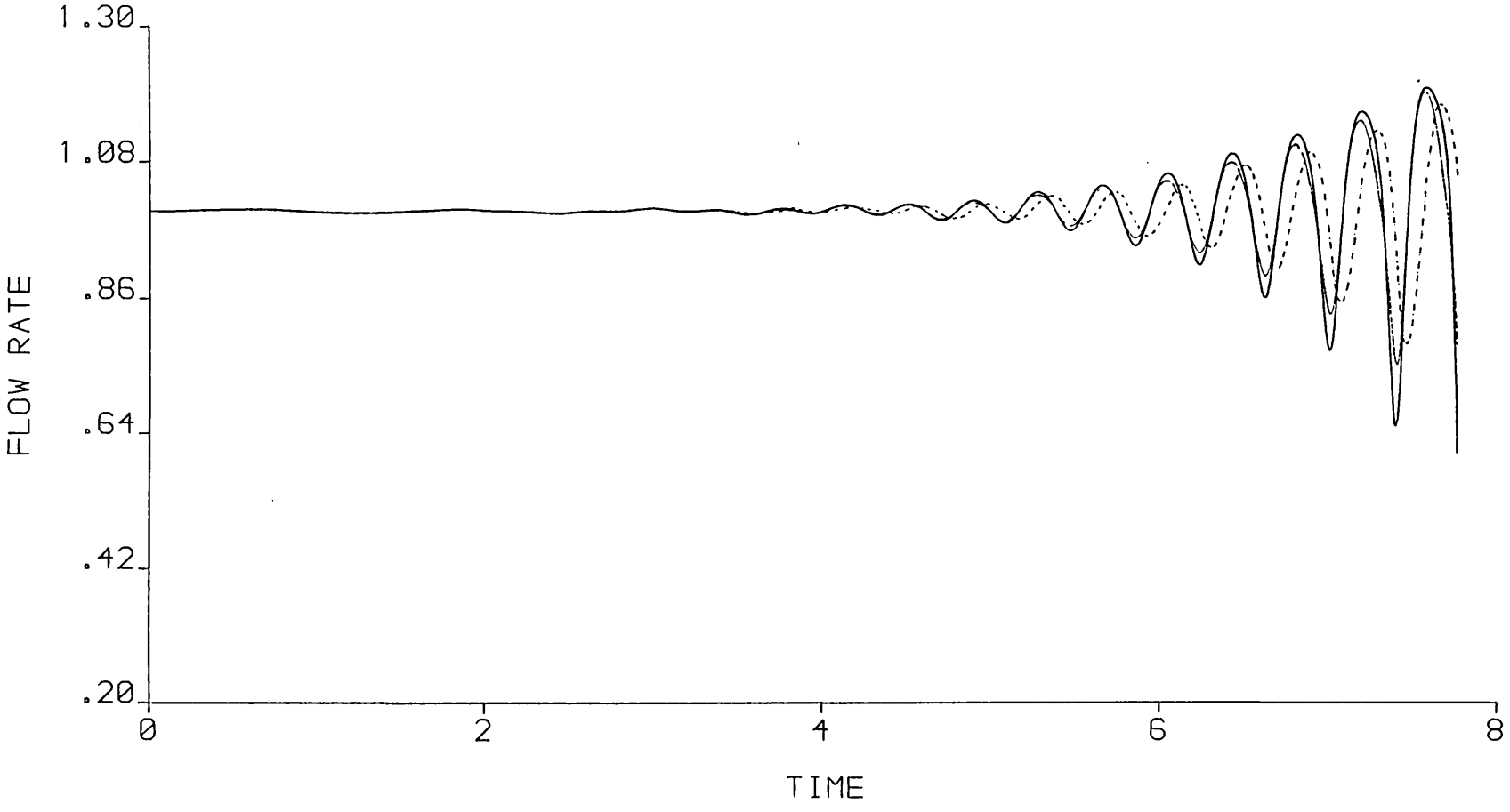



Fig 5.7.16 Effect of the introduction of the distributed parameter model with $L_4 = 1$ (cf Fig 5.7.15, note change in scales). $\Delta x = 0.1$.

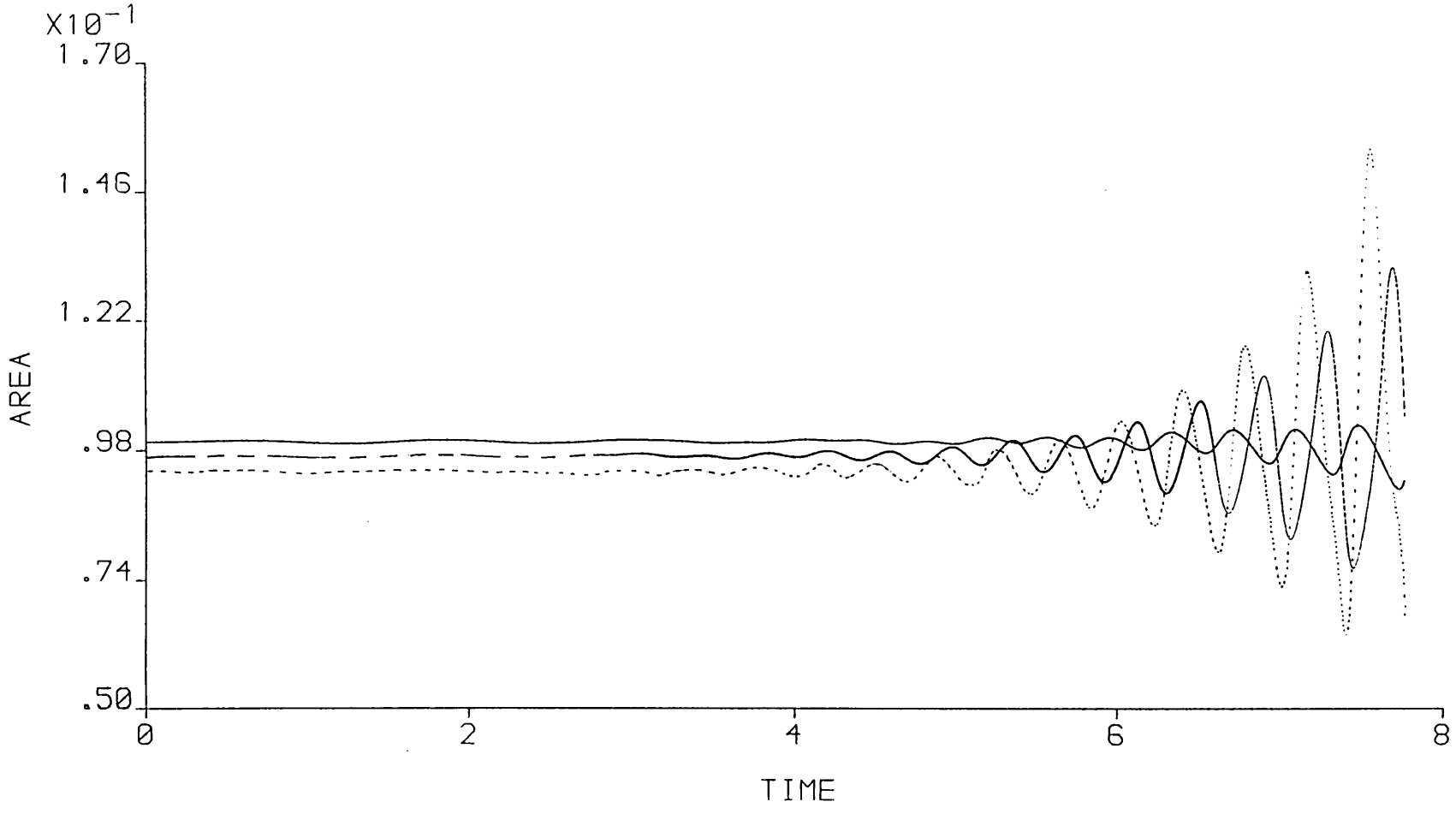



Fig 5.7.17 Area variation corresponding to the flow rate variation shown in Fig 5.7.16.

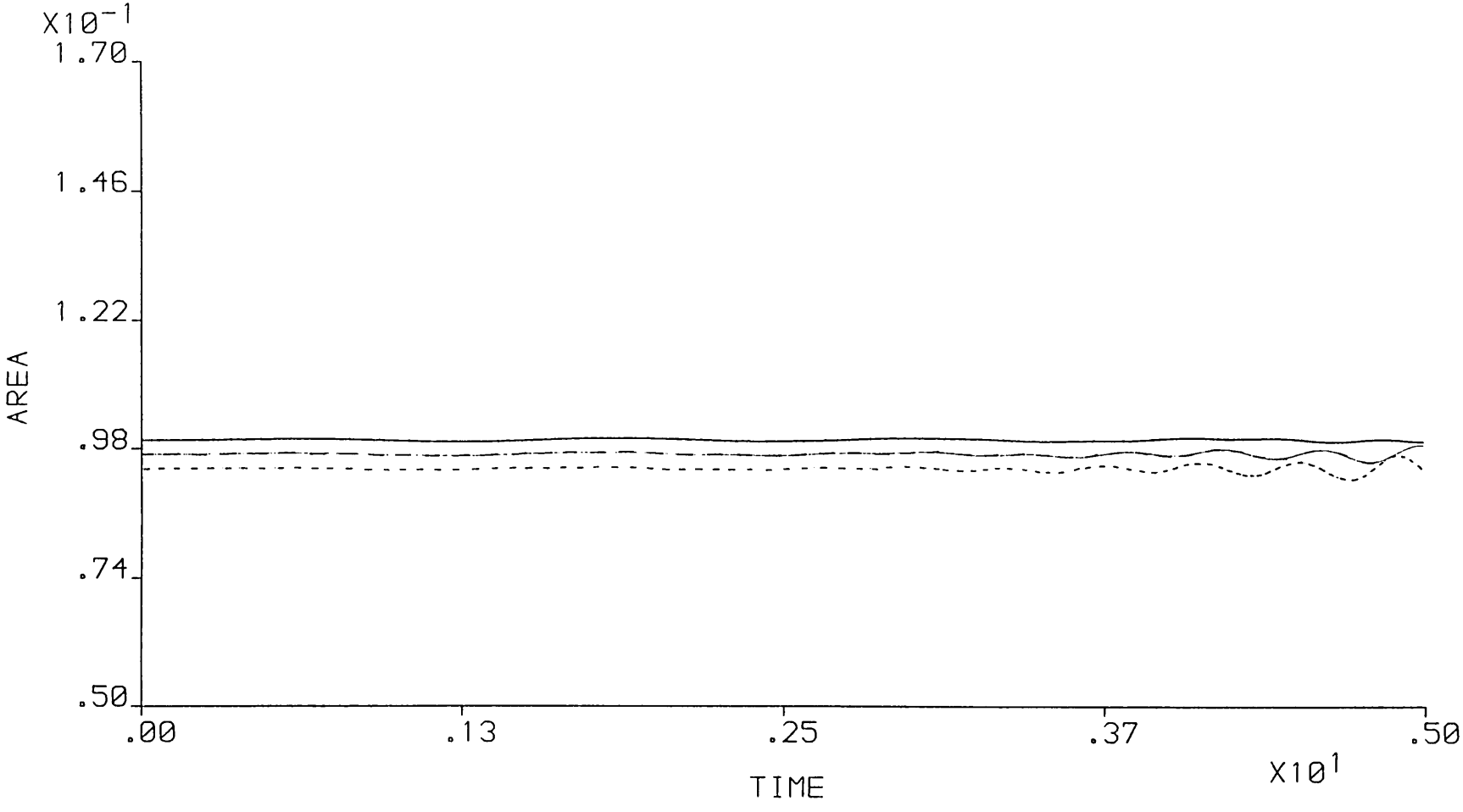



Fig 5.7.18 The results from Fig 5.7.17, for the time interval $0 \leq t \leq 5$, plotted on an expanded time scale. $\Delta x = 0.1$.

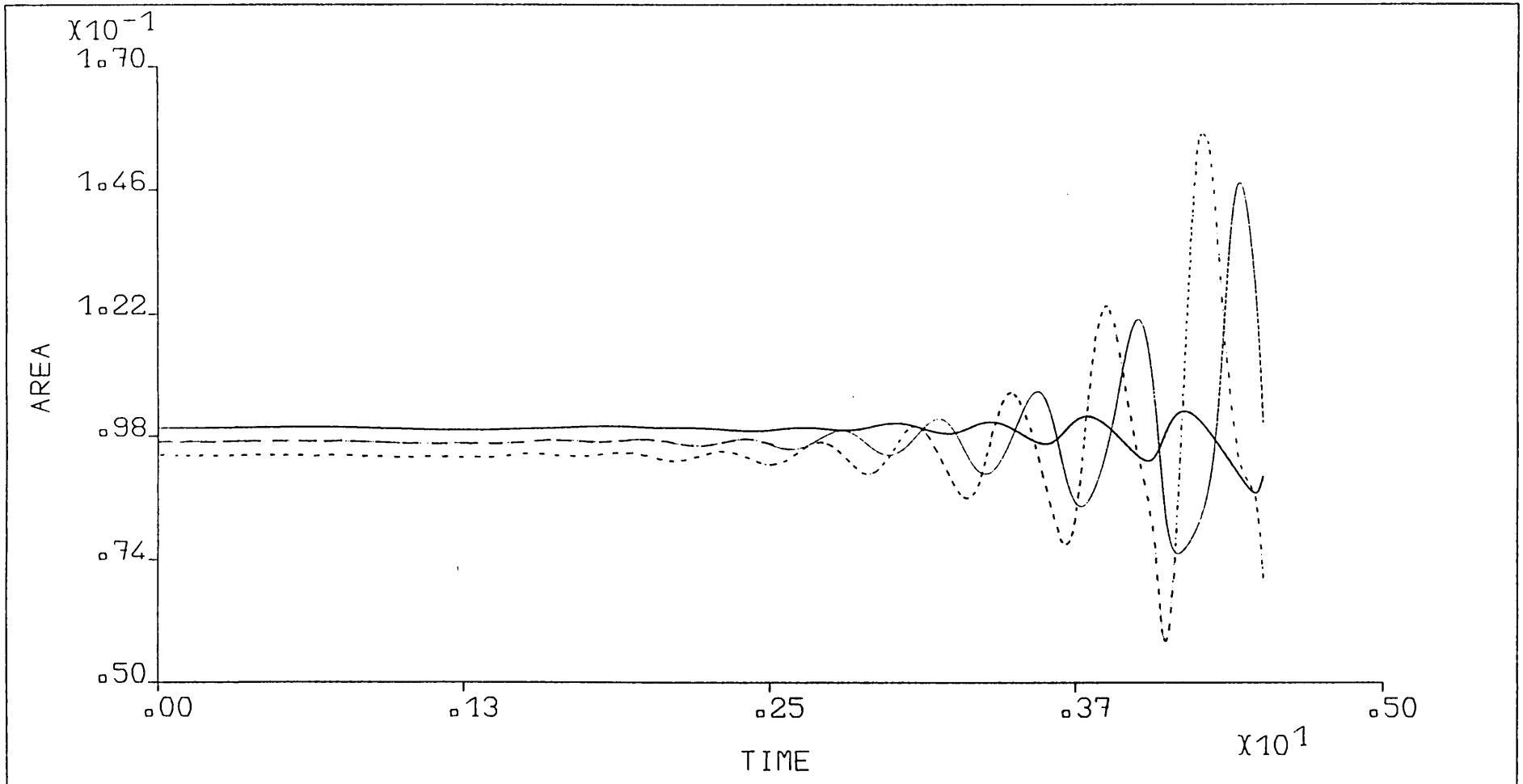



Fig 5.7.19 Effect of halving $\Delta x$ for the case shown in Fig 5.7.18. $\Delta x = 0.05$.

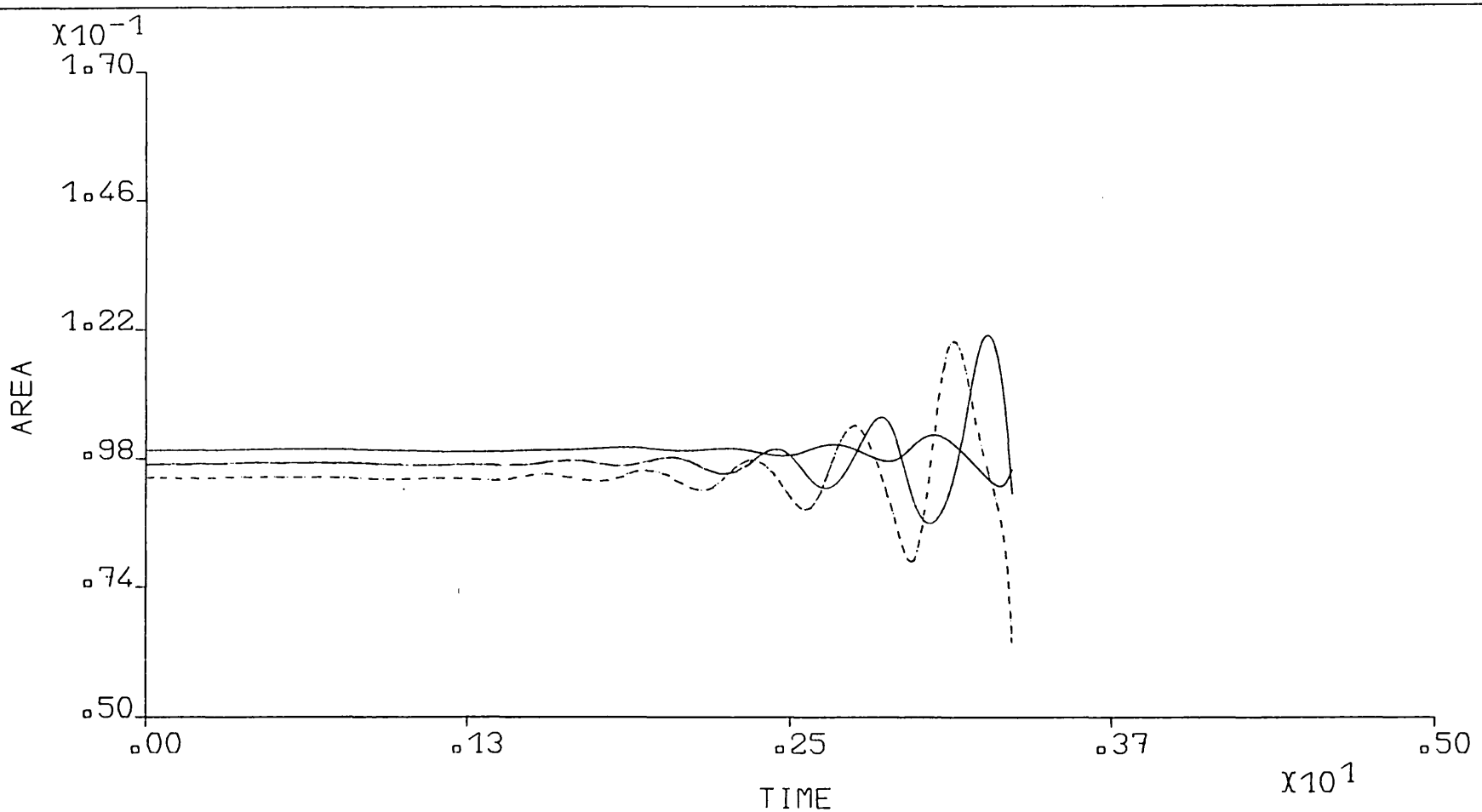



Fig 5.7.20 Effect of halving $\Delta x$ for the case shown in Fig 5.7.19. $\Delta x = 0.025$.

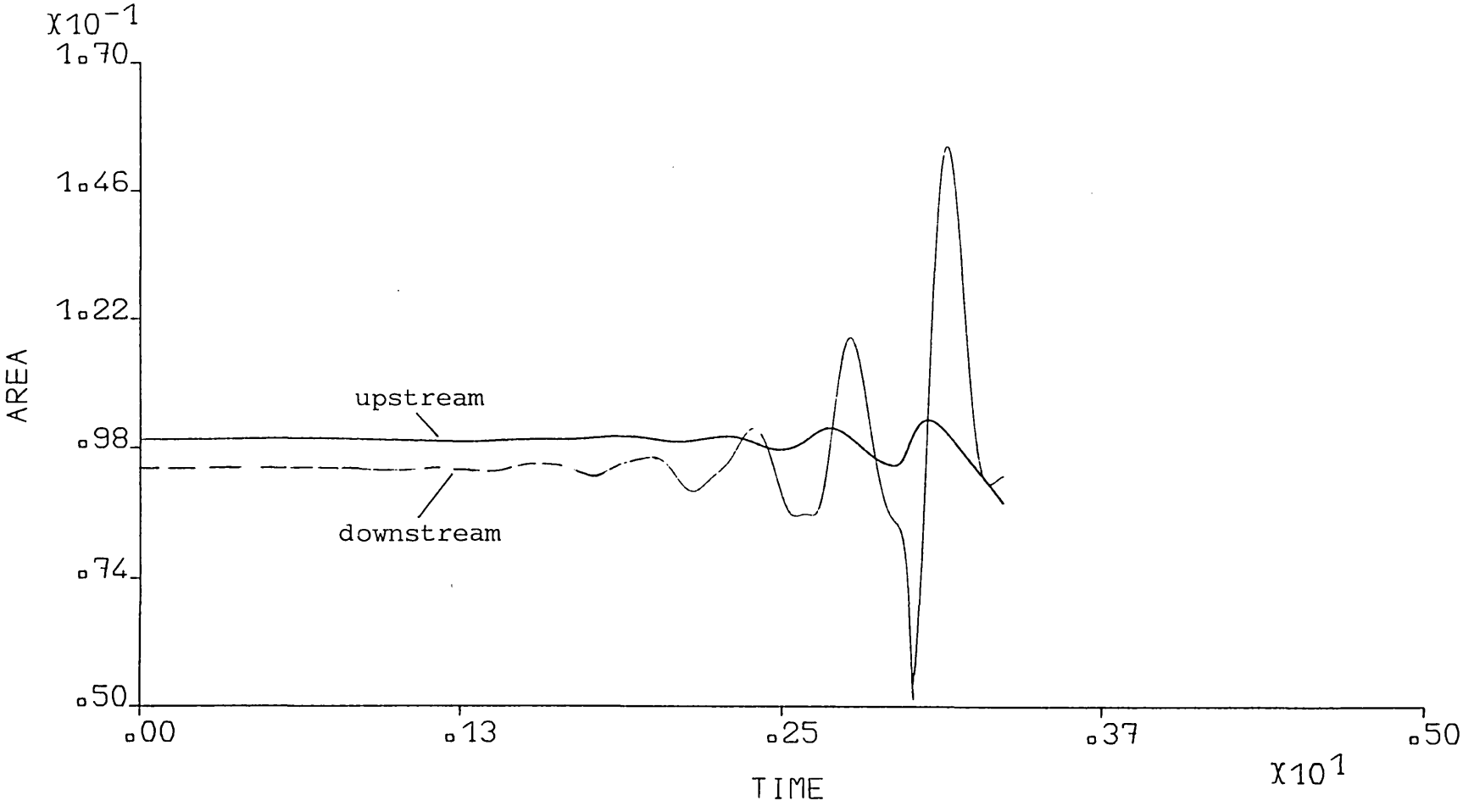



Fig 5.7.21 Effect of halving $\Delta x$ for the case shown in Fig 5.7.20. $\Delta x = 0.0125$.

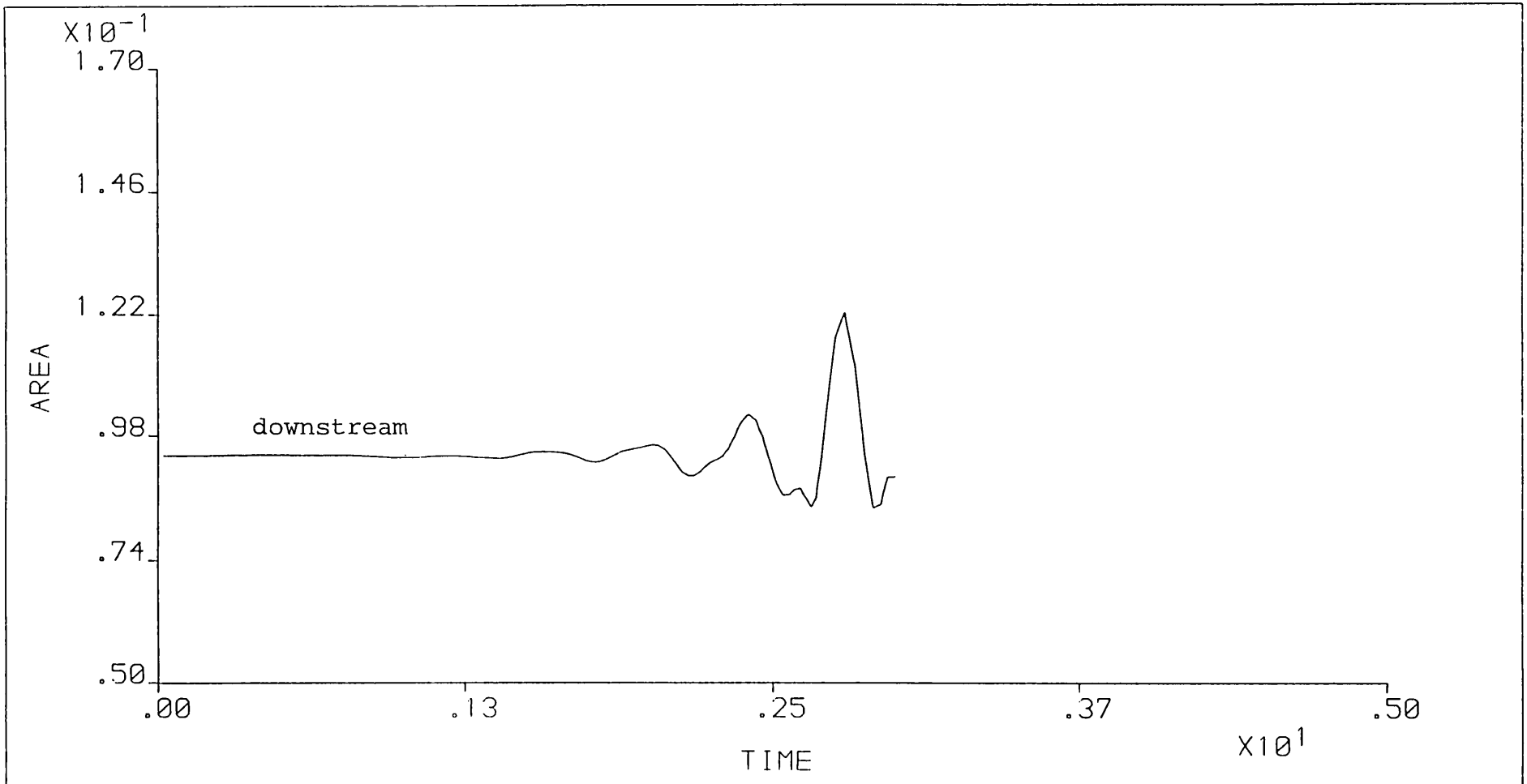



Fig 5.7.22 Effect of using the optimised scheme (see text) for the case shown in Fig 5.7.21. $\Delta x = 0.1$.

# CHAPTER 6

# INSTABILITIES

## 6.1 INTRODUCTION

This chapter is primarily concerned with an investigation of the self-excited oscillations which are commonly observed in experiments on the Starling resistor (see section 2.6). Conrad (1969) and Katz et al (1969) are among those who have observed these oscillations experimentally, while Cancelli et al (1979) and Bertram and Pedley (1982), among others, have simulated such behaviour using mathematical models. However, to date, no satisfactory explanation has been given as to their origin, etc.

The first section of this chapter examines the different types of instability observed in experiments on collapsible tubes. This is followed by a description of the methods used to investigate the stability of equilibrium states in the present model.

Finally, the unsteady flow model is used to predict the occurrence of these different types of instability and also to determine some of the important factors which affect the stability of the system. Instabilities which occur in a particular experiment on the Starling resistor are investigated by choosing initial conditions corresponding to an operating point on the appropriate P-Q characteristic.

## 6.2 TYPES OF INSTABILITY

Instabilities observed in experiments on the Starling resistor are usually oscillatory, ultimately growing into a limit cycle. Exponential type instabilities are less frequently observed due to the way in which the experiments are carried out.

There are two types of oscillation that are commonly observed in experiments on the Starling resistor. These are:

(i) a low frequency 'milking' oscillation involving most of the collapsible tube

and

(ii) a high frequency localised oscillation at the downstream end.

Bertram (1982) uses the term 'stationary' oscillation to describe the latter.

### 6.2.1 Milking Oscillations

Bertram (1982) observed that these oscillations consist of a local flattening (relative to the rest of the more or less collapsed tube) which develops in the upstream half of the tube and then moves to the downstream end. This behaviour has also been observed with the tube in a vertical position by Griffiths (1977), among others. These oscillations are found mostly at low flow rates and are of low frequency (Fig 6.2.1). Some of these oscillations in Bertram's experiment had a period of 15 s or more.

This type of oscillation, as stated by Bertram,

must be associated with wave propagation and may involve the phenomenon of 'choking'. The present model includes wave propagation, however, investigating this type of oscillation is very difficult because the oscillation is of low frequency and therefore the program must be run for a large number of time steps to simulate the oscillation. At first sight this does not appear to be a problem since because of the low frequency a larger time step seems appropriate. However, as already discussed choking may be involved in the process and to attempt to model this phenomenon a fine grid is required, together with a small time step. Thus, to run the program for a large time (ie model time), which is essential in order to observe such an oscillation, a large amount of computer time is required. It was indicated in Chapter 5 that the optimised procedure for calculating $\Delta t$ cannot be used when the curvature of the characteristics is large. If the resources were available to simulate such a process, some modification of the program would still be required to simulate the choking phenomenon and the formation of an elastic jump. Regardless of whether choking does occur, the propagation of a flattened portion of the tube will result in a region of localised curvature, which will significantly influence the size of the time step used.

Perhaps the most that can be achieved at present regarding the simulation of this type of oscillation is to model its onset and then examine the effect of model parameters on its origin. However, very often it is the

period before the process of oscillation begins that is very long and the oscillation itself, although of relatively low frequency, may have a much shorter period. Bertram has observed an oscillation of frequency 3.8 Hz, which is equivalent to a dimensionless period of 6.2 units (see Fig 6.2.1)

6.2.2 'Stationary' Oscillations

Bertram (1982) observed that these oscillations occurred when the tube formed a neck, at the downstream end only, which vibrated laterally, ie between more and less collapsed states. The frequency of these oscillations are very much greater than those of the milking type. Bertram has recorded frequencies $\approx$ 40 Hz and Rodbard and Saiki (1953) observed frequencies up to 750 Hz. The frequency of the oscillations will obviously be influenced by the properties of the collapsible tube and the fluid used (external circuitry will also have an effect, Bertram and Pedley, 1982; Cancelli and Chiocchia, 1979).

Bertram has observed that this type of oscillation occurs at high flow rates (Fig 6.2.1) and suggests that the flow through the neck is probably supercritical. The present solution scheme would need to be modified if the flow was supercritical at the upstream or downstream boundary. The solution procedure should remain unchanged when the flow is supercritical throughout the collapsible tube, provided the above modifications are made. If the flow is locally supercritical (as suggested by Bertram) the grid points and size of time step would have to be chosen very carefully.

### 6.2.3 Exponential Instability

This type of instability is less frequently observed in experiments on collapsible tubes: Bonis (1979) (see Bertram and Pedley, 1982) has reported such an instability. Bertram and Pedley (1982) have predicted the occurrence of exponential instabilities in their model.

## 6.3 STABILITY

Investigation of the stability of the complete model, ie collapsible tube plus boundary conditions, is a very difficult task. In order to proceed, it is assumed that the instabilities in the present model are associated with either the boundary conditions alone, the collapsible tube alone, or some combination of these. The approach to the problem is then to examine the stability of both the collapsible tube and the boundary conditions in isolation, and then to use this information, together with information from experimental studies, to investigate the stability of the complete model. Thus the following areas are examined:

(i) boundary condition instabilities

(ii) collapsible tube instabilities

(iii) combined instabilities.

A linear stability analysis is used for (i) and (ii). (iii) is far more difficult and the predictions from (i) and (ii) provide a useful starting point for investigation.

### 6.3.1 Boundary Condition Instabilities

Pedley (1980) produced a linear stability analysis of his model. The equilibrium states predicted

to be unstable were found to exhibit instabilities when the model equations were solved numerically. This approach is used to determine instabilities associated with the boundary conditions (lumped parameter model equations) in the present model.

The stability of an equilibrium state of the lumped parameter model is examined in the following way. It is assumed that all the variables are subjected to a small perturbation with exponential time variation, ie $A = A^* + a' e^{\sigma t}$, $u = u^* + u' e^{\sigma t}$, etc where the asterisk denotes the equilibrium value of the variable. These expressions are then substituted into the lumped parameter model equations and the non-linear terms in the perturbation quantities are neglected. The equations are then combined to eliminate the perturbation quantities. This results (for $A < 1$) in a cubic equation for $\sigma$, viz

$$c_3 \sigma^3 + c_2 \sigma^2 + c_1 \sigma + c_0 = 0 ,$$

where the coefficients are

$$c_3 = \{L_3(1-\eta) + [1-\beta(1-A^*)]I_1 + L_3\eta\}(I_2 + \alpha L_5)\frac{L_5}{2}$$

$$+ \{L_3(1-\eta) + [1-\beta(1-A^*)I_1]\}(I_2 + L_5)\frac{L_3}{2}$$

$$c_2 = \{[1-\beta(1-A^*)(R_1 + 2K_1Q^*) + 2u^* + \frac{1}{4}L_3A^*R^* - 2Q^*\}(I_2 + \alpha L_5)\frac{L_5}{2}$$

$$+ \{L_3(1-\eta) + [1-\beta(1-A^*)]I_1 - L_3\eta\}\{(R_2 + 2K_2Q^* + 2Q^*)\frac{L_5}{2} - L_5(1-\alpha)u^*$$

$$- u^*(I_2 + \alpha L_5)\} + \frac{L_3}{2}\{L_3(1-\eta) + [1-\beta(1-A^*)I_1]\}\{R_2 + 2[Q^*(K_2+1)$$

$$- u^*]\} + (I_2 + L_5)\{L_3\eta u^* - [2Q^* - (1-\beta(1-A^*))(R_1 + 2K_1Q^*)]\frac{L_3}{2}$$

$$+ [L_3(1-\eta) + (1-\beta(1-A^*))I_1]u^*\}$$

$$\mathcal{C}_1 = \{2u^* + \tfrac{1}{4}L_3A^*R^* + [1-\beta(1-A^*)](R_1+2k_1Q^*) - 2Q^*\}$$

$$\times\{(R_2 + 2k_2Q^* + 2Q^*)\tfrac{L_5}{2} - u^*(I_2+\alpha L_5) - L_5(1-\alpha)u^*\}$$

$$+ \{L_3(1-\eta) + [1-\beta(1-A^*)]I_1 + L_3\eta\}\{\tfrac{3}{2}c_1A^{*-\frac{5}{2}} - u^*(R_2 + 2k_2Q^*$$

$$+ 2Q^*) + u^{*2}\} + (I_2+L_5)\{[(1-\beta(1-A^*))(R_1+2k_1Q^*) - 2Q^*]u^* - p_1^*\beta$$

$$+ p^*(1-\beta) + [A^* + \beta(1-A^*)]\tfrac{3}{2}c_1A^{*-\frac{5}{2}} + \tfrac{1}{2}L_3A^*u^*R^* + \tfrac{1}{4}L_3A^*Q^*R^{*\prime}\}$$

$$+ \{R_2 + 2[Q^*(k_2+1) - u^*]\}\{L_3\eta u^* - \tfrac{L_3}{2}[2Q^* - (1-\beta(1-A^*))(R_1$$

$$+ 2k_1Q^*)] + u^*[L_3(1-\eta) + (1-\beta(1-A^*))I_1]\}$$

$$\mathcal{C}_0 = \{\tfrac{1}{4}L_3A^*R^* + 2u^* + [1-\beta(1-A^*)](R_1+2k_1Q^*) - 2Q^*\}\{\tfrac{3}{2}c_1A^{*-\frac{5}{2}}$$

$$- u^*[R_2 + 2k_2Q^* + 2Q^*] + u^{*2}\} + \{R_2 + 2[Q^*(k_2+1) - u^*]\}$$

$$\times\{u^*[1-\beta(1-A^*))(R_1 + 2k_1Q^*) - 2Q^*] - p_1^*\beta + p^*(1-\beta)$$

$$+ [A^* + \beta(1-A^*)]\tfrac{3}{2}c_1A^{*-\frac{5}{2}} + \tfrac{1}{2}L_3A^*u^*R^* + \tfrac{1}{4}L_3A^*Q^*R^{*\prime}\}$$

Here R* represents the resistance function evaluated at A = A*. These coefficients are more complex than those obtained from Pedley's model. This is primarily due to the inclusion of compliance in region 5 which has given rise to the terms involving $L_5$.

To determine whether any root of the cubic equation has a positive real part (indicating an unstable state), Routh's criterion could be used; this was the method employed by Pedley (1980). Indeed, the analysis would take exactly the same form since $\mathcal{C}_3$ is also positive in this case. This may be advantageous for certain values of some of the parameters, for example, $L_5 = 0$, since the coefficients would then be of a much

simpler form and the effect of individual parameters on the coefficients could be determined. However, in general, the effect of a change in a parameter on a particular coefficient or combination of coefficients is difficult to see. Further, since a standard package for determining the roots of a cubic equation is available (see section 4.3.2) it is used in the present analysis.

6.3.2 Collapsible Tube Instabilities

Pedley (1980) also made an investigation of the stability of the equations of a distributed parameter model on the assumption that 'choking' does not occur. He assumed that upstream of the constriction the equations have equilibrium solutions $A = A^*(x)$, $p = p^*(x)$, $u = u^*(x)$. In his stability analysis he assumed that the equilibrium solutions were sufficiently slowly varying with $x$ that, at each $x$, they could be regarded as uniform. Setting $A = A^* + a'(x,t)$ and similar expressions for u and p, and then linearising and eliminating $p'$ and $u'$, yielded the following equation for $a'$

$$\left\{ \frac{\partial}{\partial t} + (u^* + c^*) \frac{\partial}{\partial x} \right\} \left\{ \frac{\partial}{\partial t} + (u^* - c^*) \frac{\partial}{\partial x} \right\} a' + R(A^*) \left\{ \frac{\partial}{\partial t} + b_1 \frac{\partial}{\partial x} \right\} a' = 0 \quad , \tag{6.3.1}$$

where $c^*$ is the wave speed evaluated at area $A^*$ and $b_1 = u^* \left\{ 1 - A^* \frac{R'(A^*)}{R(A^*)} \right\}$. Equation (6.3.1) has the same form as the equation which describes roll-waves in open channels and the flow is stable if

$$u^* - c^* < b_1 < u^* + c^* \quad .$$

On the assumption that choking does not occur he concludes that instability will occur if

$$S \equiv \frac{u^*}{c^*} > - \frac{R(A^*)}{A^* R'(A^*)} \quad ,$$

which for the function R(A) defined in section 3.6 implies instability if

$$u^* \geq \tfrac{1}{2} c^* ( 1 + A^{*2} ) \approx \tfrac{1}{2} c^*$$

for very small $A^*$[I]. This analysis suggests that instabilities could occur for $\frac{1}{2} \lesssim S < 1$. Of course the larger the value of A* the larger the value of the lower bound of S.

A similar linear stability analysis was made by Ohba et al (1984b). They found that the condition for the initiation of oscillations was $c^* < \frac{1+m}{2-m} u^*$ , where

$m = 1$ for laminar flow and $m = \frac{1}{4}$ for turbulent flow. Thus $S > \frac{1}{2}$ (laminar flow) and $S > 7/5$ (turbulent flow) are the conditions required to initiate oscillation. The latter condition defines a supercritical flow.

6.3.3 Combined Instabilities

The above analysis should provide some insight into the stability of the complete model (distributed parameter model plus lumped parameter model). For example, under certain conditions one of these instabilities (boundary condition or collapsible tube) may dominate, in which case, there is no difficulty in

---

I The assumption $dA^*/dx = 0$ is probably quite reasonable in this case.

locating the unstable states of the complete model. It could be conjectured, for example, that a boundary condition instability would dominate in a short, stiff tube, whereas a collapsible tube instability might prevail in relatively long, highly compliant tubes. However, far more likely to occur is an entirely different instability resulting from a combination of the collapsible tube and the boundary conditions. Thus the stability analyses of sections 6.3.1 and 6.3.2 provide only a rough guide as to the location of instabilities of the complete model.

In experiments (which produce 'N' type P-Q characteristics) instabilities usually occur on the negative slope of the P-Q characteristic. Thus in simulating such experiments, equilibrium states corresponding to operating points in this region of the P-Q characteristic would be investigated first.

One way of speeding up the search for unstable equilibrium states is to apply a small perturbation to one of the variables: the pressure head, $p_h$, is a convenient choice.

In conclusion, to locate an unstable state, some, if not all, of the following are satisfied by the equilibrium state:

(i) boundary conditions are predicted unstable

(ii) collapsible tube is predicted unstable

(iii) operating point is in region of P-Q characteristic where instabilities in experiments occur.

Further, a small perturbation is sometimes applied to

trigger the instability.

## 6.4 RESULTS

Investigation of the stability of such a complex system is an extremely difficult task. The methods proposed which were described in section 6.3, are shown to be most useful in the present study.

There are numerous factors which can affect the stability of this system, for example, wave propagation, boundary conditions (which can involve several parameters), and part of this investigation is to determine some of the more important of these. The other area to be investigated is that of instabilities which occur in experiments on the Starling resistor. This is accomplished by relating the starting equilibrium state to an operating point on a P-Q characteristic which corresponds, as far as possible, to that obtained in an experimental study. This should provide some information on the type of oscillations which occur and the stability of such a system.

### 6.4.1 The Effect of Wave Propagation on Instabilities Associated with the Boundary Conditions

Bertram and Pedley (1982) used a lumped parameter model to describe unsteady flow in a collapsible tube held between two rigid tubes and contained in a pressurised chamber. Equilibrium states and their stability were analysed in detail. However, since this was a lumped parameter model the effect of wave propagation on stability was not included. The purpose of this section is to examine the effect of wave

propagation on these results.

It was shown in earlier chapters that the model used by Bertram and Pedley is easily incorporated as a special case of the present model, by setting $L_4 = 0$,etc. To investigate the effect of wave propagation on a particular equilibrium state a non-zero value of $L_4$ is chosen. Viscous dissipation in region 4 modifies the equilibrium state and so $R_k$ is set equal to zero at all but the first grid point (station B). Thus it is possible to start from an actual equilibrium state calculated by Bertram and Pedley. In this way some insight into the importance of unstable boundary conditions is determined.

It is conjectured that instabilities associated with the boundary conditions (lumped parameter model) can also be associated with the full model when $L_4$ is fairly short and the tube quite stiff. However, for longer and more elastic tubes it is anticipated that instabilities are not directly the consequence of the boundary conditions and may result from some mechanism in region 4 itself, or a combination of both. Instabilities in region 4 may be associated with the phenomenon of choking and whether or not choking occurs at a particular flow rate depends upon several parameters; $L_4$, R(A), $c_1$, etc. A roll wave type instability has also been proposed by Pedley (1980) (see section 6.3.2).

One of the unstable states (predicted oscillatory unstable) considered by Bertram and Pedley is now examined.

The parameter values are as follows: $L_3 = 10$, $L_4 = L_5 = 0$, $Q = 1$, $I_2 = 25$, $R_2 = 75$, $r(=I_1/I_2 = R_1/R_2) = 0.5$, $k_1 = k_2 = 0$, $c_1 = 4$ and $\Delta t = 0.02$. The upstream pressure head determined from the steady flow program is $p_h = 172.99$. Following Bertram and Pedley the solution is started at $t = 0$ with $p_h = 173$. Figs 6.4.1 and 6.4.2 show the build up of the oscillation to a limit cycle in area and flow rate respectively. These results are in excellent agreement with those of Bertram and Pedley. The flow reverses (Fig 6.4.2) during the cycle with a magnitude $\approx 1/8$ of the peak to peak value. Fig 6.4.3 shows that the flow is supercritical during part of the cycle, however, no real significance can be drawn from this since wave propagation is not possible in the lumped parameter model. It is interesting to see that the equilibrium values of u and c result in $S > \frac{1}{2}$ (possibility of a roll wave type instability in the distributed parameter model). The effect of wave propagation is now examined.

In the first test $L_4 = 1$. It was shown in section 5.7.2 that $\Delta x = 1/40$ was sufficiently small when the characteristics remained inside the cell, ie the condition $(|u| + c)_{max} \frac{\Delta t}{\Delta x} < 1$ is satisfied. However, this requires a large amount of computer time and so a method using fewer grid points and larger time steps (by allowing characteristics to cross more than one cell)

was developed. The criterion used was

$$(|u| + c)_{max} \frac{\Delta t}{\Delta x} < \text{int}\left[\frac{(|u|+c)_{max}}{||u|-c|_{min}}\right] (= nrc) \quad , \quad (6.4.1)$$

where int(z) is the integer part of z nearest zero and nrc is the number of reaches crossed. This proved a very effective method and the saving in computer time was enormous. A similar method is used here, the only difference being that an upper bound to the value of the expression on the right hand side of (6.4.1) is imposed. This is determined from a comparison of the results obtained using $\Delta x = 1/40$, with the characteristics inside the cell (nrc = 1), with those obtained using $\Delta x = 1/10$; for the case $L_4 = 1$. The value nrc = 4 is found to give the closest agreement with the standard solution. Note that this value of nrc is an upper bound and smaller values are taken automatically, when they occur, by using the formula (6.4.1). A comparison of the two cases nrc = 1 (41 grid points) and nrc = 4 (11 grid points) is shown in Fig 6.4.4. The detailed shape of the waveform is missed when nrc = 4, however, the main features, frequency, onset, etc are captured: this is all that is required in the present study.

The effect of wave propagation is now examined in some detail. Fig 6.4.4 shows the effect of imposing $p_h = 173$ at t = 0, when $L_4 = 1$. An instability grows very quickly, note the change in time scales (cf Fig 6.4.1) and ultimately 'crashes' at the downstream boundary with the area taking negative values. This breakdown results from the inability of the present model to deal with

such large amplitude oscillations. Bertram and Pedley modified the tube law to overcome this problem, however, such a modification is not made here since a change in the tube law results in a different throat pressure which may ultimately affect the equilibrium state and its stability.

The breakdown occurs at around t = 2.5. This is extremely rapid, in the case of the lumped parameter model a limit cycle took approximately 10 times longer to develop. The frequency of the oscillation is approximately 2.4 whereas for the lumped parameter model the frequency was $\approx 0.88$. It appears that the introduction of a short length of tube, $L_4 = 1$, has modified the stability of the complete system making it much more unstable.

Two factors have been introduced by choosing $L_4$ non-zero, viz

(i) the inertia of the fluid in $L_4$

and

(ii) wave propagation in this region.

Wave propagation may affect the stability of the system. The inertia will obviously affect the wave propagation, but must also affect the growth, frequency, etc of any resulting oscillation, regardless of the mechanism involved.

Based on the values of u and c at t = 0, which are constant in region 4 since the flow is inviscid, $|u + c| \approx 25.1$ and $|u - c| \approx 3.8$. Thus a disturbance

at the upstream boundary arrives at the downstream end within $\approx 1/25$ units of time, while propagation upstream takes more than six times longer.

In the lumped parameter model ($L_4 = 0$) wave propagation is instantaneous. By choosing $L_4 \neq 0$ a time delay (corresponding to the time taken for a wave to propagate the distance $L_4$) is introduced. If the present instability is a manifestation of the boundary condition instability then the phase lag, between the two boundaries, may be responsible for the earlier onset of oscillations. The inertia of the fluid in $L_4$ obviously has an effect on the frequency of the resulting oscillation.

Since $S > \frac{1}{2}$ there is the possibility that the instability is associated with the distributed parameter model or indeed, and perhaps more likely, a combination of the distributed parameter model and boundary condition instabilities. At this stage it is difficult to draw any conclusions as to the origin of the instability. The effects of larger values of $L_4$ are now investigated to give some insight into this problem.

Results for $L_4 = 3$, using 31 grid points, are illustrated in Figs 6.4.5-6.4.8. In this case a limit cycle of frequency $\approx 2$ is produced. The amplitude is $\approx 2/3$ of the amplitude of the lumped parameter model limit cycle. The frequency ($f \approx 2$) is lower than in the case $L_4 = 1$ and since the solution did not break down it is assumed that the amplitude is also less. Fig 6.4.6 shows

the behaviour at the upstream boundary, where the amplitude of the oscillation $\approx$ 1/6 of the downstream value. This reduction in amplitude is partly due to the attenuating effect of the viscous resistance at the upstream boundary. The flow rate and speed index at the downstream boundary are shown in Figs 6.4.7-6.4.8. The flow remains subcritical during a complete cycle (cf Fig 6.4.3). This is therefore an instability which does not involve choking or supercritical flow. It is interesting to see that S never falls below S = ½ during the oscillation. S > ½ is of course the condition for a roll wave type instability, associated with region 4, and may be important in this case.

The results for $L_4$ = 5 are shown in Figs 6.4.9-6.4.10. The frequency of the limit cycle is reduced once more ($f \approx 5/4$) as is its amplitude. The oscillation in area is more non-linear in this case. The collapsing phase occurs relatively slowly and consists of two stages, the latter stage consisting of an area change $\approx$ ½ of the former. In contrast the reopening phase is a single stage process and occurs very rapidly. These features are characteristic of relaxation oscillations.

It is apparent from Fig 6.4.9 that the build up of the oscillation is on a time scale associated with the travel time (upstream - downstream - upstream) of a wave in the fluid ($\approx 3/2$ units: this time is based on the values of the variables at time t = 0). This suggests the importance of the effect of boundary conditions on stability.

The limit cycle in flow rate (Fig 6.4.10) does not exhibit the two stage phenomenon observed in the area plot. However, the jerky nature is evident, with the increase in flow rate taking approximately half the time of the decrease in flow rate.

The general trend, based on the three results $L_4$ = 1, 3 and 5 is that increasing $L_4$ reduces the amplitude and frequency of the resulting oscillation. Further the oscillations take a longer time to grow and become more non-linear. With regard to stability it does not appear that the boundary conditions play a major role since the build up time of the oscillation is related to the travel time of the wave in the fluid (which links the boundary conditions). Although $S > \frac{1}{2}$ implying the possibility of a roll wave type instability, the resulting oscillation does not exhibit the characteristics of such an instability (based on their form in open channel flow). Region 4 obviously does affect the stability of the system in some way and indeed the inertia of the fluid in this region could provide a possible explanation for the change in the frequency of the limit cycle with increase in $L_4$.

In the above tests $L_3 > L_4$. A case in which $L_4 > L_3$ is now investigated to determine whether the stability of the system is significantly affected. For longer tubes more grid points are required (so as to maintain the value for $\Delta x = 1/10$) and because of the above trend (slower growth in oscillation with increase in $L_4$) a greater number of time steps. To reduce

computer time some results are computed with a larger value of nrc, viz nrc = 7[I]. Results obtained using this criterion are illustrated in Figs 6.4.11-6.4.12 for the cases $L_4 = 3$ and $L_4 = 5$. The limit cycles are qualitatively similar to those shown in Figs 6.4.5 and 6.4.9, indeed the frequencies are virtually identical. The most striking differences are in amplitude and build up of the oscillation. This is presumably due to the decrease in the number of interpolations which, as shown in section 5.3.3, can produce significant numerical damping of the physical wave. All the trends observed previously (nrc = 4) when $L_4$ was increased, are evident in these results.

The oscillation in Fig 6.4.13 is obtained using nrc = 7 for a value of $L_4 = 15$ ($> L_3 = 10$) and 151 grid points. The build up of the oscillation consists of a series of bursts, the initial bursts being separated by a time interval corresponding to the travel time of the wave in the fluid. Both the amplitude and the length of the disturbance increase with successive propagation. Ultimately a wave motion is established extending the length of region 4. The shape of the oscillation is similar to that obtained when $L_4 = 5$ (Fig 6.4.12) but the amplitude is much smaller ($\approx \frac{1}{4}$). The slower build up of the oscillation is consistent with the increased travel time associated with the greater length of region 4.

---

I It should be remembered that nrc is an upper bound and values smaller than this will frequently be taken.

The upstream area variation (Fig 6.4.14) has an amplitude $\approx \frac{1}{4}$ of that found downstream.

It is apparent that the frequency of the oscillation, although smaller than in the case $L_4 = 5$, is not as small as would be expected from the earlier results. Fig 6.4.15 shows the change in frequency with length of region 4. For small $L_4$ the frequency decreases rapidly as $L_4$ is increased, however, the change in frequency at larger $L_4$ is very much reduced. Interpolating on this curve suggests that an oscillation of frequency corresponding to that when $L_4 = 0$ would occur for $L_4 = 8.25$. This is somewhat speculative since the number of points to which the curve has been drawn are very few. Indeed the curve may contain discontinuities, which would lead to a slightly different interpretation of the results.

In conclusion the following points are noteworthy:

Increasing $L_4$ has the following effects on the oscillation; the amplitude and frequency are decreased, the shape is more non-linear and the build up takes longer.

The form of the oscillation is different from the two commonly observed types, viz 'stationary' and 'milking' oscillations. It appears that a disturbance is modified at each boundary and also as it travels through region 4. The build up of this type of oscillation involves wave propagation.

The flow remains subcritical throughout the cycle.

### 6.4.2 The Effect of Model Parameters on the Form of the Oscillations

In this section the effect of several model parameters, $I_1$, $I_2$, etc on the character of the oscillations is investigated. Consider the equilibrium state at t = 0 which is determined by the following parameter values: $Q = 0.5$, $L_3 = L_4 = 2$, $L_5 = 0$, $R_1 = k_1 = k_2 = 0$, $R_2 = 50$, $I_1 = 12.5$, $I_2 = 25$. This is taken as the standard case. The boundary conditions are predicted to be oscillatory unstable and $S < \frac{1}{2}$ at the downstream boundary (the maximum value of S occurs at the downstream boundary).

In this study some form of perturbation is applied to the upstream pressure head, $p_h$. Such a perturbation is useful since it triggers an instability much more quickly and hence reduces computer time. The results in this section were obtained by starting from an equilibrium state and applying a sinusoidal perturbation to $p_h$ of frequency unity and amplitude 1% (peak to peak).
Other types of perturbation were used to check that the oscillations were not being driven or triggered by a forcing frequency, characteristic of the complete system; although interest here is not in the cause of instability but rather in the form of the resulting oscillations.
A square wave pulse in $p_h$, sinusoidal perturbation of the downstream pressure head and stopping the forcing oscillation in $p_h$ after a certain time, all produced, ultimately, the same behaviour.

The limit cycle produced in the standard case is shown in Figs 6.4.16-6.4.18. The frequency of the limit cycle $\approx 6$ and the forcing oscillation can be observed as a low frequency modulation. This oscillation is similar to the so-called flitter observed in collapsible tube flow (Rodbard and Saiki, 1953). The amplitude of the downstream oscillation in Q is approximately $\frac{1}{3}$ of the upstream value, whereas the reverse is true in the case of the cross-secional area; in fact the ratio $\approx 2/5$.

Fig 6.4.19 shows the effect of increasing the upstream and downstream rigid tube inertia by a factor of 10 ($I_1 = 125$, $I_2 = 250$). The initial boundary conditions are again predicted to be oscillatory unstable and at the downstream boundary $S < \frac{1}{2}$ (in fact S will be less than $\frac{1}{2}$, initially, in all the tests in this section, since the parameters varied do not affect the downstream boundary values of area and flow rate). A larger amplitude ($\approx$ x 8), lower frequency ($\approx 5/2$) oscillation is produced. The modulation frequency $\approx 4/11$ in this case. The modulation must be affected by the acceleration/deceleration of the fluid in the upstream rigid tube caused by the perturbation in $p_h$. The reduction in the modulation frequency is consistent with an increase in the inertia $I_1$. The importance of the rigid tube inertias $I_1$, $I_2$ on the form of the main oscillation is now investigated by considering a change in only one of these parameters, the other corresponding to the standard case value.

Fig 6.4.20 shows the effect of increasing upstream inertia by a factor of 10 ($I_1$ = 125, $I_2$ = 25). The boundary conditions are predicted to be stable in this case. The limit cycle has a slightly greater amplitude than that in the standard case (Fig 6.4.17). A low frequency modulation is evident of frequency $\approx \frac{1}{2}$ (see expanded scale plot Fig 6.4.21). This is approximately the value found when both $I_1$ and $I_2$ were increased by a factor of 10. Thus it appears, as expected, that the modulation frequency is mainly determined by $I_1$. The frequency of the oscillation itself is the same as that in the standard case. This suggests that the frequency of the main oscillation is governed by the downstream inertia, $I_2$.

Fig 6.4.22 shows the effect of increasing the downstream rigid tube inertia, $I_2$, by a factor of 10. The boundary conditions are predicted oscillatory unstable. The onset of the oscillation occurs earlier and grows rapidly with a frequency $\approx$ 5/4. The amplitude increases until the model eventually breaks down with a negative area predicted. It appears from these results that the downstream inertia has a significant effect on the oscillations.

The effect of reducing viscous resistance is shown in Fig 6.4.23. $R_K$ is not a purely 'unsteady parameter' like inertia and so the equilibrium state is modified in this case. The boundary conditions are still predicted oscillatory unstable. The onset of the

oscillation occurs earlier and the amplitude is slightly larger than that in the standard case; the frequency is virtually the same.

The parameter $L_5$ has a stabilising effect. The values $L_5 = 1$ and $L_5 = 2$ resulted in initial boundary conditions which were predicted stable, and indeed the equilibrium states were found to be stable.

The effect of the parameters $\varepsilon$ and $\eta$ cannot be tested if either $L_3$, $L_5$ or both are zero, since the unsteady flow terms do not then appear. Since in the standard case $L_5 = 0$, and $L_5$ has a stabilising effect, then the effect of the $\eta$ parameter cannot be tested. However, $\eta$ and $\varepsilon$ have been tested in unstable flow cases and were found to have no significant effect on the form of the instability.

In conclusion:

The downstream inertia, $I_2$, appears to have a significant effect on the form of the oscillations. However, since $L_5$ was zero when this was observed (thus providing a direct link between the downstream boundary and $I_2$) it would be unwise to form any strong conclusions about the role of $I_2$.

$L_5$ has a stabilising effect.

$I_1$ has little or no effect on the main oscillation; it may have a greater effect for $L_3 = 0$. However, for $L_3$ equal to zero the equilibrium state is modified since $L_3$ is not a purely unsteady parameter (cf $L_5$); viscous effects are included in region 3 and involve $L_3$.

$R_K$ obviously affects the equilibrium state and so any conclusions regarding the effect of this parameter must be made with some care. However, the earlier onset and increase in amplitude is consistent with decreased viscous dissipation. The very slight increase in the frequency of the oscillation is presumably due to the decrease in the inertia of the fluid in region 4; the smaller viscous dissipation producing a smaller upstream area.

### 6.4.3 Instabilities in Experimental Models (Starling resistor)

In this section an attempt is made to explain some of the instabilities which occur in physical experiments on collapsible tubes. Attention is focussed on the experiment carried out by Conrad(1969). Previous theoretical investigations into the stability of flow in collapsible tubes have been based on lumped parameter or linearised distributed parameter models, and in many cases have not been related to physical experiments. Admittedly there is a lack of complete experimental data on collapsible tube flow, however, it is felt that a useful investigation of these instabilities can still be made with the available data. Relating the equilibrium state initial conditions to an operating point on the particular P-Q characteristic is shown to be useful in discussing the type and mechanism of the oscillations.

Since the present model includes wave propagation the phenomenon of choking can also occur. This is believed to be a primary mechanism for instabilities in

experiments on the Starling resistor (for example, see section 6.2).

Consider the P-Q characteristic illustrated in Fig 6.4.24. This curve is obtained from the steady flow model using parameters corresponding, as far as possible, to curve 4 of Conrad (1969); but with a stiffer tube ($c_1 = 4$). Since instabilities are most frequently observed when the operating point is on the negative slope of the P-Q characteristic, the initial conditions are chosen to correspond to an equilibrium state in this region. For $Q > 0.75$ a decrease in $p_h$ produces an increase in Q. Therefore, operating points on the curve in the region $Q > 0.75$ do not correspond to points on the same P-Q characteristic as those in the region $Q \leq 0.75$; the region $Q > 0.75$ cannot be reached by increasing $p_h$. Also, $p_1 > p_e$ for $Q > 0.67$ and $A_\beta < 1$. This is due to the value chosen for $\beta$ (= 0.58), which produces too great a pressure drop in region 3. The values of the other model parameters are: $I_1 = 12.5$, $I_2 = 25$, $L_3 = L_5 = 2$, $L_4 = 10$, $R_1 = k_1 = 0$, $R_2 = 66$, $k_2 = 204$, $p_e = 175$.

The equilibrium state $Q = 0.77$ is predicted to have exponentially unstable boundary conditions. The flow is subcritical throughout the tube, with $S \approx \frac{1}{3}$ at the downstream boundary. Starting from this equilibrium state (no perturbation applied) results in the exponential instability shown in Figs 6.4.25 - 6.4.26. Consider the following operating points obtained from the steady flow model:

| Q | $p_h$ | |
|---|---|---|
| 0.7 | 181.2 | } increasing |
| 0.75 | 188.5 | } |
| 0.76 | 187.3 | |
| 0.77 | 183.4 | (starting state) |

Assuming $p_h$ changes linearly in the interval $0.7 \leq Q \leq 0.75$, then $p_h = 183.4$ corresponds to $Q = 0.72$. This is approximately the final value of Q attained in Fig 6.4.26. Thus, starting from an equilibrium state with exponentially unstable boundary conditions, the area changes dramatically and the flow rate changes very slightly to correspond to an equilibrium state on the P-Q characteristic at the same value of $p_h$.

It is apparent that the greatest area change occurs at the downstream boundary whereas the greatest flow rate variation occurs at the upstream boundary; flow reversal occurs at the upstream boundary during the initial collapse. The smallest amplitude damped oscillations, ie those in flow rate variation at the downstream boundary, exhibit the greatest non-linearity.

It would be extremely difficult to arrange an experiment so as to observe an exponential type instability, however, Bonis (1979) (see Bertram and Pedley, 1982) has observed such instabilities.

In the following numerical experiments a square pulse perturbation or a step change in $p_h$ is applied to the initial equilibrium state in order to speed up the onset of instability or enter a region not possible using the steady flow model, respectively. Fig 6.4.27 shows a

P-Q characteristic corresponding to curve 4 of Conrad (1969). In this case $\beta = 0.5$ resulting in a smaller $(\Delta p)_{max}$ than obtained in section 4.4.3 (cf Fig 4.4.6; $\beta = 0.58$), and smaller than the experimental value. $c_1 = 1.15$, $L_5 = 0$ and all the other parameter values are as defined in the previous test.

Starting from the equilibrium state Q = 0.77 (near the valley of the characteristic) and applying a single square pulse perturbation of magnitude unity and period two, results in the curves shown in Fig 6.4.28. The boundary conditions in this case are predicted oscillatory unstable. The initial equilibrium state is a subcritical flow with $S > \frac{1}{2}$ throughout the tube. In this case the stability analysis fails and the flow quickly settles down to the original equilibrium state. The perturbation affects the upstream boundary first; however, the greatest initial area change occurs at the downstream boundary. When the wave propagates downstream, reflected waves are produced due to the change in admittance, resulting from the change in area (and hence wave speed). The propagation time (downstream) of the wave, based on the initial values of the variables, is consistent with the travel time determined from the results shown in Fig 6.4.28. Subsequent travel times depend upon the state of collapse of the tube.

The subsequent peaks at the midstream and upstream location correspond to the reflected wave from the downstream end, which decreases in amplitude as it propagates upstream due to the increase in area.

The flow rate remains subcritical throughout and the flow rate at the downstream end remains virtually constant. The wave motion is eventually damped out and the original equilibrium state is achieved. Several different values of the parameters $I_1$, $I_2$, $L_5$ and $c_1$ could not produce an instability.

The other P-Q characteristic in Fig 6.4.27 corresponds to curve 1 of Conrad (1969). Again, as above, the magnitude of $(\Delta p)_{max}$ is smaller than the experimental value. The parameter values in this case are as follows: $I_1 = I_2 = 15$, $L_5 = 2 = L_3$, $L_4 = 10$, $R_1 = k_1 = 0$, $R_2 = 18$, $k_2 = 99$, $\beta = 0.5$, $p_e = 175$, $c_1 = 1.15$. The boundary conditions for points on this P-Q characteristic ($A < 1$) are predicted stable, and indeed no instabilities arise when a perturbation is applied. Of course there is a region on the P-Q characteristic which cannot be reached using the steady flow program since the region corresponds to $S \gtrsim 1$. In this case marching upstream in the steady flow solution scheme is invalid (section 4.4.3) and thus the equilibrium state cannot be determined. However, this region can be reached using the unsteady flow program by starting at a point on the P-Q characteristic close to this region and then increasing or decreasing $p_h$, depending on whether the area is less or greater than unity, respectively. Fig 6.4.29 shows the effect of starting at $A > 1$ with $Q = 1.25$ and applying a step change in $p_h$ of -3 units. This results in $p_h$ changing from $\approx 177.3$ to $\approx 174.3$, where $p_e = 175$. The final state

should therefore correspond to an area less than unity.

The initial propagation of the wave downstream and then upstream, results in the whole tube gradually collapsing to $A \approx 1$. Subsequently there is a rapid decrease in area at the downstream end, while the upstream half of the tube collapses much more slowly; this results in a large area gradient along the tube. When A falls just below unity there is approximately an eightfold decrease in the wave speed, which results in about a fivefold increase in the time taken for a wave to propagate downstream. The time taken to propagate upstream is increased by almost two orders of magnitude since u is now close to c (Fig 6.4.30). In fact $u \approx c$ at the downstream boundary, before the wave has time to return upstream. The viscous losses must be responsible for the larger reduction in pressure at the downstream end and resulting small area. The change to super-critical flow may have been expected from consideration of the P-Q characteristic. The present solution scheme would have to be modified to deal with this situation ($u \approx c$) and therefore the subsequent behaviour cannot be discussed. However, it does seem likely that choking would be involved in any resulting instability: the distributed parameter model will have a strong influence on the instability in this case.

Fig 6.4.31 shows the effect of a step change of -1 unit in $p_h$ on an equilibrium state corresponding to $Q = 0.78$ ($A \gtrsim 1$). This point lies on the P-Q characteristic corresponding to curve 4 of Conrad (1969)

shown in Fig 6.4.27. In the present case $L_5 = 2$ and $I_1 = I_2 = 15$; all other parameter values are unchanged from the previous investigation of an operating point on this curve.

The flow is initially subcritical throughout the tube, $S < \frac{1}{2}$, and the boundary conditions are predicted oscillatory unstable.

Again, as in the previous case, the initial wave propagation downstream and then upstream, results in a gradual decrease in area over the whole tube to $A \approx 1$. Subsequently, the upstream half of the tube collapses more slowly and collapse progresses with the downstream area reaching a minimum first. Points upstream reach their minimum areas at later times, corresponding to their greater distance upstream. The reopening phase at the downstream boundary is almost a mirror image of the collapse phase; however, upstream events are quite different. The wave of opening propagates upstream, steepening as it proceeds. Fig 6.4.32 shows that the speed index also increases. When the wave reaches the upstream end it is so steep that the area changes from $\approx 0.6$ to unity very rapidly. The flow then becomes subcritical again over the whole tube. At this stage the process starts again. Fig 6.4.33 shows that the flow rate remains virtually constant at the downstream boundary throughout the oscillation. The solution eventually breaks down at the grid point adjacent to the downstream boundary with a negative area predicted. The

flow goes supercritical at this point, probably due to the discontinuity in the wave speed at A = 1.

The instability is of relatively low frequency and involves wave propagation. It occurs at a low flow rate; however, it differs in detail from the milking type oscillation described in section 6.2.1, which involves a local flattening upstream which propagates downstream. $S > \frac{1}{2}$ over the whole tube when the downstream area reaches a minimum and so perhaps some roll wave type instabiltiy is involved in this case.

Figs 6.4.35-6.4.37 show the result of starting at an operating point on the P-Q characteristic (Fig 6.4.34) with Q = 0.78 ($A \gtrsim 1$). After 1 unit of time the upstream pressure head is reduced by 1 unit, with the final value corresponding to an operating point on the negative slope with $A < 1$. The parameter values, except for $c_1$ (= 2.7), are the same as those used in the previous case. The maximum pressure drop in this case is much smaller (cf Fig 6.4.27).

The step change produces a smaller reduction in area in this case, due to the greater tube stiffness (Fig 6.4.35). A higher frequency growing oscillation is produced in this case. As before the flow rate at the downstream end remains almost constant throughout (Fig 6.4.36). The high frequency oscillations in all the variables are due to the discontinuity in the wave speed at A = 1 (Fig 6.4.37).

Again the form of the oscillations is the same as in the previous case, with the downstream end remaining

open until the steepening wave of reopening reaches the upstream boundary. Successive waves are steeper producing larger and larger area changes. The frequency and amplitude of the oscillations increase with successive propagation of the wave.

The speed index at the downstream end remains virtually constant (except for the discontinuity which occurs at A = 1) with a value $\lesssim \frac{1}{2}$. Dr Chris Bertram has observed experimentally that during some oscillations the wave speed changes with the fluid speed in such a way that S remains virtually constant (with S close to unity).

The wave speed, relative to the fluid, does not change significantly over the area range; any change in area is balanced by an opposite change in fluid velocity so as to maintain the value of the flow rate. Thus an approximation to the travel time, for $A < 1$, can be made, at least for the first cycle. After the initial wave propagation upstream and downstream, which takes approximately 1.2 units of time, three further traverses of the wave (now travelling at a much lower speed) occur before the tube reopens again at the downstream boundary.

It appears that the flow is driven to unity speed index (Fig 6.4.37). Subsequent investigation of this type of oscillation, and indeed the majority of oscillations observed in this section, must involve a model which can deal with elastic jumps.

In conclusion: two different types of instability are predicted

(i) exponential type,

(ii) low frequency, large amplitude oscillation.

Wave propagation is involved in the mechanism of the latter and the flow is driven to unity value of the speed index at some point in the tube.

As observed in the previous sections, the greatest area fluctuation occurs at the downstream boundary and the greatest flow rate fluctuation at the upstream boundary.

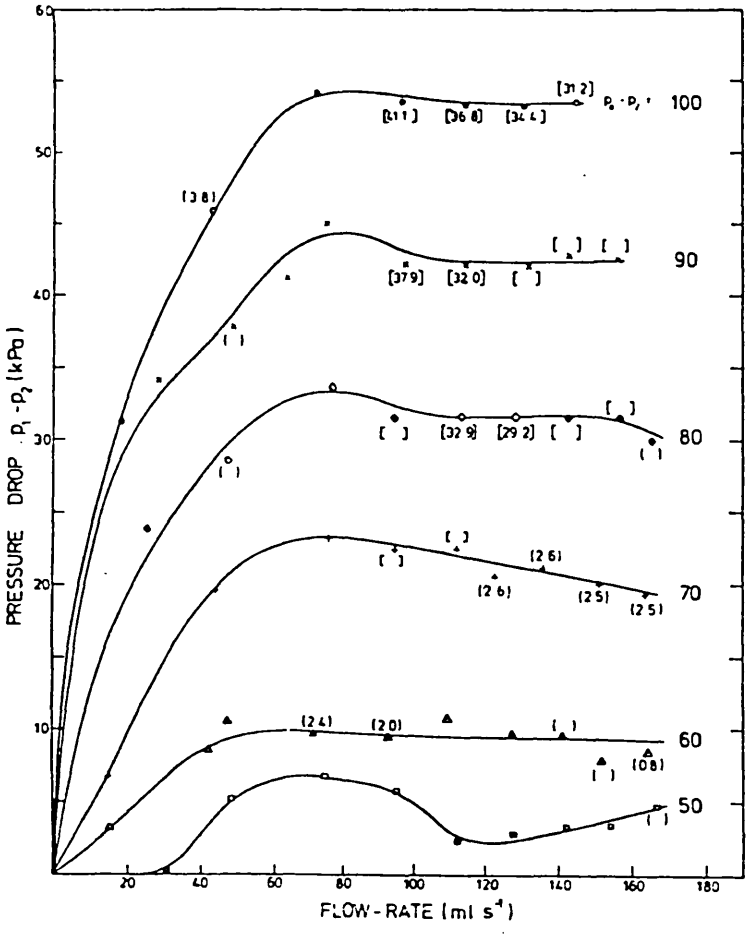



Fig 6.2.1 Experimentally determined P-Q characteristics for various values of $p_e - p_2$ = constant. ( ) indicates a low frequency 'milking' oscillation and [ ] indicates a high frequency 'stationary' oscillation. Figures in parentheses and brackets are frequencies of oscillation in Hz. (From Bertram, 1982).

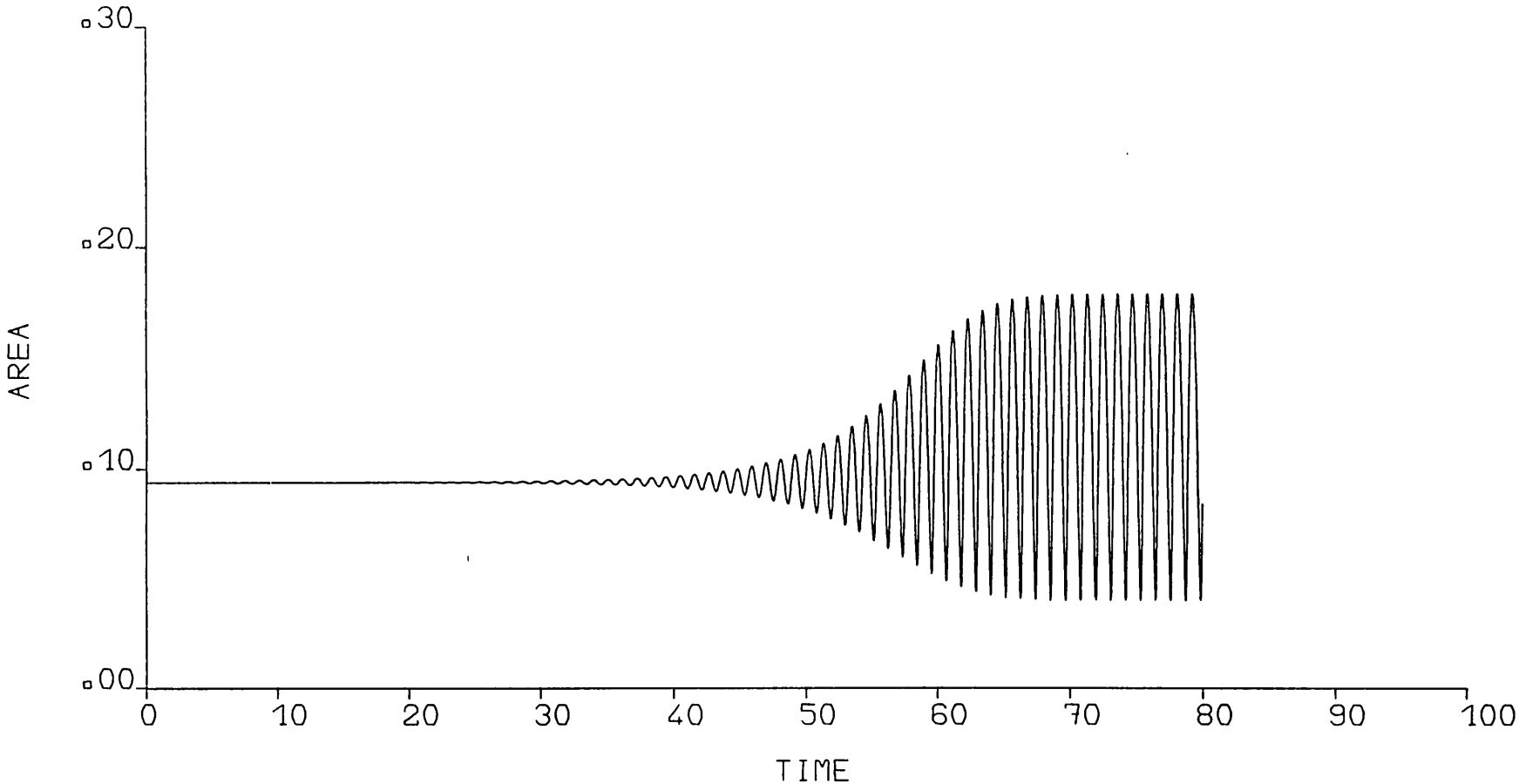



Fig 6.4.1 Standard case: limit cycle resulting from an unstable equilibrium state of the lumped parameter model of Bertram and Pedley (1982). Frequency of oscillation $\approx 0.88$. $\Delta t = 0.02$. See text for parameter values.

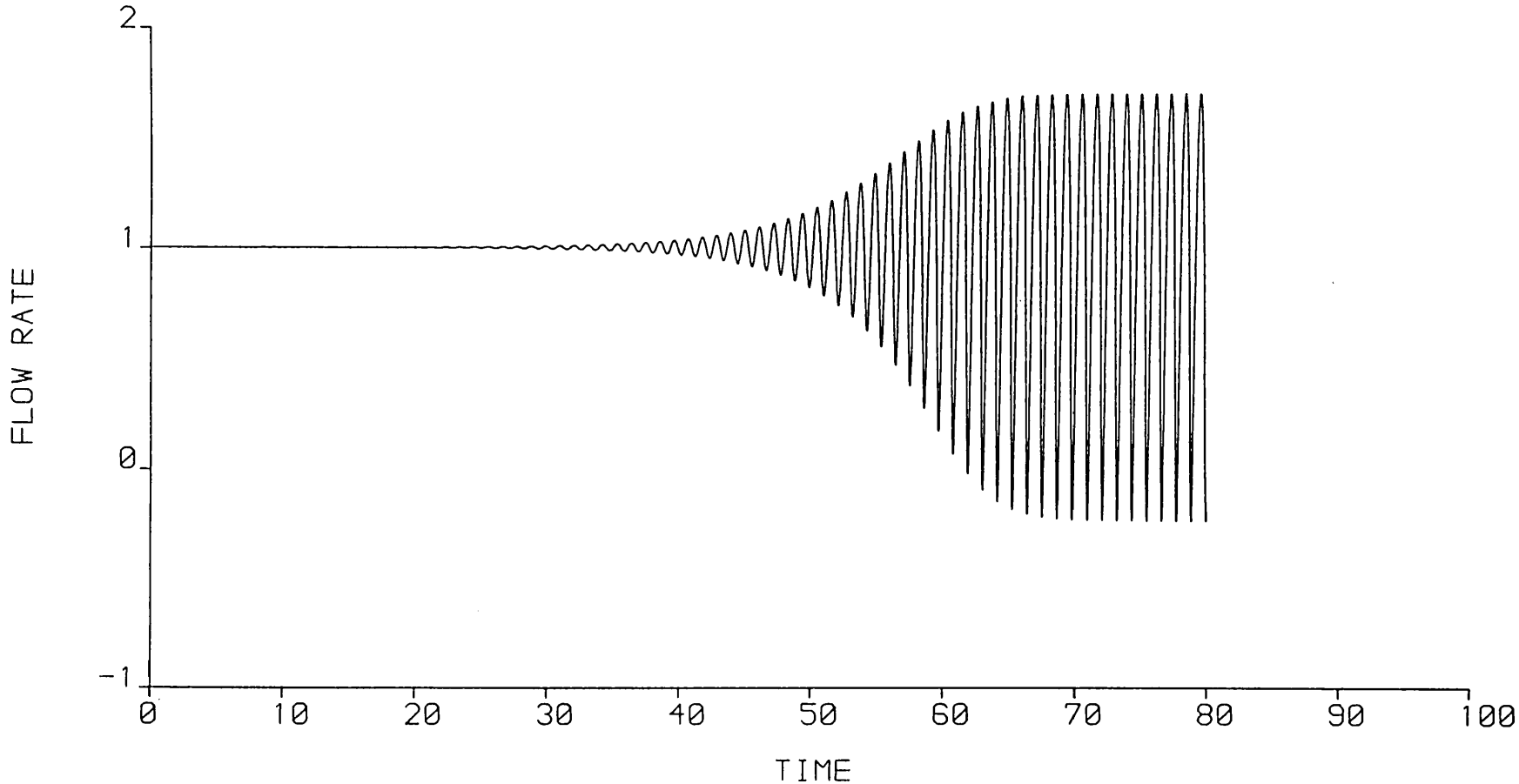



Fig 6.4.2 Limit cycle in flow rate corresponding to that in area shown in Fig 6.4.1. Note region of flow reversal.

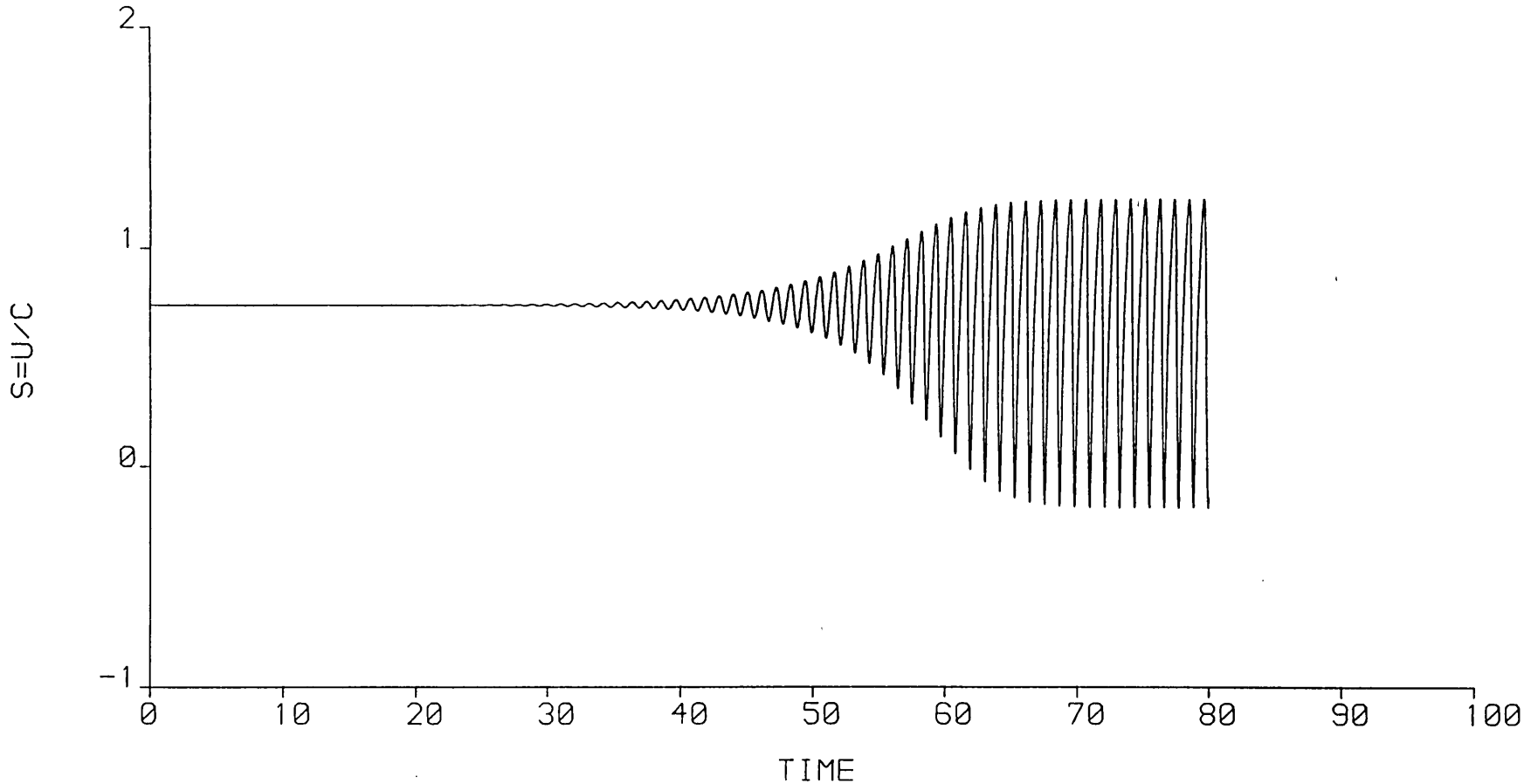



Fig 6.4.3 Limit cycle in the speed index, S, corresponding to the results shown in Figs 6.4.1 and 6.4.2. In the initial equilibrium state $S > \frac{1}{2}$.

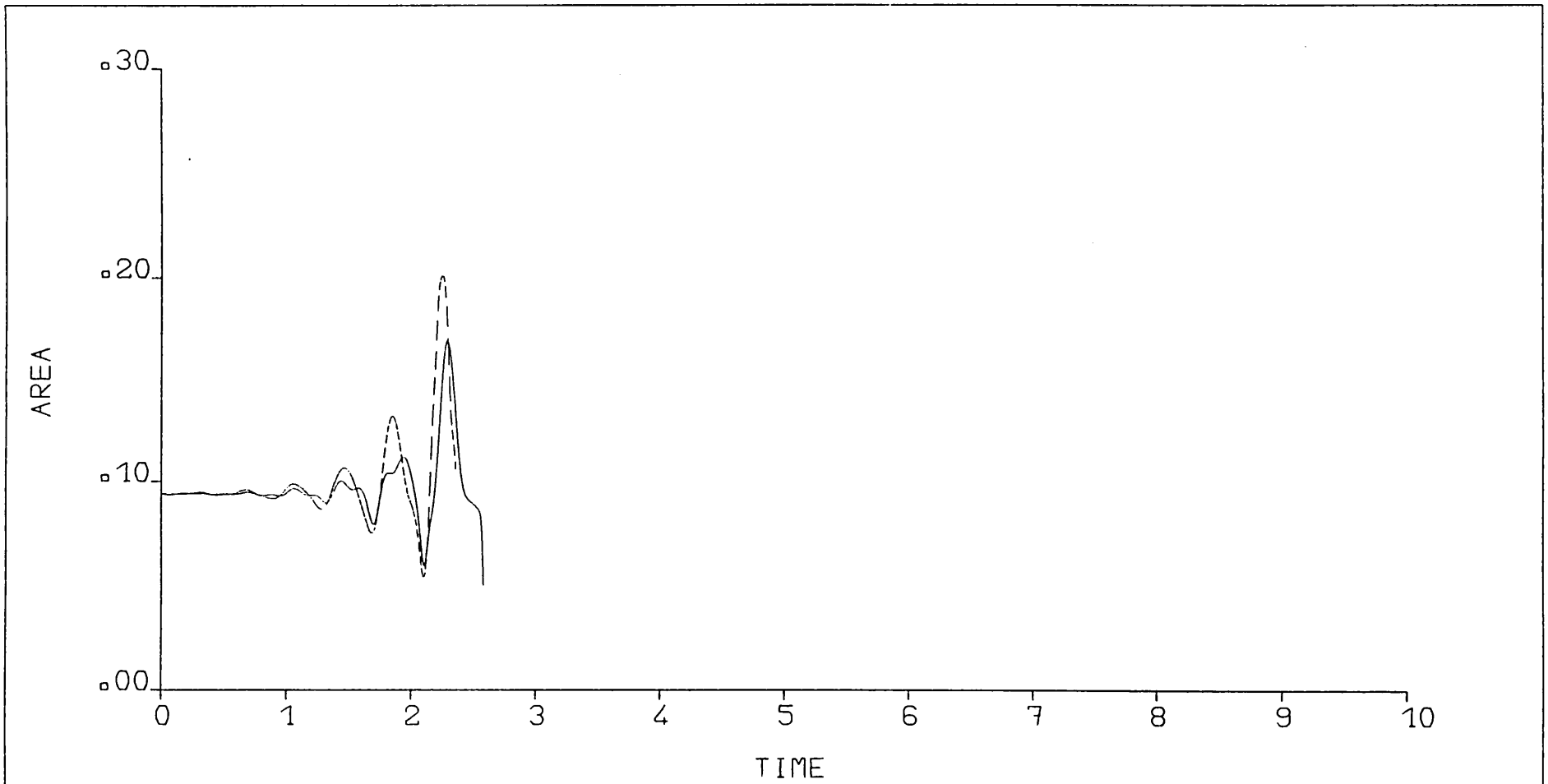



Fig 6.4.4 Comparison of standard and modified methods used to determine the time step. The solid line plot is obtained using the standard method (nrc = 1) with $\Delta x = 0.025$. Broken line corresponds to the modified method (nrc = 4) with $\Delta x = 0.1$. These results are obtained from the equilibrium state used in Fig 6.4.1 and the distributed parameter model with $L_4 = 1$ (note the change in time scale). Frequency of oscillation $\approx 2.5$.

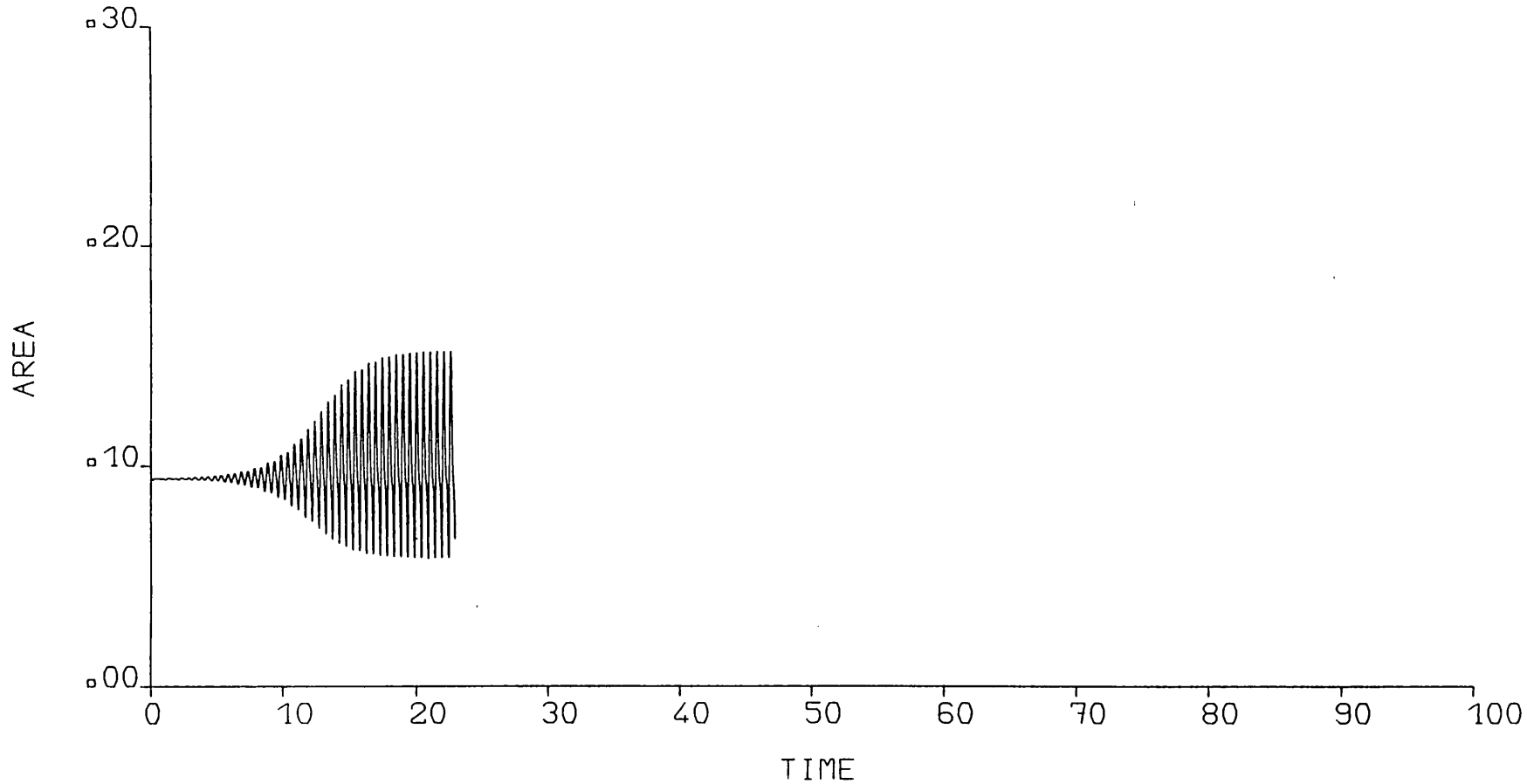



Fig 6.4.5 Limit cycle resulting from the equilibrium state used in Fig 6.4.1, with $L_4 = 3$. This plot shows the area variation at the downstream boundary. Frequency of oscillation $\approx 2$. The travel time of a wave, based on the initial values of u and c, is $\approx 0.91$. nrc = 4, $\Delta x = 0.1$.

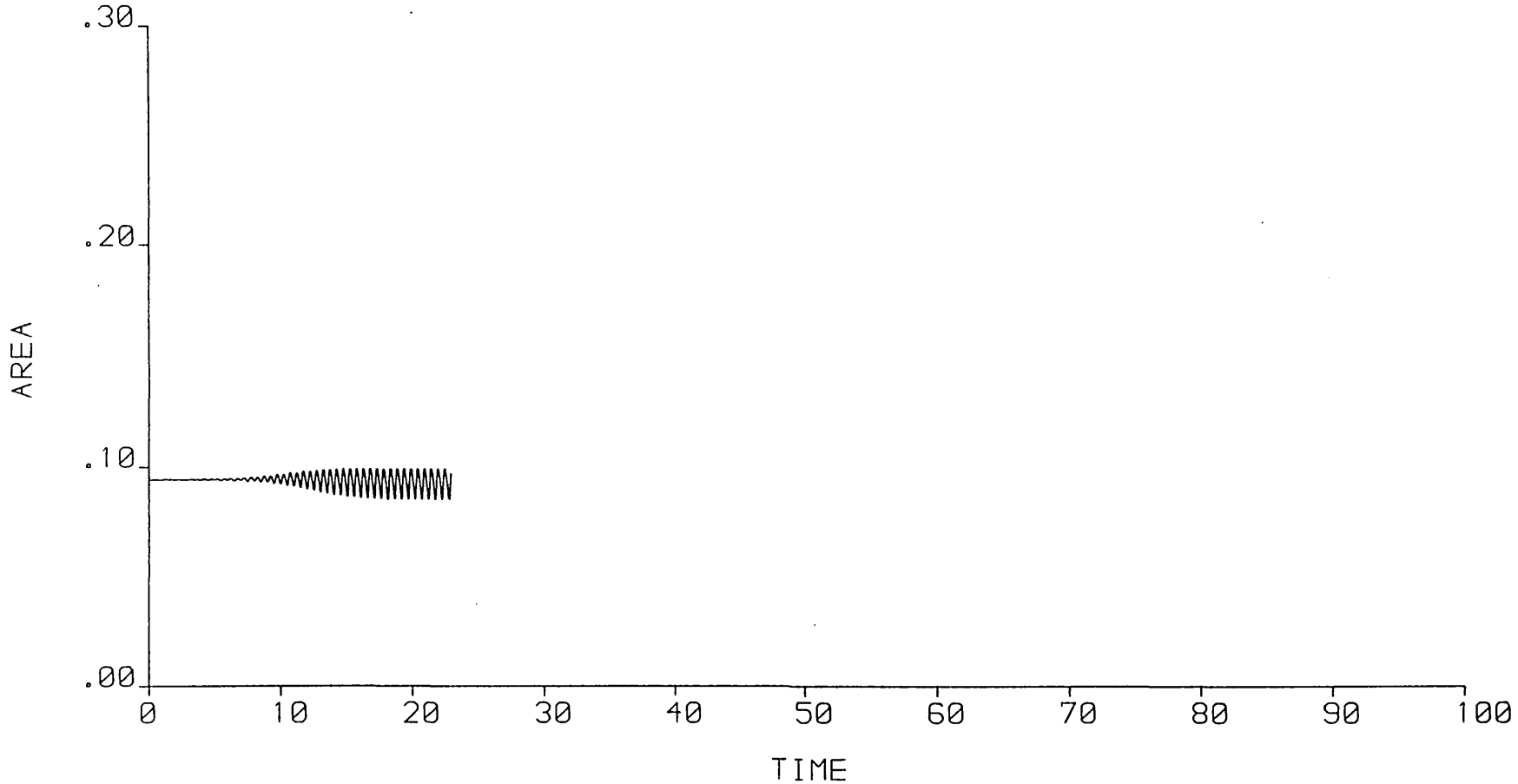



Fig 6.4.6 Limit cycle in area at the upstream boundary corresponding to that at the downstream end (see Fig 6.4.5). The amplitude ≈ 1/6 of the downstream value.

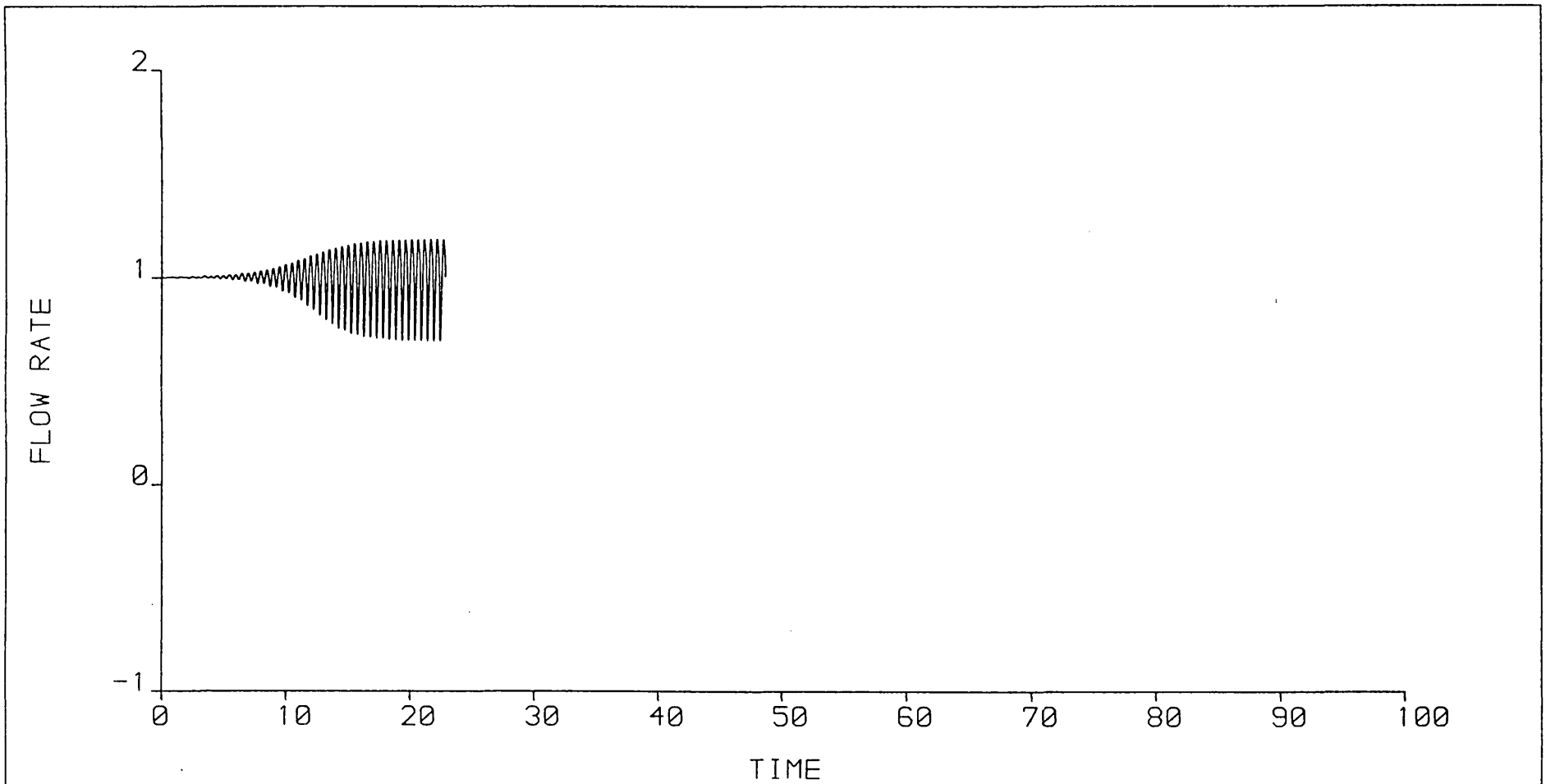



Fig 6.4.7 Limit cycle in flow rate at the downstream boundary corresponding to that in area shown in Fig 6.4.5.

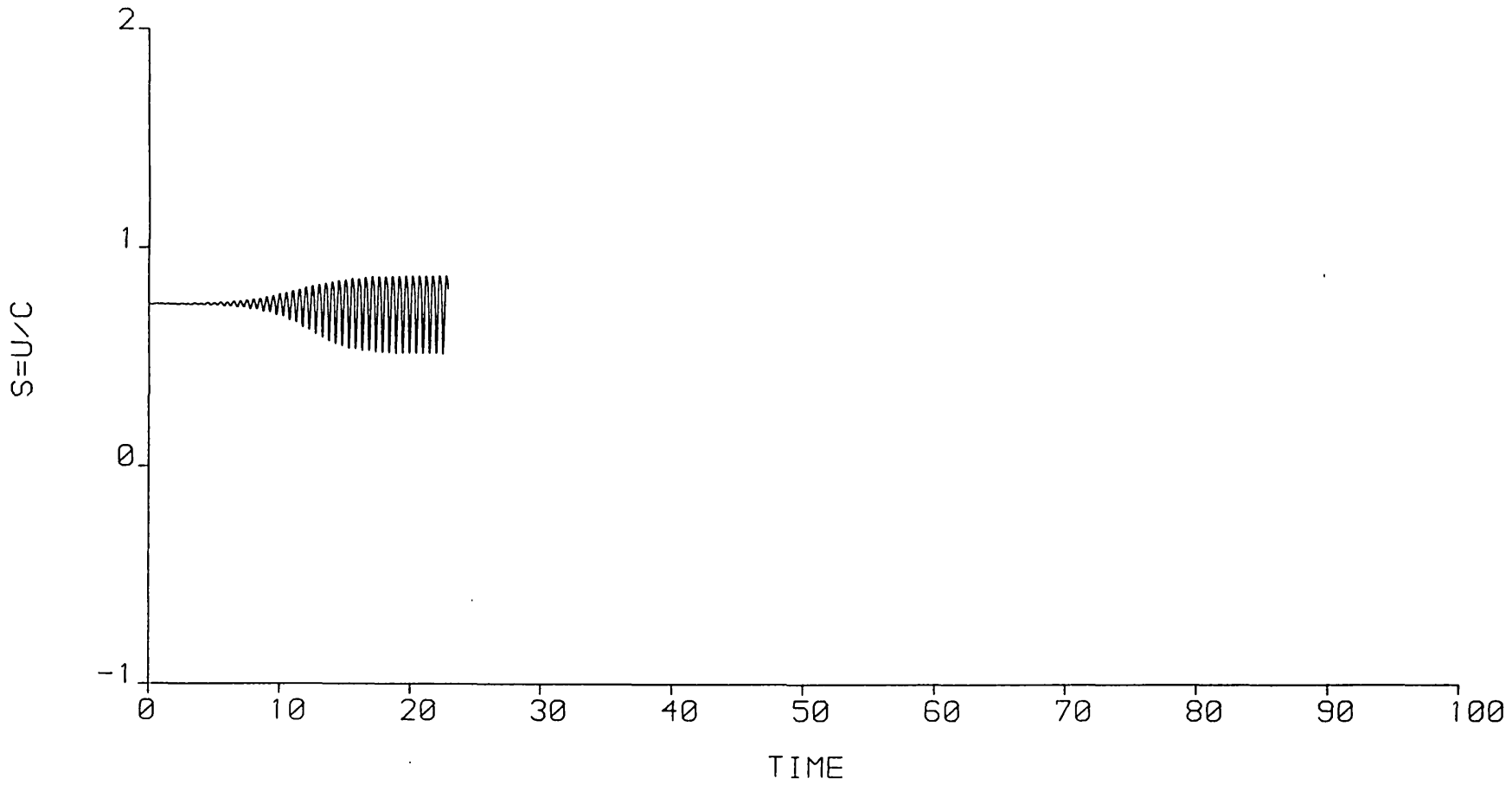



Fig 6.4.8 Limit cycle in the speed index at the downstream boundary corresponding to the results shown in Figs 6.4.5 - 6.4.7. Flow is subcritical throughout with $S > \frac{1}{2}$.

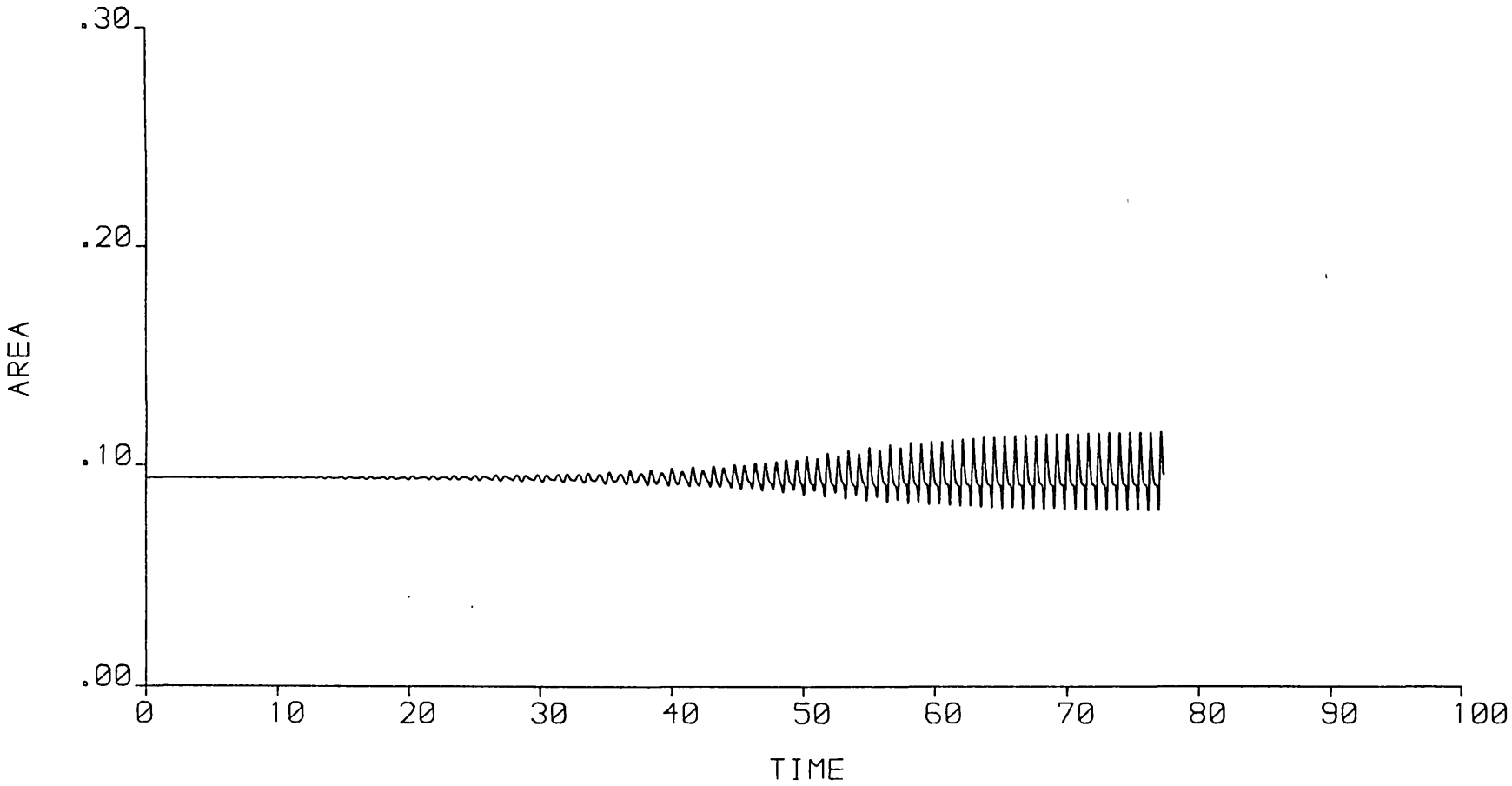



Fig 6.4.9 Limit cycle resulting from the equilibrium state used in Fig 6.4.1, with $L_4 = 5$.
This plot shows the area variation at the downstream boundary. Frequency of oscillation $\approx 1.25$. The travel time of a wave based on the initial values of u and c, is $\approx 1.5$. nrc = 4, $\Delta x = 0.1$

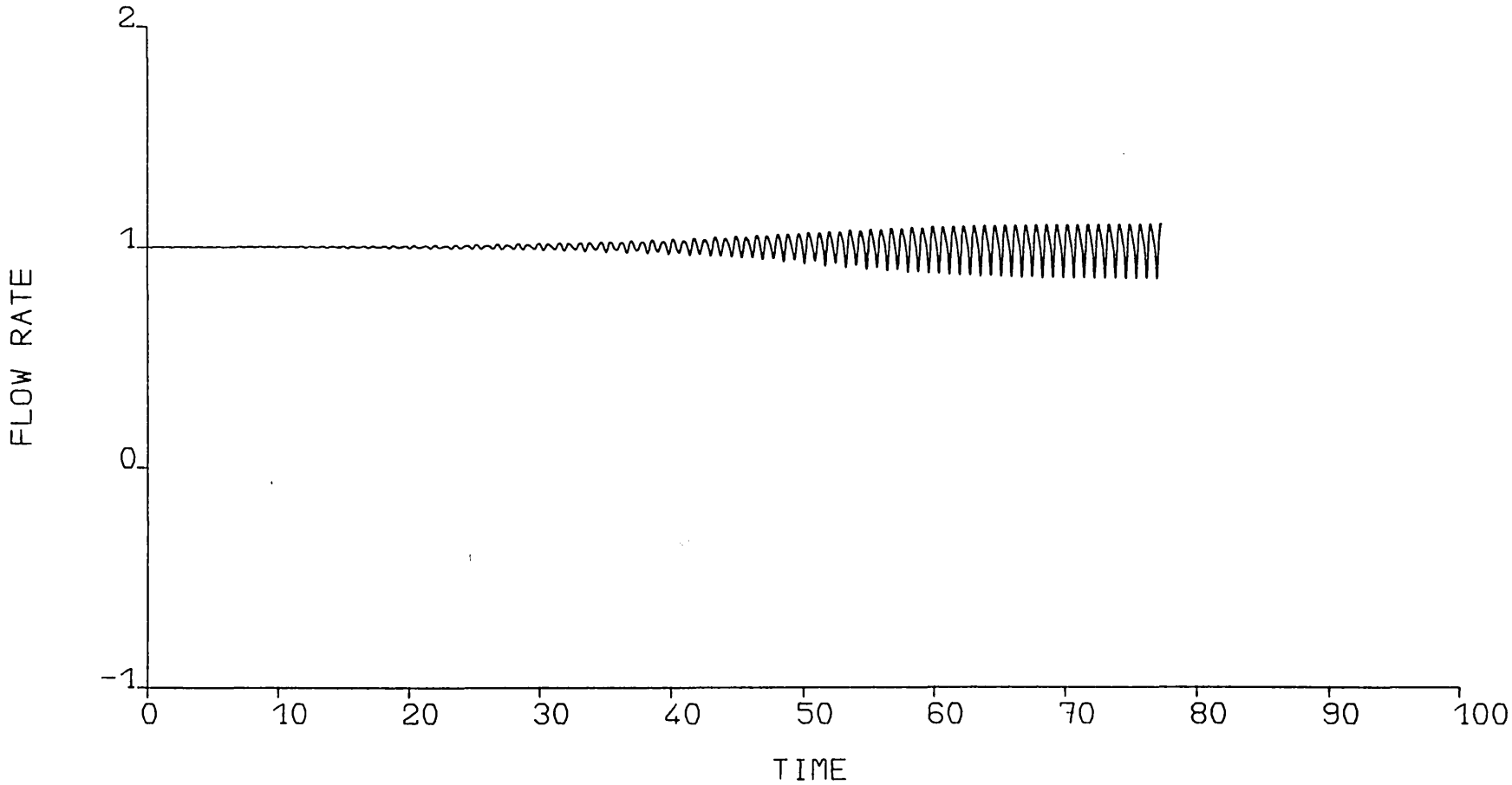



Fig 6.4.10 Limit cycle in flow rate at the downstream boundary corresponding to that in area shown in Fig 6.4.9.

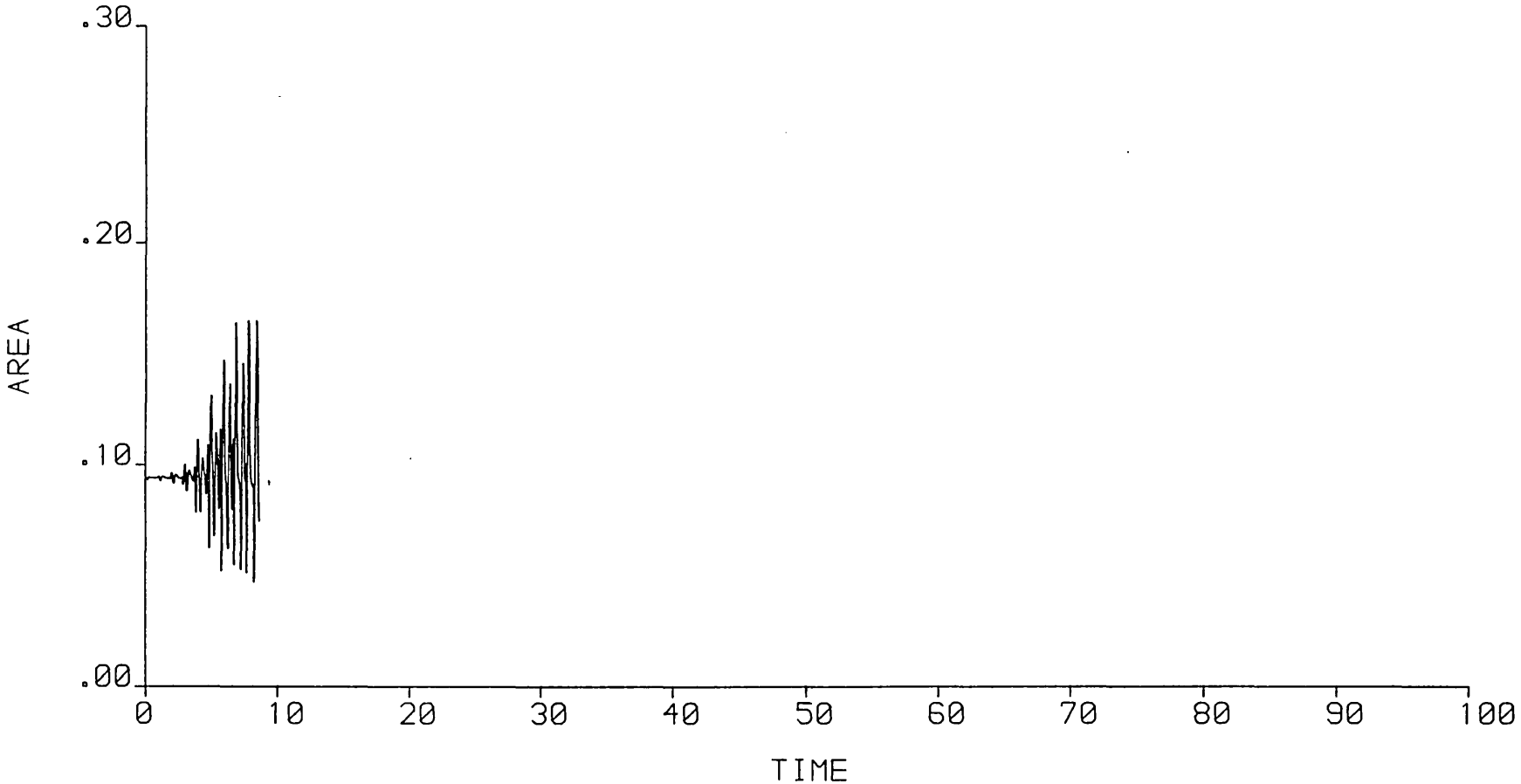



Fig 6.4.11 Effect of relaxing the criterion used to determine $\Delta t$ (cf Fig 6.4.5). nrc = 7, $L_4$ = 3, $\Delta x$ = 0.1. Frequency of oscillation $\approx$ 2.

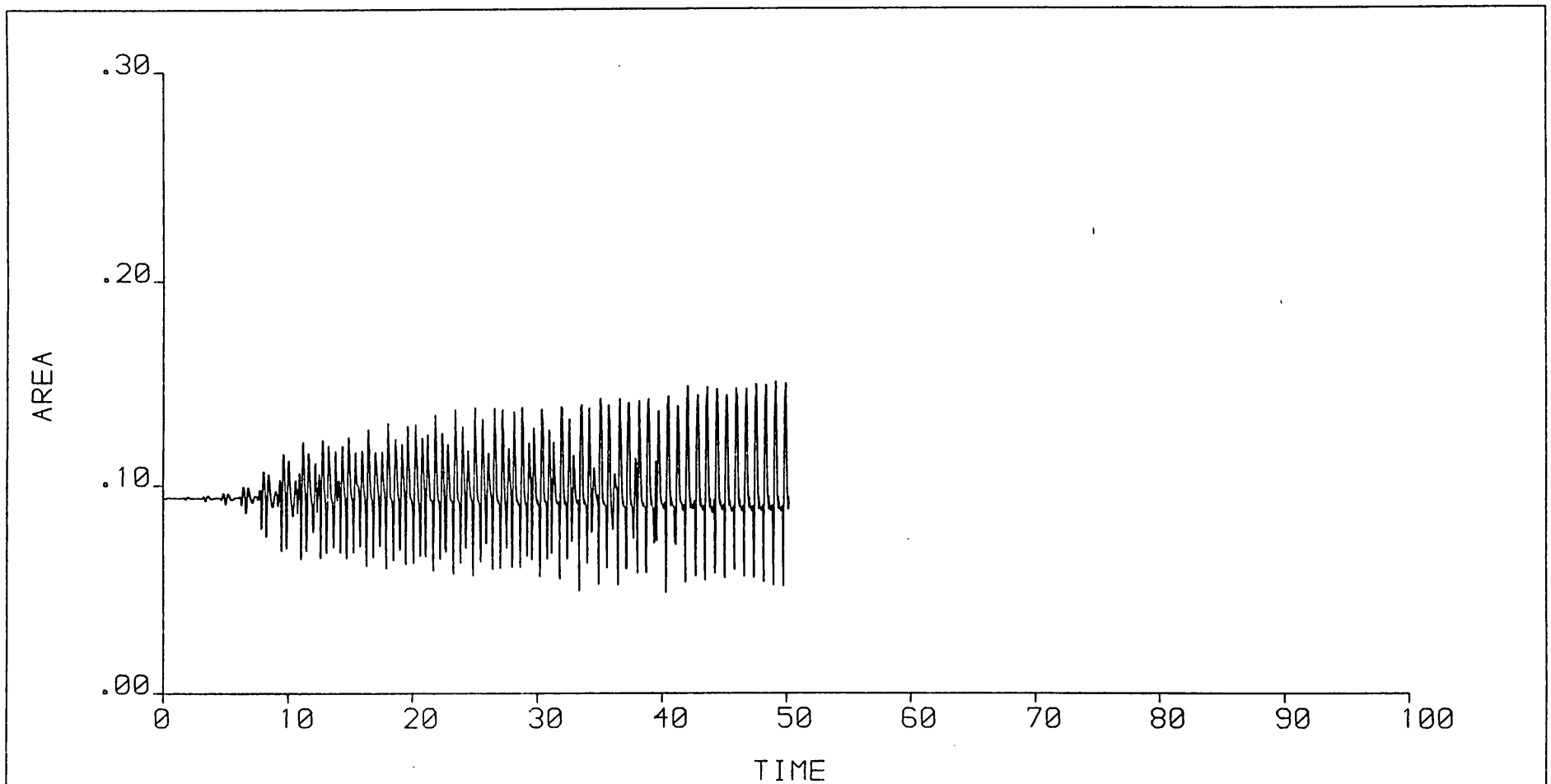



Fig 6.4.12 Effect of relaxing the criterion used to determine $\Delta t$ (cf Fig 6.4.9). nrc = 7, $L_4$ = 5, $\Delta x$ = 0.1. Frequency of oscillation $\approx$ 1.27.

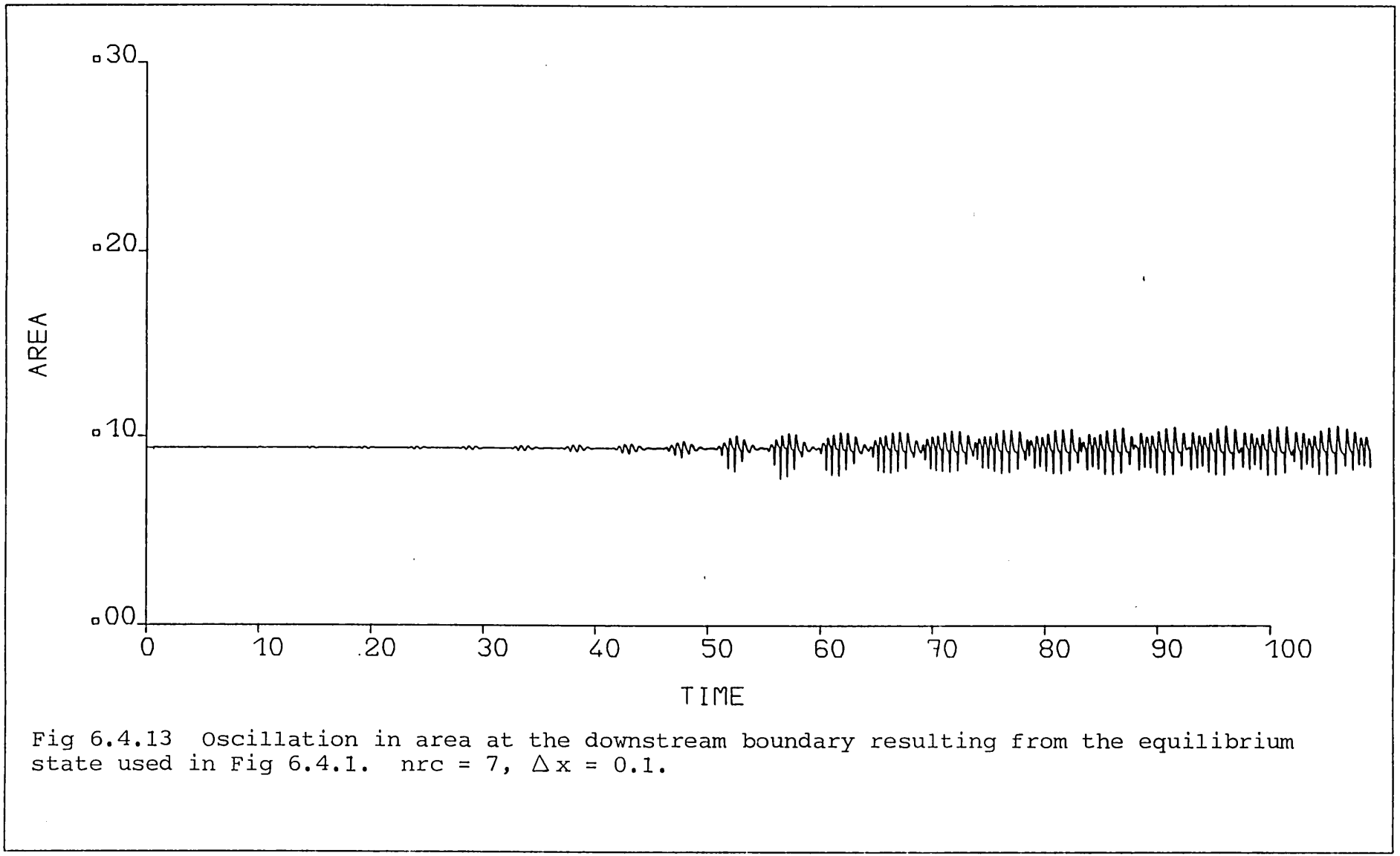



Fig 6.4.13 Oscillation in area at the downstream boundary resulting from the equilibrium state used in Fig 6.4.1. nrc = 7, $\Delta x = 0.1$.

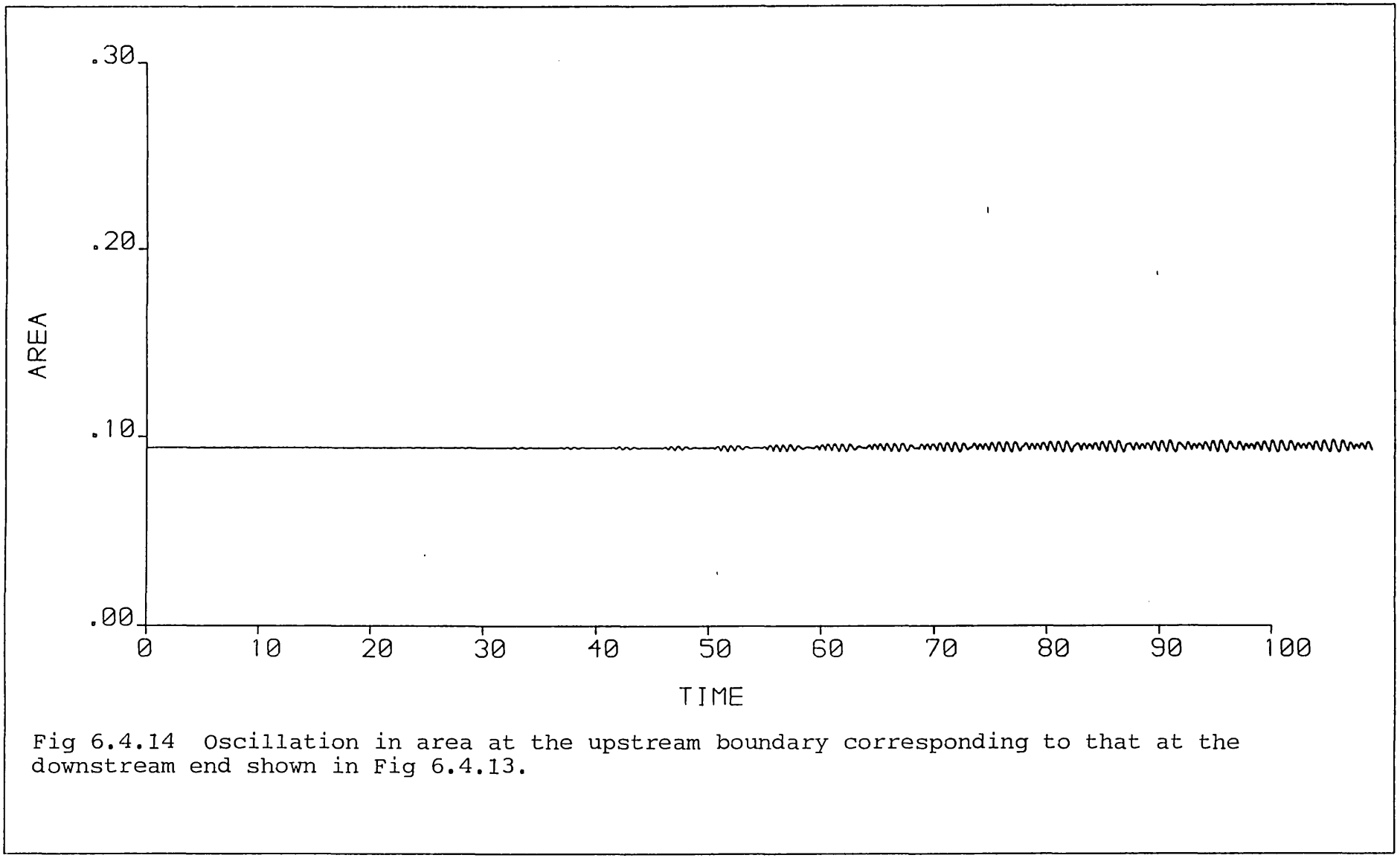



Fig 6.4.14 Oscillation in area at the upstream boundary corresponding to that at the downstream end shown in Fig 6.4.13.

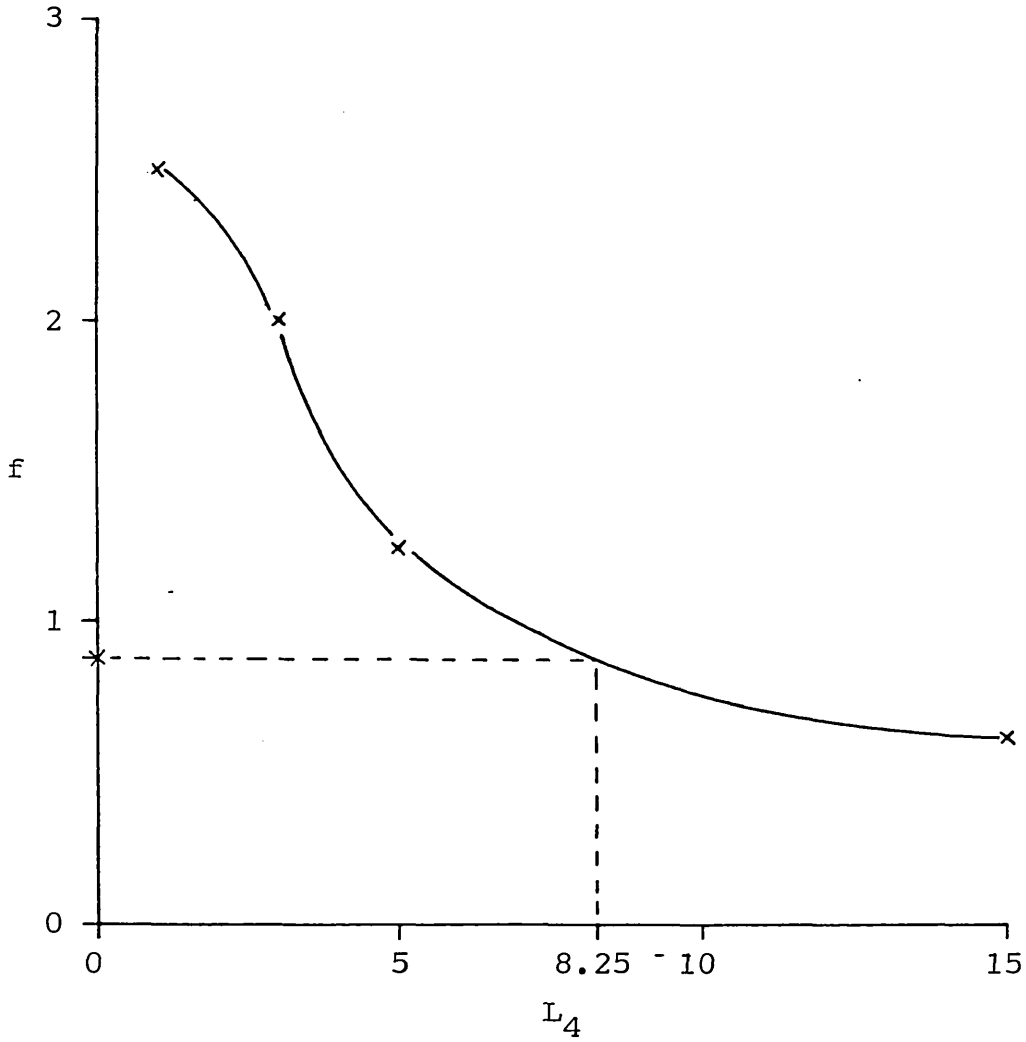



Fig 6.4.15 Frequency of limit cycle as a function of the length of region 4, based on the results of Figs 6.4.1-6.4.14.

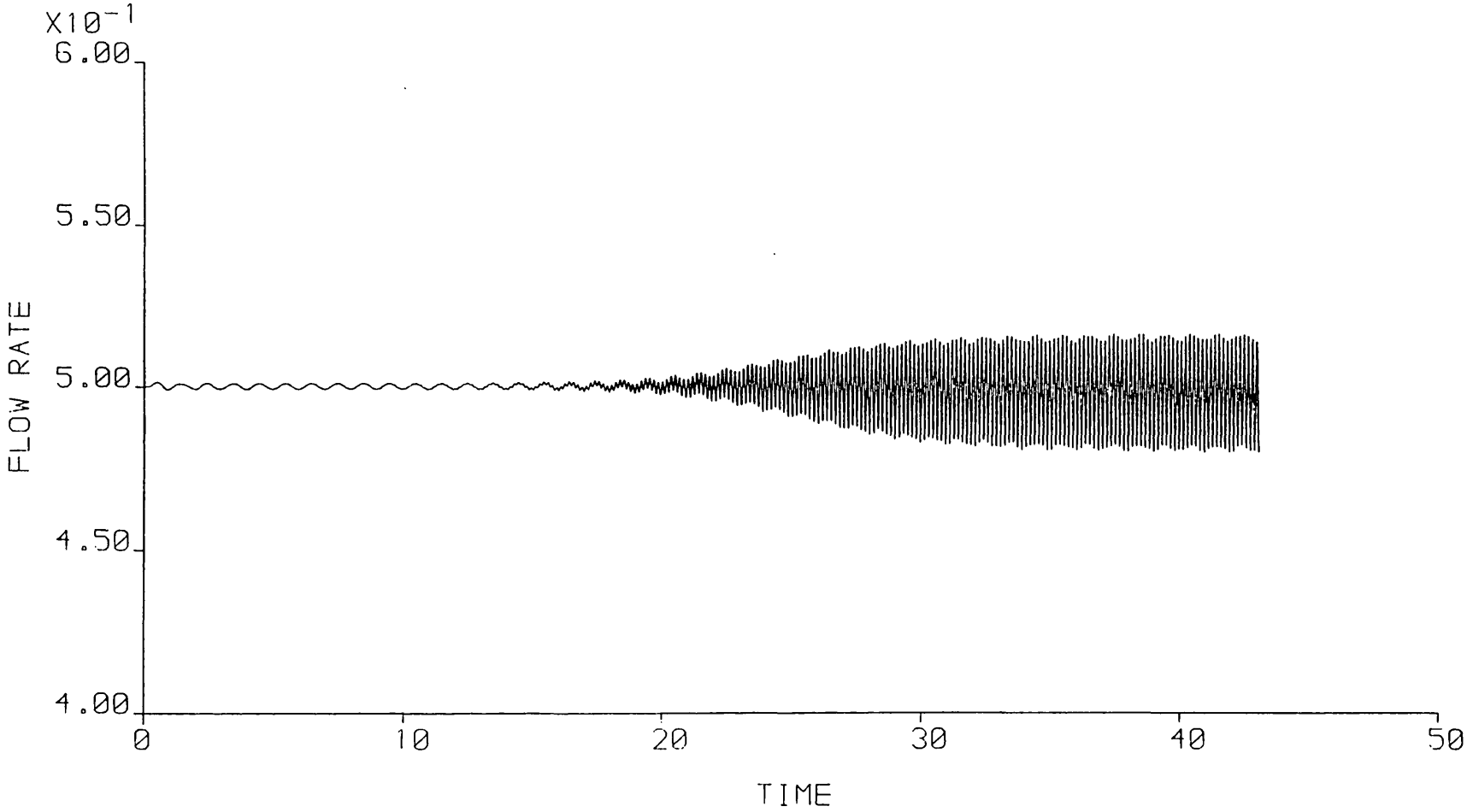



Fig 6.4.16 Limit cycle resulting from an equilibrium state which is given a sinusoidal perturbation in $p_h$ of amplitude 1% peak to peak and frequency unity. Frequency of limit cycle $\approx 6$. $I_1 = 12.5$, $I_2 = 25$, $R_k = 0.00466$.

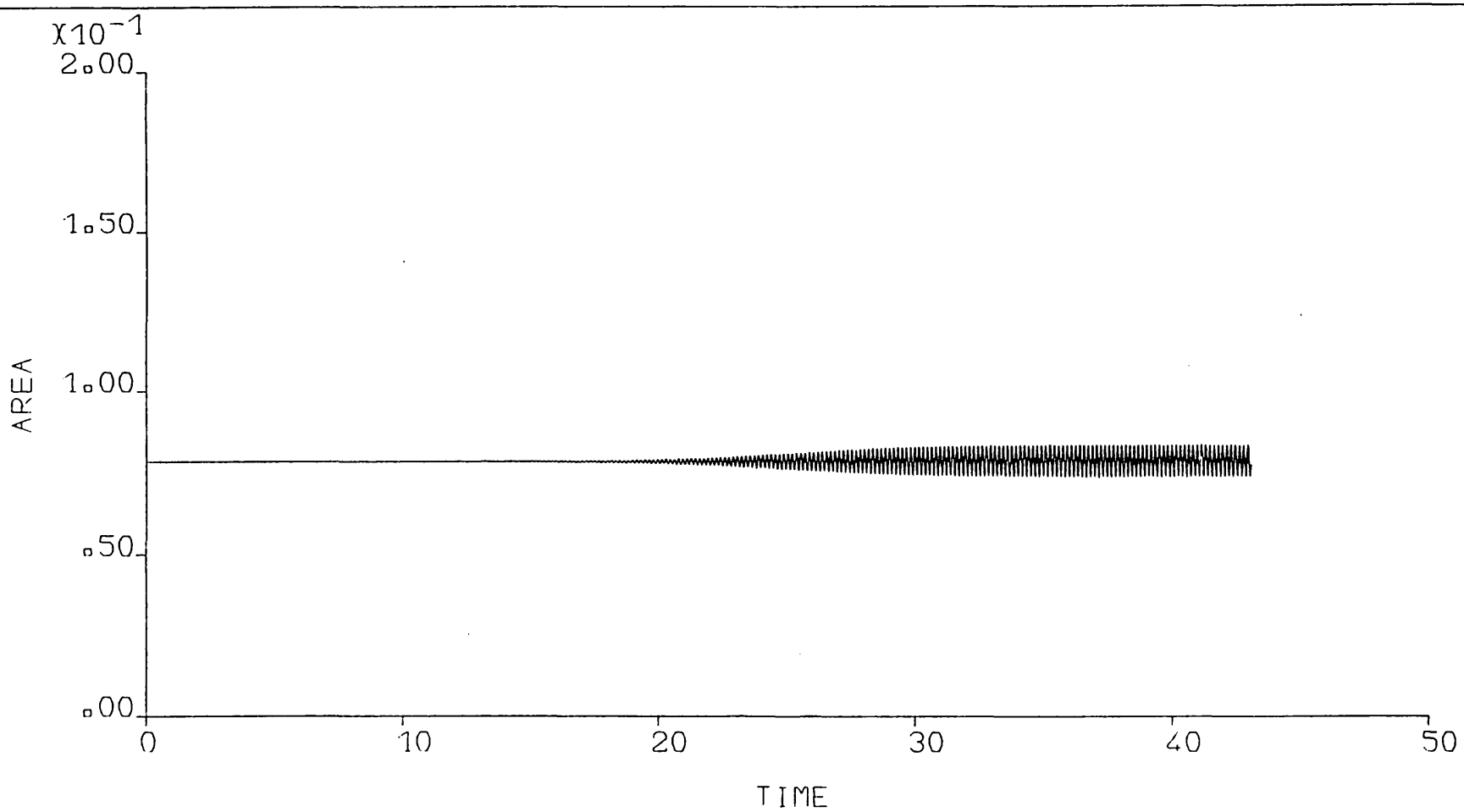



Fig 6.4 17 Limit cycle in area at the downstream boundary corresponding to that in flow rate shown in Fig 6.4.16.

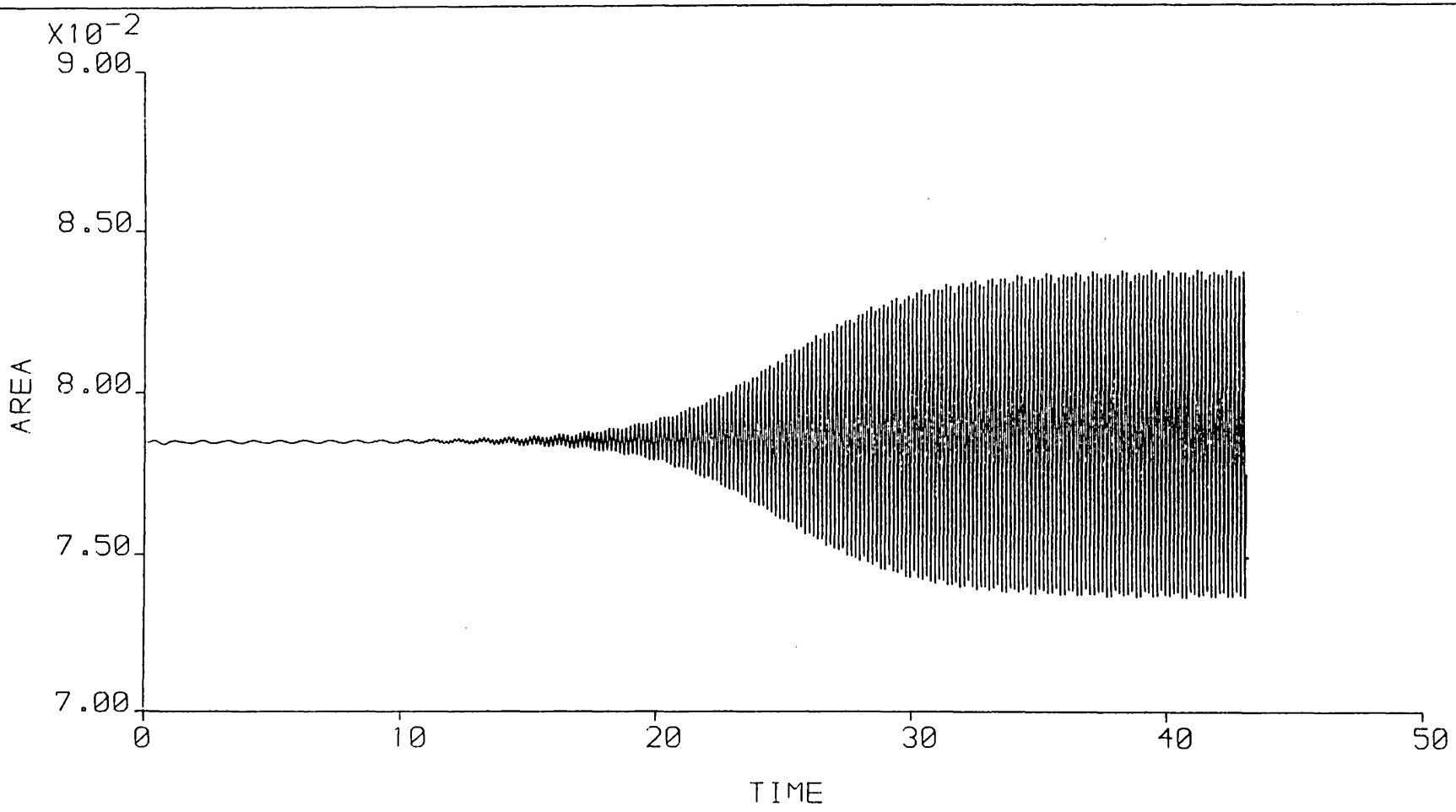



Fig 6.4.18 Limit cycle in area shown in Fig 6.4.17 plotted on an expanded area scale.

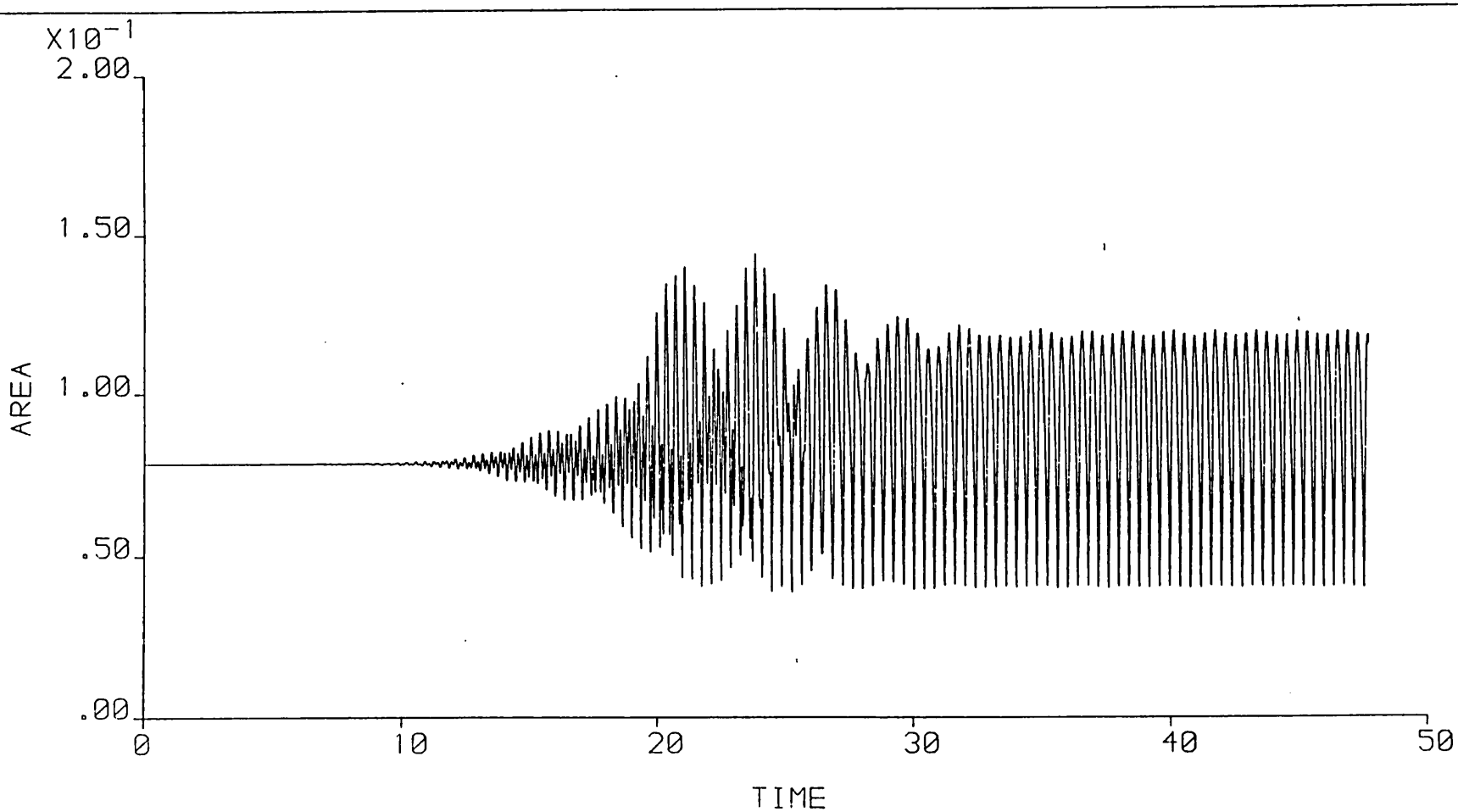



Fig 6.4.19 Effect of increasing the inertia of both rigid tubes by a factor of 10 (cf Fig 6.4.17). $I_1 = 125$, $I_2 = 250$. Frequency of limit cycle $\approx 2.5$, modulation frequency $\approx 0.36$.

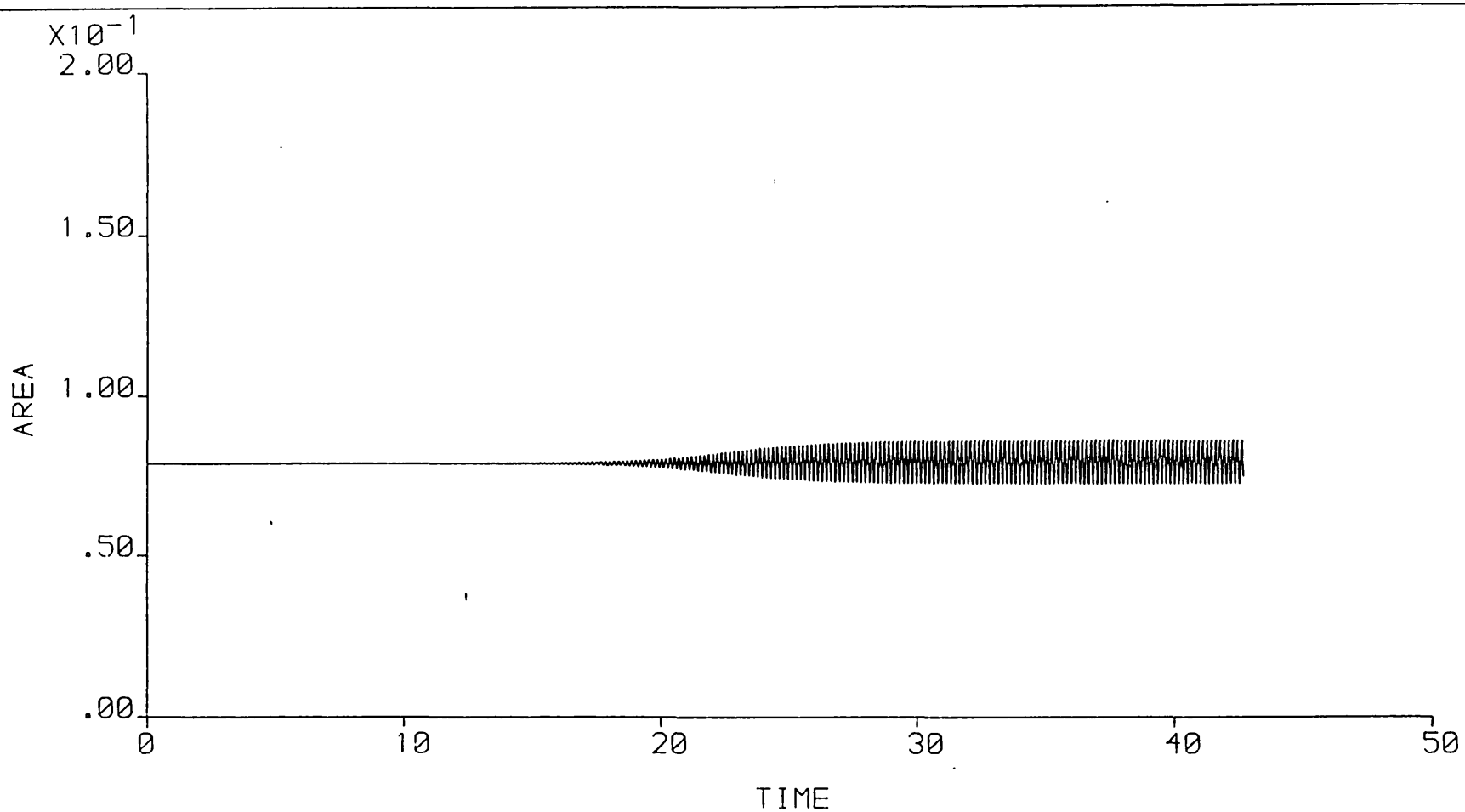



Fig 6.4.20 Effect of increasing the upstream rigid tube inertia by a factor of 10 (cf Fig 6.4.17). $I_1 = 125$, $I_2 = 25$. Frequency of limit cycle $\approx 6$.

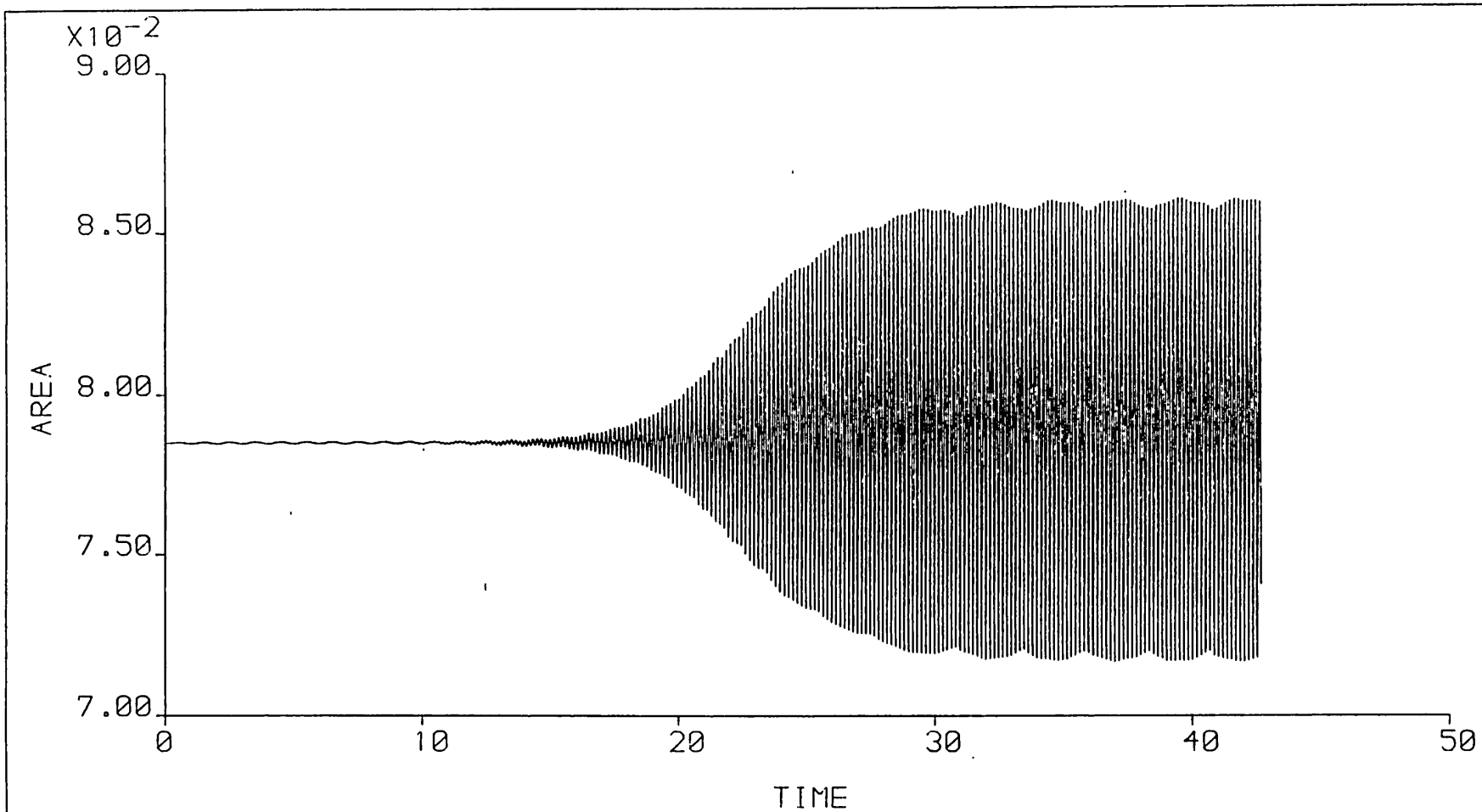



Fig 6.4.21 Limit cycle in area shown in Fig 6.4.20 plotted on an expanded area scale. Modulation frequency ≈ 0.4.

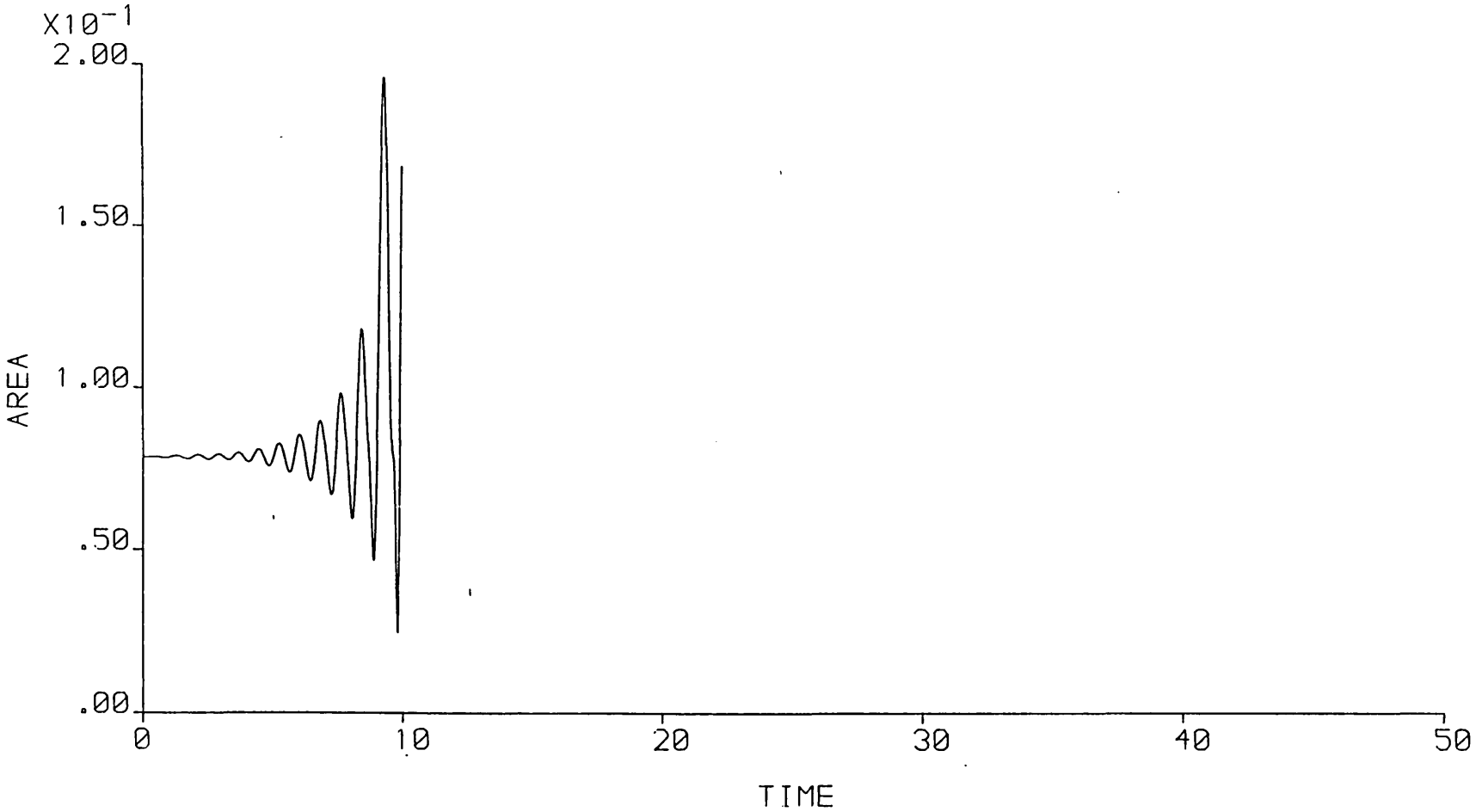



Fig 6.4.22 Effect of increasing the downstream rigid tube inertia by a factor of 10 (cf Fig 6.4.17). $I_1$ = 12.5, $I_2$ = 250. Frequency of oscillation ≈ 1.25.

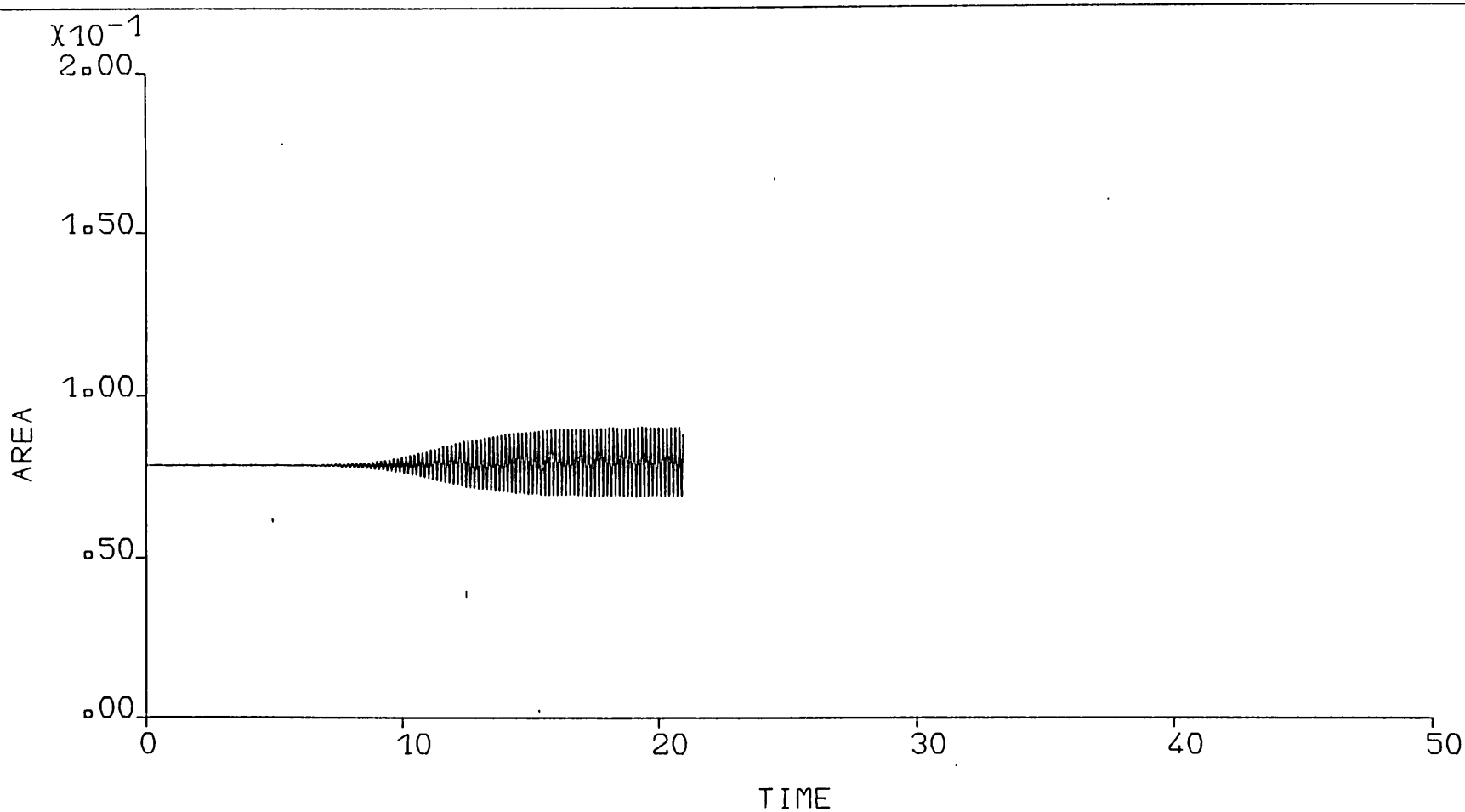



Fig 6.4.23 Effect of reducing the resistance parameter, $R_k$, by a factor of 10 (cf Fig 6.4.17). $R_k$ = 0.000466. Frequency of limit cycle ≈ 6.2.

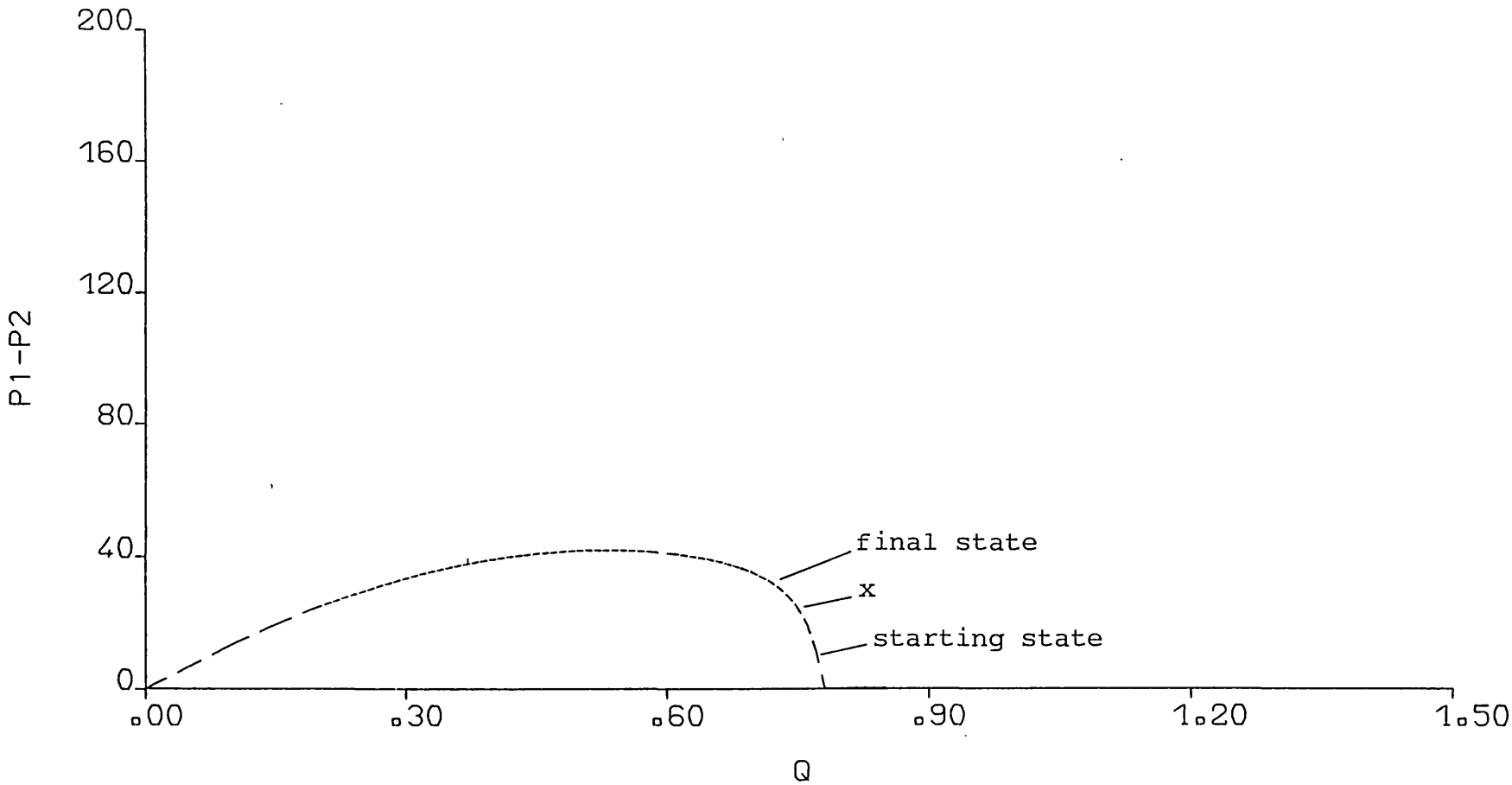



Fig 6.4.24 P-Q characteristic corresponding to curve 4 of Conrad (1969) but with $c_1 = 4$. See text for parameter values. 'x' indicates the point on the curve beyond which an increase in Q results in a decrease in $p_h$.

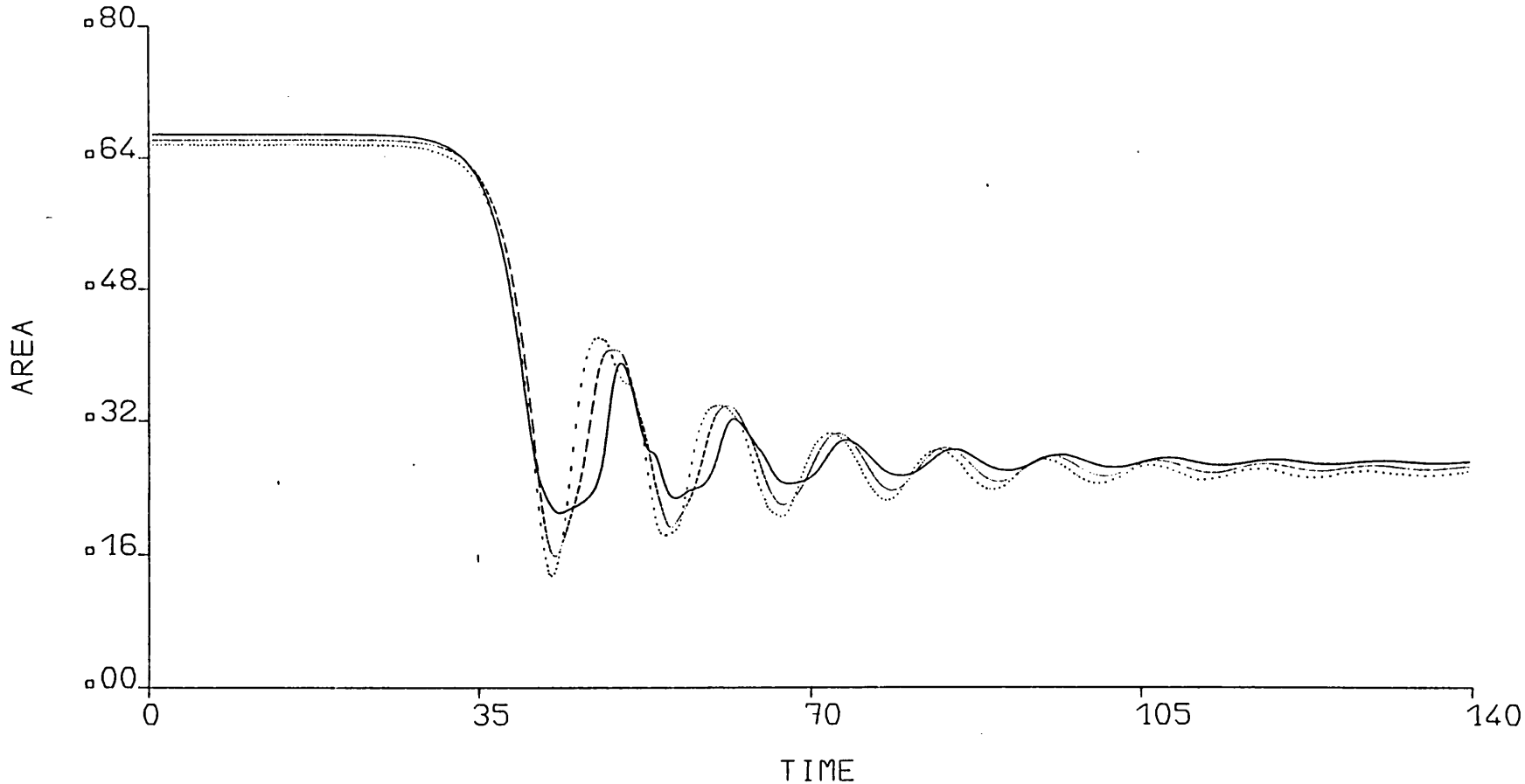



Fig 6.4.25 Exponential instability resulting from an equilibrium state on the negative slope of the P-Q characteristic shown in Fig 6.4.24. The following notation is used here: —— upstream boundary;– – – – midstream;- - - - - downstream boundary. The final state corresponds to the point on the P-Q characteristic shown in Fig 6.4.24.

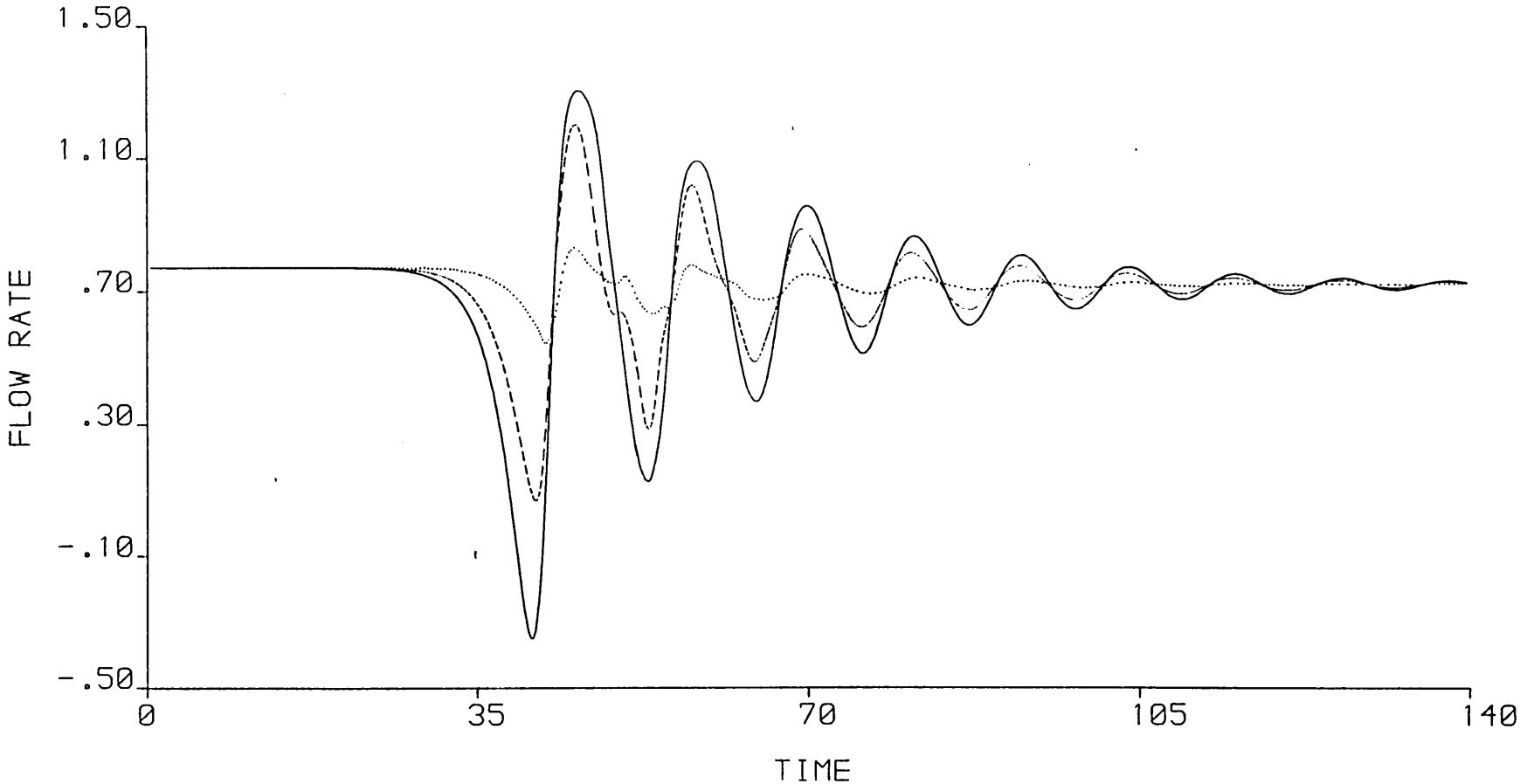



Fig 6.4.26 Exponential instability in flow rate corresponding to that in area shown in Fig 6.4.25.

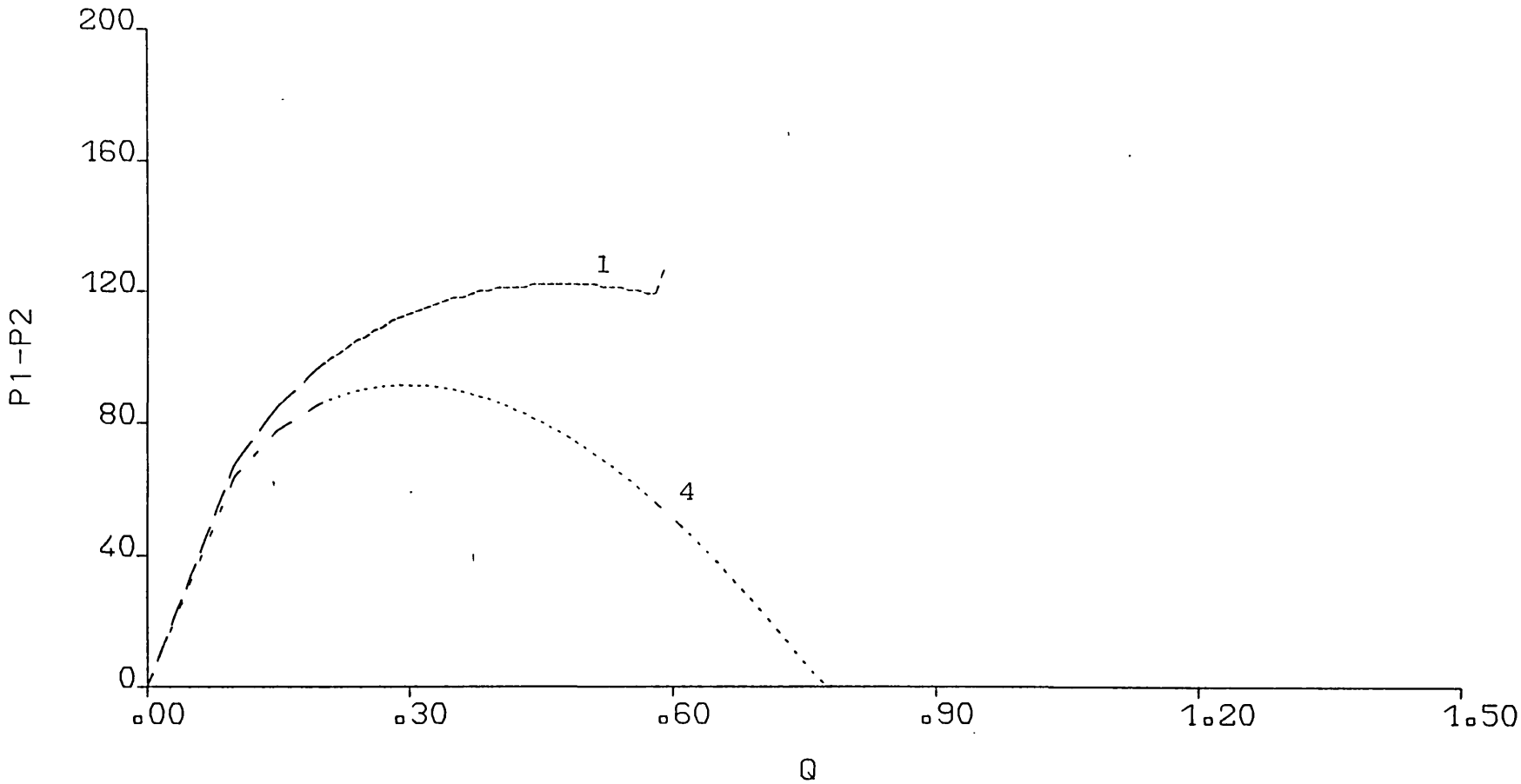



Fig 6.4.27 P-Q characteristics corresponding to curves 1 and 4 of Conrad (1969). $c_1$ = 1.15, $L_5$ = 0, $\beta$ = 0.5. See text for other parameter values.

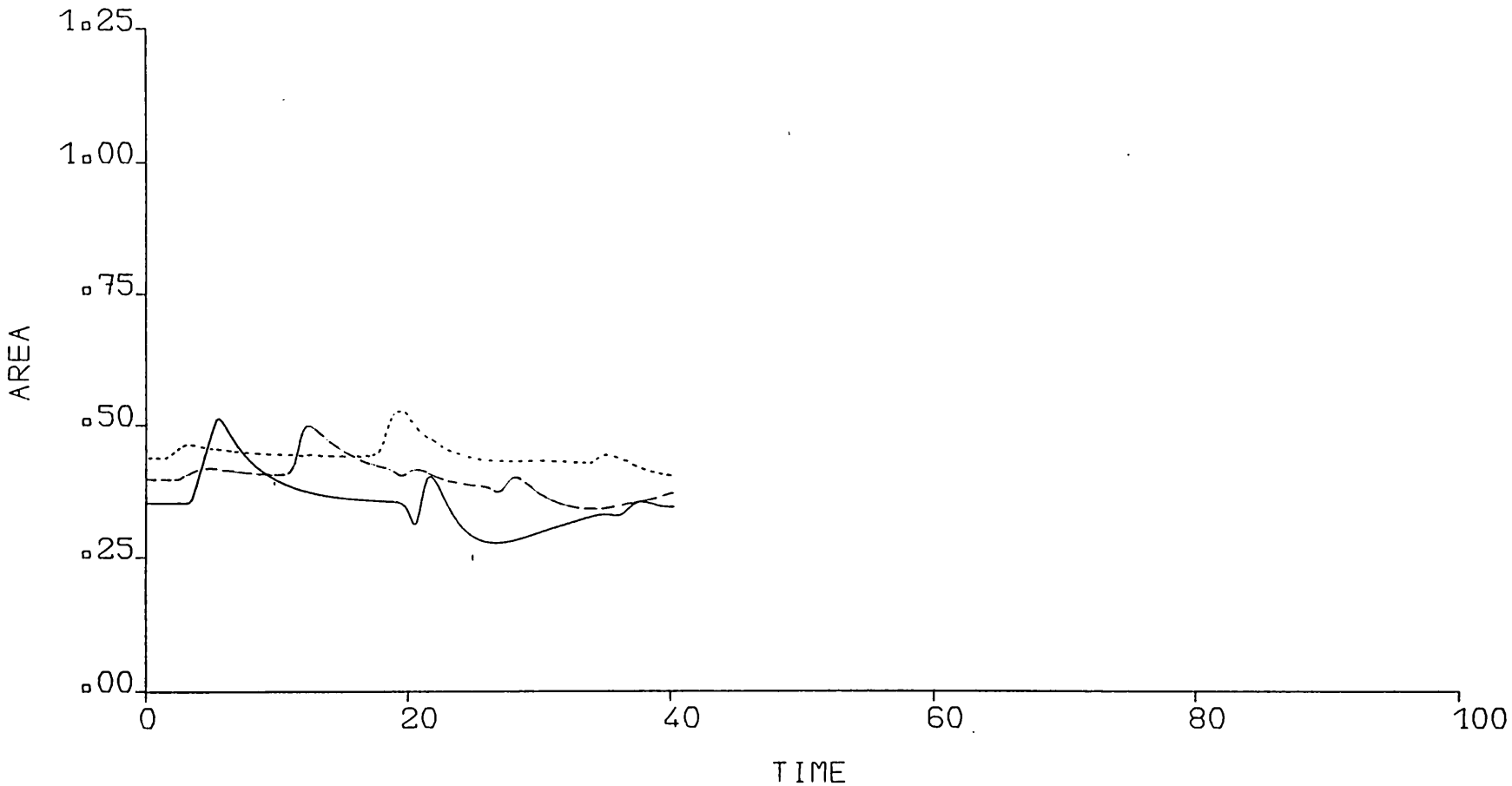



Fig 6.4.28 Results of imposing a single square pulse perturbation in $p_h$, of magnitude unity and frequency 2, on the equilibrium state corresponding to the point Q = 0.77 on curve 4 of Fig 6.4.27. In this and subsequent plots in this chapter the following notation is used: ----- upstream boundary; – – – – midstream; —— downstream boundary.

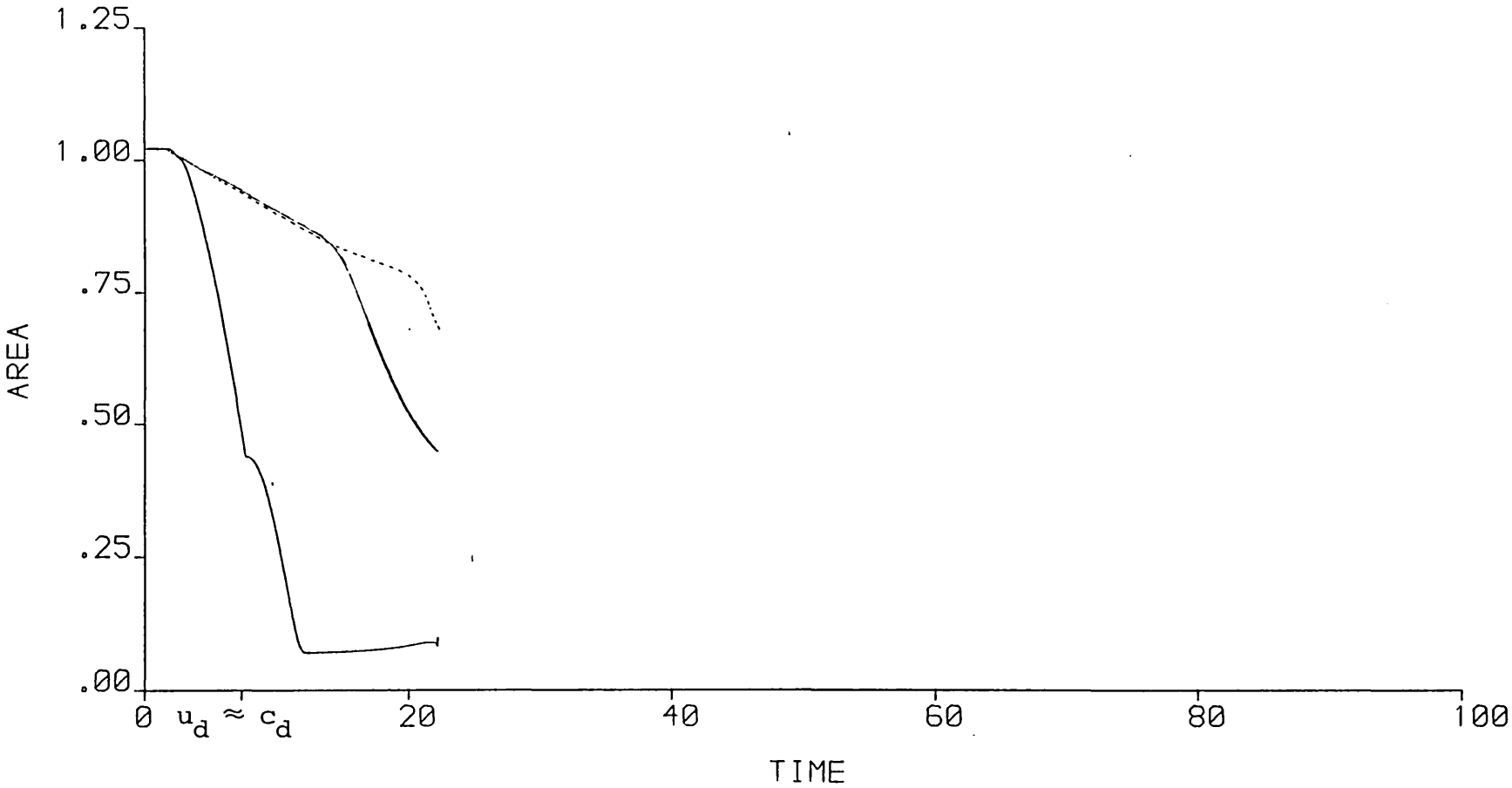



Fig 6.4.29 Effect of imposing a step change in $p_h$ of -3 units on the equilibrium state corresponding to the point Q = 1.25 on curve 1 of Fig 6.4.27. Subscript d refers to the downstream boundary.

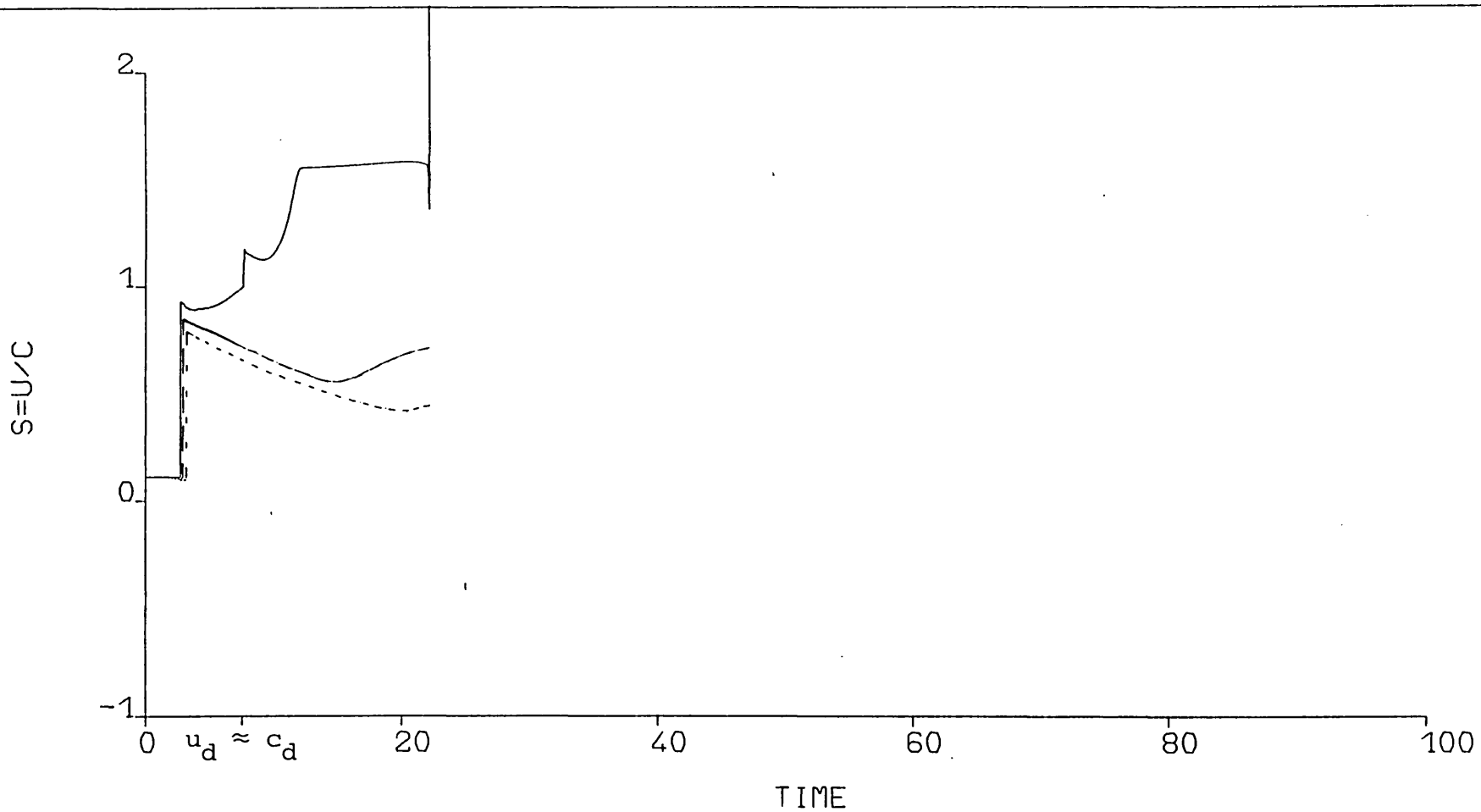



Fig 6.4.30 Variation in speed index, S, corresponding to the area variation shown in Fig 6.4.29.

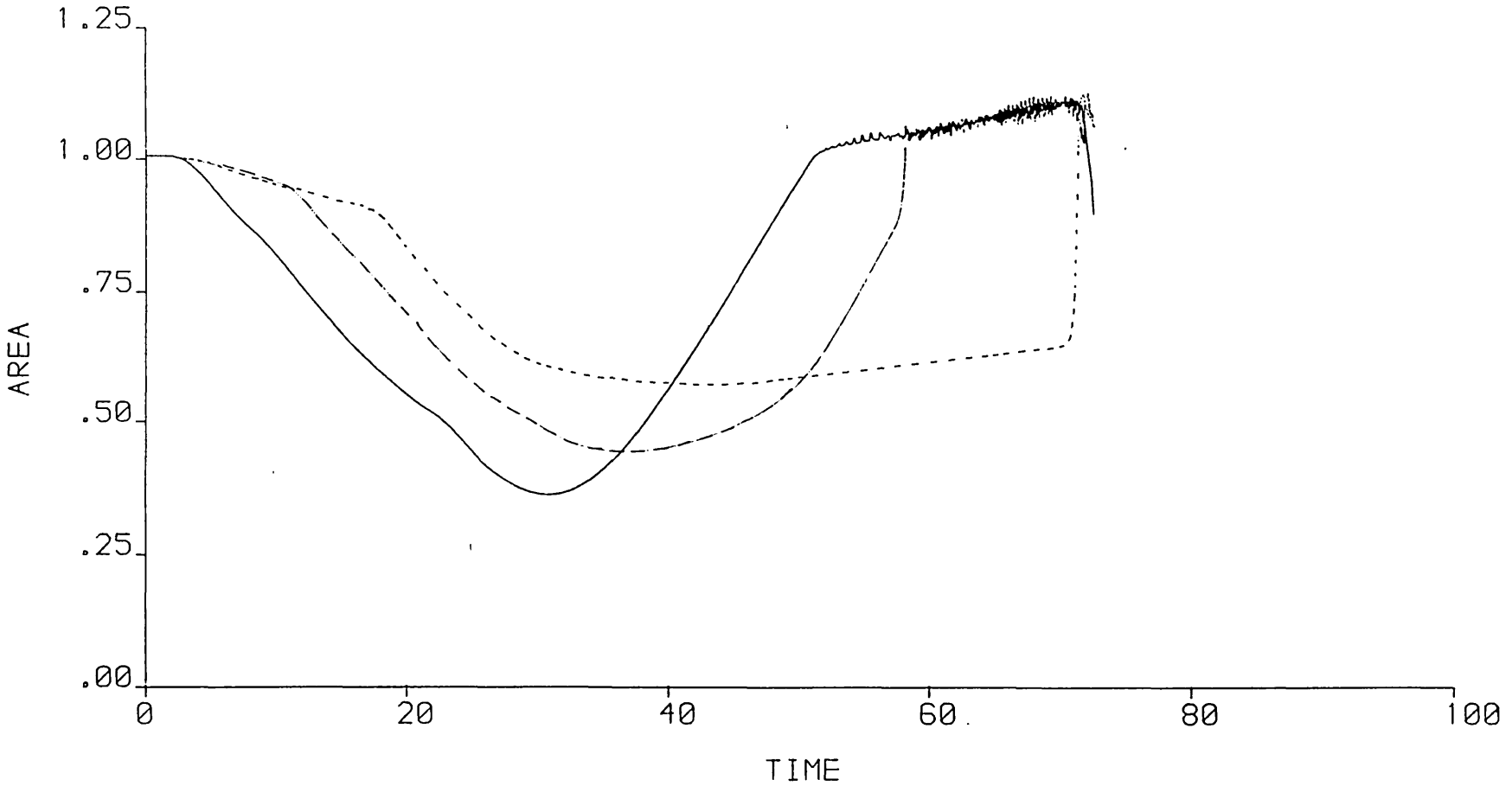



Fig 6.4.31 Effect of imposing a step change in $p_h$ of -1 unit, on the equilibrium state corresponding to Q = 0.78 on curve 4 of Fig 6.4.27. $L_5 = 2$, $I_1 = I_2 = 15$.

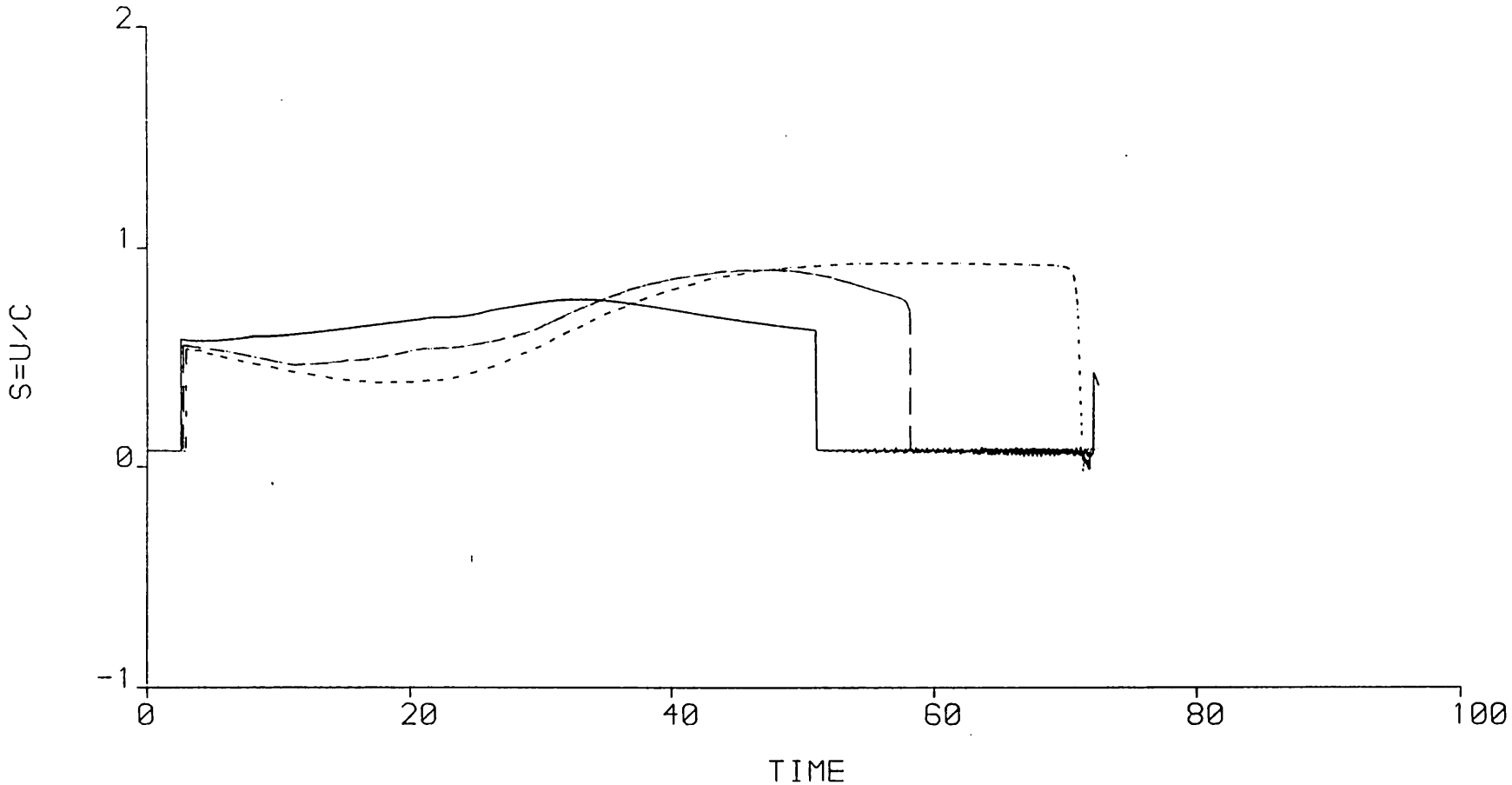



Fig 6.4.32 Variation in speed index, S, corresponding to the area variation shown in Fig 6.4.31.

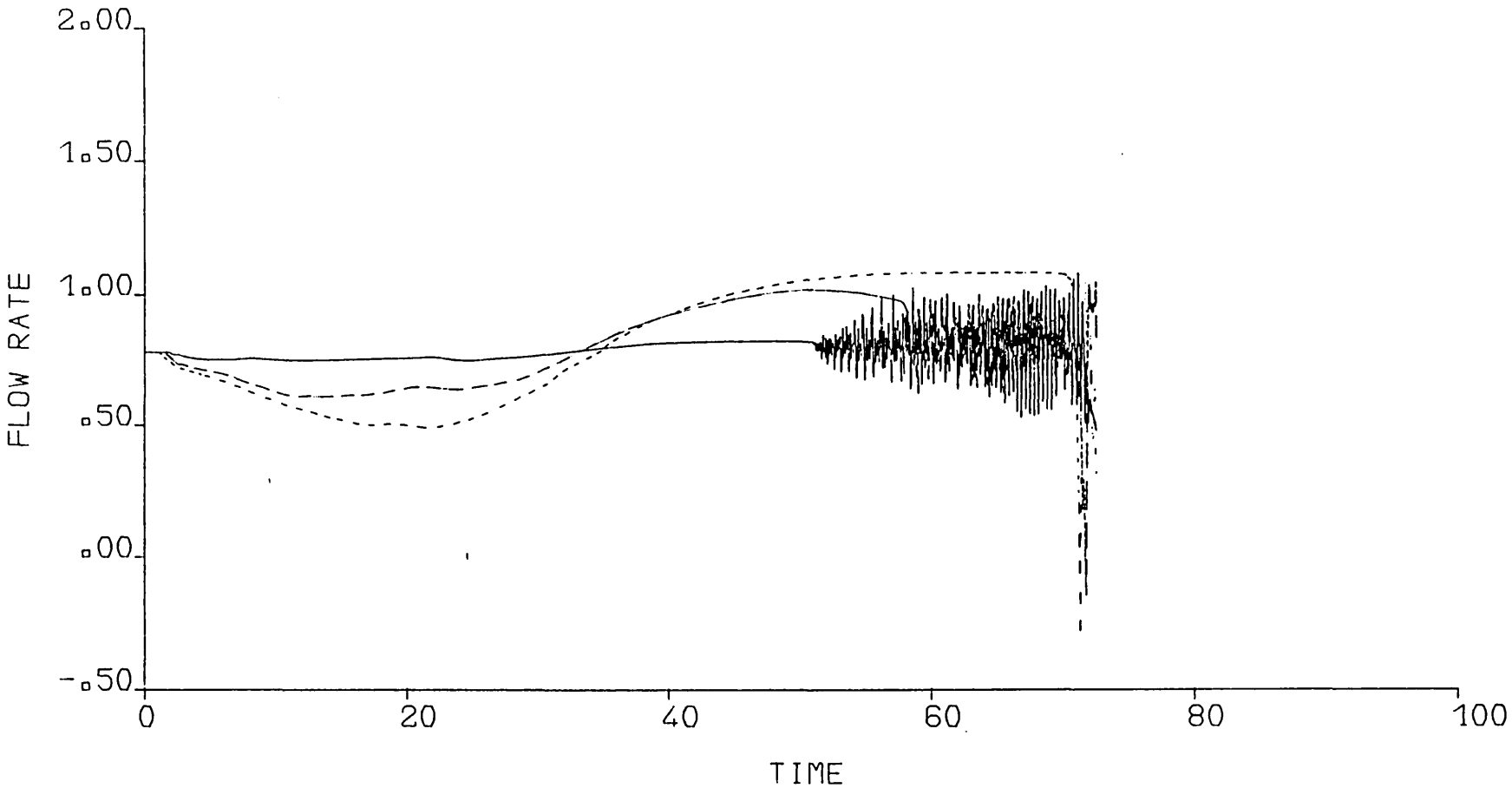



Fig 6.4.33 Variation in flow rate, Q, corresponding to the area and speed index variations shown in Figs 6.4.31 and 6.4.32, respectively.

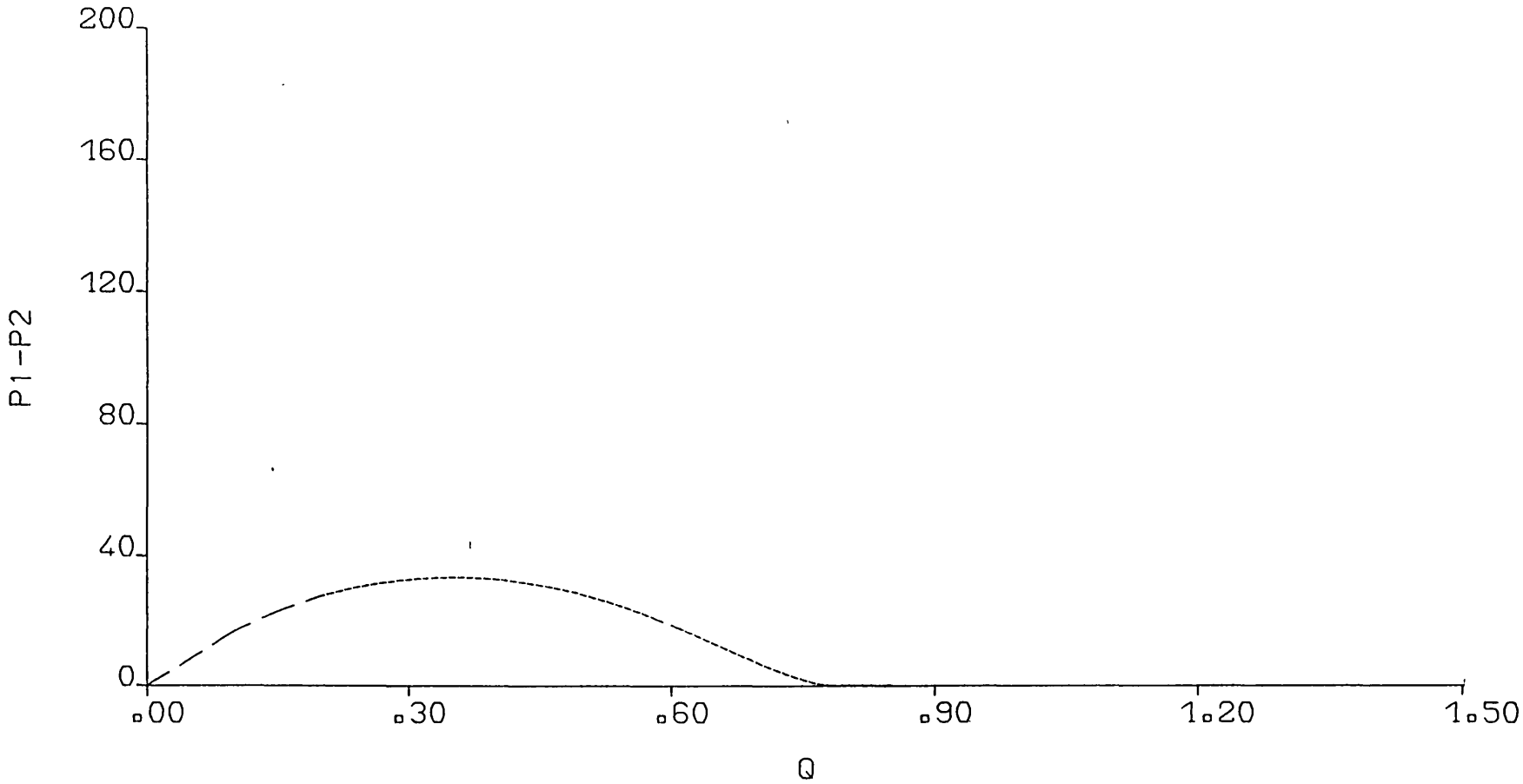



Fig 6.4.34 P-Q characteristic corresponding to curve 4 of Conrad (1969), with $c_1$ = 2.7.

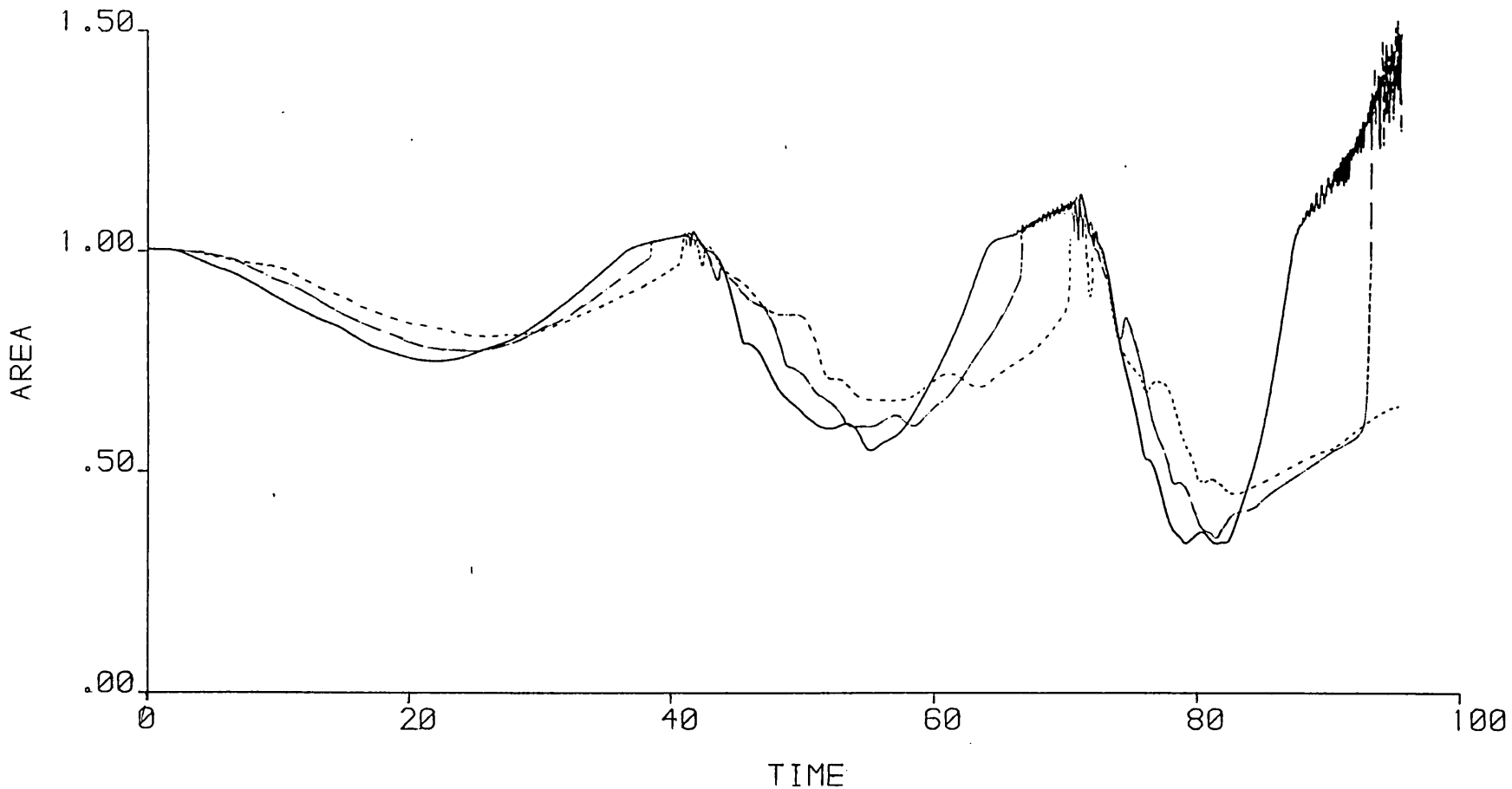



Fig 6.4.35 Effect of imposing a step change in $p_h$, of -1 unit, on an equilibrium state corresponding to the point Q = 0.78 on the characteristic shown in Fig 6.4.34.

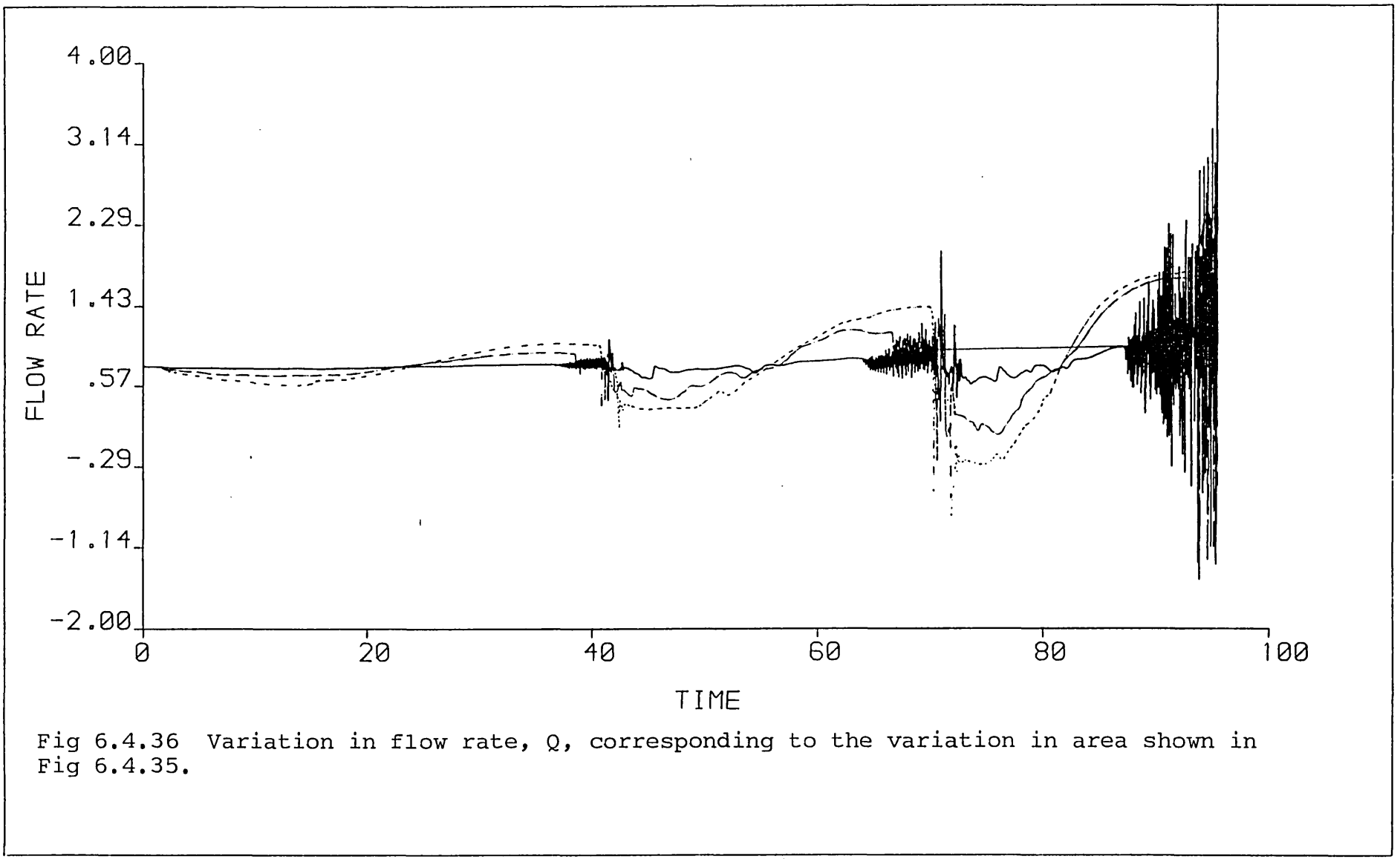



Fig 6.4.36 Variation in flow rate, Q, corresponding to the variation in area shown in Fig 6.4.35.

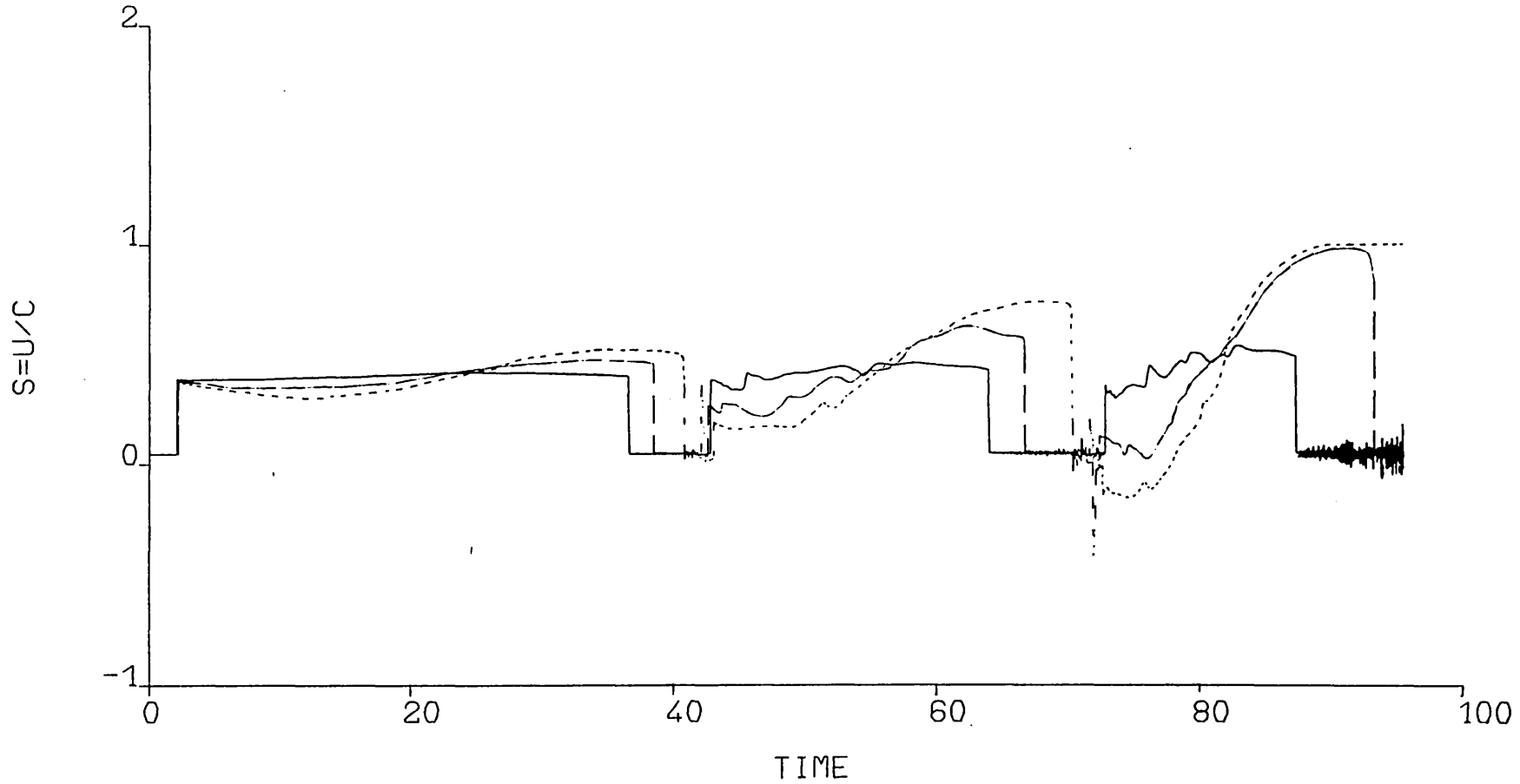



Fig 6.4.37 Variation in the speed index, S, corresponding to the variation in area and flow rate shown in Figs 6.4.35 and 6.4.36, respectively.

# CHAPTER 7

## CONCLUSIONS AND FUTURE WORK

There are several interesting conclusions, concerning unsteady flow in collapsible tubes, which arise from analysis of the research material presented in this thesis. These are now discussed and some avenues for future research in this area are suggested.

The mathematical model is shown to predict several types of instability. These are, a high frequency, small amplitude oscillation, an exponential instability and a very low frequency (<0.1) large amplitude oscillation. The first of these is found in a relatively short, relatively stiff tube. The flow is subcritical with the maximum value of the speed index, $S < \frac{1}{2}$. The boundary conditions seem to have a strong influence in this case, and it is very difficult to determine whether wave propagation is an essential part of the mechanism of this oscillation, for example, the oscillation may arise from the downstream boundary condition alone.

The second instability is of exponential type and occurs in longer tubes which are again relatively stiff. The area seems to fall rapidly, resulting in a dramatic decrease in the flow rate: the larger downstream inertia reduces outflow and the flow reverses at the upstream boundary. The final equilibrium state corresponds to a point on the P-Q characteristic at a slightly lower flow rate.

The third instability, is a low frequency large amplitude oscillation. The tube collapses to a minimum at the downstream boundary due to viscous dissipation in region 4, which reduces the pressure to a minimum at the downstream boundary; the presence of longitudinal tension would affect the position of minimum area. The tube reopens at the downstream end first, the wave of reopening steepening as it propagates upstream. Choking is ultimately involved in this instability, but cannot be investigated further without modifying the present model. Since S eventually exceeds ½ throughout the tube, a roll wave type instability may be involved. In this case the tube was of the same length as that used when the exponential type instability was observed, but the material was more flexible.

The above instabilities have features similar to some of the experimentally observed types of oscillations. The so-called flitter type instability observed by Rodbard and Saiki (1953) was a high frequency, small amplitude oscillation and exponential type instabilities have been observed by Bonis (1979) (see Bertram and Pedley, 1982). The features of the third type of oscillation, given the restrictions of the present model (for example, fixed position of the downstream boundary), are similar to those of the milking type oscillation observed by Bertram (1982).

Although the present study has been concerned primarily with unsteady flow, the results on steady flow are interesting and may be helpful in interpreting

experimental results. The steady flow analysis not only provides initial conditions for the unsteady flow model but it also enables the equilibrium states to be related to operating points on a P-Q characteristic. This is useful when investigating instabilities associated with a particular experiment. The present steady flow model is found to be superior to the previous lumped parameter models in predicting the main features of P-Q characteristics obtained in experimental studies (for example, Conrad, 1969; Brower and Scholten, 1975).

Instabilities were generally found to occur on the negative slope of the P-Q characteristics. At small values of the tube stiffness and small downstream resistance the flow is found to choke at a flow rate corresponding to an operating point on the negative slope of the P-Q characteristic; whereas for larger values of downstream resistance choking does not occur. However, in all the instabilities observed in section 6.4.3 choking ultimately occurred. This suggests that choking is likely to be involved in the oscillations observed in experiments on the Starling resistor which use a thin-walled collapsible tube.

Some parameters in the boundary conditions have a significant effect on the instabilities. The downstream rigid tube inertia, $I_2$, is found to have a big effect on the amplitude and frequency of the oscillations. The upstream inertia $I_1$ seems to have very little effect. However, it would be unwise to make any firm conclusions regarding the greater importance of $I_2$ over $I_1$ since

$L_5$ was zero in the cases considered and thus $I_2$ had a direct effect on region 4.

Another parameter which has a significant effect is $L_5$. This is found to stabilize the equilibrium state, indeed it is difficult (but not impossible) to find unstable states for $L_5 \neq 0$. A non-zero value of $L_5$ introduces a compliance and an inertia term, each of which is a crude estimate of the actual physical quantities. Again it would be unwise to propose any firm conclusion under these circumstances other than to emphasise the importance of region 5 of the model.

In all of the instabilities observed in the present study the greatest area fluctuation occurs at the downstream boundary, whereas the largest flow rate fluctuation occurs at the upstream boundary. This may be due to the steepening/flattening of pressure waves as they propagate through the fluid (see section 2.4). The asymmetry in the inertias and the resistances of the boundary conditions may also be significant.

Based on inviscid fluid flow in region 4 it is found that $L_4$ has a significant effect on the oscillations. Increasing $L_4$ reduces their amplitude and frequency and they become more non-linear. The build up time of the oscillations is also increased and this is believed to be due to the increased travel time of a wave in the fluid. This emphasises the importance of wave propagation.

The solution scheme, based on the method of

characteristics, is found to be most effective, giving a clear insight into the physical problem. Extensive testing of the method (see section 5.7) has shown it to be accurate and relatively inexpensive as regards computer time. The latter is achieved by not satisfying the CFL condition and allowing the characteristic to cross more than one grid length. The literature surveyed in connection with this method state that the CFL condition must be satisfied[‡], however, the author does not believe that the CFL condition applies directly to the scheme used in this thesis.

A linear stability analysis of the boundary conditions is shown to give a good indication of the stability of the system. In general, equilibrium states predicted unstable according to this analysis were found to be unstable, however, states predicted stable were sometimes found to be unstable. A linear stability analysis of the partial differential equations (region 4) did not give such a clear indication of the stability of the system. This perhaps emphasises the importance of the boundary conditions in the present model. The linear stability analyses, coupled with locating equilibrium states corresponding to operating points on the P-Q characteristic (usually the negative slope), provide a useful method for predicting regions of instability.

---

‡ Vardy (1976) is the only reference in which the CFL condition is not satisfied.

Several interesting avenues for future research suggest themselves. These can be divided into experimental and theoretical studies.

Many theoretical papers on flow in collapsible tubes have, in their conclusions, put emphasis on the need for more detailed experiments. The present study has again shown the significance of, for example, the rigid tube parameters which have seldom been recorded in experimental studies (two exceptions are Bertram, 1982 and a very recent publication by Ohba et al, 1984a). Thus one of the main objectives of future research should be to undertake a detailed experimental study on a Starling resistor. The parameters which have been shown to be important in the present study could then be accurately determined and so enable quantitative rather than qualitative tests to be carried out on this mathematical model.

The momentum equation in region 5 is quite a crude approximation to the flow in this region. More experiments of the type carried out by Bertram and Pedley (1983) should be undertaken to obtain more insight into the extremely difficult and important problem of flow through an oscillating constriction.

Choking is found to occur in many of the oscillations and so it is essential that future models should be able to deal with this phenomenon and the associated elastic jump. Shock-fitting or 'through' methods similar to those used by Kamm and Shapiro (1979)

could be incorporated in such models. Some modification of the solution procedure at the boundaries would also be required. The case of supercritical flow at the upstream boundary, for example, would mean that no negative slope characteristic existed at this point (downstream events cannot influence those upstream) and so a second boundary condition is required, viz constant inflow.

Some other obvious modifications which could be made to the present mathematical model are: a criterion to determine when flow separation occurs, instead of assuming separation occurs in region 5 for all $A_c<0$ (flow positive); modify the function P(A) so that the wave speed is not discontinuous at A = 1; an improved criterion to determine the number of reaches crossed by a characteristic based on its curvature.

Longitudinal tension is not included in the present model. It is an important parameter and therefore should be incorporated in future models. The present model could be modified to include this effect by using an expression similar to that proposed by McClurken et al (1981). However, a different numerical scheme would then be required since the hyperbolic character of the equations would be destroyed.

# APPENDIX A

## ELLIPTIC TUBE RESISTIVITY

The resistivity (resistance per unit length) for Poiseuille flow in an elliptic tube is well known, viz

$$R = 4\mu \frac{(a^2 + b^2)}{\pi a^3 b^3} ,$$

where $\mu$ is the dynamic viscosity and $a$, $b$ the semi-major and semi-minor axes respectively. This expression for $R$ can be rearranged in the form:

$$R(A) = 4\mu\pi \frac{(1/\delta + \delta)}{A^2} , \qquad (A.1)$$

where $A (= \pi ab)$ is the area of the ellipse and $\delta (= b/a)$ the ratio of the minor to major axes.

The equation of an ellipse centred at the origin is

$$\frac{x^2}{a^2} + \frac{y^2}{b^2} = 1 .$$

The length of the perimeter is

$$\int_C ds = \int_C [(dx)^2 + (dy)^2]^{\frac{1}{2}} .$$

The position of any point $(x, y)$ on the ellipse can also be defined by $(a\cos\theta, b\sin\theta)$. Substituting for $x$, $y$ in the above integral, yields

$$\int_C ds = 4 \int_0^{\pi/2} [a^2\cos^2\theta + b^2\sin^2\theta]^{1/2} \, d\theta$$

$$= 4a \int_0^{\pi/2} [1-(1-\delta^2)\sin^2\theta]^{1/2} d\theta \quad . \qquad (A.2)$$

At negative transmural pressures the perimeter of a rubber tube remains constant $= 2\pi a_0$, where $a_0$ is the radius of the tube in the circular configuration: this is chosen to be the radius of the rigid tube, viz $r_0$. Thus,

$$4a \int_0^{\pi/2} [1-(1-\delta^2)\sin^2\theta]^{1/2} d\theta = 2\pi r_0 \quad .$$

Rearranging the above, yields

$$\int_0^{\pi/2} [1-(1-\delta^2)\sin^2\theta]^{1/2} d\theta = \frac{\pi r_0}{2a}$$

$$= \frac{\pi^{3/2} r_0}{2} \left(\frac{\delta}{A}\right)^{1/2} \quad . \qquad (A.3)$$

Now

$$\mathcal{E}(k,\phi) = \int_0^{\phi} [1 - k^2\sin^2\Phi]^{1/2} d\Phi \quad ,$$

where $\Phi = \sin^{-1} k$ , is the elliptic integral of the second kind. Comparison of this integral with the left hand side of equation (A.3) gives $k^2 = 1-\delta^2$. Since $0 \leq \delta \leq 1$ then $0 \leq k \leq 1$ and further $0 \leq \Phi \leq \frac{\pi}{2}$ . Hence, (A.3) becomes

$$\mathcal{E}^2(k,\pi/2) = \frac{\pi^3 r_0^2 \delta}{4A} \quad .$$

Thus $$\delta = 4\mathcal{E}^2 A/\pi^3 r_0^2 \quad .$$

Substituting in (A.1) for $\delta$, yields

$$R(A) = \frac{4\mu\pi}{A^2}\left\{\frac{\pi^2 A_0}{4\mathcal{E}^2 A} + \frac{4\mathcal{E}^2}{\pi^2}\frac{A}{A_0}\right\}$$

From mathematical tables (Abramowitz and Stegun, 1965)

$$1 \leq \mathcal{E} \leq 1.5678 \quad .$$

There is no guidance as to the value of $\xi_0$ that should be used. Following Pedley (1980) the value $\pi^2/4\xi_0^2 = 1$ is chosen which corresponds approximately to the largest value of $\xi$. The expression for the resistivity then takes the simpler form

$$R(A) = \frac{4\mu\pi}{A^2}\left\{\frac{A_0}{A} + \frac{A}{A_0}\right\} .$$

Modifications to this formulation will be considered in Chapter 4.

# APPENDIX B

## METHOD OF CHARACTERISTICS

The general form of a quasi-linear system of equations for the case of two independent variables $x, t$ and dependent variables $u$, $A$ can be written in the form:

$$L_1 = A_1 \frac{\partial u}{\partial x} + B_1 \frac{\partial u}{\partial t} + C_1 \frac{\partial A}{\partial x} + D_1 \frac{\partial A}{\partial t} + E_1 = 0 \qquad (B.1)$$

$$L_2 = A_2 \frac{\partial u}{\partial x} + B_2 \frac{\partial u}{\partial t} + C_2 \frac{\partial A}{\partial x} + D_2 \frac{\partial A}{\partial t} + E_2 = 0 \ , \qquad (B.2)$$

where $A_1, A_2 \ldots, E_2$ are known functions of $x$, $t$, $u$, $A$ and first derivatives of $A$ and $u$ with respect to $x$ or $t$.

It is assumed that the above functions are continuous and that each of their derivatives arising in the subsequent analysis is also continuous. Furthermore it is assumed that the following condition does not exist:

$$\frac{A_1}{A_2} = \frac{B_1}{B_2} = \frac{C_1}{C_2} = \frac{D_1}{D_2} \ . \qquad (B.3)$$

The partial differential equations of the present model are a special case of the general system of equations (B.1) and (B.2). Setting $A_1 = A$; $B_1 = 0$; $C_1 = u$; $D_1 = 1$; $E_1 = 0$; $A_2 = u$; $B_2 = 1$; $C_2 = \frac{c^2}{A}$; $D_2 = 0$; $E_2 = RAu$, yields

$$L_1 = \frac{\partial A}{\partial t} + A \frac{\partial u}{\partial x} + u \frac{\partial A}{\partial x} = 0 \qquad (B.4)$$

$$L_2 = \frac{\partial u}{\partial t} + u \frac{\partial u}{\partial x} + \frac{c^2}{A} \frac{\partial A}{\partial x} + RAu = 0 \ , \qquad (B.5)$$

where $c = c(A)$ and $R = R(A)$ are known functions. The condition (B.3), which must not exist at any point becomes

$$\frac{A}{u} = \frac{0}{1} = \frac{Au}{c^2} = \frac{1}{0} \quad ,$$

which obviously cannot be satisfied.

Equations (B.4) and (B.5) are now combined linearly using an unknown multiplier $\lambda$. The resulting equation is

$$L = L_1 + \lambda L_2 = \left\{ \frac{\partial A}{\partial t} + \lambda \left( \frac{c^2}{A} + \frac{u}{\lambda} \right) \frac{\partial A}{\partial x} \right\}$$

$$+ \lambda \left\{ \frac{\partial u}{\partial t} + \left( u + \frac{A}{\lambda} \right) \frac{\partial u}{\partial x} \right\}$$

$$+ RAu\lambda = 0 \quad . \tag{B.6}$$

Now if $t = t(x)$ is the equation of a curve in the $x-t$ plane then the slope of the tangent at any point of the curve is $dt/dx$. Then if $u = u(x,t)$ and $A = A(x,t)$ are solutions to the equations (B.4) and (B.5) the Chain Rule gives

$$\frac{dA}{dt} = \frac{\partial A}{\partial x}\frac{dx}{dt} + \frac{\partial A}{\partial t}$$

and

$$\frac{du}{dt} = \frac{\partial u}{\partial x}\frac{dx}{dt} + \frac{\partial u}{\partial t} \quad . \tag{B.7}$$

Any two real distinct values of $\lambda$ will give two equations equivalent to (B.4) and (B.5). It is evident that a particular choice of $\lambda$ leads to a simplification. Examination of (B.6) together with (B.7) suggests that if

$$\frac{dx}{dt} = \lambda \left( \frac{c^2}{A} + \frac{u}{\lambda} \right) = u + \frac{A}{\lambda} \quad , \tag{B.8}$$

equation (B.6) becomes the ordinary differential equation

$$\frac{dA}{dt} + \lambda \frac{du}{dt} + \lambda RAu = 0 \quad , \tag{B.9}$$

where $\lambda$ depends upon the solution of (B.8), viz

$$\lambda^2 \frac{c^2}{A} - A = 0 \quad \Rightarrow \quad \lambda = \pm \frac{A}{c} \quad .$$

Substituting these values of $\lambda$ back onto (B.8), yields

$$\frac{dx}{dt} = u \pm c \quad . \tag{B.10}$$

Note that the positive value of $\lambda$ , viz $A/c$ corresponds to $dx/dt = u+c$ and that $\lambda = -A/c$ corresponds to $dx/dt = u-c$ . Substitution of these values of $\lambda$ into (B.9) results in two pairs of equations identified as the $C_+$ and $C_-$ equations:

$C_+$

$$\frac{dA}{dt} + \frac{A}{c}\frac{du}{dt} + \frac{A}{c} RAu = 0 \tag{B.11}$$

$$\frac{dx}{dt} = u + c \tag{B.12}$$

$C_-$

$$\frac{dA}{dt} - \frac{A}{c}\frac{du}{dt} - \frac{A}{c} RAu = 0 \tag{B.13}$$

$$\frac{dx}{dt} = u - c \quad . \tag{B.14}$$

Thus reduction of the original partial differential equations to two ordinary differential equations is possible in the characteristic directions given by equations (B.12) and (B.14). Equations (B.11) and (B.13) are called the compatability equations and are valid along the $C_+$ and $C_-$ characteristics respectively.

It should be noted that no mathematical approximations are made in the transformation of the original partial differential equations. Thus every solution of this set will be a solution of the original set.

## REFERENCES

Abramowitz, M and Stegun, IA (1965) Handbook of Mathematical Functions. Washington: National Bureau of Standards.

Anliker, M and Raman, KR (1966) Korotkoff sounds at diastole - a phenomenon of dynamic instability of fluid-filled shells. Int J Solids & Structures 2, 467-491.

Attinger, EO (1969) Wall properties of veins. IEEE Trans Bio-Med Eng BME-16, 253-261.

Beam, RM (1968) Finite amplitude waves in fluid-filled elastic tubes: wave distortion, shock waves and Korotkoff sounds. NASA Tech Note D-4803.

Bertram, CD (1982) Two modes of instability in a thick-walled collapsible tube conveying a flow. J Biomech 15, 223-224.

Bertram, CD and Pedley, TJ (1982) A mathematical model of unsteady collapsible tube behaviour. J Biomech 15, 39-50.

Bertram, CD and Pedley, TJ (1983) Steady and unsteady separation in an approximately two-dimensional indented channel. J Fluid Mech 130, 315-345.

Bitbol, M, Dantan, Ph, Perrot, P and Oddou, C (1982) Collapsible tube model for the dynamics of closure of the mitral valve. J Fluid Mech 114, 187-211.

Bonis, M and Ribreau, C (1977) Pressure flow relationships in collapsible tubes. In Cardio-vascular and Pulmonary Dynamics. Euromech 92, 459-466. INSERM

Brecher, GA (1952) Mechanism of venous flow under different degrees of aspiration. Am J Physiol 169, 423-433.

Brower, RW and Noordergraaf, A (1973) Pressure-flow characteristics of collapsible tubes: A reconciliation of seemingly contradictory results. Ann Biomed Eng 1, 333-355.

Brower, RW and Noordergraaf, A (1978) Theory of steady flow in collapsible tubes and veins. In Cardiovascular System Dynamics (Edited by Baan, J, Noordergraaf, A and Reines, J) 256-265, MIT Press, Cambridge, USA.

Brower, RW and Scholten, C (1975) Experimental evidence on the mechanism for the instability of flow in collapsible vessels. Med and Biol Eng 13, 839-845.

Cancelli, C and Chiocchia, G (1979) On the onset of self-excited oscillations in a collapsible tube flow with sonic index values less than one: mathematical model and numerical results. Atti Accad Naz dei Lincei - Memorie Sc fisiche ecc 15, 319-352.

Caro, CG, Pedley, TJ, Schroter, RC and Seed, WA (1978) The Mechanics of the Circulation, Oxford University Press.

Conrad, WA (1969) Pressure-flow relationships in collapsible tubes. IEEE Trans Biomed Eng BME-16, 284-295.

Conrad, WA (1980) A new model of the vocal cords based on a collapsible tube analogy. Med Res Eng 13, 7-10.

Conrad, WA (1983) Differential negative resistance in a one-mass model of the larynx with supraglottal resistance. JASA Suppl 1, 74:S116.

Conrad, WA, Cohen, ML and McQueen, DM (1978) Note on the oscillations of collapsible tubes. Med and Biol Eng and Comput 16, 211-214.

Conrad, WA, McQueen, DM and Yellin, EL (1980) Steady pressure flow relations in compressed arteries: possible origin of Korotkoff sounds. Med and Biol Eng and Comput 18, 419-426.

Courant, R, Isaacson, E and Rees, M (1952) On the solution of non-linear hyperbolic differential equations by finite differences. Comm Pure & Appl Math 5, 243-255.

Cowley, SJ (1982) Elastic jumps on fluid-filled elastic tubes. J Fluid Mech 116, 459-473.

Dawson, SV and Elliott, EA (1977) Wave speed limitation on expiratory flow - a unifying concept. J Appl Physiol 43, 498-515.

Elliott, EA and Dawson, SV (1977) Test of wave speed theory of flow limitation in elastic tubes. J Appl Physiol 43, 516-522.

Evangelisti, G (1969) Waterhammer analysis by the method of characteristics. L'Energia Elettrica 46, Pt 10, 673-692.

Flaherty, JE, Keller, JB and Rubinow, SI (1972) Post buckling behaviour of elastic tubes and rings with opposite sides in contact. SIAM J Appl Math 23, 446-455.

Fox, JA (1977) Hydraulic Analysis of Unsteady Flow in Pipe Networks. Macmillan, London.

Fry, DL (1958) Theoretical considerations of the bronchial pressure-flow-volume relationships with particular reference to the maximum expiratory flow volume curve. Phys Med Biol 3, 174-194.

Gonzalez, F, Kurzweg, UH and Jaeger, MJ (1975) Origin of Korotkoff sounds. Fed Proc 34 (3), 414.

Griffiths, DJ (1969a) Urethral elasticity and micturition hydrodynamics in females. Med and Biol Eng 7, 201-215.

Griffiths, DJ (1969b) The velocity of the urine stream during female micturition. Med and Biol Eng 7, 527-531.

Griffiths, DJ (1971a) Hydrodynamics of male micturition - I. Theory of steady flow through elastic-walled tubes. Med and Biol Eng 9, 581-588.

Griffiths, DJ (1971b) Hydrodynamics of male micturition - II. Measurements of stream parameters and urethral elasticity. Med and Biol Eng 9, 589-596.

Griffiths, DJ (1971c) Steady fluid flow through veins and collapsible tubes. Med and Biol Eng 9, 597-602.

Griffiths, DJ (1975a) Negative-resistance effects in flow through collapsible tubes: 1 Relaxation oscillations. Med and Biol Eng 13, 785-790.

Griffiths, DJ (1975b) Negative-resistance effects in flow through collapsible tubes: 2 Two-dimensional theory of flow near an elastic constriction. Med and Biol Eng 13, 791-796.

Griffiths, DJ (1975c) Negative-resistance effects in flow through collapsible tubes: 3 Two-dimensional treatment of the elastic properties of elastic constriction. Med and Biol Eng 13, 797-801.

Griffiths, DJ (1977) Oscillations in the outflow from a collapsible tube. Med and Biol Eng and Comput 15, 357-362.

Grotberg, JB and Davis, SH (1980) Fluid-dynamic flapping of a collapsible channel: sound generation and flow limitation. J Biomech 13, 219-230.

Hagen, G (1839) Ueber die bewegung des wassers in engen cylindrishchen röhren. Poggendortts Ann 46, 423-442.

Holenstein, R, Nerem, RM, and Niederer, PF (1984) On the propagation of a wave front in viscoelastic arteries. J Biomech Eng 106, 115-122.

Holmberg, JL and Wilson, TA (1970) Mechanics of the flow in an elastic tube extending from an orifice into a pressure vessel. Trans ASME, J Appl Mech 37, 812-816.

Holt, JP (1941) The collapse factor in the measurement of venous pressure; the flow of fluid through collapsible tubes. Am J Physiol 134, 292-299.

Holt, JP (1969) Flow through collapsible tubes and through in situ veins. IEEE Trans Biomed Eng BME-16, 274-283.

Jan, DL, Kamm, RD and Shapiro, AH (1983) Filling of partially collapsed compliant tubes. Trans ASME, J Biomech Eng 105, 12-19.

Kamm, RD (1982) Bioengineering studies of periodic external compression as prophylaxis against deep vein thrombosis - Part 1: Numerical studies. J Biomech Eng 104, 87-95.

Kamm, RD and Shapiro, AH (1979) Unsteady flow in a collapsible tube subjected to external pressure or body forces. J Fluid Mech 95, 1-78.

Katz, AI, Chen, Y and Moreno, AH (1969) Flow through a collapsible tube: Experimental analysis and mathematical model. Biophys J 9, 1261-1279.

Kececioglu, I, McClurken, ME, Kamm, RD and Shapiro, AH (1981) Steady, supercritical flow in collapsible tubes. Part 1: Experimental observations. J Fluid Mech 109, 367-389.

Knowlton, FP and Starling, EH (1912) The influence of variations in temperature and blood-pressure on the performance of the isolated mammalian heart. J Physiol 44, 206-219.

Knudson, RJ and Schroter, RC (1983) A consideration of density dependence of maximum expiratory flow. Respir Physiol 52, 125-136.

Korotkoff, NS (1905) A contribution to the problem of methods for the determination of the blood pressure. Imp Mil Med Acad 11, 365-367. (Trans by Geddes et al (1966) Cardiovasc Res Centre Bull 5, 57-74).

Kresch, E (1979) Compliance of flexible tubes. J Biomech 12, 825-839.

Laird, JD, Madras, PN, Jones, RT, Kantrowitz, AR, Kothari, ML, Buckley, MJ and Austen, WG (1968) Theoretical and experimental analysis of the intra aortic balloon pump. Trans Amer Soc Artif Int Organs 14, 338-343.

Lambert, RK and Wilson, TA (1972) Flow limitation in a collapsible tube. J Appl Physiol 33, 150-153.

Lighthill, MJ (1972) Physiological fluid dynamics: a survey. J Fluid Mech 52, 475-497.

Lighthill, MJ (1978) Waves in Fluids. Cambridge University Press.

Lister, M (1960) The numerical solution of hyperbolic partial differential equations by the method of characteristics. In Mathematical Methods for Digital Computers (edited by Ralston, A and Wilf, HS), 165-179. Wiley.

Mackay, RS (1958) Negative resistance. AM J Phys 26, 60-69.

Matsuzaki, Y and Fung, YC (1977) Unsteady fluid dynamic forces on a simply-supported circular cylinder of finite length conveying a flow, with applications to stability analysis. J Sound and Vibration 54, 317-330.

Matsuzaki, Y and Fung, YC (1979) Non-linear stability analysis of a two-dimensional model of an elastic tube conveying a compressible flow. Trans ASME, J Appl Mech 46, 31-36.

McClurken, ME (1978) Shape-independent area measurement in collapsible tubes by an electrical impedance technique. Proc 31st Ann Conf Eng in Medicine and Biol, Atlanta, Georgia.

McClurken, ME, Kececioglu, I, Kamm, RD and Shapiro, AH (1981) Steady, supercritical flow in collapsible tubes. Part 2: Theoretical studies. J Fluid Mech 109, 391-415.

McMahon, TA, Clark, C, Murthy, VS and Shapiro, AH (1971) Intra-aortic balloon experiments in a lumped-element hydraulic model of the circulation. J Biomech 4, 335-350.

Moreno, AH, Katz, AI, Gold, LD and Reddy, RV (1970) Mechanics of distension of dog veins and other very thin-walled tubular structures. Circulation Res 27, 1069-1080.

Nicholson, HW, Heiser, WH and Olsen, JH (1967) Wave propagation in liquid-filled elastic tubes. Bull Mech Eng Educ 6, 371-376.

Oates, GC (1975a) Fluid flow in soft-walled tubes. Part 1 Steady flow. Med and Biol Eng 13, 773-779.

Oates, GC (1975b) Fluid flow in soft-walled tubes. Part 2 Behaviour of finite waves. Med and Biol Eng 13, 780-784.

Oates, GC (1982) Effect of friction on shock like transitions in soft-walled tubes. (Tech Note). Med and Biol Eng and Comput 20, 113-116.

Ohba, K, Yoneyama, N, Shimanaka, Y and Maeda, H (1984a) Self-excited oscillation of flow in collapsible tube. Tech Rept of Kansai Univ 25, 1-13.

Ohba, K, Yoneyama, N Sakurai, A, Kajiya, F, Tomanaga, G and Kondo, Y (1984b) Self-excited oscillation of flow in collapsible tube. IV (Analysis and experiment on initiation of oscillation)

Olsen, DA, Kamm, RD and Shapiro, AH (1982) Bioengineering studies of periodic external compression as prophylaxis against deep vein thrombosis - Part II: Experimental studies on a simulated leg. J Biomech Eng 104, 96-104.

Olsen, JG and Shapiro, AH (1967) Large amplitude unsteady flow in liquid-filled elastic tubes. J Fluid Mech 29, 513-538.

Paidoussis, MP and Denise, JP (1972) Flutter of thin cylindrical shells conveying fluid. J Sound and Vibration 20, 9-26.

Pedley, TJ (1980) The Fluid Mechanics of Large Blood Vessels. Cambridge University Press.

Permutt, S and Riley, RL (1963) Hemodynamics of collapsible vessels with tone: the vascular waterfall. J Appl Physiol 18, 924-932.

Poiseuille, J (1840) Recherches experimentales sur le mouvement des liquides dans les tubes de tres petits diametres. Compt Rend 11, 961-967 and 1041-1048; 12, 112-115.

Prandtl, L (1934) Fundamentals of Hydrodynamics and Aerodynamics (trans by OG Tietjens) McGraw Hill.

Reyn, JW (1974) On the mechanism of self-excited oscillations in the flow through collapsible tubes. Delft Progr Rep, Series F: Math Eng, Math Inf Eng 1, 51-67.

Reyn, JW (1975) Perturbations of uniform flow through collapsible tubes. Delft Progr Rep Series F: Math Eng, Math Inf Eng 1, 69-81.

Rodbard, S (1955) Flow through collapsible tubes: augmented flow produced by resistance at the outlet. Circulation 11, 280-287.

Rodbard, S (1963) Autoregulation in encapsulated, passive, soft-walled vessels. Am Heart J 65, 648-655.

Rodbard, S (1966) A hydrodynamic mechanism for autoregulation of flow. Cardiologia 48, 532-535.

Rodbard, S and Saiki, H (1953) Flow through collapsible tubes. Am Heart J 46, 715-725.

Rubinow, SI and Keller, JB (1972) Flow of a viscous fluid through an elastic tube with applications to blood flow. J Theor Biol 35, 299-313.

Schoendorfer, DW and Shapiro, AH (1977) The collapsible tube as a prosthetic vocal source. Proc San Diego Biomed Symposium 16, 349-356. Academic Press, New York.

Shapiro, AH (1954) The Dynamics and Thermodynamics of Compressible Fluid Flow. Ronald Press Company, New York.

Shapiro, AH (1977a) Physiologic and medical aspects of flow in collapsible tubes. Proc 6th Canadian Cong Appl Mech Vancouver, 883-906.

Shapiro, AH (1977b) Steady flow in collapsible tubes. Trans ASME, J Biomech Eng 99, 126-147.

Shimzu, M and Tanida, Y (1983) On the mechanism of Korotkoff sound generation at diastole. J Fluid Mech 127, 315-339.

Smith, GD (1978) Numerical Solution of Partial Differential Equations: Finite Difference Methods. Oxford University Press.

Stephanoff, KD, Pedley, TJ, Lawrence, CJ and Secomb, TW (1983) Fluid flow along a channel with an asymmetric oscillating constriction. Nature 305, 692-695.

Streeter, VL, Keitzer, WF and Bohr, DF (1963) Pulsatile pressure and flow through distensible vessels. Circulation Res 13, 3-20.

Tsuji, T, Nakajima, K, Takeuchi, Y, Inoue, K, Shiroma, K, Koyama, Y, Tokuchi, K, Yoshikawa, T and Suma, K (1978) Study on haemodynamics during cardiopulmonary bypass. Artificial Organs (Japanese) 7, 435-438.

Ur, A and Gordon, M (1970) Origin of Korotkoff sounds. Am J Physiol 218, 524-529.

Vardy, AE (1976) On the use of the method of characteristics for the solution of unsteady flows in networks. Proc 2nd Int Conf on Pressure Surges BHRA, Bedford, 15-30.

Vischer, D (1979) Die selbsttätige schlauchdrossel zur gewährleistung konstanter beckenausflusse. Wasserwirtschaft 62, 346-350.

Weaver, DS and Paidoussis, MP (1977) On collapse and flutter phenomena in thin tubes conveying fluid. J Sound and Vibration 50, 117-132.

Wild, R, Pedley, TJ and Riley, DS (1977) Viscous flow in collapsible tubes of slowly-varying elliptical cross-section. J Fluid Mech 81, 273-294.

Wylie, EB and Streeter, VL (1978) Fluid Transients. McGraw Hill, New York.

Yevjevich, V and Barnes, AH (1970) Flood routing through storm drains. Part IV: Numerical computer methods of solution. Hydrology papers, Colorado State Univ, Fort Collins, Colorado.